Hybrid Magnetic Materials based on Coordination Chemistry

From Switching Magnetic Molecules to 2D Coordination Polymers

VNIVERSITAT DE VALÈNCIA

Instituto de Ciencia Molecular

Memoria presentada por Alexandre Abhervé para aspirar al grado de Doctor en Nanociencia y Nanotecnología (programa ref. 3045)

Dirigida por el Dr Eugenio Coronado Miralles y el Dr Miguel Clemente León

D. Eugenio Coronado Miralles, Catedrático y **D. Miguel Clemente León**, profesor titular, del Instituto de Ciencia Molecular (ICMol) de la Universitat de València,

CERTIFICAN:

Que el trabajo que presenta D. Alexandre Abhervé en esta memoria, bajo el título: "**Hybrid magnetic materials based on coordination chemistry: from switching magnetic molecules to 2D coordination polymers**" ha sido realizado bajo nuestra dirección en el Instituto de Ciencia Molecular de la Universitat de València.

Y para que así conste, a efectos de su presentación para optar al Grado de Doctor en Química, expedimos el presente documento.

Paterna, Febrero de 2015

Codirector	Codirector
Dr. Eugenio Coronado Miralles	Dr. Miguel Clemente León
(firma)	(firma)

à mon père

Je souhaite profiter de la publication de cet ouvrage et de ces premières lignes pour adresser quelques remerciements, et témoigner mon affection envers les personnes qui m'ont accompagné, dans la vie, dans le travail, à tout moment.

Le temps et l'énergie consacrés aux études, depuis presque 8 ans, et à la réalisation de ce travail de recherche, n'auraient été possibles sans les efforts, les sacrifices, et l'affection consacrés par mes parents pour leurs trois enfants. J'ai eu la chance d'avoir leur soutien, leur aide, et leur confiance dans chaque décision concernant ma vie et mon travail. Cet ouvrage leur est particulièrement dédié.

Dans un second temps, j'aimerais adresser mes remerciements aux personnes qui me sont les plus proches, les personnes les plus admirables qu'il m'a été donné de rencontrer :

A Vincent, Georgy, Morgane ; votre soutien, puis votre amitié, sont les plus belles choses qui me soient arrivées, et continuent de me combler. A Damien, Fred, Flo ; j'ai eu la chance de croiser aussi votre chemin, l'amitié s'est installée très vite. Vous m'avez ensuite soutenu, et ainsi permis de maintenir la tête haute, à un moment où j'aurai pu renoncer. A vous tous, je dédie également cette thèse.

A une famille incroyable dont je suis fier, mes frangins Jean-Marc et Romain, mes belles sœurs Delphine et Laëtitia, neveux, cousins, oncles, tantes, grands-parents, Abhervé et Lamour ! Et à ma deuxième famille, Tata Malou, Gérard, Nelly et mon « grand frère » Eric.

A tous mes amis bretons, connus principalement pendant mes années à Brest, Youssef, Christophe, Line, Matthias, Guillaume, Charlène, David, Nolwenn, Laëtitia, Thibault, Julien, Caro, Clémence, Marie, Angie, Amaury, Zélie, Isabelle, Tchaz, Greg, Matthieu et Nicolas.

A mes amis galiciens, en particulier mes « parents galiciens » María et Paco, et à ceux qui ont participé avec moi à cette aventure du jumelage Lesneven – As Pontes, pour tous les moments d'amitié et de fraternité partagés chaque été en votre compagnie, notamment avec la bande Christophe, David, Ewen, Guillaume, Jérôme et François-Xavier.

Au fil du temps et des rencontres, on a parfois l'opportunité de rencontrer des personnes sincères, bienveillantes et humbles, des valeurs primordiales mais très souvent oubliées, notamment dans la « communauté scientifique ». J'ai eu cette chance, je pense tout d'abord à Mauri, à qui je dois mon intégration à Valencia et au sein du groupe ; à Sam, qui m'a apporté tellement de choses, soutien, rire, tendresse, et réconfort ; et bien sûr, à cette bande de potes, dont j'ai parfois peine à imaginer qu'ils soient amenés à devenir de sérieux chercheurs, mon ami Michele, José Jaime (« Equipo India »), Gustavo, Marc, et Ramón. Enfin j'aimerais remercier, pour leur amitié, le non moins dingue Walter, Juampi, mes « Valenciens préférés » Paco, María, Eva, Jose et Carles, le « McGiver de l´ICMol » Angel, l'irremplaçable Carlos, mes compatriotes et compagnons de comptoir Yoann, Florence, Jérémy, Martin et Laëtitia, la belle et rayonnante Thaïs ainsi que les collègues survivants du Master, et les potes du football qui, comme moi, ont judicieusement préféré suivre la vocation de scientifiques.

Plus sérieusement enfin, ce travail ne pouvait pas se faire à la force de mes bras et de mon ingéniosité relatives. Je remercie les personnes qui ont contribuées à l'obtention des résultats présentés dans cet ouvrage : tout d'abord, Eugenio Coronado et Miguel Clemente, directeurs de cette thèse, pour leur aide constante dans la réalisation de ce travail de recherche; je souhaite témoigner toute ma reconnaissance à Miguel, pour ses conseils et la transmission de ses connaissances, et bien davantage pour les qualités humaines, la présence, la confiance, et l'enthousiasme ; Mauri López pour les composés basés sur le ligand bppCOOH et l'enseignement des différentes techniques de travail au laboratoire, Carlos Gómez et Martin Verneret pour le travail sur les anilates, Samuel Mañas et Elena Pinilla pour le travail de délamination et les mesures AFM, Chema Martínez et Gloria Agustí pour les mesures magnétiques, Juan Modesto Clemente pour les ajustements de propriétés magnétiques et calculs théoriques, Guillermo Mínguez pour la partie cristallographie, Jaursup Boonmak pour les clusters de Fe^{III}, ainsi que Raphael Marx et Joris van Slageren de Institut für Physikalische Chemie, Universität Stuttgart pour les mesures de HF-EPR.

Quisiera dedicar la publicación y las primeras líneas de este manuscrito para intentar agradecer y expresar mi cariño hacía las personas que me han acompañado en la vida, en el trabajo, y en todo momento.

El tiempo y la energía, dedicados a los estudios desde hace casi 8 años y la realización de este trabajo de investigación, no hubieran sido posibles sin los esfuerzos, los sacrificios y el cariño de mis padres a sus tres hijos. He tenido la gran suerte de tener, siempre, su apoyo, su ayuda y su confianza en cada decisión que tomaba en relación con mi vida y mi trabajo. Este manuscrito les está particularmente dedicado.

Por otra parte, me gustaría dirigir mis agradecimientos a las personas más cercanas y admirables que he tenido la suerte de conocer:

Vincent, Georgy, Morgane; vuestro apoyo y vuestra amistad, son las cosas más bonitas que me hayan ocurrido y que siguen llenándome. Damien, Fred, Flo; he tenido también la suerte de cruzar vuestro camino, la amistad se instaló rápidamente. Luego me habéis apoyado y así permitido de resistir en vez de rendirme. A todos vosotros, os dedico también esta Tesis.

A una familia increíble de la cual estoy muy orgullosos: mis hermanos Jean Marc y Romain, mis cuñadas Delphine y Laëtitia, mis sobrinos, primos, tios, tias, abuelos, Abhervé y Lamour. Y a mi secunda familia: Tata Malou, Gérard, Nelly y mi “hermano mayor” Eric.

A todos mis amigos bretones, encontrados principalmente durante mis años pasados en Brest, Youssef, Christophe, Line, Matthias, Guillaume, Charlène, David, Nolwenn, Laëtitia, Thibault, Julien, Caro, Clémence, Marie, Angie, Amaury, Zélie, Isabelle, Tchaz, Grec, Matthieu y Nicolas.

A mis amigos gallegos, en particular a mis “padres gallegos” María y Paco y a los que han participado conmigo en esta aventura de hermanamiento Lesneven – As Pontes, por todos estos momentos de amistad y fraternidad compartidos cada verano, en particular con la pandilla compuesta por Christophe, David, Ewen, Guillaume, Jérôme y François-Xavier.

A lo largo del tiempo y de los encuentros, tenemos a veces la oportunidad de conocer a personas sinceras, bondadosas y humildes, valores primordiales pero a menudo olvidados en «la comunidad científica». Tuve esta suerte. Pienso en primer lugar en Mauri, a quien debo mi integración en Valencia y en el grupo. A Sam que me ha aportado tantas cosas, apoyo, risas, cariño y consuelo; y naturalmente a esta pandilla de colegas, que me cuesta a veces imaginar que puedan ser serios investigadores, mi amigo Michele, José Jaime (« Equipo India »), Gustavo, Marc, y Ramón. Para acabar, me gustaría agradecerles su amistad a, no el menos loco Walter, a Juampi, a mis « Valencianos preferidos» » Paco, María, Eva, Jose y Carles, al « McGiver del ICMol » Angel, al irremplazable Carlos, a mis compatriotas y compañeros de barra Yoann, Florence, Jérémy, Martin y Laëtitia, a la bella y radiante Thais así que a los colegas supervivientes del Master y a los del futbol quien, como yo han preferido, con acierto, seguir la vocación científica.

De manera más seria y para acabar, este trabajo no hubiera podido hacerse sin la fuerza de mis brazos ni sin mi ingenio relativo. Le agradezco su contribución para la obtención de los resultados presentados en este manuscrito: en primer lugar, a Eugenio Coronado y Miguel Clemente, directores de esta tesis, por su ayuda constante en la realización de este trabajo de investigación. Todo mi reconocimiento a Miguel por sus consejos y transmisión de conocimientos y más si cabe, por los valores humanos: su presencia, su confianza y su entusiasmo. A Mauri Lopez, por los compuestos basados en el ligando bppCOOH y la enseñanza de las distintas técnicas de trabajo en el laboratorio. A Carlos Gómez y a Martin Verneret por el trabajo sobre los anilatos, a Samuel Mañas y a Elena Pinilla por el trabajo sobre la deslaminación y medidas de AFM. A Chema Martinez y a Gloria Agustí por las medidas magnéticas. A Juan Modesto Clemente por los ajustes de las propiedades magnéticas y cálculos teóricos. A Guillermo Minguez por la parte cristalográfica. A Jaursup Boonmak por los clústeres de Fe^{III}, así que a Raphael Marx y Joris van Slageren del Institut für Physikalische Chemie, Universität Stuttgart, por las medidas de HF-EPR.

« If you wanna tease you gotta shake me please
Shake da buddha cyco takin' da coco
You got understanding: I'm just a fonkey junky monkey! »

Goz

TABLE OF CONTENTS

Introduction

Chapter 1

Chapter 1. Introduction

1. Multifunctional Hybrid Materials

For more than 5000 years, organic-inorganic hybrid materials created by men via skill and serendipity have been part of human culture and customs. The first hybrid materials made by humanity were based on organically modified clays, and were used along history for artistic, social, environmental, industrial and commercial uses.[1] Before Antiquity, clay and soil were mixed with decaying urine to enhance laundry processes. In America, pre-Colombian civilizations created a well-known pigment, the Maya blue. This pigment was a combination of a natural organic dye (blue indigo) with a micro-fibrous clay (palygorskite). This resulting hybrid is characterized by a strong blue coloring, which is much more stable towards weathering and biodegradation than the indigo dye alone.[2]

Today, hybrid materials represent not only a new field of basic research where creative chemists can express themselves, but also an apportunity to develop more applications thanks to their remarkable new properties and multifunctional nature. For over two decades, synthetic methods based on the so-called “soft chemistry” have been developed to prepare hybrid materials. They have attracted strong interest both in academia and industry, as they constitute a versatile route towards multifunctionality and device integration, and have led to collaborations between chemists, physicists and biologists. It is therefore possible, with the “soft chemistry” processes, to design multifunctional hybrid materials with perfect control over their composition, structure and shape. Some of these hybrids are increasingly impacting important fields such as energy, environment and nanomedicine.[3] A fundamental characteristic of these materials consists on the easiness of their processing, leading to films, membranes, fibers, powders, monoliths, micro- and nano-patterns.

The versatility of the building-block approach provided by coordination chemistry allows the design of new molecular materials by self-assembling of building blocks of different natures (organic, inorganic or organometallic), that combine several physical properties of interest, such as ferromagnetism, conductivity, superconductivity, optical activity or non-linear optics. This chemical approach allows for a careful design of the material with specific supramolecular interactions between the different building blocks. The combination of these subunits has permitted the coexistence or even the synergy of different properties in a single material. It is also possible, by the control of the molecular structure, to tune the properties of the material. Most of the research has been focused in the use of three-dimensional (3D) host structures. Still, much effort is now devoted to the design of layered solid-state structures, as they offer new possibilities thanks to their processability and chemical versatility. Furthermore, they lead to new physical properties derived from their two-dimensional (2D) character. Most of the research in this area started very recently after the discovery of graphene and other 2D systems made out of atomically thin layers.[4] The development of exfoliation/delamination techniques for a wide range of layered materials has allowed the design of new multifunctional materials and their integration into devices.

The main focus of this thesis is the design of new multifunctional hybrid compounds based on spin-crossover complexes combined with magnetic polyoxometalates or with magnetic networks. A second goal is the processing of some of these compounds on surfaces via self-assembly or top-down delamination processes. An introduction to these materials together with their physical properties is now presented.

2. Spin-Crossover Materials

2.1. Spin-Crossover Phenomenon

Spin-crossover (SCO) or spin-transition complexes are an interesting class of switchable molecules that change its spin state configuration under the influence of external perturbations such as a change in temperature, pressure or light irradiation.[5] A thermal spin transition in a SCO material results in changes in several of its physical properties,[6] including magnetic moment, color, molecular structure,[7] dielectric constant,[8] and electrical resistance.[9] Therefore, this is a typical example of molecular bistability. Since the first reports of Cambi *et al.*,[10] several hundreds of mononuclear or multinuclear spin crossover complexes have been synthesized and characterized as bulk (powder or single crystal) or diluted (solid or liquid) materials. Functional liquid crystals,[11] Langmuir–Blodgett and other thin films,[12] nanoparticles[12f,13] and surface patterns[5,12e,14] of spin-transition materials have also been isolated.[15] Their macroscopic properties are mainly understood on the basis of electron–phonon coupling and elastic properties of the crystal lattice.[16] At the molecular level, this phenomenon has been fully rationalized by ligand field theory.[17]

Spin-crossover is typically observed in *d*-block metal complexes. As a consequence of the splitting of the energy of the *d* orbitals into the t_{2g} and e_g sets in an octahedral ligand field, certain strength transition metal complexes may exist in either the high-spin (HS) or low-spin (LS) state, depending on the nature of the ligand field about the metal ion.[18] In weak fields, the ground state is HS where the spin multiplicity is a maximum, the *d* electrons being distributed over the t_{2g} and e_g sets, whereas strong fields stabilize the LS state with minimum multiplicity, the t_{2g} set being completely occupied before electrons are added to the e_g set. For intermediate fields, the energy difference between the two states may be sufficiently small in such a way that the application of an external perturbation induces a spin-crossover between the higher enthalpy of the LS state and the greater electronic and vibrational entropy of the HS

state (Scheme 1). Most commonly, this transition is induced by a change in temperature. The HS state is stabilized relative to the LS as the transition temperature is raised, so that above the transition temperature the HS state becomes the thermodynamic ground state of the compound. This spin-transition results in an elongation of the metal-ligand bond lengths and a color change of the system. Equations that treat the magnetic transition as a thermodynamic equilibrium between starting materials (LS) and products (HS) are required to reproduce the behavior. This phenomenon could be shown by octahedral complexes with d^n (n = 4 – 7) configuration, though the family of Fe^{II} complexes is the most investigated.[19] For Fe^{II} (d^6 configuration), spin-transition occurs between the diamagnetic LS state (S = 0), characterized by a $t_{2g}^6e_g^0$ configuration ($^1A_{1g}$ state in octahedral symmetry), and the HS state (S = 2) with the $t_{2g}^4e_g^2$ configuration, which has four unpaired electrons and thus is strongly paramagnetic ($^5T_{2g}$ state).[18] The majority of these complexes exhibit a N_6 coordination sphere,[20] but other examples with a N_5O[21], N_4O_2,[22] N_4S_2[21,23] or N_4C_2[24] coordination sphere are also reported. Two other important families of SCO complexes are Fe^{III} complexes (d^5 configuration) with a N_4O_2 coordination sphere,[25] and Co^{II} complexes (d^7 configuration).[26] Finally, Morgan and co-workers have reported some examples of Mn^{III} (d^4 configuration) spin-crossover complexes.[27]

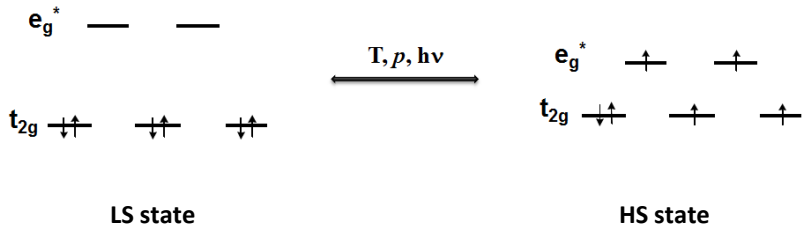

Scheme 1. Schematic illustration of SCO for a d^6 metal center.

Cooperativity in the solid lattice is a fundamental aspect for the SCO material, since it determines the efficiency with which structural changes at individual metal ion sites are transmitted through the bulk material, and therefore, control the form of the transition (Figure 1).[28] Cooperative spin-transitions, which involve large structural

changes between the two electronic states, are common in Fe^{II} compounds,[29] rare in Fe^{III} compounds[25] and almost unknown in other SCO complexes. Such structural changes in the molecular shape depend on the nature of the metal ion as well as the metal-ligand combinations.[30] For example, spin-crossover in octahedral d^6 (S = 2 → S = 0) and d^5 (S = $^5/_2$ → S = $^3/_2$) metal ions generally involves greater structural changes than for d^4 (S = 2 → S = 1) and d^7 (S = $^3/_2$→ S = $^1/_2$), since it involves a greater depopulation of the antibonding e_g orbital. On the other hand, the largest structural changes are observed for group 15 ligand donors (N and P), whose metal-ligand bonds contract by 10-13% during spin-crossover.[15] The form of the transition is also determined by the dimensionality and strength of inter-molecular interactions in the bulk solid.[19] There are several possibilities. In some cases, the metal complexes may be linked by covalent bonding when they are contained in a polynuclear complex or coordination polymer.[31] Alternatively, in a molecular crystal, they arise from weaker hydrogen bonding, π-π interactions or simple intermolecular contacts.[32] These secondary interactions usually induce most cooperative spin transitions than those observed in coordination polymers. Solid state cooperativity reflects changes in the energy of the solid lattice due to the elastic forces. Thus, it is not possible to understand it just considering each bonding interaction individually. it is a sum of all the intermolecular interactions and steric contacts in the crystal lattice the responsible of the cooperativity of the spin-transition. For instance, planar or wedge shaped aromatic ligand donor groups presenting intermolecular π-π interactions are particularly efficient to induce cooperativity, not because of the π-π interactions (which are weak), but because they present a large contact surface area between neighboring molecules. On other hand, hydrogen bonds, as other short intermolecular contacts, appear to work equally well to transmit structural changes through the bulk material. This allows changes in molecular shape during spin-crossover to be propagated between molecules more efficiently through these elastic forces.

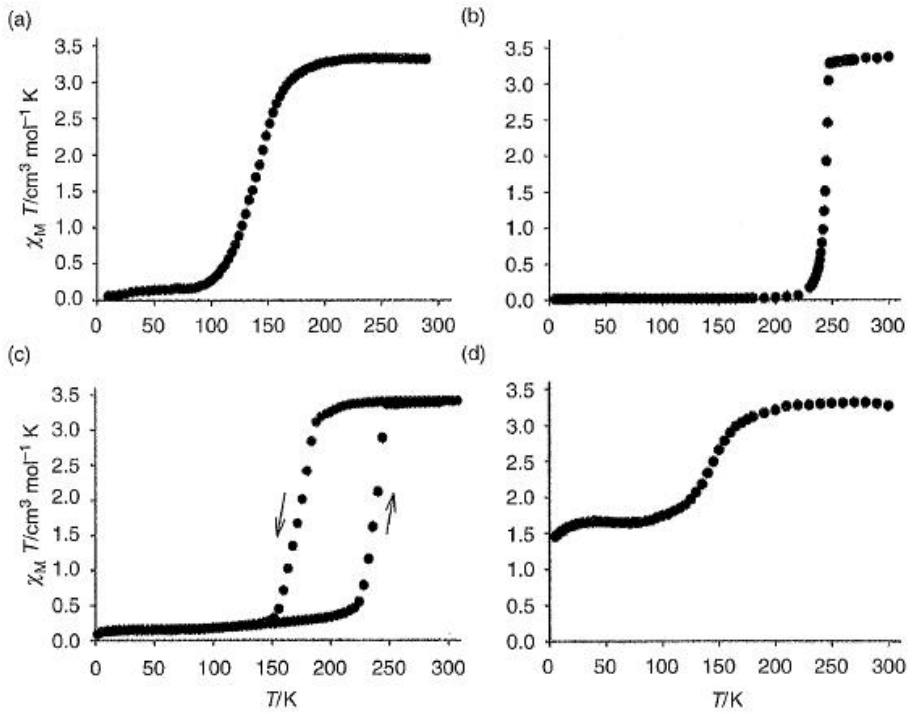

Figure 1. Four representative spin-crossover transitions of molecular Fe^{II} complexes, illustrating the different types of cooperativity that can be observed. (a) Gradual transition. (b) Abrupt transition. (c) With thermal hysteresis. (d) Incomplete transition.[15]

Since these materials can be considered as binary switches, many potential applications based on spin-crossover can be envisaged, such as memories, switching devices, sensors[33] or MRI contrast agents.[34] The main advantages of using such molecule-based materials are that (i) transitions can be obtained even at nanometric scale, (ii) the switching can occur at technologically relevant temperatures, (iii) they involve a change in electronic states, resulting in very fast transitions (at least at the molecular level), and (iv) they can be easily functionalized, providing a wide range of flexibility to design new materials. Cooperative SCO systems can also exhibit a thermal hysteresis, an useful property for memory applications in electronic devices.[13e] For

example, following the pioneering ideas of Olivier Kahn, several multi-nuclear complexes (also called coordination polymers) have been synthesized displaying hysteresis around room temperature.[35] Finally, spin-crossover can be used to modulate other physical phenomena at the molecular level.[36] Some examples are the salts of spin-transition cations and conducting metal/dithiolene anions, where contraction of the cation sub-lattice can cause a change in the conductivity at the spin-transition temperature,[37] or more recently, the switching in the electrical conductivity (with differences in conductivity between 50 and 300%) in polypyrrole conductive films with incorporated SCO compounds.[38] The possible applications of SCO are the causes of the great interest in understanding the solid-state chemistry and physics of spin-state transformations. The final goal could be the design of switchable materials with predictable bulk properties.

2.2. Light-Induced Excited Spin-State Trapping (LIESST) Effect

Light is an effective way to interact with a molecular system. The photoinduction of spin-transition in a Fe^{II} SCO material was first observed by McGarvey *et al* in solution,[39] and then by Decurtins *et al.*[40] in the solid state. These authors demonstrated the possibility of converting a LS state into a metastable HS state by using a green light irradiation. This phenomenon, called Light-Induced Excited Spin-State Trapping (abbreviated as LIESST), was originally observed for Fe^{II} complexes at low temperatures (≤ 50 K). Hauser showed later that red light may switch the system back to the LS state (reverse-LIESST).[41]

Irradiation of the sample at low temperatures (LS state) induces a spin-allowed $^1A_1 \cdot {}^1T_n$ transition (Figure 2). The photoexcited state presents a very short lifetime (a few nanoseconds), inducing fast relaxation of the system back to the $^1A_1$ ground state. A second decay path is possible thanks to the spin orbit coupling, which enables an "intersystem crossing" (ISC) step with $\Delta S = 1$ to the intermediate states $^3T_1$ or $^3T_2$. These spin states can in turn decay via two possible ISC, one implies the relaxation to the $^1A_1$ ground state, the other to the metastable $^5T_2$ state. In this last case, the system

remains trapped in the HS state with a very long lifetime if the thermal energy (K_BT) is lower than the energy barrier between HS and LS potential surfaces (ΔE^0_{HL}).

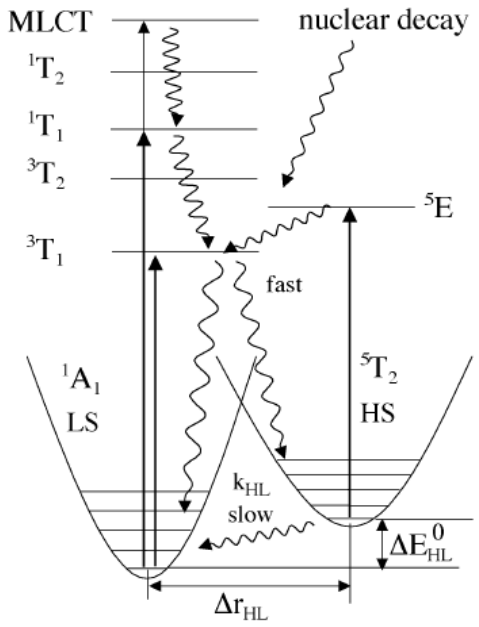

Figure 2. Jablonski diagram of a d^6 spin-crossover system.

The LIESST effect has been observed in a large number of Fe^{II} systems. Figure 3 shows a typical measurement of the T_{LIESST} temperature for a mononuclear SCO complex, $[Fe(1\text{-bpp})_2](BF_4)_2$ (1-bpp = 2,6-bis(pyrazol-1-yl)pyridine).[42] The photomagnetic properties of SCO complexes are typically recorded with a SQUID magnetometer coupled to an optical source through an optical fiber. The magnetic response is expressed as the $\chi_M T$ product (χ_M is the molecular magnetic susceptibility and T the temperature). Light irradiation is applied to the material at 10 K, and results in the population of the paramagnetic HS state through the LIESST phenomenon. This can be observed by a sharp increase of the magnetic signal. The irradiation is only stopped when saturation of the signal is reached, that is when an equilibrium is operating between the population and relaxation of the excited state. The

temperature is then slowly increased at a rate of 0.3 K.min^{-1} and the magnetic behavior recorded. The magnetic response of the light-induced HS state remains almost constant until the energy barrier between HS and LS can be overcome thermally, typically up to 40-50 K. Then, $\chi_M T$ drastically decreases and rapidly recovers its initial value. The minimum of the $\delta\chi_M T/\delta T$ *vs. T* curve determines the T_{LIESST} temperature.

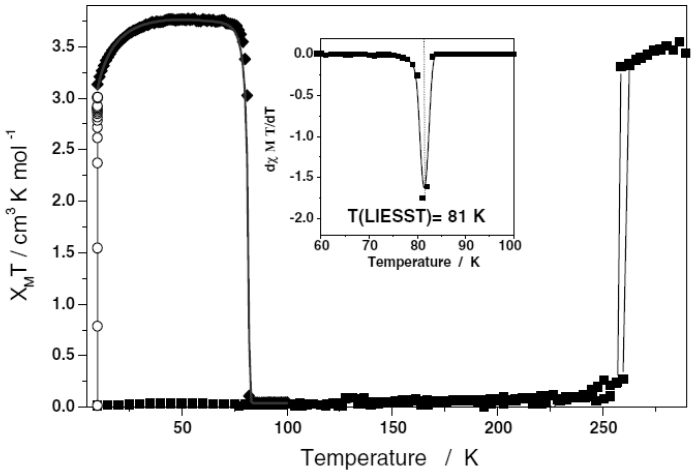

Figure 3. The LIESST behavior of $[Fe(1\text{-}bpp)_2](BF_4)_2$. ■ = Data recorded in the cooling and warming mode without irradiation; ○ = data recorded with irradiation at 10 K; ♦ = T_{LIESST} measurement, data recorded in the warming mode with the laser turned off after irradiation for one hour. The inset graph shows the derivative $\delta\chi_M T/\delta T$ plot as function of the temperature.

In order to compare thermal spin-transition $T_{1/2}$ and T_{LIESST} temperatures, magnetic and photomagnetic studies of many SCO materials have been carried out. It has been observed that these physical properties are related, and the general equation, $T_{LIESST} = T_0 - 0.3\ T_{1/2}$, has been proposed.[43] Experimentally, T_0 is a function of the rigidity of the ligand donor sphere bound to the Fe^{II} center. Thus, complexes of monodentate ligands follow the equation with T_0 = 100 K, while complexes of bidentate ligands show T_0 =

120 K,[43] and tridentate tris-heterocyclic ligands give T_0 = 150 K.[44] Until now, the T_{LIESST} database compiles the properties of more than 80 SCO materials and five parallel T_0 lines have been obtained with respectively, values of 100, 120, 150, 180 and 200 K (Figure 4). A general tendency, noticeable for all the T_0 lines, is a decrease of T_{LIESST} with the increase of $T_{1/2}$, reflecting the fact that the higher the thermal spin-transition occurs, the less photomagnetic information remains.

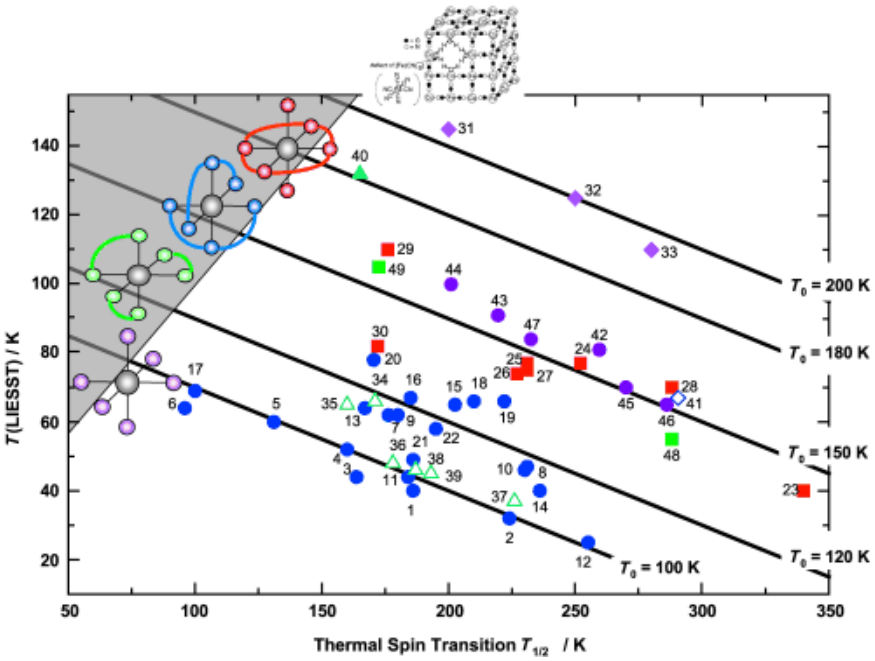

Figure 4. Variation of T_{LIESST} vs. $T_{1/2}$ for spin-crossover compounds. Data taken from reference 45. The region in gray is meaningless as T_{LIESST} temperature has to be inferior or at least equal to $T_{1/2}$ temperature.

Since LIESST compounds are effectively photo-activated molecular switches, there is great interest in finding new compounds with high operating temperatures (that is, with maximum T_{LIESST}). In the last 10 years, the T_{LIESST} record has been progressively shifted from 60 K to 130 K for a pure Fe^{II} SCO material[24,46] and even 150 K in Prussian Blue analogs.[47]

2.3. Spin-Crossover Complexes based on the 2,6-bis(pyrazol-1-yl)pyridine (1-bpp) ligand

Derivatives of 2,6-bis(pyrazol-1-yl)pyridine (1-bpp) and 2,6-bis(pyrazol-3-yl)pyridine (3-bpp) have been thoroughly used for the preparation of SCO Fe^{II} complexes, which can show unusual and useful switching properties. Furthermore, derivatives of these ligands have been used for the preparation of strongly emissive lanthanide complexes.[48] In particular, Fe^{II} complexes of 1-bpp and its derivatives have proven to be interesting SCO compounds as they often exhibit spin transitions near room temperature.[49] Another advantage for this family of complexes is that they often exhibit the LIESST effect described in the previous paragraph.[50] Photoconversions of 80-100% during irradiation are common for samples that exhibit thermal spin-crossover around room temperature. Depending on the $T_{1/2}$ values, the T_{LIESST} are usually between 65 and 100 K.[42,51]

Synthetic routes have been developed for the functionalization of almost every site of the 1-bpp ligand. Substitution at the pyrazole 3-position can modify the steric environment of the coordinated Fe^{II} ion, giving some control over its spin state[52] (Scheme 2, A). Alternatively, substitution at the pyrazole 4-position or pyridine 4-position allows modification of the periphery of the complex, without perturbing the Fe^{II} center (Scheme 2, B and C).[53] As the Fe^{II} complexes of all these derivatives often undergo thermal spin-crossover at accessible temperatures, we can conclude that no other ligand system used in spin-crossover research is so synthetically flexible.

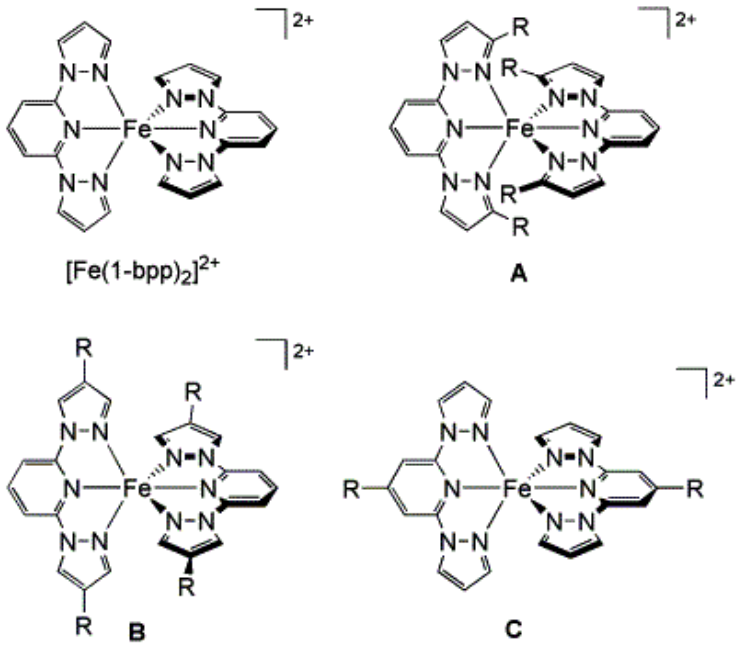

Scheme 2. Structure of $[Fe^{II}(1\text{-bpp})_2]^{2+}$, and the orientation of ligand substituents at the pyrazole 3-position (A), the pyrazole 4-position (B) and the pyridine 4-position (C).[49]

Most syntheses of 4-substituted-1-bpp ligands begin from commercially available 2,6-dihydroxyisonicotinic acid. After a halogenation step, this is readily converted to 2,6-bis(pyrazol-1-yl)pyridine-4-carboxylic acid (bppCOOH, see Scheme 3).[54] From there, a variety of functional group transformations are available. This is the most common route for attaching additional functionality to the 1-bpp pyridine ring. However, the formation of spin-crossover Fe^{II} complexes of bppCOOH had not been reported until this thesis (see Chapter 2).[55]

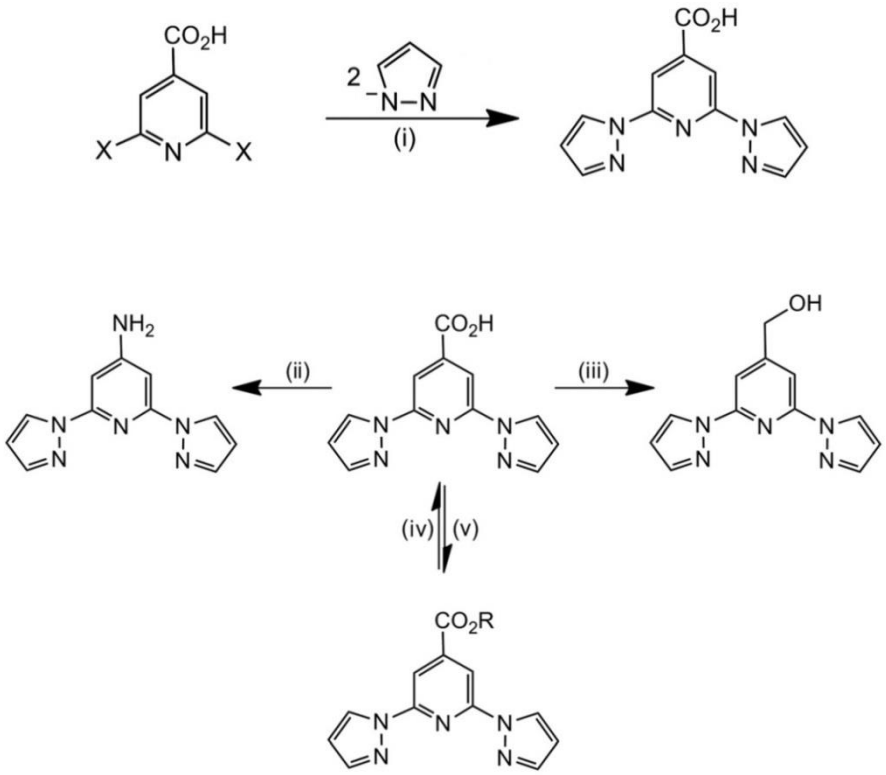

Scheme 3. Synthetic routes to 4-substituted-1-bpp derivatives. Typical reaction conditions: (i) diglyme, 110-130 ºC, 3-5 days. (ii) $COCl_2$, THF; NaN_3, acetone-water; CF_3CO_2H, benzene; K_2CO_3, MeOH. (iii) $NaBH_4$, EtOH. (iv) ROH, H_2SO_4 (cat). (v) LiOH, THF then dil. HCl.

This complex is an interesting precursor to exploit the well-known coordination capability of the carboxylate ligand of bppCOOH to link the Fe^{II} spin-crossover complex to high nuclearity clusters or extended magnetic networks, providing an additional functionality. Furthermore, this carboxylate group could be used for the grafting of the complex on metal oxide surfaces, which is an essential step for the preparation of devices based on the spin-crossover phenomenon.[56] Finally, we have used bppCOOH as precursor of other 1-bpp ligands that have been linked to a polyoxometalate (see

Section 3 and Chapter 3) opening the way to the combination of spin-crossover and the interesting electronic and magnetic properties of the polyoxometalate (single-ion magnet behavior, see Section 4).

3. Functionalized Polyoxometalates

Polyoxometalates (POMs) are discrete anionic metal-oxygen clusters with a great diversity of sizes, nuclearities, and shapes. The metal (M) is an early transition metal in a high oxidation state, usually V(IV,V), Mo(VI), or W(VI). They represent a large family of compounds with numerous applications in catalysis, material science, and medicine.[57] This wide range of uses is mainly due to their redox activity and their acidic properties as well as to the structural and configurational diversity of these anionic oxo-clusters (Figure 5).

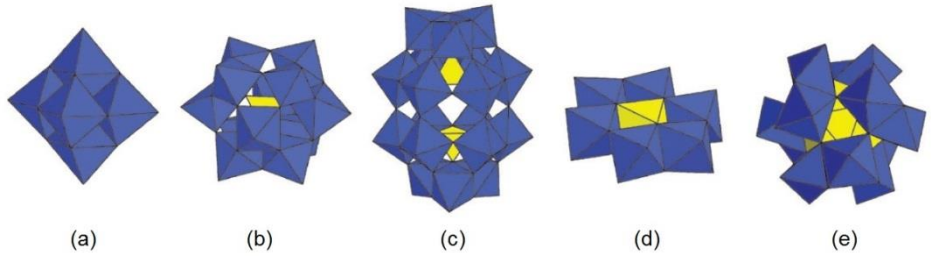

Figure 5. Some basic POM structures in polyhedral representation: (a) Lindqvist $[M_6O_{19}]^{n-}$, (b) Keggin $[\alpha\text{-}XM_{12}O_{40}]^{n-}$, (c) Dawson-Wells $[\alpha\text{-}X_2M_{18}O_{62}]^{n-}$, (d) Anderson $[H_xXM_6O_{24}]^{n-}$, (e) Dexter-Silverton $[XM_{12}O_{42}]^{8-}$. Color code: MO_6 octahedral, blue; XO_n polyhedral, yellow.[58]

Traditionally, these molecular-metal oxides were mostly used in catalysis. Still, owing to their structural and electronic versatilities, they have been used since the 1990's as model systems in molecular magnetism. Furthermore, they have been used as magnetic components of hybrid molecular materials. POMs have been incorporated

into hybrid systems by combining them with various inorganic[59] and organic subunits.[60] As mentioned in Section 1, the combination of inorganic and organic components into a single material is an appealing strategy in order to enhance new properties. Thus, further applications of hybrid POMs have been reached in photocatalysis,[61] biology,[62] and magnetism.[60,63]

Many works have been published concerning coordination complexes or organometallic fragments connected to a POM through a bridging μ-oxo ligand. However, structures of transition metal-substituted POMs are generally unpredictable, since they are generally formed under hydro/solvothermal conditions. A second and more controllable approach is to graft organic ligands onto the POM frameworks, and use them as building blocks to link to transition metal ions via a well-defined coordination mode.[64] This strategy is an effective approach to fabricate POM-functionalized macrostructures with interesting properties. These hybrid systems present the advantages of the covalent interaction, leading to: (i) robust systems, which are not affected by the media (ionic strength, temperature or pH), (ii) rationally designed and predictable structures. Adequate functionalization of POMs allows the preparation of multifunctional hybrid systems that feature the combined intrinsic properties of each component, as well as new properties originating from the combination of these components. Synthetic methodologies to achieve such hybrid POMs via this strategy require an organic molecule that reacts with several POMs and that exhibits free coordination sites in order to link to common transition metal cations. Interestingly, discrete species as well as polymeric compounds can be obtained with this strategy, selectivity being achieved by fine tuning of the experimental conditions. In order to design predictable structures with robust organic functionalization, attention has turned to polyalkoxo functionalization. The tris-alkoxo functionalization has been reported both in organic media[65] and in aqueous conditions.[66] For example, reactions of the tris(hydroxymethyl)methane-derived ligands, $(HOCH_2)_3CR$ (R = NO_2, CH_2OH, and CH_3), with $[N(C_4H_9)_4]_3[H_3V_{10}O_{28}]$ in acetonitrile yield the hybrid structure $[N(C_4H_9)_4]_2[V_6O_{13}\{(OCH_2)_3CR\}_2]$, where opposite

sides of the Lindqvist POM are capped by the organic ligands. Because of its electronic and structural features, this functionalization is reported to be robust, even in presence of water, making it a suitable choice for further chemistry and for various applications under ambient conditions.[67] Similar tris-alkoxo ligands were also successfully incorporated into Dawson-Wells[68] (Figure 6) and Anderson structures.[69]

Figure 6. Representation of tris-alkoxo functionalization of Dawson-Wells structure [R-CONH-C$(CH_2O)_3P_2V_3W_{15}O_{59}]^{6-}$. VO_4 yellow, WO_4 blue, PO_4 green.

More recently, complexation of these functionalized POMs has been investigated. For example, an amino group on a tris-alkoxo capping ligand was reacted with pyridinecarbaldehyde, giving rise to a monodentate or bidentate coordination site linked to the tris-alkoxo-functionalized Anderson POM through an amide function.[69b] However, first attempts to complex metal ions failed and led to fast precipitation of POMs. Indeed, the high-negative charge of POM-based building blocks is responsible for precipitation of the complexes. Thus, the choices of metallic precursors and experimental conditions are crucial in order to achieve complexation on organic-inorganic hybrid POMs. A more promising approach is the introduction of polydentate coordination sites onto the POMs, in order to accommodate a larger range of photoactive transition metal cations. Hasenknopf, Hanan *et al.* prepared tris-alkoxo-pyridyl ligands of various denticity (from pyridyl to bipyridyl(bpy) and terpyridyl (tpy)) and reported their grafting on Anderson Mn-templated molybdates, Lindqvist

vanadates and Dawson-Wells vanadotungstates.[70] Some of these hybrid structures have been resolved by single-crystal X-ray analysis (Figure 7). The authors reported the successful complexation of $\{Ru^{III}Cl_3\}$ and $\{Pd^{II}Cl\}^+$ moieties on a tpy-functionalized POM and the isolation of the pure hybrids. In particular, the formation of $[N(C_4H_9)_4]_5H[P_2W_{15}V_3O_{62}(C_{20}H_{17}N_4O)RuCl_3]$ was characterized by ^1H NMR, high-resolution ESI-mass spectrometry, IR and UV-Vis absorption spectroscopies.

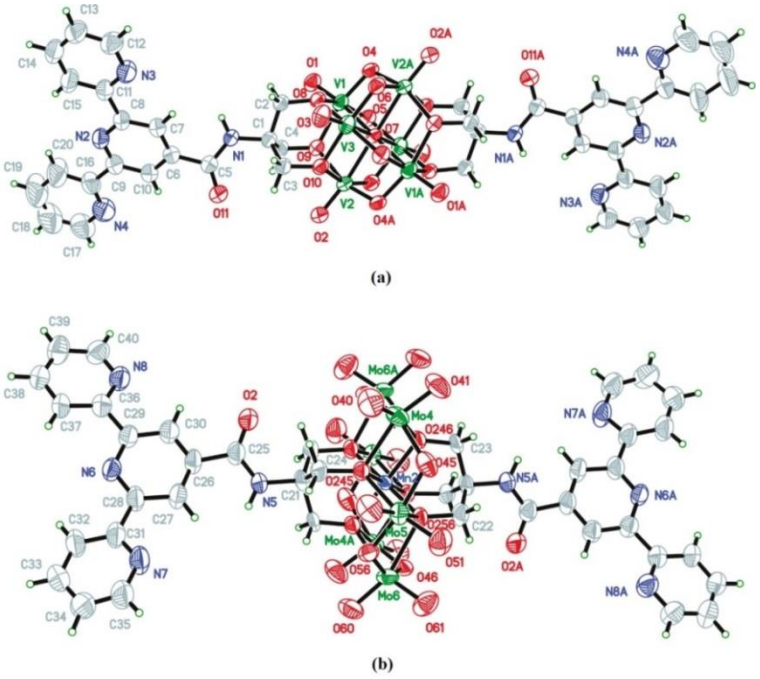

Figure 7. ORTEP diagram of (a) Lindqvist $(C_{16}H_{36}N)_2[V_6O_{19}(C_{20}H_{17}N_4O)_2]$ and (b) Anderson $(C_{16}H_{36}N)_3[MnMo_6O_{24}(C_{20}H_{17}N_4O)_2]$ (thermal ellipsoids are drawn at 50% probability). Counterions and solvents were omitted for clarity.[70]

An alternative to the polyalkoxo functionalization can be provided by the replacement of terminal oxo ligand O^{2-} by imido ligands RN^{2-}, where R groups can be ligands for transition metal ions or preformed transition metal complexes. This strategy allowed the preparation of polymeric or discrete hybrid POMs. In particular,

Peng *et al.* reported the formation of a discrete and polymeric hybrid POMs by coordination of the tpy-functionalized Lindqvist POMs with Fe^{II} ion (Figure 8).[71] The complexation of the functionalized POM with one tpy ligand was quantitative at room temperature in both CH_3CN and DMSO, as confirmed by ^1H NMR and UV-Vis spectroscopies, but the $Fe^{II}(tpy)_2$-POM coordination polymers turned out to precipitate upon formation.

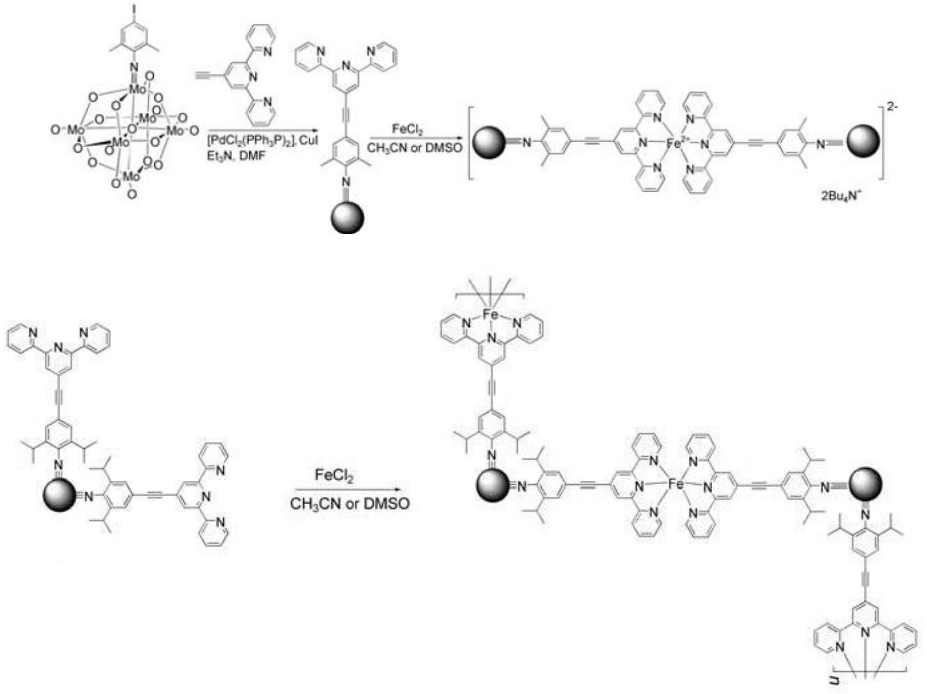

Figure 8. Synthesis of the polynuclear (top) and polymeric (bottom) hybrid POMs by ligand coordination to Fe^{II}.

Very recently the interest for magnetic POMs has moved towards the design of single-molecule magnets (SMMs, see Section 4) and their use as molecular spin-qubits in nanospintronic devices.[72] In this thesis we have tried to make use of the synthetic approaches for development of organic-inorganic hybrid POMs reported in this section to prepare new hybrid POMs that could combine the magnetic properties of the POM

(SMM behavior) with an additional property such as spin-crossover, by functionalization with a 1-bpp ligand derivative and metal ion complexation (see Chapter 3).

4. Single-Molecule Magnets (SMMs)

The area of molecular nanomagnets received its first major impetus in the 90's. Studies of zero-dimensional molecular systems had been pursued, with an academic competition to find the molecule with the highest ground-state spin. This situation changed drastically in 1991 with the discovery that a family of dodecametallic manganese cages {Mn_{12}}, with a spin ground state of S = 10 exhibited magnetic hysteresis of molecular origin at low temperature (Figure 9).[73] This was a behavior only previously observed in bulk ferromagnets or in magnetic nanoparticles. The key physical property of single-molecule magnets (SMMs) is slowing of magnetization (M) relaxation at low temperature giving rise to a blocking of the magnetization below a given temperature, which provokes the hysteretic behavior. This hysteresis is shown for a single crystal of Mn_{12} (Figure 10). When the relaxation is slow, then M will have some remnant value at zero field. Applying the field in the opposite direction will eventually force M back to nil and then ultimately saturate M in the opposite sense. Removing the field leaves an equal but opposite remnant magnetization. This gives bistability in zero applied field as M can take one of two values. The molecule 'remembers' the sense of the field that was applied to it. This immediately led to proposals that such molecules could be used to store information.

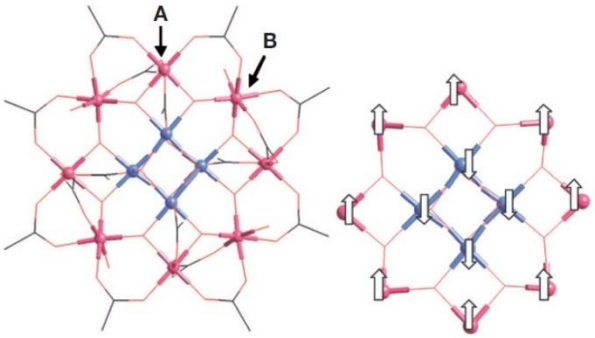

(a) (b)

Figure 9. (a) Crystal structure of $[Mn_{12}O_{12}(O_2CMe)_{16}(H_2O)_4]$, with Mn^{III} and Mn^{IV} ions in pink and blue, respectively, and highlighting the two structurally distinct Mn^{III} ions (A and B). (b) Representation of the ground-state spin structure, leading to an S = 10 state.[74]

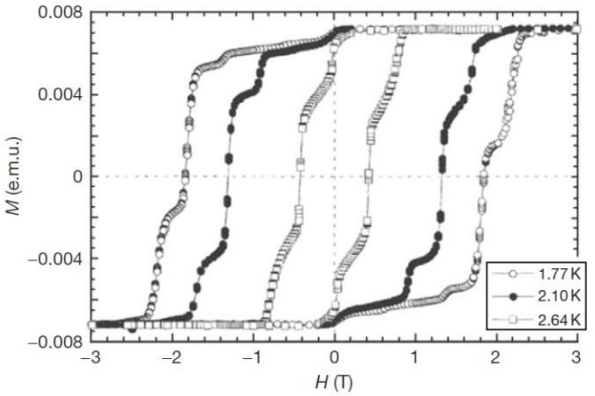

Figure 10. $M(H)$ curves, showing magnetic hysteresis, for a single crystal of $[Mn_{12}O_{12}(O_2CMe)_{16}(H_2O)_4]\cdot 2MeCO_2H\cdot 4H_2O$ with the applied field along the easy axis of magnetization.[75]

The slow magnetic relaxation of SMMs originates from uniaxial magnetic anisotropy (D) and a high-spin (HS) ground state (S_T). This relaxation is observed below a certain 'blocking' temperature (T_B). Depending on the temperature, this relaxation obeys two processes. At high temperatures, the relaxation time, τ, is thermally activated and the theoretical energy barrier Δ is equal to $\Delta = |D|S_T^2$ for an integer spin,

and $\Delta = |D|(S_T^2 - {}^1/_4)$ for a half-integer spin. At very low temperatures, quantum tunnelling of the magnetization (QTM) governed by the transverse anisotropy (E), becomes the fastest pathway of relaxation. Experimentally, a crossover occurs between these two regimes called thermally-assisted QTM. In this intermediate range of temperature, the thermal energy barrier is "short-cut" by quantum tunnelling, and an effective barrier, Δ_{eff}, smaller than Δ, is found. The steps in the *M* vs *H* curves observed in Figure 10 are due to this tunneling. In many SMM systems, this regime is the only one seen experimentally before τ becomes temperature independent.[76] This Δ_{eff} can be derived from direct measurement of relaxation, but more often is derived from alternating current (AC) susceptibility measurements where a small oscillating external magnetic field is applied at a range of frequencies and temperatures. The frequency (ω) at which a maximum in the out-of-phase component of the susceptibility is observed at a specific temperature is related to the relaxation time constant (τ) by $\omega\tau = 1$. By repeating this measurement over a range of temperatures (Figure 11), the thermal energy barrier to relaxation, Δ_{eff}, can be determined from the Arrhenius equation $\tau = \tau_0 \exp(\Delta_{eff}/T)$. Hence, fitting to a plot of $\ln(\tau)$ versus $1/T$ gives Δ_{eff} as the slope of the line. For initial measurements on $\{Mn_{12}\}$, $\Delta_{eff} = 43$ cm^{-1} with $\tau_0 = 2.1\text{x}10^{-7}$ s.[77] This corresponds to relaxation times of tens of years below 2 K.

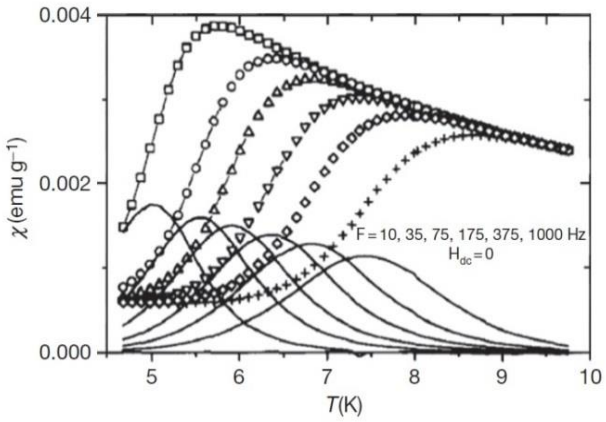

Figure 11. In-phase and out-of-phase (solid lines) components of the AC magnetic susceptibility of $[Mn_{12}O_{12}(O_2CMe)_{16}(H_2O)_4]\cdot 2MeCO_2H\cdot 4H_2O$.[78]

The first SMMs reported contained Mn^{III} ions as $\{Mn_{12}\}$. The second important family are the $\{Mn_6\}$ cages reported by Milios *et al.*[79] These cages contain two oxide bridges, and are best described as two $\{Mn^{III}_3O\}$ triangles linked via oxygen atoms derived from the derivatized oxime ligands. One of these $\{Mn_6\}$ cages has the highest energy barrier (86 K) for loss of magnetization of any 3*d* polymetallic complex. The largest known SMM has the formula $[Mn_{84}O_{72}(O_2CMe)_{78}(OMe)_{24}(OH)_6(MeOH)_{12}(H_2O)_{42}]$.[80] Several Fe^{III}-based SMMs have also been reported. The most important is the $[Fe_8O_2(OH)_{12}(tacn)_6]Br_8$, which has an S = 10 ground state with D = -0.20 cm^{-1}, and a barrier to relaxation of magnetization with $\Delta_{eff} \approx 23$ K,[81] and a family of tetranuclear cages of formula $[Fe_4(OR)_6L_3]$ (R = Me, Et; L = β-diketonate). These tetranuclear Fe^{III} SMMs are important because they can easily modified simply by changing the alkoxide or β-diketonate present in the reaction. This has led to the first reports where the properties of an SMM are retained when the SMM is bound to a surface.[82] Other SMMs containing polynuclear complexes of 3*d* ions are Ni^{II}-based SMMs, including a $\{Ni_{12}\}$ ring[83] and several $\{Ni_4\}$ heterocubanes,[84] or Co^{II} SMMs.[85]

In 2003, a new class of SMMs was reported which contain only a single paramagnetic metal ion.[86] The first example was reported by Ishikawa in the lanthanoid complexes of general formula $[LnPc]^-$, with phthalocyanines as ligands. These magnetic molecules, also known as single-ion magnets (SIMs), represent the limit of miniaturization of a nanomagnet, as they are based on a magnetically anisotropic single metal ion. The second family of reported SIMs was the $[Ln(W_5O_{18})_2]^{9-}$ (Ln = Tb, Dy, Ho and Er) POMs reported by our group.[87] The first SIM containing a 3*d* transition-metal center was reported by Long *et al.* in 2010. The system consisted of a Fe^{II} complex displaying a trigonal-pyramidal structure (Figure 12a) that retained the magnetization when an external direct-current (dc) field was applied.[88] After this discovery, the family of 3*d* transition-metal complexes with a SIM behavior has quickly grown with the addition of new Fe^{II} and Co^{II} complexes with a variety of coordination geometries.[89] Since then, SIM behavior has been extended to other *d* metals such as

Mn^{III}. Thus, SIM behavior of $Ph_4P[Mn(opbaCl_2)(py)_2]$ ($H_4opbaCl_2$ = *N,N'*-3,4-dichloro-*o*-phenylenebis(oxamic acid); py = pyridine),[90] a $[Mn^{III}Co^{III}]$ complex,[91] and $[Mn\{(OPPh_2)_2N\}_3]$[92] (Figure 12b) was reported in 2013. Very recently, a fourth example of Mn^{III} complex with field-induced slow relaxation of *M* has been found in compound $Na_5[Mn(L\text{-tart})_2]\cdot 12H_2O$ (L-tart = L-tartrate).[93]

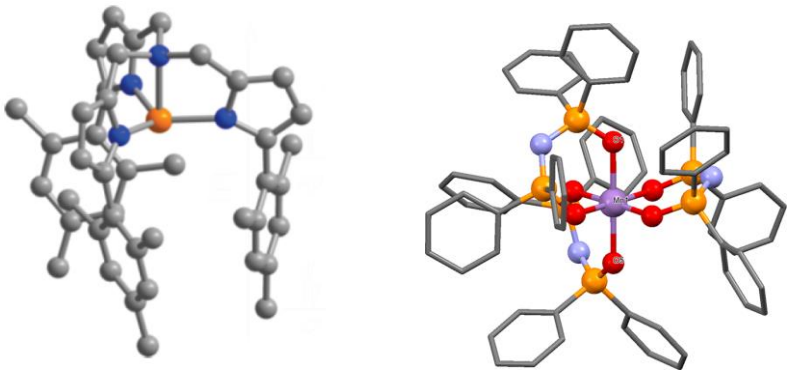

(a) (b)

Figure 12. (a) Crystal structure of $K[(tpa^{Mes})Fe]$. Color code: Fe = orange, C = gray, N = blue. (b) Crystal structure of the mononuclear complex $[Mn\{(OPPh_2)_2N\}_3]$. Color code: Mn = purple, C = gray, N = blue, O = red, P = orange.

However, to our knowledge SIM behavior in POMs has only been found in POM containing lanthanoids. In this thesis, we report the SIM behavior in a Mn^{III} Anderson POM functionalized with 1-bpp ligand (see Chapter 3).

5. Multifunctional Magnetic Networks

The search for new molecule-based magnets was a very active area in the beginning of molecular magnetism in the 80's. In the last years, the interest has been focused in the preparation of multifunctional magnetic networks since these materials provide unique opportunities to design, from a wise selection of the molecular building blocks, crystal structures exhibiting cooperative magnetism in combination with a

second property of interest. A rational approach to design multifunctional materials consists of creating hybrid solids constituted by two networks formed by two molecular fragments, where each network furnishes distinct physical properties. A coexistence of the two physical properties is anticipated if the two networks are quasi-independent, while the interaction among them could lead to the onset of new properties. Recent activity in this field has been focused in the design of materials for which physical properties can be tuned by applying an external stimulus in view of their potential applications as chemical switches, memories or molecular sensors.[94] Most of the responsive magnetic materials obtained so far are one-network materials in which the magnetic order is tuned by light or pressure.[95] Two-network materials, formed by a magnetic lattice and a switchable molecular component, are promising candidates for the preparation of multifunctional responsive materials. The preparation of new hybrid magnets with inserted spin-crossover complexes is ascribed in this line of research.

5.1. Oxalate-Based Hybrid Magnets with Inserted Spin-Crossover Complexes

Bimetallic oxalate-bridged compounds have been thoroughly used as magnetic lattice of multifunctional magnetic materials. They are formed by polymeric anionic networks $[M^{II}M^{III}(ox)_3]^-$,with M^{II} (Mn, Fe, Ni, Cu, Cr, Zn) and M^{III} (Cr, Fe, Ru, Mn) linked through bis-bidentate bridging oxalate ligands. The structure of the bimetallic compounds of formula $(XR_4)[M^{II}M^{III}(ox)_3]$ is composed by 2D or 3D anionic networks (Figure 13), and an inserted cation (XR_4, X = N, P; R = Ph, nPr, nBu…), which template the network formation. In most cases, they present a polymeric 2D honeycomb-like anionic network in which the adjacent Mn^{II} and Cr^{III} ions present the opposite chirality. Notice that, depending on the nature of the templating cation (size, shape and charge), other magnetic networks, different from the 2D honeycomb-like network, can also be obtained with dimensionalities ranging from 0D to 3D. The most extensive one is represented by the family of 3D chiral structures in which the chirality of a templating

cation of the type $[Z^{II}(bpy)_3]^{2+}$ (Z^{II} = Fe, Co, Ni, Ru) induces the building blocks to adopt a homochiral configuration.

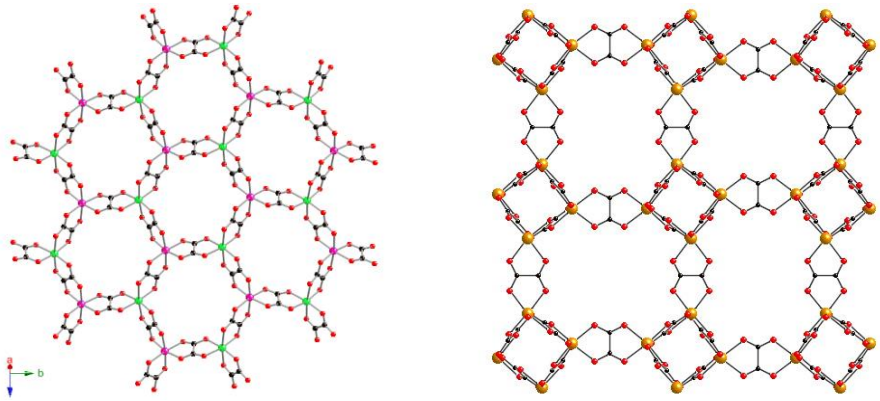

(a) (b)

Figure 13. 2D (a) and 3D (b) extended anionic networks based on the oxalate ligand.

The right choice of the templating cations allows the introduction of new properties to the hybrid system. Therefore, cooperative magnetic properties (ferro-, ferri- or antiferromagnetism) from the oxalate-based network can coexist with electronic properties from the molecular cations. The use of different charge-compensating molecular cations has provided many examples of multifunctional materials[96] combining the long-range magnetic ordering of the oxalate network with paramagnetism,[97] photochromism,[98] electrical conductivity,[99] proton conductivity,[100] ferroelectricity,[101] chirality[102] or single-molecule magnet behavior from the cation.[103]

In this context, spin crossover cations are particularly suitable to prepare multifunctional magnetic materials since they represent one of the best examples of molecular bistability. This may open a way to design switching magnets in which the magnetic ordering of the oxalate network could be tuned taking advantage of the possibility of inducing the spin-crossover phenomenon by applying an external stimulus such as light or pressure. Multifunctional materials exhibiting both spin-crossover and magnetic interaction have been obtained by combining a spin-crossover

cation with the oxalate-based anionic framework. Fe^{II} spin-crossover complexes have led to the growth of 3D bimetallic oxalate-based compounds, which present magnetic properties very sensitive to the changes of size of the inserted cation, although the inserted Fe^{II} complexes do not present clear spin-crossover behavior.[104] Fe^{III} spin crossover cationic complexes based on the Schiff-base ligand $H_2(sal_2\text{-trien})$ (= *N*,*N*'-disalicylidenetriethylene-tetramine, see Scheme 4) and derivatives have been used for the growth of 2D and 3D bimetallic oxalate-based magnets in the search of responsive magnetic materials.[105] They have led to 2D or chiral and achiral 3D networks depending on the ligand derivative and the synthesis conditions. Interestingly, subtle chemical changes in the X-sal_2-trien substituent have led to 2D compounds (X = H, 3-CH_3O-, 3-Br-, 4-Br- and 3Cl-), chiral 3D compounds (X = 5-Cl and 5-Br) or achiral 3D compounds containing Mn^{II} and Cr^{III} centers of both chiralities (X = 5-CH_3O, 5-CF_3O). The most interesting results were obtained for the family of compounds $[Fe^{III}(sal_2\text{-trien})][Mn^{II}Cr^{III}(ox)_3]\cdot G$ (G= CH_2Cl_2, $CHBr_3$, CH_2Br_2 and $CHCl_3$) formed by alternating layers of a 2D oxalate-based network, $[Fe^{III}(sal_2\text{-trien})]^+$ complexes and solvent molecules (Figure 14).

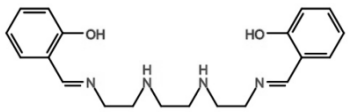

Scheme 4. $H_2(sal_2\text{-trien})$.

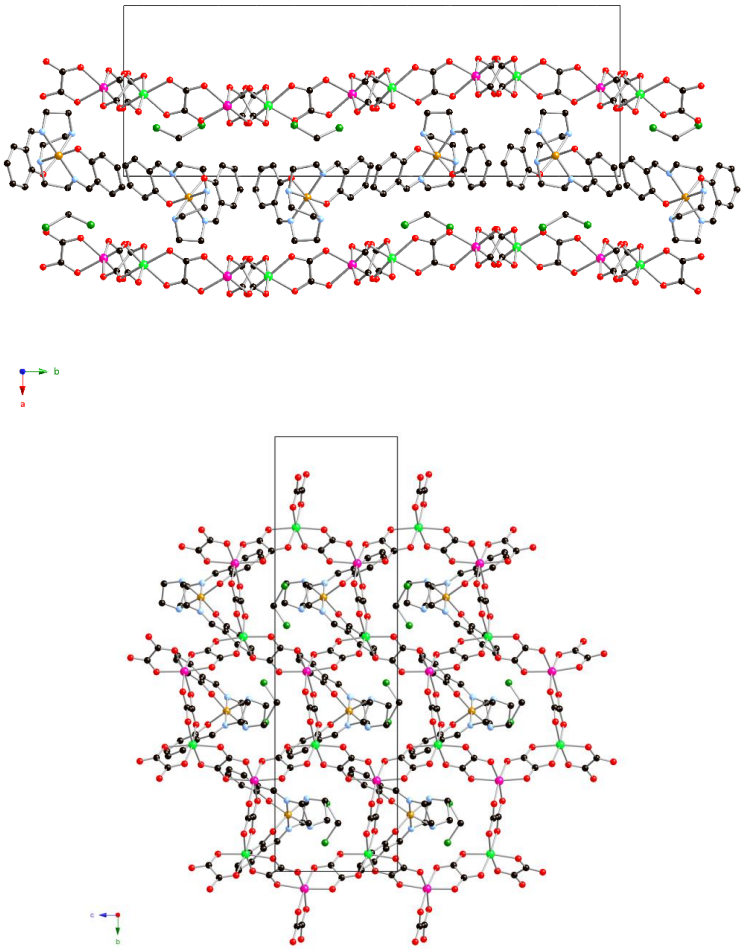

Figure 14. Structure of $[Fe^{III}(sal_2\text{-trien})][Mn^{II}Cr^{III}(ox)_3]\cdot CH_2Cl_2$. Projection in the *ab* plane (top). Projection in the *bc* plane (bottom). Color code: Fe = orange, Cr = green, Mn = pink, C = black, N = blue, O = red, Cl = dark green.[105e]

The magnetic properties of these compounds indicate the coexistence of a partial or complete spin-crossover and a long-range ferromagnetic ordering of the oxalate networks. In the compound of formula $[Fe^{III}(sal_2\text{-trien})][Mn^{II}Cr^{III}(ox)_3]\cdot CH_2Cl_2$, there is a complete spin-crossover between 150 and 350 K and a long-range ordering of the network at 5.6 K.[105b] Furthermore, this family of compounds shows that the confinement of spin crossover cations into extended networks induces an unexpected

property, LIESST effect, something very unusual for Fe^{III} spin-crossover complexes. For the compound $[Fe^{III}(sal_2\text{-trien})][Mn^{II}Cr^{III}(ox)_3]\cdot CH_2Cl_2$, the photomagnetic characterization shows the presence of a LIESST effect below 42 K (Figure 15).[105e] By changing CH_2Cl_2 for other halogenated solvents in the synthesis ($CHBr_3$, CH_2Br_2 and $CHCl_3$), it is possible to tune the temperature of the thermal and photoinduced spin-crossover. The replacement of CH_2Cl_2 by bulkier solvents in the structure increases interlamellar distance between the layers of the oxalate network and reduces the chemical pressure on the inserted spin-crossover compound. This induces a shift of $T_{1/2}$ to lower temperatures and therefore a shift of T_{LIESST} to larger values.[105h] Unfortunately, the photo-induced spin conversion of the inserted Fe^{III} complex has a negligible influence on the magnetic behavior of the 2D oxalate network as the magnetic ordering of this type of networks is not sensitive to the change in size of the inserted cation.

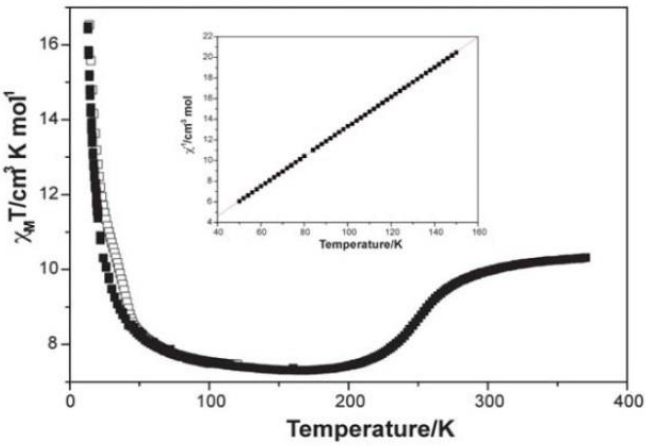

Figure 15. Magnetic and Photo-Magnetic behavior for $[Fe^{III}(sal_2\text{-trien})][Mn^{II}Cr^{III}(ox)_3]\cdot CH_2Cl_2$. ■ Magnetic behavior measured in dark. □ Photo-Magnetic behavior measured after irradiation by 647 nm wavelength laser. Inserted graph: Curie-Weiss law between 50 K and 150 K.

5.2. Anilate-Based Magnets

Recently, replacement of the oxalate ligand by larger 2,5-dihydroxy-1,4-benzoquinone dianion derivatives of formula $C_6O_4X_2^{2-}$ (anilates, X_2An^{2-}; X = Cl, Br or I, see Scheme 5) in bimetallic networks has been explored. These ligands, which show coordination modes similar to the oxalate ligand, present additional advantages: (i) they are easy to modify or functionalize by simply changing the X group; (ii) they present higher ordering temperatures; (iii) their bigger size may enable the introduction of a larger library of cations in order to prepare multifunctional molecular materials.

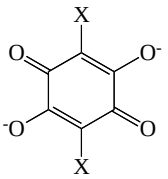

X = Cl, Br, I (X_2An^{2-}), or H ($dhbq^{2-}$).

Scheme 5. 2,5-dihydroxy-1,4-benzoquinone dianion derivatives.

The coordination modes and the ability to act as bridging ligands of these anilate derivatives to afford many different coordination frameworks have been summarized by Kitagawa and Kawata.[106] Thus, the ligand $dhbq^{2-}$ and its derivatives, mainly with X = Cl, have been extensively studied, alone or in combination with other ligands (mainly N-donor ones), to prepare several compounds with different dimensionalities and structures, spanning from isolated monomers, dimers and oligomers to extended one-dimensional (1D), 2D and 3D structures. Some interesting coordination polymers based on the anilate bridging ligand are the 2D honeycomb layers formed with $dhbq^{2-}$ and its Cl derivative (chloranilate, Cl_2An^{2-}).[107] In these compounds, the structure is similar to that shown by the oxalate-based honeycomb layers although all are homometallic (*i.e.*, they contain two M^{II} or two M^{III} ions instead of one M^{II} and one M^{III} ions). The examples of the $[M^{II}_2L_3]^{2-}$ series are: $[M^{II}_2(dhbq)_3]^{2-}$ (M^{II} = Mn and Cd) and $[M^{II}_2(Cl_2An)_3]^{2-}$ (M^{II} = Cu, Co, Cd and Zn).[107a,b] With two M^{III} ions the layers are neutral

and the reported examples to date are $[M^{III}_2(dhbq)_3]\cdot 24H_2O$ (M^{III} = Y, La, Ce, Gd, Yb and Lu), $[M^{III}_2(Cl_2An)_3]\cdot 12H_2O$ (M^{III} = Sc, Y, La, Pr, Nd, Gd, Tb, Yb, Lu, see Figure 16a) and $[Y^{III}_2(Br_2An)_3]\cdot 12H_2O$.[107c,d,e] An additional interest of the $dhbq^{2-}$ and X_2An^{2-} ligands is related to the formation of a 3D structure with a (10,3)-*a* topology, similar to the one observed with oxalate.[108] This 3D structure with a (10,3)-*a* topology has been reported for $[NBu_4]_2[M^{II}_2(dhbq)_3]$ (M^{II} = Mn, Fe, Ni, Co, Zn and Cd) and $[NBu_4]_2[Mn^{II}_2(Cl_2An)_3]$ (Figure 16b).[109] Albeit, the magnetic properties of the only two magnetically characterized 2D derivatives ($[M^{II}_2(Cl_2An)_3]^{2-}$ with M^{II} = Mn and Cu) lack of interest since they show weak antiferromagnetic M^{II}-M^{II} interactions mediated by the Cl_2An^{2-} bridges.[107b,f]

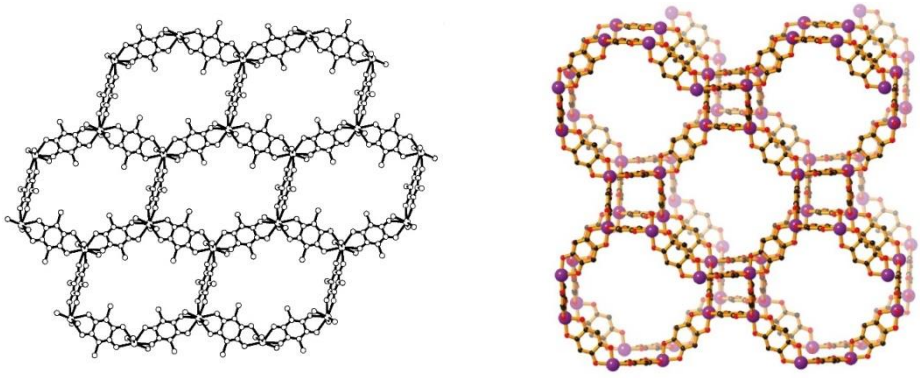

(a) (b)

Figure 16. 2D (a) and 3D (b) extended networks based on the anilate ligand.

Recently, our group obtained the first 2D heterometallic lattices based on the anilate ligand with a honeycomb structure in the family of layered ferrimagnets $A[M^{II}M^{III}(X_2An)_3]\cdot G$ (A = $[(H_3O)(phz)_3]^+$ (phz = phenazine) or NBu_4^+; M^{II} = Mn, Fe, Co, etc.; M^{III} = Cr, Fe; X = H, Cl, Br, I; G = water or acetone) (Figure 17).[110] In this family, it has been observed that the anilate derivatives offer the possibility to tune the ordering temperatures by simply changing the substituents in the anilate bridging ligand. In the $Mn^{II}Cr^{III}$ derivatives, T_c is ranging from 5.5 to 6.3, 8.2 and 11.0 K (for X = Cl, Br, I and H, respectively, see Figure 18). Furthermore, depending on the cation and X substituent,

the 2D bimetallic ferrimagnets can be porous and/or chiral. Indeed, the chiral compound $[(H_3O)(phz)_3][Mn^{II}Cr^{III}(Cl_2An)_3(H_2O)]$ and the compounds $[(H_3O)(phz)_3][Mn^{II}M^{III}(Br_2An)_3]\cdot G$ (M^{III} = Cr and Fe) present an eclipsed disposition of the layers, generating hexagonal channels that may be filled with different guest molecules, opening the way to the synthesis of new porous magnets.

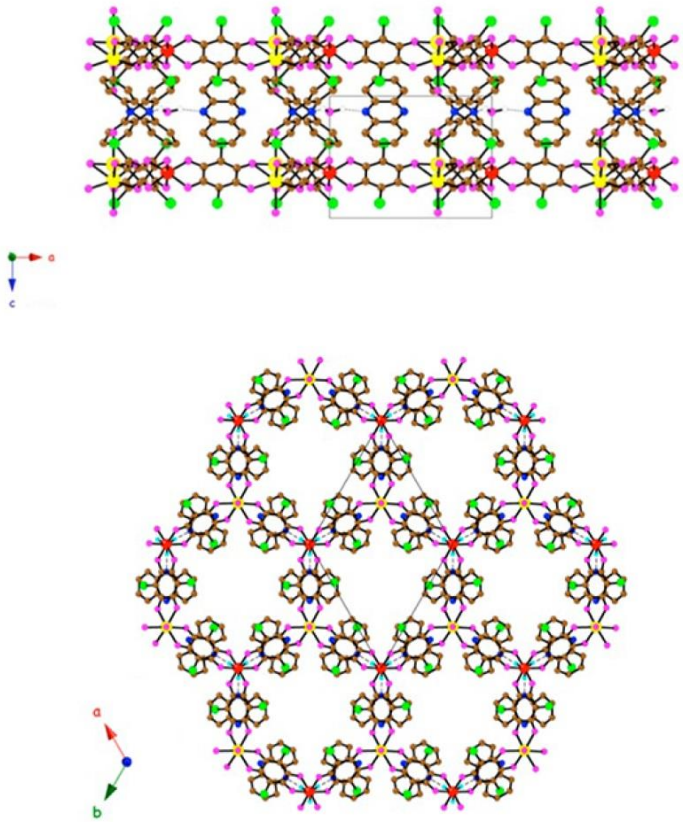

Figure 17. Structure of $[(H_3O)(phz)_3][Mn^{II}Cr^{III}(Cl_2An)_3(H_2O)]$. Projection in the *ac* plane (top). Projection in the *ab* plane (bottom). Color code: Cr = red, Mn = yellow, C = brown, N = blue, O = pink, Cl = green, H = cyan.

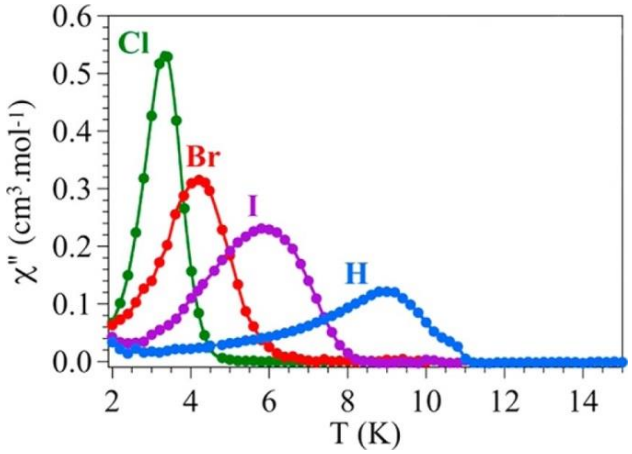

Figure 18. Thermal variation of the out-of-phase (χ_m'') AC susceptibility at 1 Hz of the series of $[NBu_4][Mn^{II}Cr^{III}(X_2An)_3]$ (X = Cl, Br, I and H).

In this thesis we have explored the insertion of spin-crossover cations in anilate-based bimetallic lattices to prepare a new family of multifunctional magnetic materials as it was already done in the oxalate family (see Chapter 4).[111] On the other hand, the bigger size of the anilate ligand compared to the oxalate one leads to hexagonal cavities that are twice larger than those of the oxalate-based layers. This bigger size represents an interesting feature of the anilate-based layers, since it will allow the inclusion of the spin-crossover cation within these cavities (see Chapter 5). Finally, the weak interaction between the layers of these 2D coordination polymers (CPs) has allowed the opportunity to process them as 2D nanosheets, prepared by exfoliation processes. In the following section, exfoliation of 2D layered materials is introduced.

6. Exfoliation of 2D Layered Materials

The research on layered materials has evolved from the elucidation of their laminar structure and the study of the intercalated molecules to the first attempts to exfoliate or delaminate them into individual, atomically thin nanosheets. This culminated with the discovery of graphene,[4a,112] which resulted in a new explosion of

interest in 2D materials. Similar processes have been demonstrated for different types of materials, including graphene, MoS_2 and other related structures, layered oxides, and clays. The diverse range of properties of known layered materials means that their exfoliated counterparts will be equally diverse, leading to applications in electronics, photonics, energy storage, structural composites, drug delivery, hydrogen catalysts, barrier layers, and coatings. By stacking layers of different materials including graphene, it will also be possible to produce new hybrid devices with unprecedented functionalities. As exfoliation methods increase in their sophistication and effectiveness, 2D layered materials will become central to nanotechnology in the 21st century. This should be accompanied by an expansion of the range of layered materials that can be exfoliated.[4b]

Layered crystals present strong chemical bonds in-plane but display weak out-of-plane bonding due to van der Waals interactions. This allows them to be exfoliated into individual nanosheets, which can be micrometers wide but less than a nanometer thick. Although in the ideal case such nanosheets consist of single monolayers, they are often manifested as incompletely exfoliated flakes comprising a small number (<10) of stacked monolayers. There are many types of layered materials, which can be grouped into diverse families. The simplest are the atomically thin, hexagonal sheets of graphene,[112] and hexagonal boron nitride (h-BN),[113] then transition metal dichalcogenides (TMDs) (such a MoS_2 and WSe_2),[114] metal trichalcogenides, metal halides (such as PbI_2 and $MgBr_2$),[115] layered metal oxides (such as MnO_2, MoO_3 and $LaNb_2O_7$) and layered double hydroxides (LDHs) (such as $Mg_6Al_2(OH)_{16}$),[116] and layered silicates (or clays)[117]. More recently, the exfoliation of coordination polymers (CPs) has gained attention. The versatility of CPs and the ability to tune their properties makes them attractive additions to the range of 2D materials.[118] Furthermore, the nanostructural control of CPs has become increasingly interesting due to their unique size- and shape-dependent properties, which differ from those of bulk crystals.

A strategy for exfoliation is to expose the layered material to ultrasonic waves in a solvent. Such waves generate cavitation bubbles that collapse into high-energy jets, breaking up the layered crystallites and producing exfoliated nanosheets (Figure 19).[4b] Modeling has shown that if the surface energy of the solvent is similar to that of the layered material, the energy difference between the exfoliated and reaggregated states will be very small, removing the driving force for reaggregation. In "good" solvents (those with appropriate surface energy), the exfoliated nanosheets are stabilized against reaggregation.

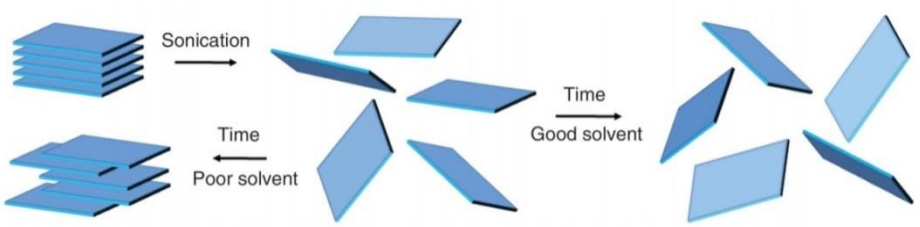

Figure 19. Sonication-assisted liquid exfoliation.

These top-down delamination processes are an effective approach to fabrication of 2D CPs. In 2010, a bidimensional mixed-copper CP, $[Cu_2Br(isonicotinato)_2]_n$, was delaminated by ultrasonication in solution by Zamora *et al*.[119] Single sheets of the CP were characterized by Atomic Force Microscopy (AFM). In 2011, Xu *et al.* reported the exfoliation in acetone of the layered MOF $[Zn(TPA)(H_2O)DMF]_n$ (TPA = terephthalic acid) (Figure 20).[120] More recently, Cheetam *et al.* reported the exfoliation of non-porous hybrid framework materials based on the 2,2-dimethylsuccinate (DMS) ligand, characterized by Transmission Electron Microscopy (TEM) and AFM.[121] The fully exfoliated nanosheets characterized under AFM display a thickness of 1 nm, which corresponds to the thickness of one elementary host layer.

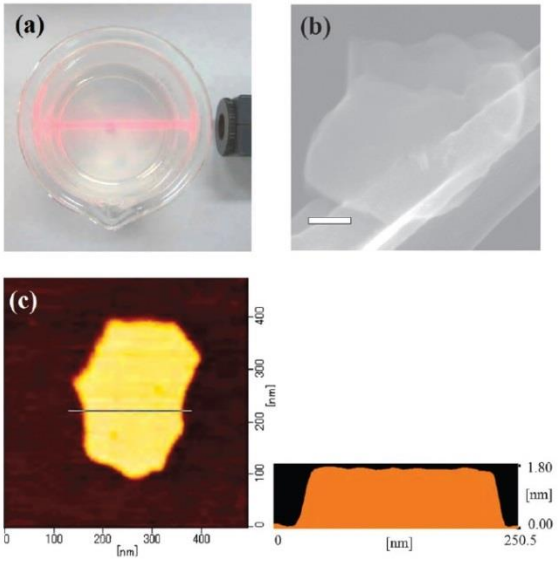

Figure 20. (a) Photograph of the colloidal suspension in acetone of the MOF $[Zn(TPA)(H_2O)DMF]_n$ nanosheets with demonstration of the Tyndall effect. (b) The SEM morphology of the MOF nanosheets on a copper grid. Scale bar: 100 nm. (c) AFM topography image and height profile of a MOF nanosheet deposited on a mica substrate, with thickness of ~1.5 nm and lateral dimensions of 200-300 nm.

Ultrasonication-assisted solvent exfoliation has a number of limitations in its current form, as the monolayer yield is far too low for many applications. To date, only a few examples of soft-delamination process (without ultrasonication) have been reported, such as the fully delamination of the CP $[Cu(\mu\text{-}pym_2S_2)(\mu\text{-}Cl)]_n \cdot nY$, by immersion of the crystals in water.[122] As such, it is necessary to develop methods that do not rely on ultrasonication, in order to improve the quality of the layer and its thickness. This can be achieved by solvent-free exfoliation processes. To date, the micromechanical exfoliation (the so-called Scotch tape method) is the most efficient way to produce clean, highly crystalline and atomically thin nanosheets of layered material, which one suitable for investigation of their intrinsic thickness-dependent properties. Despite the simplicity of this method, it can provide extremely high quality samples. In a typical mechanical exfoliation process, the 2D material is first peeled off

from its bulk crystals by using adhesive Scotch tape (Figure 21). These freshly cleaved thin crystals on Scotch tape are brought into contact with a target substrate, typically a Silicon (Si) or Silicon oxide (SiO_2) substrate, and rubbed by using tools such as plastic tweezers to further cleave them. After the Scotch tape is removed, layers of the 2D material are left on the substrate. This exfoliation method produces flakes with different sizes and thicknesses randomly distributed over the substrate, and only a small fraction of these flakes are atomically thin. Nevertheless, using an optical microscope, the contrast difference between the thin flakes and the substrate in the color optical image can determine the thinnest flakes left on the SiO_2 substrate.[123] Recently, a rapid method to identify single- to quindecuple-layer 2D nanosheets such as graphene, MoS_2, WSe_2, and TaS_2 on SiO_2/Si has been developed,[124] by measuring the optical contrast difference of nanosheets and substrate and analyzing these differences with the program ImageJ.[125] To date, this mechanical technique has been used only for the delamination of graphite and simple 2D inorganic materials, such as metal oxides, metal hydroxides and chalcogenides. The micromechanical exfoliation of more sophisticated 2D architectures, such as CPs, is still missing from the literature.

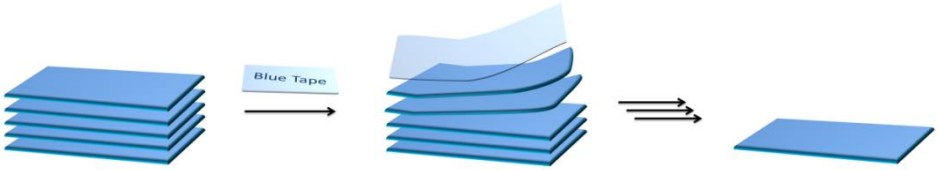

Figure 21. Mechanical exfoliation.

In this thesis, we have developed for the first time exfoliation processes in multifunctional compounds based in 2D anilate-bridged networks. This represents a novelty in three aspects; i) they are not neutral 2D layered compounds as other CPs so far exfoliated, ii) they present more complex structures containing two different functional subnetworks (ferrimagnetic anilate-based networks and spin-crossover cation) and, iii) mechanical exfoliation has been used for the first time for delaminate a CP. These results are included in Chapter 5.

7. Summary and Aims of the Work

The general objective of this thesis is the preparation of multifunctional molecular compounds combining the switching properties of spin-crossover complexes with other magnetic properties of interest. To reach this goal, we have used three strategies; covalent functionalization of a well-known family of spin-crossover complexes (Fe^{II} complexes of 1-bpp, chapters 2 and 3), formation of salts of cationic spin-crossover complexes and anionic extended networks (chapters 4 and 5) and preparation of polynuclear complexes of tetranuclear Schiff-base ligands that could lead to spin-crossover behavior (chapter 6).

Synthesis, structural and magnetic characterizations of the new spin-crossover complex $[Fe^{II}(bppCOOH)_2](ClO_4)_2$ are presented in Chapter 2 (bppCOOH, Scheme 3). This complex presents an abrupt spin transition at 383 K and shows LIESST effect until 60 K. The functionalization of 1-bpp with a carboxylate group has been performed to achieve the grafting of the complex on metal oxide surfaces, which is a necessary step for the preparation of devices based on the spin-crossover behavior, and to link the Fe^{II} spin-crossover complex to high nuclearity clusters or extended magnetic networks, providing an additional functionality (magnetic ordering or slow relaxation of magnetization). The complex presented in this chapter seems to be an excellent candidate to reach those purposes.

Furthermore, bppCOOH is a suitable precursor for the preparation of other 1-bpp derivatives (Scheme 6). Thus, in Chapter 3, the functionalization of the 1-bpp ligand with the triol motif tris(hydroxymethyl)aminomethane (TRIS), an useful functional group for the grafting to POMs, has been tried in the search of a POM hybrid showing spin-crossover as additional functionality. The synthesis of the ligand TRIS-bpp and the preparation of the hybrid Anderson POM $((n\text{-}Bu)_4N)_3[Mn^{III}Mo^{VI}_6O_{24}(TRIS\text{-}bpp)_2]$ (**1**) are the first steps to reach this goal (see Scheme 7). Magnetic measurements show that this 1-bpp-functionalized POM presents a SIM behavior.

In this chapter we also present two polymeric compounds obtained by complexation of Fe^{II} on the hybrid POM in the search of spin-crossover behavior. Recrystallisation in dimethylformamide of the precipitate obtained after reaction of Fe^{II} with the functionalized POM **1** affords the compound $[Fe^{II}(H_2O)(C_3H_7NO)]_2[Mn^{III}Mo^{VI}_6O_{24}(TRIS\text{-}bpp)_2](OH)\cdot(H_2O)$ (**2**). The structure of **2** has been resolved by single-crystal X-ray diffraction. This compound presents a 2D layered network, with presence of micropores, and shows a SIM behavior. The Fe^{II} ion is coordinated to one 1-bpp from a POM. The octahedral coordination is completed with one dimethylformamide and water solvent molecules and one oxo group from a neighboring POM. Due to this, it remains in the HS state. Elemental Analysis, IR and UV-Visible spectroscopies of the precipitate obtained by direct reaction of Fe^{II} with **1** is consistent with the formula $((n\text{-}Bu)_4N)[Fe^{II}(Mn^{III}Mo^{VI}_6O_{24}(TRIS\text{-}bpp)_2)]$ (**3**). Magnetic characterization of this polymer show that it remains in the LS state. Furthermore, it presents a SIM behavior.

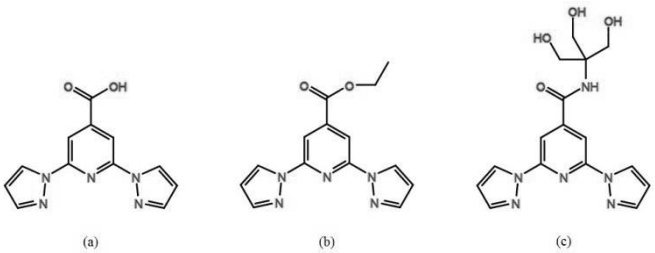

Scheme 6. Functionalized 1-bpp ligands. (a) bppCOOH, (b) bppCOOEt and (c) TRIS-bpp.

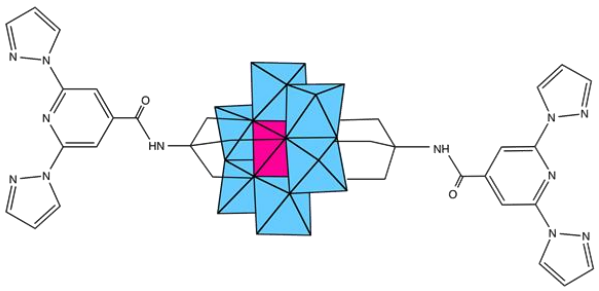

Scheme 7. Structure of functionalized POM in **1**.

Motivated by the interesting results obtained with bimetallic oxalate-based networks, we have explored the use of Fe^{II} and Fe^{III} spin-crossover complexes for the preparation of hybrid multifunctional materials based on the anilate ligand, in the search of a new family of hybrid magnets combining spin-crossover and magnetic ordering. The preparation and characterization of five novel compounds, formed by cationic complexes of hexadentate Schiff-base ligands (H_2(sal$_2$-trien) and derivatives, and tren(imid)$_3$, see Scheme 8) and anionic anilate-based bimetallic networks, are presented in Chapter 4. The four compounds $[Fe^{III}$(sal$_2$-trien)$][Mn^{II}Cr^{III}(Cl_2An)_3]\cdot(CH_2Cl_2)_{0.5}(CH_3OH)(H_2O)_{0.5}(CH_3CN)_5$, $[Fe^{III}$(4-OH-sal$_2$-trien)$][Mn^{II}Cr^{III}(Cl_2An)_3]\cdot$(solvate), $[Fe^{III}$(sal$_2$-epe)$][Mn^{II}Cr^{III}(Br_2An)_3]\cdot(CH_3CN)_4$(solvate) and $[Fe^{III}$(5-Cl-sal$_2$-trien)$][Mn^{II}Cr^{III}(Br_2An)_3]\cdot(CH_2Cl_2)(CH_3OH)(H_2O)_4(CH_3CN)_{1.5}$(solvate) present a 2D network with a honeycomb structure. Magnetic properties indicate that the Fe^{III} complexes remain in their HS or LS state, while the anilate networks present a ferrimagnetic ordering with significantly high ordering temperatures for this type of 2D network (ca. 10 K). The compound $[Fe^{II}(tren(imid)_3)]_2[Mn^{II}Cl_2Cr^{III}(Cl_2An)_3]Cl\cdot(CH_3OH)(CH_2Cl_2)_3(CH_3CN)_{0.5}$ presents a 1D anionic anilate-based network, surrounded by the $[Fe^{II}(tren(imid)_3)]^{2+}$ cations, and shows coexistence of a spin-crossover of half of the Fe^{II} complexes between 280 and 100 K and a ferrimagnetic ordering from the bimetallic anilate-based network below 2.6 K.

The search of other anilate-based hybrid magnets has been continued in Chapter 5. The structure and magnetic properties of $[Fe^{III}$(acac$_2$-trien)$][Mn^{II}Cr^{III}(Cl_2An)_3]\cdot(CH_3CN)_2$ and $[Fe^{III}$(acac$_2$-trien)$][Mn^{II}Cr^{III}(Br_2An)_3]\cdot(CH_3CN)_2$ are presented in this chapter. The size of the smaller spin-crossover cation ($[Fe^{III}$(acac$_2$-trien)$]^+$, see Scheme 8), has afforded a new type of layered structure, with the cation inserted within the hexagonal cavities of the 2D anilate layers. This is in contrast with the alternating cationic and anionic layers found in the 2D compounds reported in Chapter 4. As in most of these compounds, the inserted cation remains in its HS state, and the anilate network shows a magnetic ordering around 10 K. Both liquid and

micromechanical exfoliation processes have been tried for compounds with these two types of 2D structures $[Fe^{III}(acac_2\text{-trien})][Mn^{II}Cr^{III}(Br_2An)_3]\cdot(CH_3CN)_2$, and $[Fe^{III}(sal_2\text{-trien})][Mn^{II}Cr^{III}(Cl_2An)_3]\cdot(CH_2Cl_2)_{0.5}(CH_3OH)(H_2O)_{0.5}(CH_3CN)_5$. This would enable processing of these compounds and could lead to new properties as a result of their nanometric size. In this chapter we show that it is possible to exfoliate these compounds by these two methods. The best results have been obtained by micromechanical exfoliation (scotch-tape method) giving rise to nanosheets with lateral dimensions ranging from 500 nm to about 5 µm, and well-defined edges and angles. The thickness of the thinnest nanosheets, around 2 nm, suggests the delamination into at least bilayers of the two anilate compounds. To our knowledge, this is the first time that exfoliation is achieved in hybrid coordination polymers formed by cationic and anionic networks opening the way to the study of these magnetic layers in the two-dimensional limit.

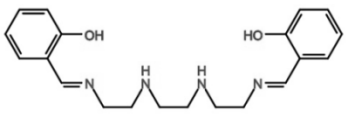

$H_2(sal_2\text{-trien})$

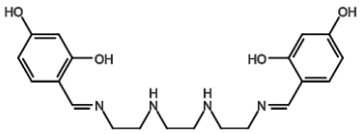

$H_2(4\text{-OH-}sal_2\text{-trien})$

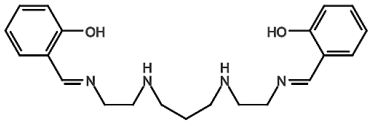

$H_2(sal_2\text{-epe})$

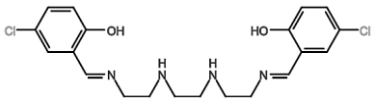

$H_2(5\text{-Cl-}sal_2\text{-trien})$

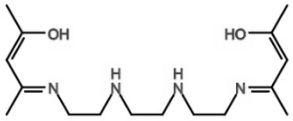

$H_2(acac_2\text{-trien})$

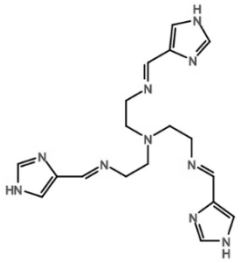

$Tren(imid)_3$

Scheme 8. Ligands of the Fe^{III} and Fe^{II} complexes.

Finally, the preparation and the characterization of a new family of Fe^{III} polynuclear complexes based on tetradentate Schiff-base ligands (Scheme 9) is presented in Chapter 6. The change of counterions or the presence of a substituent on the Schiff-base ligand has an influence on the nuclearity of the cluster, as this has resulted in the preparation of octanuclear and hexanuclear clusters with ring structures and a tetranuclear neutral cluster, with an unusual nonplanar arrangement of the Fe^{III} ions. The presence of pairs of HS Fe^{III} ions bridged by μ-oxo or μ-hydroxo ligands gave rise to strong antiferromagnetic interactions. Thus, the use of tetradentate Schiff-base ligands is a suitable strategy to obtain polynuclear complexes with interesting topologies.

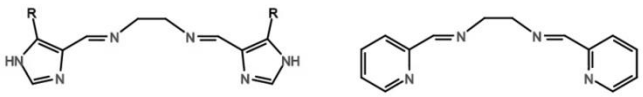

Scheme 9. Tetradentate Schiff-base ligands. R = H or CH_3.

[1] Nicole, L., Laberty-Robert, C., Rozes, L., Sanchez, C. *Nanoscale* **2014**, *6*, 6267-6292.

[2] (a) Del Rio, M. S., Martinetto, P., Reyes-Valerio, C., Dooryhee, E., Suarez, M. *Archaeometry* **2006**, *48*, 115-130. (b) Berke, H. *Chem. Soc. Rev.* **2007**, *36*, 15-30.

[3] (a) Sanchez, C., Ribot, F. *New J. Chem.* **1994**, *18*, 1007-1047. (b) Gómez-Romero, P., Sanchez, C. *Functional Hybrid Materials*, Wiley-VCH, Weinheim, **2004**. (c) Kickelbick, G. *Hybrid Materials: Strategies, Syntheses, Characterization and Applications*, Wiley-VCH, Weinheim, **2007**. (d) Sanchez, C., Shea, K. J., Kitagawa, S. *Hybrid Materials, Chem. Soc. Rev.*, **2011**, *40*, 453-1152.

[4] (a) Geim, A. K. *Science* **2009**, *324*, 1530-1534. (b) Nicolosi, V., Chhowalla, M., Kanatzidis, M. G., Strano, M. S., Coleman, J. N. *Science* **2013**, *340*, 1420-1438.

[5] (a) Gütlich, P., Hauser, A., Spiering, H. *Angew. Chem. Int. Ed.* **1994**, *33*, 2024-2054. (b) Gütlich, P., Goodwin, H. A. *Top. Curr. Chem.* **2004**, 233-235. (c) Létard, J.-F. *J. Mater. Chem.* **2006**, *16*, 2550-2559. (d) Sato, O., Tao, J., Zhang, Y.-Z. *Angew. Chem. Int. Ed.*

2007, *46*, 2152-2187. (e) Kitchen, J. A., Brooker, S. *Coord. Chem. Rev.* **2008**, *252*, 2072-2092. (f) Weber, B. *Coord. Chem. Rev.* **2009**, *253*, 2432-2449. (g) Halcrow, M. A. *Coord. Chem. Rev.* **2009**, *253*, 2493-2514. (h) Murray, K. S. *Aust. J. Chem.* **2009**, *62*, 1081-1101. (i) Gaspar, A., Seredyuk, M., Gütlich, P. *J. Mol. Struct.* **2009**, *924-926*, 9-19. (j) Brooker, S., Kitchen, J. A. *Dalton Trans.* **2009**, 7331-7340. (k) Koudriavtsev, A. B., Linert, W. *J. Struct. Chem.* **2010**, *51*, 335-365.

[6] Kahn, O., Kröber, J., Jay, C. *Adv. Mater.* **1992**, *4*, 718-728.

[7] König, E. *Prog. Inorg. Chem.* **1987**, *35*, 527-622.

[8] (a) Bousseksou, A., Molnár, G., Demont, P., Menegotto, J. *J. Mater. Chem.* **2003**, *13*, 2069-2071. (b) Bonhommeau, S., Guillon, T., Daku, L. M. L., Demont, P., Costa, J. S., Létard, J.-F., Molnár, G., Bousseksou, A. *Angew. Chem. Int. Ed.* **2006**, *45*, 1625-1629.

[9] Matsuda, M., Tajima, H. *Chem. Lett.* **2007**, *36*, 700-701.

[10] Cambi, L., Szego, L. *Ber. Drsch. Chem. Ges. B* **1931**, *64*, 2591-2598.

[11] (a) Galyametdinov, Y., Ksnevofontov, V., Prosvirin, A., Ovchinnikov, I., Ivanova, G., Gütlich, P., Haase, W. *Angew. Chem. Int. Ed.* **2001**, *40*, 4269-4271. (b) Seredyuk, M., Gaspar, A.B., Ksenofontov, V., Reiman, S., Galyametdinov, Y., Haase, W., Rentschler, E., Gütlich, P. *Chem. Mater.* **2006**, *18*, 2513-2519. (c) Seredyuk, M., Gaspar, A. B. Ksenofontov, V., Galyametdinov, Y., Kusz, J., Gütlich, P. *Adv. Funct. Mater.* **2008**, *18*, 2089-2101. (d) Bodenthin, Y., Pietsch, U., Mhwald, H., Kurth, D. G. *J. Am. Chem. Soc.* **2005**, *127*, 3110-3114. (e) Bodenthin, Y., Schwarz, G., Tomkowicz, Z., Geue, T., Haase, W., Pietsch, U., Kurth, D. G. *J. Am. Chem. Soc.* **2009**, *131*, 2934-2941. (f) Gaspar, A., Seredyuk, M., Gütlich, P. *Coord. Chem. Rev.* **2009**, *253*, 2399-2413. (g) Grondin, P., Siretanu, D., Roubeau, O., Achard, M.-F., Clérac, R. *Inorg. Chem.* **2012**, *51*, 5417-5426. (h) Hayami, S., Razaul Karim, M., Hoon Lee, Y. *Eur. J. Inorg. Chem.* **2013**, 683-696. (i) Gaspar, A. B., Seredyuk, M. *Coord. Chem. Rev.* **2014**, *268*, 41-58.

[12] (a) Létard, J.-F., Nguyen, O., Soyer, H., Mingotaud, C., Delhaes, P., Kahn, O. *Inorg. Chem.* **1999**, *38*, 3020-3021. (b) Roubeau, O., Agricole, B., Clérac, R., Ravaine, S. *J. Phys. Chem. B* **2004**, *108*, 5184-5195. (c) Roubeau, O., Natividad, E., Agricole, B., Ravaine, S. *Langmuir* **2007**, *23*, 3110-3117. (d) Thibault, C., Molnár, G., Salmon, L., Bousseksou, A., Vieu, C. *Langmuir* **2010**, *26*, 1557-1560. (e) Cavallini, M. *Phys. Chem. Chem. Phys.* **2012**, *14*, 11867-11876. (f) Shepherd, H. J., Molnár, G., Nicolazzi, W., Salmon, L., Bousseksou, A. *Eur. J. Inorg. Chem.* **2013**, 653-661. (g) Tanaka, D., Aketa, N., Tanaka, H., Tamaki, T., Inose, T., Akai, T., Toyama, H., Sakata, O., Tajiri, H., Ogawa, T. *Chem. Commun.* **2014**, *50*, 10074-10077.

[13] (a) Coronado, E., Galán-Mascarós, J. R., Monrabal-Capilla, M., García-Martínez, J., Pardo-Ibáñez, P. *Adv. Mater.* **2007**, *19*, 1359-1361. (b) Forestier, T., Mornet, S., Daro, N., Nishihara, T., Mouri, S., Tanaka, K., Fouché, O., Freysz, E., Létard, J.-F. *Chem. Commun.* **2008**, 4327-4329. (c) Volatron, F., Catala, L., Rivière, E., Gloter, A., Stéphan, O., Mallah, T. *Inorg. Chem.* **2008**, *47*, 6584-6586. (d) Boldog, I., Gaspar, A. B., Martínez, V., Pardo-Ibañez, P., Ksenofontov, V., Bhattacharjee, A., Gütlich, P., Real, J. A. *Angew. Chem. Int. Ed.* **2008**, *47*, 6433-6437. (e) Larionova, J., Salmon, L., Guari, Y., Tokarev, A., Molvinger, K., Molnár, G., Bousseksou, A. *Angew. Chem. Int. Ed.* **2008**, *47*, 8236-8240. (f) Forestier, T., Kaiba, A., Pechev, S., Denux, D., Guionneau, P., Etrillard, C., Daro, N., Freysz, E., Létard, J.-F. *Chem. Eur. J.* **2009**, *15*, 6122-6130. (g) Bousseksou, A., Molnár, G., Salmon, L., Nicolazzi, N. *Chem. Soc. Rev.* **2011**, *40*, 3313-3335. (h) Chakraborty, P., Boillot, M.-L., Tissot, A., Hauser, A. *Angew. Chem. Int. Ed.* **2013**, *52*, 7139-7142. (h) Tissot, A. *New J. Chem.* **2014**, *38*, 1840-1845. (i) Dugay, J., Giménez-Marqués, M., Kozlova, T., Zandbergen, H. W., Coronado, E., van der Zant, H. S. J. *Adv. Mater.* **2015**, *DOI: 10.1002/adma.201404441*.

[14] (a) Cobo, S., Molnár, G., Real, J. A., Bousseksou, A. *Angew. Chem. Int. Ed.* **2006**, *45*, 5786-5789. (b) Molnár, G., Cobo, S., Real, J. A., Carcenac, F., Daran, E., Vieu, C., Bousseksou, A. *Adv. Mater.* **2007**, *19*, 2163-2167. (c) Agustí, G., Cobo, G., Gaspar, A. B., Molnár, G., Ould Moussa, N., Szilágyi, P. Á., Pálfi, V., Vieu, C., Muñoz, M. C., Real, J. A., Bousseksou, A. *Chem. Mater.* **2008**, *20*, 6721-6732. (d) Cavallini, M., Bergenti, I., Milita, S., Ruani, G., Salitros, I., Qu, Z.-R., Chandrasekar, R., Ruben, M. *Angew. Chem. Int. Ed.* **2008**, *47*, 8596-8600.

[15] Halcrow, M. A. (Ed) *Spin-Crossover Materials, Properties and Applications.* Wiley, Chichester, UK, **2013**.

[16] Spiering, H., Boukheddaden, K., Linares, J., Varret, F. *Phys. Rev. B* **2004**, *70*, 184106.

[17] Hauser, A. *Top. Curr. Chem.* **2004**, *233*, 49-58.

[18] Gütlich, P., Garcia, Y., Goodwin, H. A. *Chem. Soc. Rev.* **2000**, *29*, 419-427.

[19] (a) Hauser, A., Jeftić, J., Romstedt, H., Hinek, R., Spiering, H. *Coord. Chem. Rev.* **1999**, *190-192*, 471-491. (b) Halcrow, M. A. *Chem. Commun.* **2013**, *49*, 10890-10892.

[20] (a) Gütlich, P., Goodwin, H. A. (Eds) *Top. Curr. Chem.* **2004**, vols. 233-235. Springer, Berlin/Heidelberg, Germany. (c) Atmani, C., El Hajj, F., Benmansour, S., Marchivie, M., Triki, S., Conan, F., Patinec, V., Handel, H., Dupouy, G., Gómez-García, C. J. *Coord.*

Chem. Rev. **2010**, *254*, 1559-1569. (d) Gütlich, P. *Eur. J. Inorg. Chem.* **2013**, 581-591. (e) Heider, S., Petzold, H., Chastanet, G., Schlamp, S., Rüffer, T., Weber, B., Létard, J.-F. *Dalton Trans.* **2013**, *42*, 8575-8584.

[21] Krüger, H.-J. *Coord. Chem. Rev.* **2009**, *253*, 2450-2459.

[22] (a) Petrouleas, V., Tuchagues, J.-P. *Chem. Phys. Lett.* **1987**, *137*, 21-25. (b) Boinnard, D., Bousseksou, A., Dworkin, A., Savariault, J. M., Varret, F., Tuchagues, J.-P. *Inorg. Chem.* **1994**, *33*, 271-281. (c) Psomas, G., Bréfuel, N., Dahan, F., Tuchagues, J.-P. *Inorg. Chem.* **2004**, *43*, 4590-4594. (d) Salmon, L., Bousseksou, A., Donnadieu, B., Tuchagues, J.-P. *Inorg. Chem.* **2005**, *44*, 1763-1773. (e) Zhang, L., Xu, G.-C., Xu, H.-B., Zhang, T., Wang, Z.-M., Yuan, M., Gao, S. *Chem. Commun.* **2010**, *46*, 2554-2556.

[23] Grillo, V. A., Gahan, L. R., Hanson, G. R., Stranger, R., Hambley, T. W., Murray, K. S., Moubaraki, B., Cashion, J. D. *J. Chem. Soc., Dalton Trans.* **1998**, 2341-2348.

[24] Costa, J. S., Balde, C., Carbonera, C., Denux, D., Wattiaux, A., Desplanches, C., Ader, J. P., Gütlich, P., Létard, J.-F. *Inorg. Chem.* **2007**, *46*, 4114-4119.

[25] Nihei, M., Shiga, T., Maeda, Y., Oshio, H. *Coord. Chem. Rev.* **2007**, *251*, 2606-2621.

[26] (a) Krivokapic, I., Zerara, M., Daku, M. L., Vargas, A., Enachescu, C., Ambrus, C., Tregenna-Piggott, P., Amstutz, N., Krausz, E., Hauser, A. *Coord. Chem. Rev.* **2007**, *251*, 364-378. (b) Hayami, S., Komatsu, Y., Shimizu, T., Kamihata, H., Lee, Y. H. *Coord. Chem. Rev.* **2011**, *255*, 1981-1990. (c) Cowan, M. G., Olguín, J., Narayanaswamy, S., Tallon, J. L., Brooker, S. *J. Am. Chem. Soc.* **2011**, *134*, 2892-2894.

[27] (a) Morgan, G. G., Murnaghan, K. D., Müller-Bunz, H., McKee, V., Harding, C. J. *Angew. Chem. Int. Ed.* **2006**, *45*, 7192-7195. (b) Martinho, P. N., Gildea, B., Harris, M. M., Lemma, T., Naik, A. D., Müller-Bunz, H., Keyes, T. E., Garcia, Y., Morgan, G. G. *Angew. Chem. Int. Ed.* **2012**, *51*, 12597-12601. (c) Pandurangan, K., Gildea, B., Murray, C., Harding, C. J., Müller-Bunz, H., Morgan, G. G. *Chem. Eur. J.* **2012**, *18*, 2021-2029.

[28] Real, J. A., Gaspar, A. B., Muñoz, M. C. *Dalton Trans.* **2005**, 2062-2079.

[29] Halcrow, M. A. *Polyhedron* **2007**, *26*, 3523-3576.

[30] König, E. *Prog. Inorg. Chem.* **1987**, *35*, 527-622.

[31] Muñoz, M. C., Real, J. A. *Coord. Chem. Rev.* **2011**, *255*, 2068-2093.

[32] (a) Real, J. A., Gaspar, A. B., Niel, V., Muñoz, M. C. *Coord. Chem. Rev.* **2003**, *236*, 121-141. (b) Halcrow, M. A. *Chem. Soc. Rev.* **2011**, *40*, 4119-4142.

[33] (a) Létard, J.-F., Guionneau, P., Goux-Capes, L. *Top. Curr. Chem.* **2004**, *235*, 221-249. (b) Garcia, Y., Ksenofontov, V., Mentior, S., Dîrtu, M. M., Gieck, C., Bhatthacharjee, A., Gütlich, P. *Chem. Eur. J.* **2008**, *14*, 3745-3758.

[34] Venkataramani, S., Jana, U., Dommaschk, M., Sonnichsen, F. D., Tuczek, F., Herges, R. *Science* **2011**, *331*, 445-448.

[35] Kahn, O., Martinez, C. J. *Science* **1998**, *279*, 44-48.

[36] Gaspar, A. B., Ksenofontov, V., Seredyuk, M., Gütlich, P. *Coord. Chem. Rev.* **2005**, *249*, 2661-2676.

[37] (a) Dorbes, S., Valade, L., Real, J. A., Faulmann, C. *Chem. Commun.* **2005**, 69-71. (b) Faulmann, C., Dorbes, S., Garreau de Bonneval, B., Molnár, G., Bousseksou, A., Gómez-García, C. J., Coronado, E., Valade, L. *Eur. J. Inorg. Chem.* **2005**, 3261-3270. (c) Takahashi, K., Cui, H.-B., Okano, Y., Kobayashi, H., Einaga, Y., Sato, O. *Inorg. Chem.* **2006**, *45*, 5739-5741. (d) Faulmann, C., Jacob, K., Dorbes, S., Lampert, S., Malfant, I., Doublet, M.-L., Valade, L., Real, J. A. *Inorg. Chem.* **2007**, *46*, 8548-8559. (e) Takahashi, K., Cui, H.-B., Okano, Y., Kobayashi, H., Mori, H., Tajima, H., Einaga, Y., Sato, O. *J. Am. Chem. Soc.* **2008**, *130*, 6688-6689.

[38] Koo, Y.-S., Galán-Mascarós, J. R. *Adv. Mater.* **2014**, *26*, 6785-6789.

[39] McGarvey, J. J., Lawthers, I. *J. Chem. Soc. Chem. Comm.* **1982**, *16*, 906-907.

[40] Decurtins, S., Gütlich, P., Köhler, C. P., Spiering, H., Hauser, A. *Chem. Phys. Lett.* **1984**, *105*, 1-4.

[41] Hauser, A. *Chem. Phys. Lett.* **1986**, *124*, 543-548.

[42] Money, V. A., Costa, J. S., Marcén, S., Chastenet, G., Elhaik, J., Halcrow, M. A., Howard, J. A. K., Létard, J.-F. *Chem. Phys. Lett.* **2004**, *391*, 273-277.

[43] Létard, J.-F., Capes, L., Chastanet, G., Moliner, N., Létard, S., Real, J.-A., Kahn, O. *Chem. Phys. Lett.* **1999**, *313*, 115-120.

[44] Marcén, S., Lecren, L., Capes, L., Goodwin, H. A., Létard, J.-F. *Chem. Phys. Lett.* **2002**, *358*, 87-95.

[45] Létard, J.-F., Guionneau, P., Nguyen, O., Costa, J. S., Marcén, S., Chastanet, G., Marchivie, M., Goux-Capes, L. *Chem. Eur. J.* **2005**, *11*, 4582-4589.

[46] Costa, J. S., Guionneau, P., Létard, J.-F. *J. Phys. Conf. Ser.* **2005**, *21*, 67-72.

[47] (a) Shimamoto, N., Ohkoshi, S. S., Sato, O., Hashimoto, K. *Inorg. Chem.* **2002**, *41*, 678-684. (b) Lebris, R., Mathonière, C., Létard, J.-F. *Chem. Phys. Lett.* **2006**, *426*, 380-386.

[48] Halcrow, M. A. *Coord. Chem. Rev.* **2005**, *249*, 2880-2908.

[49] Halcrow, M. A. *Coord. Chem. Rev.* **2009**, *253*, 2493-2514.

[50] (a) Mohammed, R., Chastanet, G., Tuna, F., Malkin, T. L., Barrett, S. A., Kilner, C. A., Létard, J.-F., Halcrow, M. A. *Eur. J. Inorg. Chem.* **2013**, 819-831. (b) Šalitroš, I., Fuhr, O., Kruk, R., Pavlik, J., Pogány, L., Schäfer, B., Tatarko, M., Boča, R., Linert, W., Ruben, M. *Eur J. Inorg. Chem.* **2013**, 1049-1057.

[51] (a) Carbonera, C., Costa, J. S., Money, V. A., Elhaïk, J., Howard, J. A. K., Halcrow, M. A., Létard, J.-F. *Dalton Trans.* **2006**, 3058-3066. (b) Pritchard, R., Lazar, H., Barrett, S. A., Kilner, C. A., Asthana, S., Carbonera, C., Létard, J.-F., Halcrow, M. A. *Dalton Trans.* **2009**, 6656-6666. (c) Money, V. A., Carbonera, C., Elhaïk, J., Halcrow, M. A., Howard, J. A. K., Létard, J.-F. *Chem. Eur. J.* **2007**, *13*, 5503-5514.

[52] Holland, J. M., Barrett, S. A., Kilner, C. A., Halcrow, M. A. *Inorg. Chem. Commun.* **2002**, *5*, 328-332.

[53] (a) Rajadurai, C., Fuhr, O., Kruk, R., Ghafari, M., Hahn, H., Ruben, M. *Chem. Commun.* **2007**, 2636-2638. (b) Nihei, M., Han, L., Oshio, H. *J. Am. Chem. Soc.* **2007**, *129*, 5312-5313. (c) Tovee, C. A., Kilner, C. A., Barrett, S. A., Thomas, J. A., Halcrow, M. A. *Eur. J. Inorg. Chem*. **2010**, 1007-1012. (d) González-Prieto, R., Fleury, B., Schramm, F., Zoppellaro, G., Chandrasekar, R., Fuhr, O., Lebedkin, S., Kappes, M., Ruben, M. *Dalton Trans.* **2011**, *40*, 7564-7570. (e) Takahashi, K., Hasegawa, Y., Sakamoto, R., Nishikawa, M., Kume, S., Nishibori, E., Nishihara, H. *Inorg. Chem.* **2012**, *51*, 5188-5198. (f) Alam, M. S., Stocker, M., Gieb, K., Müller, P., Harvono, M., Student, K., Grohmann, A. *Angew. Chem. Int. Ed.* **2010**, *49*, 1159-1163.

[54] (a) Vermonden, T., Branowska, D., Marcelis, A. T. M., Sudhölter, E. J. R. *Tetrahedron*, **2003**, *59*, 5039-5045. (b) Klein, C., Baranoff, E., Grätzel, M., Nazeeruddin, M. K. *Tetrahedron Lett.* **2011**, *52*, 584-587.

[55] Abhervé, A., Clemente-León, M., Coronado, E., Gómez-García, C. J., López-Jordà, M. *Dalton Trans.* **2014**, *43*, 9406-9409.

[56] (a) Alam, M. S., Stocker, M., Gieb, K., Müller, P., Harvono, M., Student,K., Grohmann, A. *Angew. Chem. Int. Ed.* **2010**, *49*, 1159-1163. (b) Shen, C., Harvono, M., Grohmann, A., Buck, M., Weidner, T., Ballay N., Zharkinov, M. *Langmuir* **2008**, *24*, 12883-12891.

[57] (a) Pope, M. T. *Comprehensive Coordination Chemistry II*, **2004**, *4*, 635-678. (b) Hill, C. L. *Chem. Rev.* **1998**, *98*, 1-2.

[58] Proust, A., Thouvenot, R., Gouzerh, P. *Chem. Commun.* **2008**, 1837-1852.

[59] (a) Wang, M. S., Xu, G., Zhang, Z. J., Guo, G. C. *Chem. Commun.* **2010**, *46*, 361-376. (b) Yamase, T., Pope, M. T. (Eds) *Polyoxometalate Chemistry for Nano-composite Design*, Kluwer Academic/Plenum Publishers, New York, **2002**. (c) Sadakane, M., Steckhan, E. *Chem. Rev.* **1998**, *98*, 219-237.

[60] (a) Coronado, E., Gómez-García, C. J. *Chem. Rev.* **1998**, *98*, 273-296. (b) Coronado, E., Giménez-Saiz, C., Gómez-García, C. J. *Coord. Chem. Rev.* **2005**, *249*, 1776-1796.

[61] Bonchio, M., Carraro, M., Scorrano, G., Bagno, A. *Adv. Synth.Catal.* **2004**, *346*, 648-654.

[62] (a) Feng, Y., Han, Z., Peng, J., Lu, J., Xue, B., Li, L., Ma, H., Wang, E. *Mat. Lett.* **2006**, *60*, 1588-1593. (b) Geisberger, G., Paulus, S., Carraro, M., Bonchio, M., Patzke, G. R. *Chem. Eur. J.* **2011**, *17*, 4619-4625.

[63] Clemente-Juan, J., Clemente-León, M., Coronado, E., Galán-Mascarós, J., Giménez-Saiz, C., Gómez-García, C. J. *C.R. Acad. Sci. Paris, t. 1, Série II c*, **1998**, 305-317.

[64] (a) Zhu, Y., Yin, P., Xiao, F., Li, D., Bitterlich, E., Xiao, Z., Zhang, J., Hao, J., Liu, T., Wang, Y., Wei, Y. *J. Am. Chem. Soc.* **2013**, *135*, 17155-17160. (b) Bar-Nahum, I., Cohen, H., Neumann, R. *Inorg. Chem.* **2003**, *42*, 3677-3684.

[65] (a) Chen, Q., Goshorn, D., Scholes, C., Tan, X., Zubieta, J. *J. Am. Chem. Soc.* **1992**, *114*, 4667-4681. (b) Chen, Q., Zubieta, J. *Inorg. Chim. Acta* **1992**, *198-200*, 95-100.

[66] Müller, A., Meyer, J., Bögge, H., Stammler, A., Botar, A., Anorg, Z., *Allg. Chem.* **1995**, *621*, 1818-1831.

[67] Zeng, H., Newkome, G., Hill, C. L. *Angew. Chem. Int. Ed.* **2000**, *39*, 1772-1774.

[68] (a) Hou, Y., Hill, C. L. *J. Am. Chem. Soc.* **1993**, *115*, 11823-11830. (b) Pradeep, C. P., Long, D. L., Newton, G., Song, Y. F., Cronin, L. *Angew. Chem. Int. Ed.* **2008**, *47*, 4388-4391.

[69] (a) Hasenknopf, B., Delmont, R., Herson, P., Gouzerh, P. *Eur. J. Inorg. Chem.* **2002**, *5*, 1081-1087. (b) Marcoux, P., Hasenknopf, B., Vaissermann, J., Gouzerh, P. *Eur. J. Inorg. Chem.* **2003**, *13*, 2406-2412.

[70] Santoni, M-P.; Pal, A. K.; Hanan, G. S.; Hasenknopf, B. *Inorg. Chem.* **2011**, *50*, 6737-6745.

[71] Kang, J.; Xu, B.; Peng, Z.; Zhu, X.; Wei, Y.; Powell, D. R. *Angew. Chem. Int. Ed.* **2005**, *44*, 6902-6905.

[72] Clemente-Juan, J. M., Coronado, E., Gaita-Ariño, A. *Chem. Soc. Rev.* **2012**, *41*, 7464–7478.

[73] Sessoli, R., Gatteschi, D., Caneschi, A., Novak, M. A. *Nature* **1993**, *365*, 141-143.

[74] Winpenny, R. E. P., McInnes, E. J. L. *Molecular Nanomagnets.* Walton, R. I., Bruce, D. W., O'Hare, D., Eds. Wiley, Chichester, UK, **2010**.

[75] Thomas, L., Lionti, F., Ballou, R., Gatteschi, D., Sessoli, R., Barbara, B. *Nature* **1996**, *383*, 145-147.

[76] Jeon, I. R., Clérac, R. *Dalton Trans.* **2012**, *41*, 9569–9586.

[77] Sessoli, R., Gatteschi, D., Caneschi, A., Novak, M.A. *Nature* **1993**, *365*, 141-143.

[78] Novak, M. A., Sessoli, R., Caneschi, A., Gatteschi, D. *J. Magn. Magn. Mater.* **1995**, *146*, 211-213.

[79] (a) Milios, C. J., Inglis, R., Vinslava, A., Bagai, R., Wernsdorfer, W., Parsons, S., Perlepes, S. P., Christou, G., Brechin, E. K. *J. Am. Chem. Soc.* **2007**, *129*, 12505-12511. (b) Milios, C. J., Vinslava, A., Wernsdorfer, W., Moggach, S., Parsons, S., Perlepes, S. P., Christou, G., Brechin, E. K. *J. Am. Chem. Soc.* **2007**, *129*, 2754-2755.

[80] Tasiopoulos, A. J., Vinslava, A., Wernsdorfer, W., Abboud, K. A., Christou, G. *Angew. Chem. Int. Ed.* **2004**, *43*, 2117-2121.

[81] Sangregorio, C., Ohm, T., Paulsen, C., Sessoli, R., Gatteschi, D. *Phys. Rev. Lett.* **1997**, *78*, 4645-4648.

[82] (a) Mannini, M., Pineider, F., Sainctavit, P., Danieli, C., Otero, E., Sciancalepore, C., Talarico, A. M., Arrio, M.-A., Comia, A., Gatteschi, D., Sessoli, R. *Nat. Mater.* **2009**, *8*, 194-197. (b) Mannini, M., Pineider, F., Danieli, C., Totti, F., Sorace, L., Sainctavit, P., Arrio, M.-A., Otero, E., Joly, L., Cezar, J. C., Cornia, A., Sessoli, R. *Nature* **2010**, *468*, 417-421.

[83] Andres, H., Basler, R., Blake, A. J., Brechin, E. K., Cadiou, C., Chaboussant, G., Grant, C. M., Güdel, H.-U., Harris, S. G., Murrie, M., Parsons, S., Paulsen, C., Semadini, F., Villar, V., Wernsdorfer, W., Winpenny, R. E. P. *Chem Eur. J.* **2002**, *8*, 4867-4876.

[84] (a) Lawrence, J., Yang, E.-C., Edwards, R., Olmstead, M. M., Ramsey, C., Dalal, N. S., Gantzel, P. K., Hill, S., Hendrickson, D. N. *Inorg. Chem.* **2008**, *47*, 1965-1974. (b) Ferguson, A., Lawrence, J., Parkin, A., Sanchez-Benitez, J., Kamenev, K. V., Brechin, E. K., Wernsdorfer, W., Murrie, M. *Dalton Trans.* **2008**, 6409-6414. (c) Moragues-Canova, M., Helliwell, M., Ricard, L., Riviere, E., Wernsdorfer, W., Brechin, E. K., Mallah, T. *Eur. J. Inorg. Chem.* **2004**, 2219-2222.

[85] Murrie, M. *Chem. Soc. Rev.* **2010**, *39*, 1986-1995.

[86] Ishikawa, N., Sugita, M., Ishikawa, T., Koshihara, S.-Y., Kaizu, Y. *J. Am. Chem. Soc.* **2003**, *125*, 8694-8695.

[87] AlDamen, M. A., Clemente-Juan, J. M., Coronado, E., Martí- Gastaldo, C., Gaita-Ariño, A. *J. Am. Chem. Soc.* **2008**, *130*, 8874-8875.

[88] Freedman, D. E., Harman, W. H., Harris, T. D., Long, G. J., Chang, C. J., Long, J. R. *J. Am. Chem. Soc.* **2010**, *132*, 1224-1225.

[89] Gómez-Coca, S., Cremades, E., Aliaga-Alcalde, N., Ruiz, E. *Inorg. Chem.* **2014**, *53*, 676-678.

[90] Vallejo, J., Pascual-Álvarez, A., Cano, J., Castro, I., Julve, M., Lloret, F., Krzystek, J., De Munno, G., Armentano, D., Wernsdorfer, W., Ruiz-García, R., Pardo, E. *Angew. Chem. Int. Ed.* **2013**, *52*, 14075-14079.

[91] Ishikawa, R., Miyamoto, R., Nojiri, H., Breedlove, B. K., Yamashita, M. *Inorg. Chem.* **2013**, *52*, 8300-8302.

[92] Grigoropoulos, A., Pissas, M., Papatolis, P., Psycharis, V., Kyritsis, P., Sanakis, Y. *Inorg. Chem*. **2013**, *52*, 12869-12871.

[93] Craig, G. A., Marbey, J. J., Hill, S., Roubeau, O., Parsons, S., Murrie, M. *Inorg. Chem.* **2015**, *54*, 13-15.

[94] Coronado, E., Mínguez Espallargas, G. *Chem. Soc. Rev.* **2013**, *42*, 1525-1539.

[95] (a) Sato, O., Iyoda, T., Fujishima, A., Hashimoto, K. *Science*, **1996**, *272*, 704-705. (b) Coronado, E., Giménez-López, M. C., Levchenko, G., Romero, F. M., García-Baonza, V., Milner, A., Paz-Pasternak, M. *J. Am. Chem. Soc.* **2005**, *127*, 4580-4581. (c) Coronado, E., Giménez-López, M. C., Korzeniak, T., Levchenko, G., Romero, F. M., Segura, A., García-Baonza, V., Cezar, J. C., De Groot, F. M. F., Milner A., Paz-Pasternak, M. *J. Am. Chem. Soc.* **2008**, *130*, 15519-15532. (d) Ohkoshi, S.–I., Imoto, K., Takano, S., Tokoro, H. *Nature Chem.* **2011**, *3*, 564-569.

[96] Clemente-León, M., Coronado, E., Martí-Gastaldo C., Romero, F. M. *Chem. Soc. Rev.* **2011**, *40*, 473-497.

[97] (a) Clemente-León, M., Galán-Mascarós, J. R., Gómez-García, C. J. *Chem. Commun.* **1997**, 1727-1728. (b) Coronado, E., Galán-Mascarós, J. R., Gómez-García, C. J., Martínez-Agudo, J. M. *Adv. Mater.* **1999**, *11*, 558-561. (c) Coronado, E., Galán-Mascarós, J. R., Gómez-García, C. J., Ensling, J., Gütlich, P. *Chem. Eur. J.* **2000**, *6*, 552-563.

[98] (a) Bénard, S., Yu, P., Audière, J. P., Rivière, E., Clèment, R., Ghilhem, J., Tchertanov, L., Nakatami, K. *J. Am. Chem. Soc.* **2000**, *122*, 9444-9454. (b) Aldoshin, S. M., Sanina, N. A., Minkin, V. I., Voloshin, N. A., Ikorskii, V. N., Ovcharenko, V. I., Smirnov, V. A., Nagaeva, N. K. *J. Mol. Struct.* **2007**, *826*, 69-74.

[99] (a) Coronado, E., Galán-Mascarós, J. R., Gómez-García, C. J., Laukhin, V. *Nature* **2000**, *408*, 447-449. (b) Alberola, A., Coronado, E., Galán-Mascarós, J. R., Giménez-Saiz, C., Gómez-García, C. J. *J. Am. Chem. Soc.* **2003**, *125*, 10774-10775. (c) Galán-Mascarós, J. R., Coronado, E., Goddard, P. A., Singleton, J., Coldea, A. I., Wallis, J. D., Coles, S. J., Alberola, A. *J. Am. Chem. Soc.* **2010**, *132*, 9271-9273. (d) Coronado, E., Galán-Mascarós, J. R., Gómez-García, C. J., Martínez-Ferrero, E., Van Smaalen, S. *Inorg. Chem.* **2004**, *43*, 4808-4810. (d) Zhang, B., Zhang, Y., Zhu, D. *Chem. Commun.* **2012**, *48*, 197-199.

[100] (a) Okawa, H., Shigematsu, A., Sadakiyo, M., Miyagawa, T., Yoneda, K., Ohba, M., Kitagawa, H. *J. Am. Chem. Soc.* **2009**, *131*, 13516-13522. (b) Pardo, E., Train, C., Contard, G., Boubekeur, K., Fabelo O., Liu, H., Dkhil, B., Lloret, F., Nakagawa, K., Tokoro, H., Ohkoshi, S. –I., Verdaguer, M. *J. Am. Chem. Soc.* **2011**, *133*, 15328-15331.

(c) Sadayiko, M., Okawa, H., Shigematsu, A., Ohba, M., Yamada, T., Kitagawa, H. *J. Am. Chem. Soc.* **2012**, *134*, 5472-5475. (d) Okawa, H., Sadakiyo, M., Yamada, T., Maesato, M., Ohba, M., Kitagawa, H. *J. Am. Chem. Soc.* **2013**, *135*, 2256-2262.

[101] (a) Endo, T., Akutagawa, T., Noro, S. I., Nakamura, T. *Dalton Trans.* **2011**, *40*, 1491-1496. (b) Pardo, E., Train, C., Liu, H., Chamoreau, L.-M., Dkhil, B., Boubekeur, K., Lloret, F., Nakatani, K., Tokoro, H., Ohkoshi, S.-i., Verdaguer, M. *Angew. Chem. Int. Ed*. **2012**, *51*, 8356-8360.

[102] (a) Andrés, R., Gruselle, M., Malézieux, B., Verdaguer, M., Vaissermann, J. *Inorg. Chem.* **1999**, *38*, 4637-4646. (b) Andrés, R., Brissard, M., Gruselle, M., Train, C., Vaissermann, J., Malézieux, B., Jamet, J. P., Verdaguer, M. *Inorg. Chem.* **2001**, *40*, 4633-4640. (c) Clemente-León, M., Coronado, E., Dias, J. C., Soriano-Portillo, A., Willett, R. D. *Inorg. Chem.* **2008**, *47*, 6458-6463. (d) Train, C., Gheorghe, R., Krstic, V., Chamoreau, L. M., Ovanesyan, N. S., Rikken, G. L. J. A., Gruselle M., Verdaguer, M. *Nat. Mater.* **2008**, *7*, 729-734. (e) Train, C., Nuida, T., Gheorghe, R., Gruselle, M., Ohkoshi, S.-I. *J. Am. Chem. Soc.* **2009**, *131*, 16838-16843. (f) Gruselle, M., Li, Y., Ovanesyan, N., Markhaev, V., Shilov, G., Mushenok, F., Train, C., Aldoshin, S. *Chirality* **2013**, *25*, 444-448.

[103] Clemente-León, M., Coronado, E., Gómez-García, C. J., López-Jordà, M., Camón, A., Repollés, A., Luis, F. *Chem. Eur. J.* **2014**, *20*, 1669-1676.

[104] Coronado, E., Galán-Mascarós, J. R., Giménez-López, M. C., Almeida, M., Waerenborgh, J. C. *Polyhedron* **2007**, *26*, 1838-1844.

[105] (a) Clemente-León, M., Coronado, E., Giménez-López, M. C., Soriano-Portillo, A., Waerenborgh, J. C., Delgado, F. S., Ruiz-Pérez, C. *Inorg. Chem.* **2008**, *47*, 9111-9120. (b) Clemente-León, M., Coronado, E., López-Jordà, M., Mínguez Espallargas, G., Soriano-Portillo, A., Waerenborgh, J. C. *Chem. Eur. J.* **2010**, *16*, 2207-2219. (c) Clemente-León, M., Coronado, E., López-Jordà, M. *Dalton Trans.* **2010**, *39*, 4903-4910. (d) Clemente-León, M., Coronado, E., López-Jordà, M., Waerenborgh, J. C. *Inorg. Chem.* **2011**, *50*, 9122-9130. (e) Clemente-León, M., Coronado, E., López-Jordà, M., Desplanches, C., Asthana, S., Wang, H., Létard, J.-F. *Chem. Sci.* **2011**, *2*, 1121-1127. (f) Clemente-León, M., Coronado, E., López-Jordà, M. *Eur. J. Inorg. Chem.* **2013**, 753-762. (g) Ben Djamâa, A., Clemente-León, M., Coronado, E., López-Jordà, M. *Polyhedron* **2013**, *64*, 142-150. (h) Clemente-León, M., Coronado, E., López-Jordà, M., Waerenborgh, J. C., Desplanches, C., Wang, H., Létard, J.-F., Hauser, A., Tissot, A. *J. Am. Chem.* Soc. **2013**, *135*, 8655-8667.

[106] Kitagawa, S., Kawata, S. *Coord. Chem. Rev.* **2002**, *224*, 11-34.

[107] (a) Weiss, A., Riegler, E., Robl, C. *Z. Naturforsch., B* **1986**, *41B*, 1501-1505. (b) Luo, T., Liu, Y., Tsai, H., Su, C., Ueng, C., Lu, K. *Eur. J. Inorg. Chem.* **2004**, 4253-4258. (c) Abrahams, B. F., Coleiro, J., Hoskins, B. F., Robson, R. *Chem. Commun.* **1996**, 603-604. (d) Abrahams, B. F., Coleiro, J., Ha, K., Hoskins, B. F., Orchard, S. D., Robson, R. *J. Chem. Soc., Dalton Trans.* **2002**, 1586-1594. (e) Robl, C. *Mater. Res. Bull.* **1987**, *22*, 1483-1491. (f) Shilov, G. V., Nikitina, Z. K., Ovanesyan, N. S., Aldoshin, S. M., Makhaev, V. D. *Russ. Chem. Bull.* **2011**, *60*, 1209-1219.

[108] Coronado, E., Galán-Mascarós, J. R., Gómez-García, C. J., Martínez-Agudo, J. M. *Inorg. Chem.* **2001**, *40*, 113-120.

[109] Abrahams, B. F., Hudson, T. A., McCormick, L. J., Robson, R. *Cryst. Growth Des.* **2011**, *11*, 2717-2720.

[110] Atzori, M., Benmansour, S., Mínguez Espallargas, G., Clemente-León, M., Abhervé, A., Gómez-Claramunt, P., Coronado, E., Artizzu, F., Sessini, E., Deplano, P., Serpe, A., Mercuri, M. L., Gómez-García, C. J. *Inorg. Chem.* **2013**, *52*, 10031-10040.

[111] Abhervé, A., Clemente-León, M., Coronado, E., Gómez-García, C. J., Verneret, M. *Inorg. Chem.* **2014**, *53*, 12014-12026.

[112] (a) Geim, A. K., Novoselov, K. S. *Nat. Mater.* **2007**, *6*, 183-191. (b) Novoselov, K. S., Fal'ko, V. I., Colombo, L., Gellert, P. R., Schwab, M. G., Kim, K. *Nature* **2012**, *490*, 192-200.

[113] Golberg, D. *ACS Nano* **2010**, *4*, 2979-2993.

[114] (a) Wang, Q. H., Kalantar-Zadeh, K., Kis, A., Coleman, J. N., Strano, M. S. *Nat. Nanotechnol.* **2012**, *7*, 699-712. (b) Wilson, J. A., Yoffe, A. D. *Adv. Phys.* **1969**, *18*, 193-335.

[115] Coleman, C. C., Goldwhite, H., Tikkanen, W. *Chem. Mater.* **1998**, *10*, 2794-2800.

[116] (a) Ma, R. Z., Sasaki, T. *Adv. Mater.* **2010**, *22*, 5082-5104. (b) Bizeto, M. A., Shiguihara, A. L., Constantino, V. R. L. *J. Mater. Chem.* **2009**, *19*, 2512-2525. (c) Nalawade, P., Aware, B., Kadam, V. J., Hirlekar, R. S. *J. Sci. Ind. Res.* **2009**, *68*, 267-272.

[117] (a) Luckham, P. F., Rossi, S. *Adv. Colloid. Interface Sci.* **1999**, *82*, 43-92. (b) Velde, B. *Introduction to Clay minerals: Chemistry, Origins, Uses, and Environmental Significance*, **1992**, Chapman & Hall, London, UK.

[118] Beldon, P. J., Tominaka, S., Singh, P., Saha Dasgupta, T., Bithell, E. G., Cheetham, A. K. *Chem. Commun.* **2014**, *50*, 3955-3957.

[119] Amo-Ochoa, P., Welte, L., Gonzáles-Prieto, R., Sanz Miguel, P. J., Gómez-García, C. J., Mateo-Martí, E., Delgado, S., Gómez-Herrero, J., Zamora, F. *Chem. Commun.* **2010**, *46*, 3262-3264.

[120] Li, P.-Z., Maeda, Y., Xu, Q. *Chem. Commun.* **2011**, *47*, 8436-8438.

[121] (a) Tan, J.-C., Saines, P. J., Bithell, E. G., Cheetham, A. K. *ACS Nano* **2012**, *6*, 615-621. (b) Saines, P. J., Tan, J.-C., Yeung, H. H.-M., Barton, P. T., Cheetham, A. K. *Dalton Trans.* **2012**, *41*, 8585-8593.

[122] Gallego, A., Hermosa, C., Castillo, O., Berlanga, I., Gómez-García, C. J., Mateo-Martí, E., Martínez, J. I., Flores, F., Gómez-Navarro, C., Gómez-Herrero, J., Delgado, S., Zamora, F. *Adv. Mater.* **2013**, *25*, 2141-2146.

[123] Castellanos-Gomez, A., Navarro-Moratalla, E., Mokry, G., Quereda, J., Pinilla-Cienfuegos, E., Agraït, N., van der Zant, H. S. J., Coronado, E., Steele, G. A., Rubio-Bollinger, G. *Nano Research* **2013**, *6(3)*, 191-199.

[124] (a) Li, H., Wu, J., Huang, X., Lu, G., Yang, J., Lu, X., Xiong, Q., Zhang, H. *ACS Nano* **2013**, *7*, 10344-10353. (b) Li, H., Wu, J., Yin, Z., Zhang, H. *Acc. Chem. Res.* **2014**, *47*, 1067-1075.

[125] Schneider, C. A., Rasband, W. S., Eliceiri, K. W. *Nat. Methods* **2012**, *9*, 671-675.

A Spin-Crossover Complex based on a 2,6-bis(pyrazol-1-yl)pyridine (1-bpp) Ligand Functionalized with a Carboxylate Group

Chapter 2

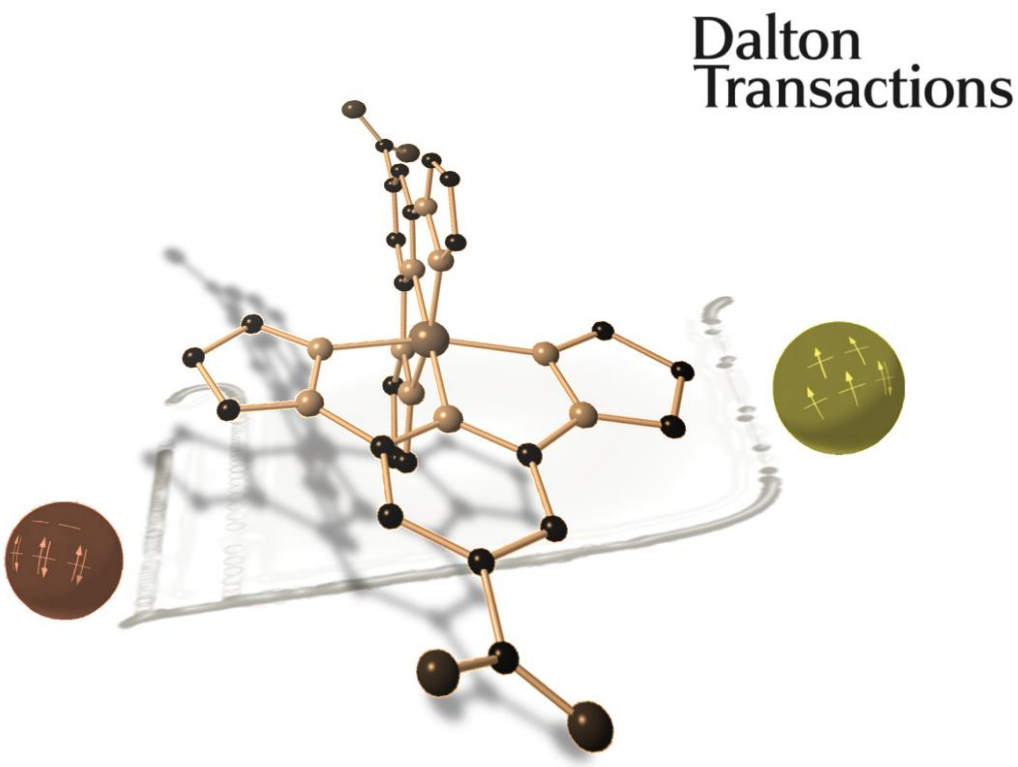

Abhervé, A., Clemente-León, M., Coronado, E., Gómez-García, C. J., López-Jordà, M. *Dalton Trans.* **2014**, *43*, 9406-9409.

Chapter 2. A Spin-Crossover Complex based on a 2,6-bis(pyrazol-1-yl)pyridine (1-bpp) Ligand Functionalized with a Carboxylate Group

Combining Fe^{II} with the carboxylate-functionalized 2,6-bis(pyrazol-1-yl)pyridine (bppCOOH) ligand results in the spin-crossover compound $[Fe(bppCOOH)_2](ClO_4)_2$ which shows an abrupt spin transition with $T_{1/2}$ of *ca.* 380 K and a T_{LIESST} of 60 K due to the presence of a hydrogen-bonded linear network of complexes.

Introduction

Spin crossover (SCO) complexes are one of the most spectacular examples of molecular bistability. In these systems low-spin (LS) to high-spin (HS) transitions can be triggered through a variety of external stimuli (e.g. temperature, pressure or electromagnetic radiation). In addition to the interesting fundamental aspects of this phenomenon, these systems are of growing interest in the area of functional materials due to their possible applications as sensors, memories or switching devices.[1] The most studied SCO systems are based on Fe^{II} complexes that undergo spin crossover between their diamagnetic LS (S = 0) and paramagnetic HS (S = 2) configurations.[2] The change of electronic configuration is accompanied by drastic changes in the optical and magnetic properties of these compounds.[3] Thus, under given experimental conditions, the same material can be found in two states exhibiting different optical and magnetic behaviors. Abrupt transformations with hysteretic behavior are expected for systems with strong intermolecular interactions.

An interesting series of spin crossover compounds are bis-chelated Fe^{II} complexes of tridentate ligands based on 2,6-bis(pyrazol-1-yl)pyridine (1-bpp), which can be functionalized at its periphery with a variety of substituents.[4] The spin change in these materials is usually very abrupt and takes place with thermal hysteresis close to room temperature.[5] In addition, $[Fe(1\text{-}bpp)_2]^{2+}$ salts have the advantage of exhibiting spin-

crossover induced by irradiation: light-induced excited spin state trapping effect (LIESST)[6] at high temperatures with relatively long lifetimes of the photoinduced metastable states.[7] Substitution on the pyridine ring allows functional groups to be included at the periphery of the $[Fe(1\text{-}bpp)_2]^{2+}$ center without significantly perturbing the Fe^{II} center.[8] This approach has afforded spin-crossover compounds with a variety of different pendant functionalities, coordination polymers or complexes for deposition on surfaces.[9,10,11,12,13,14] In an attempt to improve these results, we have added a carboxylate group to this ligand (bppCOOH, see Scheme 1). The well-known coordination capability of the carboxylate ligand could enable binding to metal ions or grafting on metal oxide surfaces, which are essential steps for the preparation of devices based on the spin-crossover phenomenon.[15] As a first step in this direction, herein we present the synthesis, and structural and magnetic characterization of the $[Fe^{II}(bppCOOH)_2](ClO_4)_2$ compound.

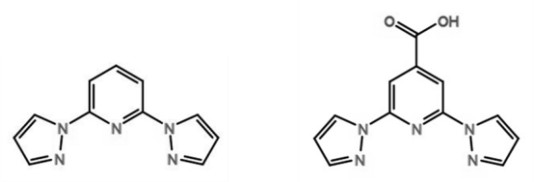

Scheme 1. Molecular structure of the 1-bpp (left) and bppCOOH (right) ligands.

Results and Discussion

Synthesis

Slow diffusion of diethyl ether on the mixture solution of $Fe(ClO_4)_2{\cdot}xH_2O$ and bppCOOH in a 1 : 2 molar ratio in acetone yielded crystals of compound $[Fe(bppCOOH)_2](ClO_4)_2$.

Structure

The structure of the compound was revealed by single crystal X-ray diffraction at 120 K and confirmed by the powder X-ray diffraction pattern (Figure S1, ESI†). It

crystallizes in a monoclinic crystal system with the centrosymmetric *C*2/*c* space group. The asymmetric unit is composed of half of the $[Fe(bppCOOH)_2]^{2+}$ cation (Figure 1) and one perchlorate anion. The central Fe^{II} ion of the complex is coordinated by six nitrogen atoms from two tridentate bppCOOH ligands with a distorted octahedral coordination geometry close to the ideal D_{2d} symmetry associated to a $[Fe(1\text{-}bpp)_2]^{2+}$ center (trans-N(pyridyl)–Fe–N(pyridyl) angle (ϕ) of 180° and dihedral angle between the least squares planes of the two ligands (θ) of 87°). Fe–N bond lengths are in the range 1.888(4)–1.981(2) Å, typical of LS Fe–N lengths for this type of ligand.9 Neighboring $[Fe(bppCOOH)_2]^{2+}$ cations are linked through hydrogen bonds between the carboxylate groups ($d_{O1\cdots O3}$ = 2.671 Å, Figure 2), forming a chain that runs along the *b* axis. These chains are linked through intermolecular interactions that involve the pyrazole groups and the carboxylate groups of neighboring molecules giving rise to layers of complexes on the *bc* plane separated by layers of perchlorate anions (Figure S2, ESI†). Finally, $[Fe(bppCOOH)_2]^{2+}$ complexes of neighboring layers present short contacts involving CH groups of the pyrazole rings (Figure S2, ESI†). The presence of the carboxylate groups causes packing which is different to that found in many salts of $[Fe(1\text{-}bpp)_2]^{2+}$ and derivatives. This is the so called "terpyridine embrace" crystal packing motif, a four-fold layer formed by π–π and edge-to-face C–X⋯π interactions between pyrazole groups of neighboring molecules, which leads to a face-to-face configuration of the pyrazole groups with intermolecular distances of between 3.4 and 3.6 Å.[16] In contrast to this, in our compound the shortest intermolecular contacts of the pyrazole groups are with the carboxylate oxygen atoms of a complex belonging to a neighboring chain (Figure S2, ESI†).

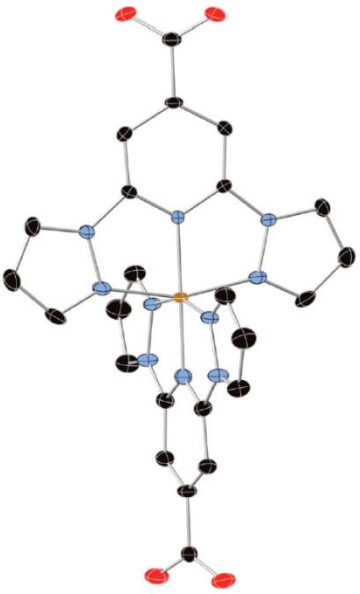

Figure 1. X-ray structure of the complex $[Fe^{II}(bppCOOH)_2]^{2+}$ (C(black), N(blue), O(red) and Fe(yellow)) (hydrogen atoms omitted for clarity).

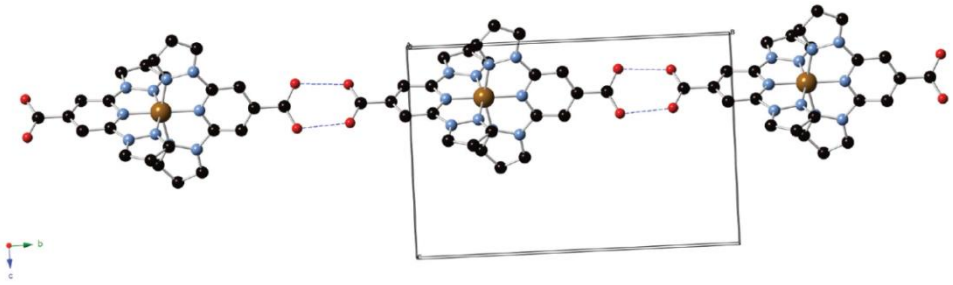

Figure 2. Supramolecular 1D hydrogen-bonded chain structure of the complex $[Fe^{II}(bppCOOH)_2](ClO_4)_2$. The counter ions and hydrogen atoms are omitted for clarity.

Magnetic properties

The temperature dependence of the magnetic susceptibility of the compound was studied in heating and cooling modes. In the temperature range 2–370 K, the product of the molar magnetic susceptibility times the temperature, $\chi_M T$ (Figure 3), shows a

value close to 0, typical of a diamagnetic LS state (S = 0). Above this temperature, there is a sharp increase to a saturated HS value of 3.3 cm^3 K mol^{-1}, which corresponds to 100% of Fe^{II} in the HS state (S = 2). This is consistent with the structure solved at 120 K which shows distances typical of LS Fe^{II}. The same behavior is observed in heating and cooling modes with a small thermal hysteresis of 3 K ($T_{1/2}\uparrow$ = 384 K and $T_{1/2}\downarrow$ = 381 K, with $T_{1/2}$ = temperature of 50% HS → LS conversion). The presence of a thermal hysteresis loop clearly demonstrates the existence of a significant level of cooperativity probably due to the presence of intermolecular interactions mediated by the hydrogen-bonds between neighboring $[Fe(bppCOOH)_2]^{2+}$ complexes. A similar cooperative behavior has been observed for $[Fe^{II}(L)_2H](ClO_4)_3 \cdot MeOH$ (L = 4′-(4‴-pyridyl)-1,2′:6′1″-bis(pyrazolyl)pyridine), which also contains hydrogen-bonded chains of complexes.[17] Finally, it is worth mentioning that the $T_{1/2}$ of this complex is noticeably higher than that of the unsubstituted 1-bpp Fe^{II} complex (260 K)[18] but similar to that of other 1-bpp Fe^{II} complexes with substituents in the fourth position of the pyridine ring[5,9,13,19,20] or 2,6-bis(pyrazol-3-yl)pyridine (3-bpp) Fe^{II} complexes.[21]

In the heating mode the differential scanning calorimetry (DSC) measurement exhibited an endothermic peak centered at 383 K which corresponds to the LS to HS transition. Upon cooling an exothermic peak centered at 381 K was observed and could be assigned to the HS to LS transition, in good agreement with the magnetic measurements (Figure S3 and Table S2, ESI†).

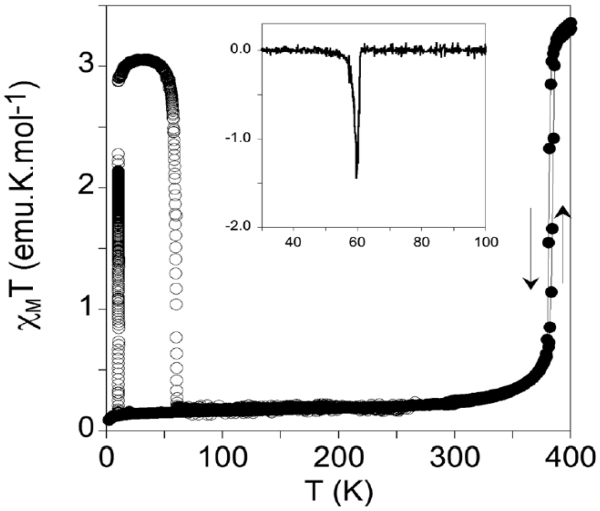

Figure 3. Thermal variation of $\chi_M T$ for $[Fe^{II}(bppCOOH)_2](ClO_4)_2$. Full circles: data recorded in the cooling and heating modes without irradiation; empty circles: data recorded after irradiation at 10 K. The inset graph shows the temperature dependence of the first derivative of $\chi_M T$ with respect to the temperature.

For the photomagnetic measurements the compound was irradiated with green light (λ = 532 nm, optical power 3.4 mW cm^{-2}) at 10 K in a SQUID magnetometer. A drastic increase of the magnetic signal was observed. After about two hours, the irradiation was switched off. The temperature was then increased at a rate of 0.3 K min^{-1} and the magnetic susceptibility recorded. The $\chi_M T$ value after irradiation was higher than the value recorded in the dark at temperatures below 60 K (Figure 3, empty circles). The fraction of Fe^{II} photoconverted after irradiation was calculated to be 90%. The LIESST temperature (T_{LIESST}), defined as the minimum of the derivate of $\chi_M T$ with temperature, is 60 K. This value can be compared with those previously obtained for other 1-bpp compounds. Létard *et al.* have shown that a linear correlation between the thermal spin crossover temperature and T_{LIESST} holds generally for Fe^{II} complexes. In particular, for the $Fe(1\text{-}bpp)_2$ family, the two physical quantities may be related by the formula: $T_{LIESST} = T_0 - 0.3\ T_{1/2}$, with T_0 = 150 K.[7b,16] Taking $T_{1/2}$ = 382 K as the mean value of $T_{1/2}\uparrow$ and $T_{1/2}\downarrow$, a T_{LIESST} of 35.4 K is expected (well below the

observed one of 60 K). Interestingly, the other Fe(1-bpp)$_2$ derivative with a high $T_{1/2}$ showing LIESST effect is the [Fe(L)$_2$](BF$_4$)$_2$ complex (L = 2,6-bis(4-iodopyrazol-1-yl)pyridine) with a reported $T_{1/2}$ > 360 K and an experimental T_{LIESST} of 54 K.[16] Therefore, there is a reasonable agreement between the data of the two compounds. Further studies needed to understand the photomagnetic behavior of this compound (structure and relaxation kinetics of the photoinduced metastable state) are in progress.

Conclusion

In conclusion, we have demonstrated that the functionalization of the 1-bpp ligand with a carboxylate group is a suitable strategy for the preparation of new spin-crossover complexes. The presence of a carboxylate group linked to this spin-crossover complex makes it a useful synthon for the preparation of polynuclear metal complexes, polymers (metal–organic frameworks, MOFs) or for anchoring to metal-oxide surfaces/nanostructures. The preliminary results obtained by us show that some of these goals are possible. Thus, reaction of [Fe(bppCOOH)$_2$]$^{2+}$ complex with Fe^{3+} ions gives rise to a nonanuclear cluster formed by an iron trimer coordinated to six partially deprotonated [Fe(bppCOOH)$_2$]$^{2+}$ units. Furthermore X-ray photoelectron spectroscopy (XPS) measurements of a glass substrate covered with Al_2O_3 that has been immersed into an acetonitrile solution of [Fe(bppCOOH)$_2$](ClO$_4$)$_2$ confirm the deposition of the complex.

Acknowledgements

The authors thank the European Union (Project HINTS and ERC Advanced Grant SPINMOL), the Spanish MINECO (Project Consolider-Ingenio in Molecular Nanoscience CSD2007-00010, and projects MAT2011-22785 and CTQ-2011-26507) and the Generalitat Valenciana (Prometeo and ISIC-NANO Programs) for financial support. The authors also thank J. M. Martínez-Agudo and Dr G. Agustí-López, University of Valencia, for magnetic measurements.

Notes and references

[1] (a) O. Kahn and C. Jay Martinez, *Science* 1998, **279**, 44; (b) J. F. Létard, P. Guionneau and L. Goux-Capes, *Top. Curr. Chem.* 2004, **235**, 221; (c) T. Mahfoud, G. Molnar, S. Cobo, L. Salmon, C. Thibault, C. Vieu, P. Demont and A. Bousseksou, *Appl. Phys. Lett.* 2011, **99,** No. 053307; (d) D. Aravena and E. Ruiz, *J. Am. Chem. Soc.* 2012, **134**, 777; (c) N. Baadji and S. Sanvito, *Phys. Rev. Lett.* 2012, **108,** 217201.

[2] See for general reviews: *Spin Crossover in Transition Metal Compounds, Topics in Current Chemistry*, eds. P. Gütlich and H.A. Goodwin, Springer Verlag, Berlin, Heidelberg, New York, 2004, vols. *233-235*; *Spin-Crossover Materials: Properties and Applications*, ed. M. A. Halcrow, Wiley, 2013, ISBN: 978-1-119-99867-9.

[3] P. Gütlich, A. Hauser and H. Spiering, *Angew. Chem. Int. Ed. Engl*. 1994, **33**, 2024.

[4] M. A. Halcrow, *Coord. Chem. Rev.* 2005, **249**, 2880.

[5] M. A. Halcrow, *Coord. Chem. Rev.* 2009, **253**, 2493.

[6] (a) S. Decurtins, P. Gütlich, C. P. Köhler, H. Spiering and A. Hauser, *Chem. Phys. Lett.* 1984, **105**, 1; (b) S. Decurtins, P. Gütlich, K. M. Hasselbach, A. Hauser and H. Spiering, *Inorg. Chem.* 1985, **24**, 2174.

[7] (a) T. Buchen, P. Gütlich, K. H. Sugiyarto and H. A. Goodwin, *Chem. Eur. J.* 1996, **2,** 1134; (b) S. Marcen, L. Lecren, L. Capes, H. A. Goodwin and J. F. Létard, *Chem. Phys. Lett*. 2002, **358**, 87; (c) G. Chastanet, C. A. Tovee, G. Hyett, M. A. Halcrow and J. F. Létard, *Dalton Trans.* 2012, **41,** 4896.

[8] T. D. Roberts, M. A. Little, L. J. K. Cook, S. A. Barrett, F. Tuna and M. A. Halcrow, *Polyhedron* 2013, **64**, 4.

[9] C. Rajadurai, O. Fuhr, R. Kruk, M. Ghafari, H. Hahn and M. Ruben, *Chem. Commun.* 2007, 2636.

[10] M. Nihei, L. Han and H. Oshio, *J. Am. Chem. Soc.* 2007, **129**, 5312-5313.

[11] C. A. Tovee, C. A. Kilner, S. A. Barrett, J. A. Thomas and M. A. Halcrow, *Eur. J. Inorg. Chem*. 2010, 1007.

[12] R. González-Prieto, B. Fleury, F. Schramm, G. Zoppellaro, R. Chandrasekar, O. Fuhr, S. Lebedkin, M. Kappes and M. Ruben, *Dalton Trans.* 2011, **40**, 7564.

[13] K. Takahashi, Y. Hasegawa, R. Sakamoto, M. Nishikawa, S. Kume, E. Nishibori and H. Nishihara, *Inorg. Chem.* 2012, **51**, 5188.

[14] M. S. Alam, M. Stocker, K. Gieb, P. Müller, M. Harvono, K. Student and A. Grohmann, *Angew. Chem. Int. Ed.* 2010, **49**, 1159.

[15] (a) C. Shen, M. Harvono, A. Grohmann, M. Buck, T. Weidner, N. Ballay and M. Zharkinov, *Langmuir* 2008, **24**, 12883; (b) A. Bousseksou, G. Molnár, L. Salmon and N. Nicolazzi, *Chem. Soc. Rev.* 2011, **40**, 3313.

[16] R. Pritchard, H. Lazar, S. A. Barrett, C. A. Kilner, S. Asthana, C. Carbonera, J. F. Létard and M. A. Halcrow, *Dalton Trans.* 2009, 6656.

[17] C. Rajadurai, R. Kruk, F. Schramm, S. Brink, O. Fuhr, M. Ghafari, R. Kruk and M. Ruben, *Inorg. Chem.* 2006, **45**, 10019.

[18] J. M. Holland, J. A. McAllister, Z. Lu, C. A. Kilner, M. Thornton-Pett and M. A. Halcrow, *Chem. Commun.* 2001, 577.

[19] M. Nihei, T. Maeshima, Y. Kose and H. Oshio, *Polyhedron* 2007, **26**, 1993.

[20] I. Salitros, O. Fuhr, A. Eichhöfer, R. Kruk, J. Pavlik, L. Dlhán, R. Boca and M. Ruben, *Dalton Trans.* 2012, **41**, 5163

[21] I. A. Gass, S. R. Batten, G. M. Forsyth, B. Moubaraki, C. J. Schneider and K. S. Murray, *Coord. Chem. Rev.*, 2011, **255**, 2058.

Associated Content:

Electronic Supplementary Information (ESI) for Dalton Transactions

Experimental section

2,6-dibromoisonicotinic acid and the 2,6-di(1H-pyrazol-1-yl)isonicotinic acid (bppCOOH) were prepared according to the literature methods.[1] All other chemicals are commercially available and were used as received without further purification.

Synthesis of $[Fe(bppCOOH)_2](ClO_4)_2$.

A solution of $Fe(ClO_4)_2,xH_2O$ (25 mg, 0.10 mmol) in acetone (2 mL) was added to a solution of bppCOOH (57 mg, 0.20 mmol) in acetone (10 mL) and the mixture was stirred for 15 minutes. Red prismatic crystals of $[Fe(bppCOOH)_2](ClO_4)_2$ suitable for X-ray diffraction were obtained by slow diffusion of diethyl ether into this solution. The composition of crystals of $[Fe(bppCOOH)_2](ClO_4)_2$, checked by microanalysis, shows a Fe:Cl ratio close to 1:2.

Structural characterization.

A single crystal of $[Fe(bppCOOH)_2](ClO_4)_2$ was mounted on a glass fibre using a viscous hydrocarbon oil to coat the crystal and then transferred directly to the cold nitrogen stream for data collection. X-ray data were collected at 120 K on a Supernova diffractometer equipped with a graphite-monochromated Enhance (Mo) X-ray Source (λ = 0.71073 Å). The program CrysAlisPro, Oxford Diffraction Ltd., was used for unit cell determinations and data reduction. Empirical absorption correction was performed using spherical harmonics, implemented in the SCALE3 ABSPACK scaling algorithm. Crystal structure was solved by direct methods with the SIR97 program,[2] and refined against all F^2 values with the SHELXL-97 program,[3] using the WinGX graphical user interface.[4] Non-hydrogen atoms were refined anisotropically, and hydrogen atoms were placed in calculated positions refined using idealized geometries (riding model)

and assigned fixed isotropic displacement parameters. A summary of the data collection and structure refinements is provided in Table 1. A 0.5 mm glass capillary was filled with a polycrystalline sample of $[Fe(bppCOOH)_2](ClO_4)_2$ and mounted and aligned on a Empyrean PANalytical powder diffractometer, using CuKα radiation (λ = 1.54177 Å). A total of 2 scans were collected at room temperature in the 2θ range 5-40°.

Physical characterizations.

The Fe:Cl ratios were measured on a Philips ESEM X230 scanning electron microscope equipped with an EDAX DX-4 microsonde.

Differential scanning calorimetry (DSC) measurements under nitrogen atmosphere were performed in a Mettler Toledo DSC 821e apparatus with warming and cooling rates equal to 5 $K \cdot min^{-1}$. A correction from the sample holder was automatically applied. The heat flow thus measured ($\Delta H/\Delta t$) was used in the calculation of the approximate specific heat function as follows:

$$\frac{\Delta H}{\Delta T} = \frac{\Delta H}{\Delta t} \cdot \frac{M}{\beta \cdot m}$$

where *m* is the mass of the sample, *M* its molecular weight and *b* the heating (cooling) rate.

Magnetic measurements were performed with a Quantum Design MPMS-XL-5 SQUID magnetometer in the 2 to 400 K temperature range with an applied magnetic field of 0.1 T at a scan rate of 1 $K.min^{-1}$ on a polycrystalline sample with a mass of 18.07 mg. Photomagnetic measurements were performed irradiating with a Diode Pumped Solid State Laser DPSS-532-20 from Chylas coupled *via* an optical fibre to the cavity of the SQUID magnetometer. The optical power at the sample surface was adjusted to 3.4 $mW.cm^{-2}$, and it was verified that it resulted in no significant change in magnetic response due to heating of the sample. The photomagnetic samples consisted of a thin layer of compound whose weight was obtained by comparison of a thermal spin

crossover curve with that of a more accurately weighted sample of the same compound.

Table S1. Crystallographic data for $[Fe(bppCOOH)_2](ClO_4)_2$.

Formula	$FeC_{24}H_{18}N_{10}O_{12}Cl_2$
M_r	765.23
Crystal size	0.03*0.03*0.02
T /K	120
Crystal system	Monoclinic
Space group	$C2/c$
a /Å	17.2679(8)
b /Å	16.0585(6)
c /Å	10.7907(5)
α /º	90.000(5)
β /º	105.264(5)
γ /º	90.000(5)
V /Å^3	2886.7(2)
Z	4
ρ_{calc} /g.cm^{-3}	1.761
$\mu(Mo_{K\alpha})$ /mm^{-1}	0.793
Reflns collected	3312
Independent reflns	2368
$R1(F)$,[a] I >2σ(I)	0.0517
$wR2(F^2)$,[b] all data	0.1171

[a] $R = \sum||F_o| - |F_c||/\sum|F_o|$. [b] $R_w = \{\sum[w(|F_o| - |F_c|)]^2/\sum[w|F_o|^2]\}^{1/2}$

Table S2. DSC data for $[Fe(bppCOOH)_2](ClO_4)_2$.

T (K)	ΔH (KJ.mol^{-1})	ΔS (J.mol^{-1}.K^{-1})
383	18.9	45.3
381	17.2	44.9

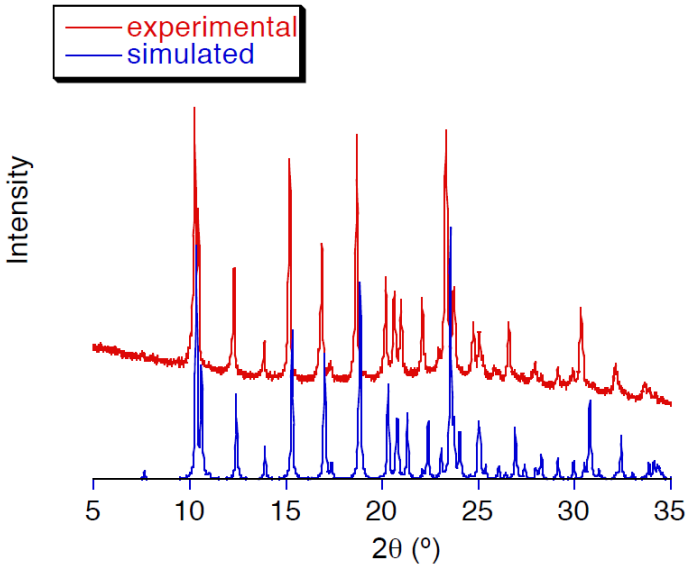

Figure S1. Experimental powder X-ray diffraction pattern (top) and simulated one (bottom) of $[Fe(bppCOOH)_2](ClO_4)_2$ at room temperature.

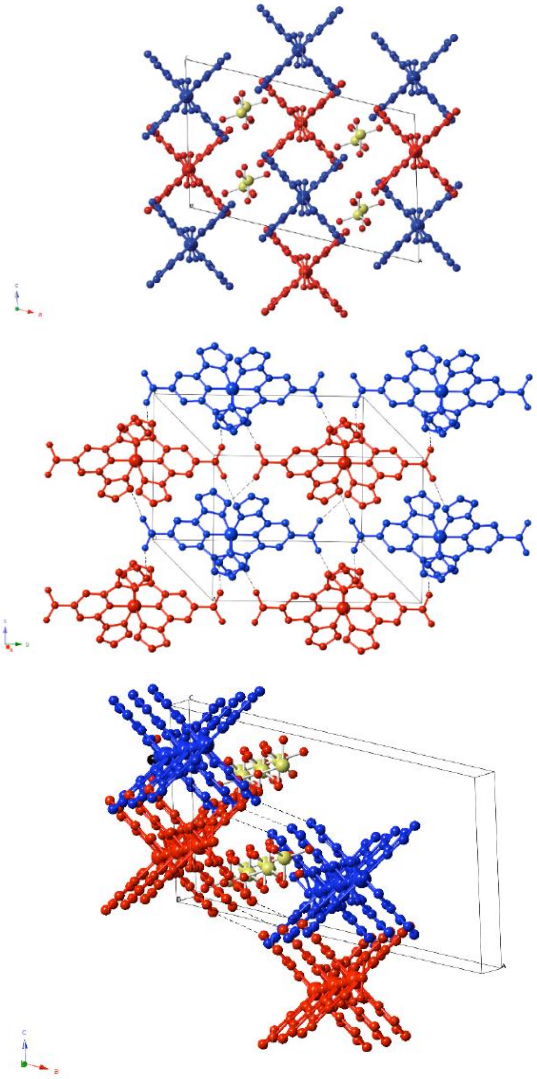

Figure S2. Projection of the structure of $[Fe(bppCOOH)_2](ClO_4)_2$ in the *ac* plane with the $[Fe(bppCOOH)_2]^{2+}$ belonging to the same hydrogen-bonded chain colored in red or blue (top); view of a layer of $[Fe(bppCOOH)_2]^{2+}$ complexes with the intermolecular interactions between complexes belonging to different hydrogen-bonded chains as dashed lines (center); view of two layers of $[Fe(bppCOOH)_2]^{2+}$ complexes with the intermolecular interactions between complexes belonging to different layers as dashed lines (bottom).

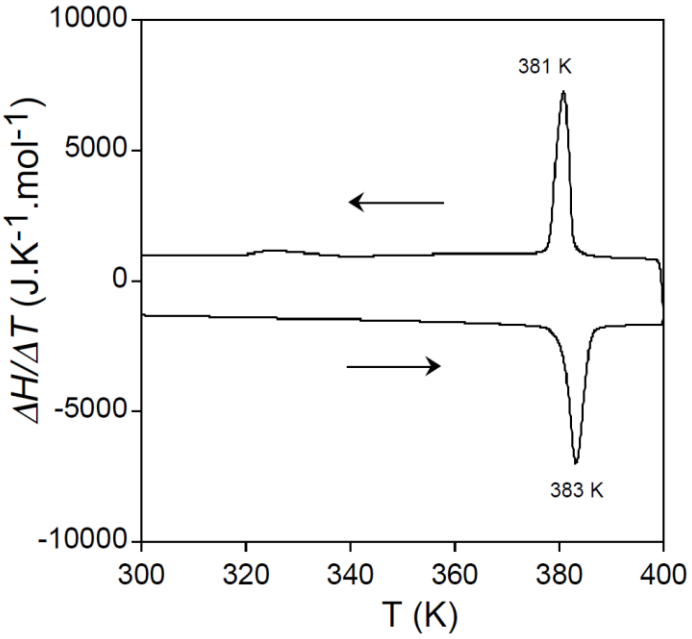

Figure S3. Differential scanning calorimetry of $[Fe(bppCOOH)_2](ClO_4)_2$: The corresponding thermodynamic parameters are gathered in Table S2.

---

[1] (a) R.-A. Fallahpour, *Synthesis* 2000, **8**, 1138; (b) T. Vermonden, D. Branowska, A. T. M. Marcelis and E. J. R. Sudhölter, *Tetrahedron* 2003, **59**, 5039.

[2] A. Altomare, M. C. Burla, M. Camalli, G. L. Cascarano, C. Giacovazzo, A. Guagliardi, A. G. G. Moliterni, G. Polidori and R. Spagna, *J. Appl. Cryst*. 1999, **32**, 115.

[3] G. M. Sheldrick, *Acta Cryst.* 2008, **A64,** 112.

[4] L. J. Farrugia, *J. Appl. Cryst.* 2012, **45**, 849.

Field-Induced Slow Relaxation of Magnetization in Mn^{III} Anderson POMs and their Functionalization with 2,6-bis(pyrazol-1-yl)pyridine (1-bpp)

Chapter 3

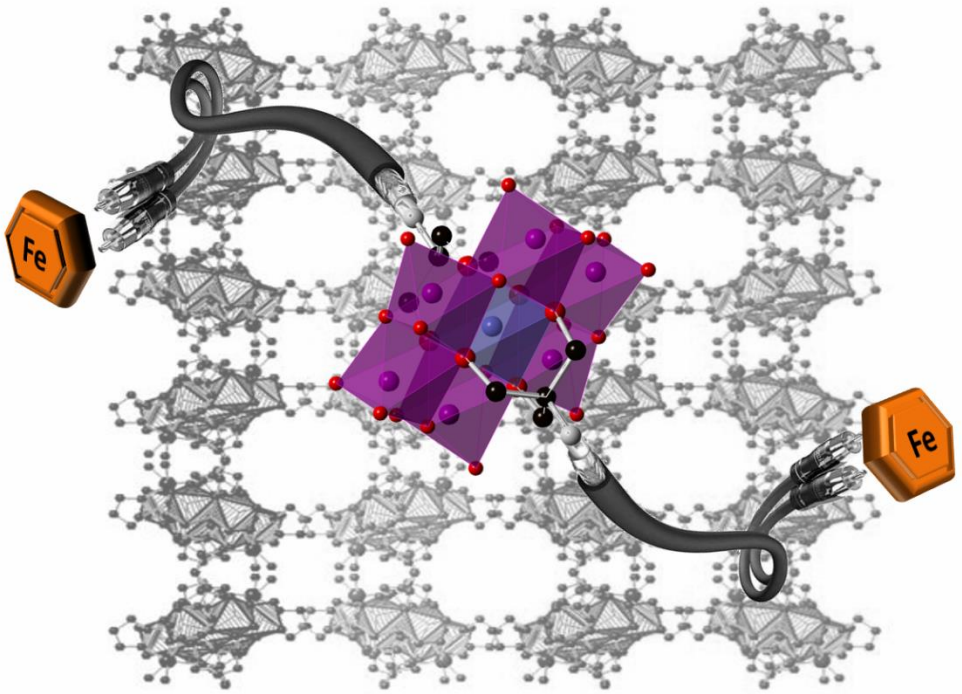

Chapter 3. Field-Induced Slow Relaxation of Magnetization in Mn^{III} Anderson POMs and their Functionalization with 2,6-bis(pyrazol-1-yl)pyridine (1-bpp).

Abstract

The synthesis and crystal structure of the Anderson POM functionalized with 2,6-bis(pyrazol-1-yl)pyridine (1-bpp) ligand are reported. The resulting compound can be formulated as $(C_{16}H_{36}N)_3[MnMo_6O_{24}(C_{16}H_{15}N_6O)_2]\cdot(C_4H_9NO)_2\cdot(H_2O)_{2.5}$ (**1**). High-field electron paramagnetic resonance (HF-EPR) and alternating-current (AC) susceptibility measurements show that **1** presents a significant negative axial zero-field splitting and field-induced slow relaxation of magnetization due to the presence of isolated Mn^{III} anisotropic magnetic ions. Complexation with Fe^{II} of **1** gives rise to a 2D cationic network of formula $[Fe(H_2O)(C_3H_7NO)]_2[MnMo_6O_{24}(C_{16}H_{15}N_6O)_2](OH)\cdot(H_2O)\cdot(C_3H_7NO)_3$ (**2**) and an anionic 1D polymeric network of formula $(C_{16}H_{36}N)[Fe(MnMo_6O_{24}(C_{16}H_{15}N_6O)_2)]\cdot(H_2O)_4$ (**3**). Crystal structure of **2** has been solved. Magnetic properties of **3** shows that Fe^{II} remains in the LS state, while that of **2** remains in the HS state due to coordination to oxygens from a neighboring POM and dimethylformamide and water solvent molecules. Finally, AC susceptibility measurements of **2** and $(C_{16}H_{36}N)_3[MnMo_6O_{18}\{(OCH_2)_3CNH_2\}_2]$ (**4**) confirm field-induced slow relaxation of magnetization of Mn^{III} Anderson POMs.

Introduction

Polyoxometalates (POMs) are a family of molecular-metal oxides. Thanks to their structural versatility, their electronic behavior can be modulated chemically. This results in a rich landscape of magnetic, catalytic, and redox properties, which, together with their chemical robustness, are currently attracting particular interest in areas like catalysis, medicine, molecular magnetism and molecular spintronics.[1,2] To further extend these applications, they have been extensively combined with organic donors

and transition metal complexes to form hybrid multifunctional materials. A rational approach to design this type of materials is the functionalization of POMs with organic ligands that are then linked to transition metal ions via a well-defined coordination bond.[3] This strategy is an effective approach, which affords rationally designed, predictable and consistent POM-based structures with interesting properties.[4] One of the most successful strategies is the tris-alkoxo-amide tripodal functionalization of POMs. With this strategy, a large variety of organic ligands have been incorporated into Lindqvist, Anderson and Dawson structures, which have been in some cases linked to metal ions. Some examples are the coordination polymers of hexavanadates coordinated to Mn^{II}, Co^{II}, Ni^{II} and Zn^{II} [5] or Tb^{III} ions[6] and the formation of Anderson, Dawson and Lindqvist structures functionalized with metalloporphyrins.[7,8.9] Other discrete or polymeric complexes have been obtained from tris-alcoxo-pyridyl ligands of various denticity (pyridyl,[10] bipyridyl[11,12] and terpyridine[13]). In the case of tridentate ligands, the terpyridine-functionalized Anderson and Dawson POMs coordinated to $\{PdCl\}^{+}$ and $\{RuCl_3\}$ moieties respectively have been reported.[13]

In this work, we have incorporated another tridentate ligand, 2,6-bis(pyrazol-1-yl)pyridine (1-bpp) (Scheme 1) into an Anderson POM in the search of functionalized magnetic POMs. The formation of coordination complexes with this 1-bpp functionalized POM could lead to other properties of interest. Indeed, Fe^{II} complexes of 1-bpp have been extensively studied for spin-crossover research as the spin change with temperature in these materials is usually very abrupt and takes place with thermal hysteresis close to room temperature.[14,15] Furthermore, these complexes have the advantage of exhibiting spin-crossover induced by irradiation (light-induced excited spin state trapping effect, LIESST) at high temperatures with relatively long lifetimes of the photoinduced metastable states.[15b] In addition to this, *d* metal (Ru^{II} and Pt^{II}) and lanthanoid complexes of 1-bpp derivatives are luminescent in solution or in the solid state and have been used as dyes for dye-sensitised solar cells (DSCs).[16]

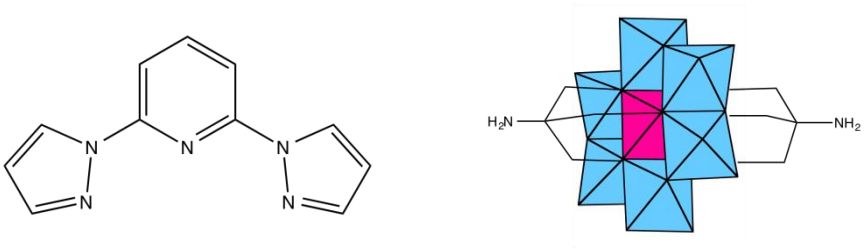

Scheme 1. Molecular structure of 1-bpp (left) and **4** (right).

In this chapter, we report the synthesis, structure and spectroscopic characterization of the 1-bpp-functionalized Anderson POM $(C_{16}H_{36}N)_3[MnMo_6O_{24}(C_{16}H_{15}N_6O)_2]\cdot(C_4H_9NO)_2\cdot(H_2O)_{2.5}$ (**1**), which presents a field-induced slow relaxation of magnetization, as shown by magnetic characterization and high-frequency EPR spectra, and the formation of compounds $[Fe(H_2O)(C_3H_7NO)]_2[MnMo_6O_{24}(C_{16}H_{15}N_6O)_2](OH)\cdot(H_2O)\cdot(C_3H_7NO)_3$ (**2**) and $(C_{16}H_{36}N)[Fe(MnMo_6O_{24}(C_{16}H_{15}N_6O)_2)]\cdot(H_2O)_4$ (**3**) by coordination of **1** with Fe^{II}. The structure of **2** and the magnetic properties of **2** and **3** are also reported. Finally, the magnetic properties of one of the simplest Anderson POM with Mn^{III} reported in the literature, the $(C_{16}H_{36}N)_3[MnMo_6O_{18}\{(OCH_2)_3CNH_2\}_2]$ (**4**) compound (Scheme 1),[17] have been measured for the first time as a reference to demonstrate that the field-induced slow relaxation of magnetization is general for this type of structure. We have to take into account that, while unfunctionalized Anderson-type polyoxomolybdates with Mn^{II}, Fe^{III}, Ni^{II}, and Zn^{II} have been reported in the literature,[17] all Mn^{III} Anderson POM structures reported so far correspond to functionalized POMs with a large variety of ligands.

Results and discussion

Syntheses

1-bpp-functionalized Anderson POM (**1**) was synthesized in several steps following adapted literature procedures (Scheme 2). The starting material for the preparation of the functionalized POM was a tris-(hydroxymethyl)-functionalized 1-bpp (TRIS-bpp),

which was obtained from 1-bpp-4´-carboxyethylester. The ester was obtained by esterification with ethanol of the carboxylate 1-bpp derivative (bppCOOH). The functionalization of the POM was performed in dry dimethylacetamide (DMAc). It can also be performed with similar conditions in dry acetonitrile but it gives rise to a less pure product in a lower yield. Single crystals were obtained by slow evaporation of the DMAc solution of the compound. ^{1}H NMR spectra confirm the purity of TRIS-bpp and **1** and the grafting of 1-bpp to the POM in **1** (Figure S1 in the Supporting Information, SI). As observed previously in terpyridine-functionalized Anderson POM,[13] the electronic influence of the cluster (paramagnetic Mn^{III}) induces changes in the chemical shifts of the methylene protons of the ligand but not in those of the aromatic ones. Further characterization of **1** by elemental analysis, IR spectroscopy (Figure S2 in the SI), microanalysis and electrospray ionization mass spectrometry (ESI-MS) is consistent with the bifunctionalization of the POM. Microanalysis shows a Mn/Mo ratio close to 1:6. Figure S3 in the SI shows the ESI-MS (negative mode) analysis of a solution of **1** in acetonitrile. The three most intense peaks appear at m/z values of 543.2, 814.8 and 935.9, which correspond respectively to the $[MnMo_6O_{24}(C_{16}H_{15}N_6O)_2]^{3-}$ ($[\mathbf{1}]^{3-}$), $[(H)MnMo_6O_{24}(C_{16}H_{15}N_6O)_2]^{2-}$ (H^+ + $[\mathbf{1}]^{3-}$) and $[(C_{16}H_{36}N)MnMo_6O_{24}(C_{16}H_{16}N_6O)_2]^{2-}$ (Tetrabutylammonium $(TBA)^+$ + $[\mathbf{1}]^{3-}$) species. The charge of the species present in the spectrum has been unambiguously characterized by single ion recording (SIR) at the highest resolution of the spectrometer with monoisotopic peaks separated by 1/z. Figure S4 in the SI shows the isotopic distributions of the most intense peaks. As these peaks arise from species in which the POM remains intact, we can conclude that the structure of the polyanion is preserved in solution.

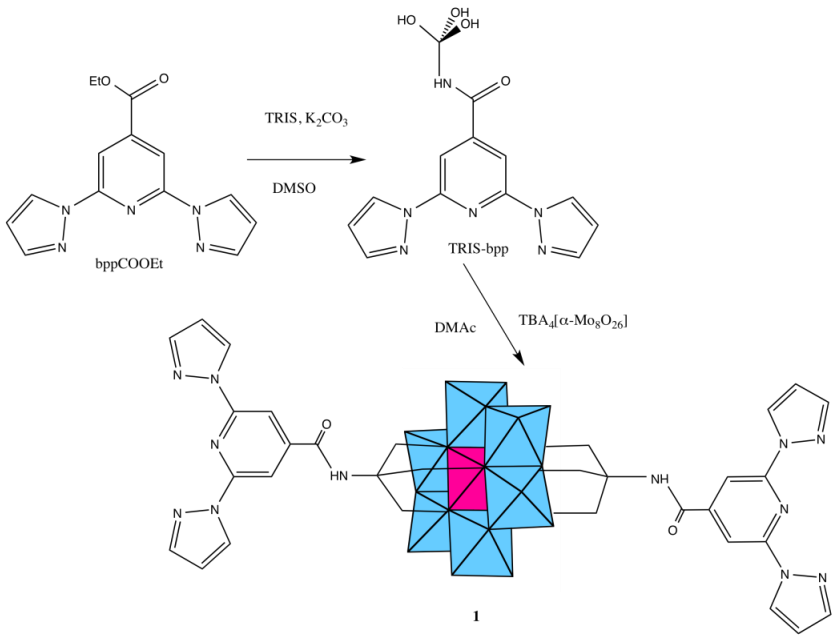

Scheme 2. Synthesis of TRIS-bpp and **1**.

When **1** was reacted with Fe^{II} in acetone or acetonitrile, a precipitate immediately formed, as observed in Lindqvist POM functionalized with terpyridine.[18] The precipitation takes place after the addition of one equivalent of Fe^{2+} to the POM suggesting the formation of a polymeric compound in which every POM is coordinated to two Fe^{II}, which, at the same time, are coordinated to two 1-bpp from two POMs (Scheme 3). Elemental analysis of this precipitate is consistent with the formula $(C_{16}H_{36}N)[Fe(MnMo_6O_{24}(C_{16}H_{15}N_6O)_2)]\cdot(H_2O)_4$ (**3**). Furthermore, microanalysis show a Fe:Mn:Mo ratio close to 1:1:6 and IR spectrum (Figure S2 in the SI) and magnetic properties (see below) are consistent with coordination of two 1-bpp to Fe^{II}. Unfortunately it was not possible to grow single crystals of this compound to solve the structure. If two equivalent of Fe^{II} are added, an orange precipitate is obtained with a Fe:Mn:Mo ratio close to 2:1:6. This could indicate that Fe^{II} are either coordinated to 1-bpp from the POM or act as counterion. This precipitate was partially soluble in polar aprotic solvents such as dimethylsulfoxide (DMSO), DMAc and dimethylformamide (DMF). This dissolution may involve dissociation of the 1-bpp-metal coordination bond

as observed in pyridyl-functionalized hexavanadates.[5] Indeed, recrystallization in DMF of the compound gave rise to polymeric compound **2**, in which octahedral coordination around Fe^{II} is completed with DMF and water solvent molecules and oxo groups from neighboring POM (see below). The presence of DMF and water molecules coordinated to the M^{II} (Mn, Co, Ni, Zn) metals has also been observed in pyridyl-functionalized hexavanadates.[5]

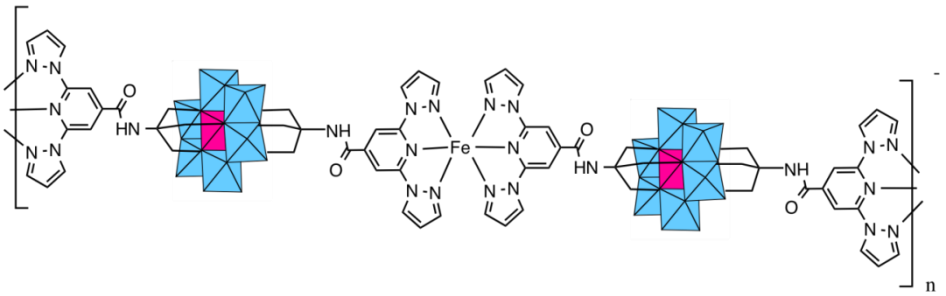

3

Scheme 3. Proposed structure for the polymeric network of **3**.

Structure

1 crystallizes in the monoclinic space group $P2_1/n$. The asymmetric unit is composed by two half crystallographically independent anions, three TBA^+ cations, two DMAc solvent molecules and water molecules that present some disorder. The two crystallographically independent anions contain an inversion center placed in the Mn. They present the common Anderson POM structure with six MoO_6 octahedral edge-sharing units forming a hexagon around the central MnO_6 octahedron. As both alkoxo ligands from the 1-bpp ligand are directly linked to the Mn^{III} ion, this corresponds to the δ isomer of the Anderson structure (Figure 1).[19] All metal atoms essentially lie in a common plane, with a maximum deviation of 0.003 Å from the best least-squares plane for the cluster with Mn1 and 0.02 Å for that with Mn2. The octahedral coordination geometry of the central Mn^{III} ion is quite regular, with three Mn-O distances of 1.961(3), 1.977(3) and 2.014(3) Å for Mn1 and 1.913(3), 2.019(3) and 2.022(3) Å for Mn2, and cis-O-Mn-O bond angles comprised between 87.00(10)° and

93.00(11)° and trans-O-Mn-O angles of 180° due the presence of an inversion center in Mn. In contrast to previous Mn^{III} complexes exhibiting a slow relaxation of magnetization, the coordination sphere around Mn^{III} does not exhibit a marked tetragonal distortion.[20] It should be noted that the rigidity of the POM framework prevents the Mn^{III} ion from undergoing marked Jahn-Teller distortions. Due to this, the coordination octahedron is only very slightly elongated (Mn1) or compressed (Mn2). The small distortions observed correspond to a slight compression of the octahedron, bringing the two faces capped by the organic ligands closer together, as in other Mn^{III} Anderson POMs.[17,19] Indeed, distances between these two faces of the octahedron (2.186-2.189 Å) are much shorter than those between other faces (2.312-2.338 Å). The two crystallographically independent POMs present a different orientation. They are surrounded by TBA^+ cations and solvent molecules (Figure S5 in the SI). The shortest distance between Mn^{III} belonging to different POMs is 14.317 Å. Hydrogen bonds are observed between the terminal oxo groups of the POM and water molecules. Furthermore, the NH groups of the two POMs form hydrogen bonds with a DMAc molecule and a water molecule. Powder X-ray diffraction of **1** confirms the structure of the compound (Figure S6 in the SI).

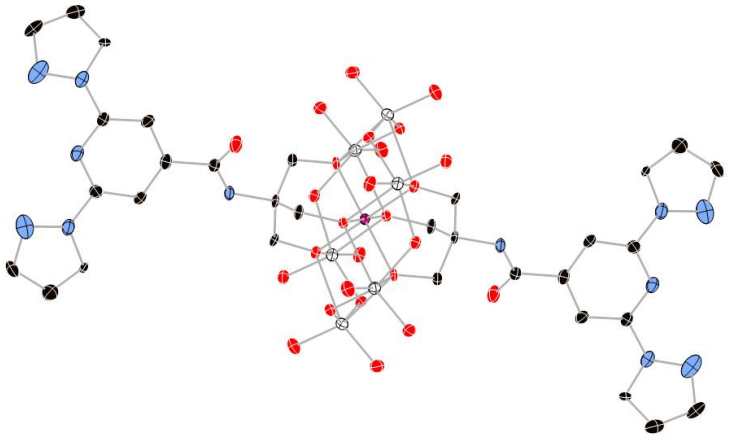

Figure 1. View of the structure of the functionalized-POM in compound **1**. (Mn (pink), Mo (white), C (black), N (blue), O (red)). Hydrogen atoms have been omitted for clarity.

2 crystallizes in the monoclinic space group *C*2/*c*. The asymmetric unit is composed by half crystallographically independent anion and one crystallographically independent Fe coordinated to a DMF and water molecule. Furthermore, it contains half crystallographically independent OH^- and water molecules. The structure of the anion is the same as that of the 1-bpp-functionalized Anderson POM found in **1** with an inversion center placed in Mn, but, in contrast to **1**, it presents a two dimensional (2D) polymeric structure (Figure 2). Thus, each functionalized Anderson POM is coordinated to two Fe^{II} ions through the two tridentate 1-bpp ligands and to other two Fe^{II} ions through two oxo ligands linked to two Mo ions (Mo2). The octahedral coordination around Fe^{II} is completed with one DMF and water solvent molecules and the oxo ligand from a neighboring POM mentioned above. This gives rise to a 2D network in the *bc* plane formed by interconnected $[Fe^{II}(H_2O)(C_3H_7NO)]_2[Mn^{III}Mo^{VI}_6O_{24}(C_{16}H_{15}N_6O)_2]^+$ units (Figure 2). The octahedral coordination geometry of the central Mn^{III} presents three Mn-O distances of 1.906(11), 1.998(11) and 2.034(12) Å, cis-O-Mn-O bond angles comprised between 87.1(5)° and 92.9(5)° and trans-O-Mn-O angles of 180° due the presence of an inversion center in Mn. Fe^{II} presents a more distorted octahedral coordination geometry. The shortest distance is that with the O atom from DMF (1.985(19) Å). Fe-O distances to the water molecule and oxo ligand from POM are intermediate (2.128(16) and 2.206(13) Å), while Fe-N distances to the 1-bpp ligand range from 2.182(16) to 2.224(16) Å. These distances indicate that Fe^{II} is in the high-spin state. A lateral view of two neighboring layers, shown in Figure S7 in the SI, allows distinguishing the microporous channels, which are formed along the crystallographic *c*-axis. These pores are occupied by three disordered DMF solvent molecules (see SI). Beside these DMF molecules, the space between the cationic layers is occupied by water solvent molecules and OH- groups, which are connected through hydrogen bond interactions with NH groups and POM oxo groups from the layers. Hydrogen bond formation agrees with the presence of half crystallographically independent OH^- anion (O200 in Figure S7 in the SI), which counterbalances the positive charge of the 2D layer.

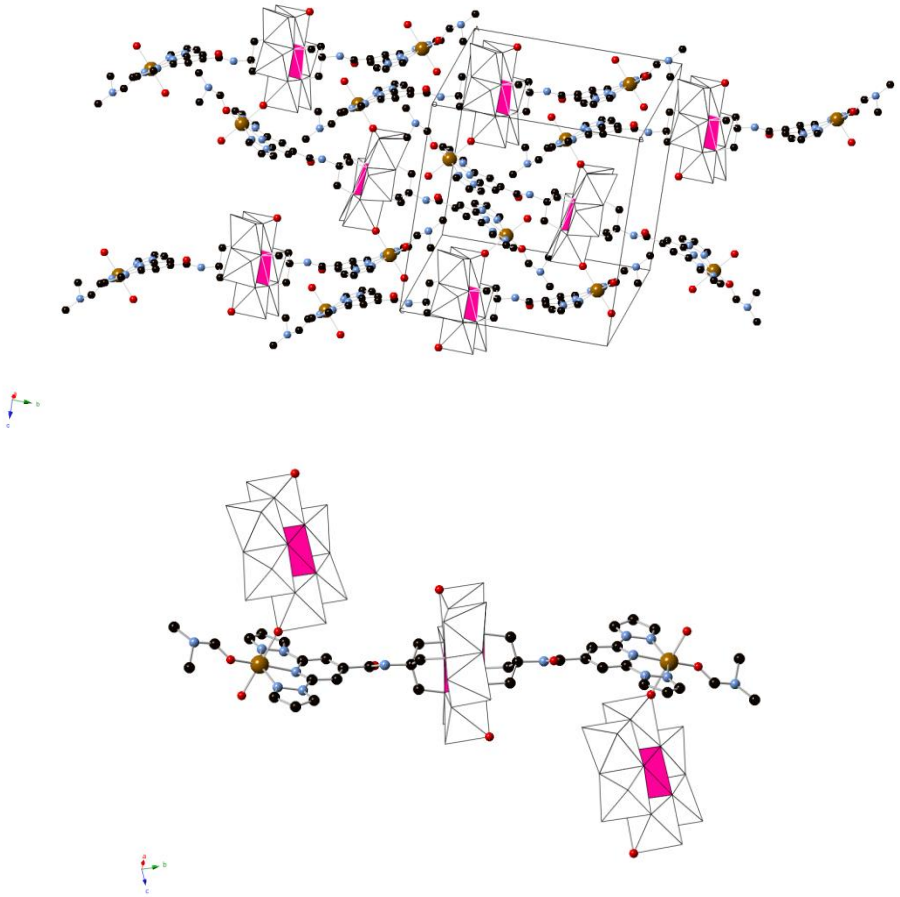

Figure 2. View of a layer of functionalized-POMs linked through Fe^{2+} ions in the structure of **2** (top) and view of the repeating trimeric unit with two coordinated POMs. (Fe (yellow), Mn (pink), Mo (white), C (black), N (blue), O (red)). Red oxygen atoms from the POM are those coordinated to Fe^{2+} ions. Hydrogen atoms have been omitted for clarity.

Magnetic properties

Temperature dependence of the product of the molar magnetic susceptibility times the temperature ($\chi_m T$) of a powdered sample of **1** is shown in Figure 3. $\chi_m T$ value at room temperature (2.9 cm^3 mol^{-1} K) is consistent with an isolated Mn^{III} with S = 2

and g = 2.0. Upon cooling, the $\chi_m T$ value remains constant until 40 K. Below this temperature, there is an abrupt decrease which indicates that there is an appreciable zero-field-splitting as observed in other Mn^{III} mononuclear complexes.[20] This is further confirmed by the isothermal magnetization (M) curves of **1** in the temperature range of 2–10 K, which cannot be superposed at high H/T values (Figure 4). This indicates that there is a strong magnetic anisotropy of the ground state of Mn^{III}. From simultaneous fitting of susceptibility and magnetization data using the Magpack program, a *D* value = -3.24 cm^{-1}, a *E* value = 0 and a g value = 2 have been obtained. A more precise value of the negative axial anisotropy and a rhombic term presence was confirmed by high-field electron paramagnetic resonance (HF-EPR, see below).

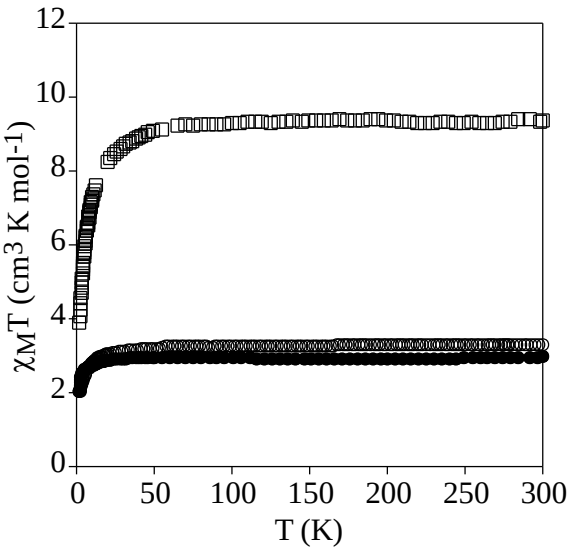

Figure 3. Temperature dependence of $\chi_m T$ of **1** (full circles), **2** (empty squares) and **3** (empty circles).

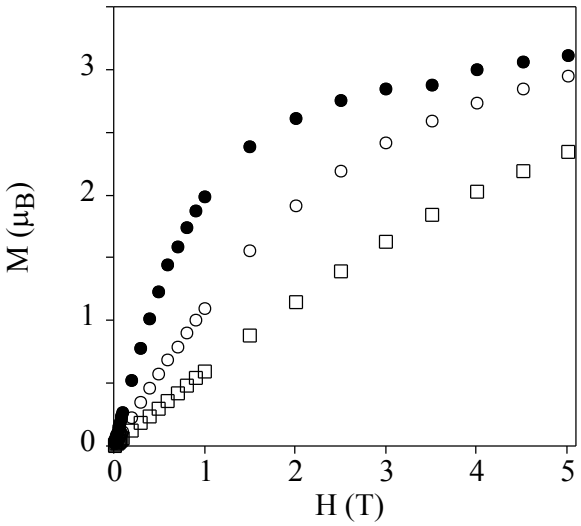

Figure 4. Isothermal magnetization of **1** at 2 K (full circles), 5 K (empty circles) and 10 K (empty squares).

The relaxation properties of **1** were studied by susceptibility measurements performed with an alternating magnetic field (AC susceptibility). In the absence of a magnetic field, no signal in the out of phase molar susceptibility (χ_m") is observed. When a magnetic field of 0.5 T is applied, strong frequency-dependent peaks in both the in phase molar susceptibility (χ_m') and χ_m" appear with clear maxima of χ_m" below 3 K (Figure 5), as observed for other Mn^{III} showing field induced slow relaxation of the magnetization.[20] This is a clear indication that **1** presents a SIM behavior (Figure 5). These maxima appear at lower temperature than those of compound $Ph_4P[Mn(opbaCl_2)(py)_2]$ ($H_4opbaCl_2$ = N,N'-3,4-dichloro-o-phenylenebis(oxamic acid), py = pyridine, and Ph_4P^+ = tetraphenylphosphonium cation) (4 K)[20a] but higher than those of compounds $[Mn^{III}$(5-TMAM(*R*)-salmen)$(H_2O)Co^{III}(CN)_6]\cdot 7H_2O\cdot$MeCN (5-TMAM(*R*)-salmen = (*R*)-*N*,*N*-(1-methylethylene)bis(5-trimethylammoniomethylsalicylideneiminate)[20b] and $[Mn^{III}\{(OPPh_2)_2N\}_3]$[20c] (lower than 2.3 K). On the other hand, the values of the relaxation time, which are calculated from the maximum of χ_m" at a given frequency ($\tau = 1/2\pi\nu$), follow the Arrhenius law

characteristic of a thermally activated mechanism ($\tau = \tau_0 \exp(E_a/k_BT)$). The calculated values of the pre-exponential factor and the activation energy (τ_0 = 3.9 10^{-7} s and E_a = 14.4 cm^{-1}) are consistent with those of the four other Mn^{III} complexes showing this behavior.[20]

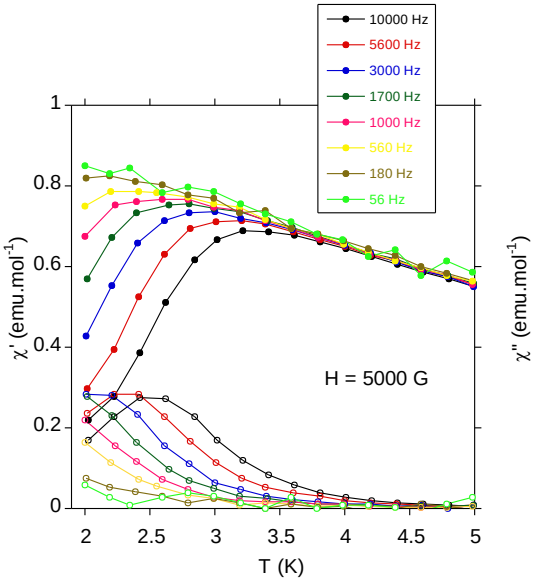

Figure 5. Temperature dependence of the in-phase AC susceptibility (χ_m') (filled symbols) and the out-of-phase AC susceptibility (χ_m") (empty symbols) of **1** under an applied field of 0.5 T.

HF-EPR is a useful technique to study mononuclear Mn^{III} complexes.[21] HF-EPR spectra of a pressed pellet of **1** in eicosane at different temperatures and frequencies (see Table S1 in the SI) are shown in Figures 6 and Figures S8 and S9 in the SI. Simulations of these spectra using the EasySpin simulation software[22] clearly confirm the negative sign of *D*. All simulations were done using the following set of parameters: *D* = -5.24 cm^{-1}, *E* = 0.39 cm^{-1} and g_{iso} = 1.98. Interestingly, the slightly distorted octahedral geometry of Mn^{III} in the Anderson POM gives rise to higher axial zero field splitting parameters than values found in literature for other Mn^{III} complexes presenting a clear tetrahedral elongation of the coordination sphere of Mn^{III},[21]

including those showing a SIM behavior ($D \approx -3.4$ cm^{-1}).[20] On the other hand, the rhombic E-term is slightly lower than most of these complexes ($E \approx 0.5$-0.7 cm^{-1})[20a,b,c] but higher than that found for $Na_5[Mn(L\text{-tart})_2]\cdot 12H_2O$ ($E = 0.032$ cm^{-1}).[20d]

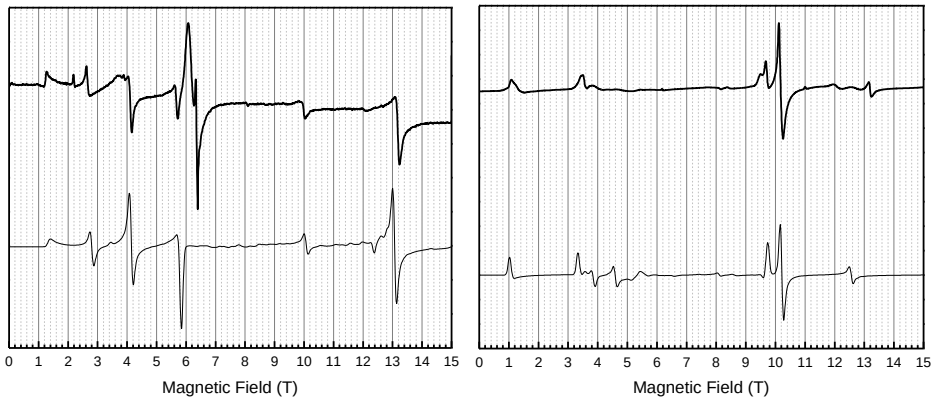

Figure 6. HF-EPR spectra of **1** (bold: experiment, thin: simulation) at 180 GHz (left) and 370 GHz (right) and 10 K. Note that the strong signals at 6.4 T (left) and 13.2 T (right) are at g = 2 and caused by some impurity.

Temperature dependence of $\chi_m T$ of powdered samples of **2** and **3** are shown in Figure 3. $\chi_m T$ values at room temperature (9.4 cm^3 mol^{-1} K for **2** and 3.4 cm^3 mol^{-1} K for **3**) are close to the expected contributions for an isolated Mn^{III} with S = 2 and g = 2.0 plus two Fe^{II} in the LS state for **3** and in the HS state for **2**. These data are consistent with metal-ligand distances in the structure of **2** that indicate that Fe^{II} is in the HS state. This is in agreement with the crystal field splitting caused by the coordination of Fe^{II} with O atoms (N_3O_3 coordination sphere), whose strength is lower than that caused by the N atoms in **3**. In fact, in **3**, Fe^{II} is coordinated to two 1-bpp ligands leading to a LS state of Fe^{II}. Finally, as spin-crossover of other 1-bpp derivatives has been observed at temperatures well above 300 K,[23] $\chi_m T$ of **3** has been measured up to 400 K. Unfortunately, $\chi_m T$ remains close to LS values indicating that no spin-crossover is taking place in this polymer.

The relaxation properties of **2**, **3** and **4** were studied by AC susceptibility

measurements. As in **1,** strong frequency-dependent peaks χ_m' and χ_m" appear under an applied magnetic field of 0.5 T below 3 K. This is a clear indication that field-induced slow relaxation of magnetization is a common feature for this type of structure (Figures 7 and S10 in the SI).

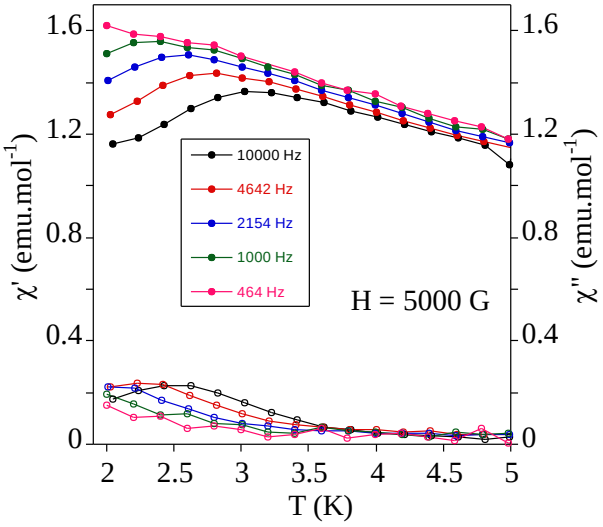

Figure 7. Temperature dependence of the in-phase AC susceptibility (χ_m') (filled symbols) and the out-of-phase AC susceptibility (χ_m") (empty symbols) of **2** under an applied field of 0.5 T.

Conclusions

In this work, two tridentate 1-bpp ligands have been incorporated into an Anderson POM in compound **1** by using the tris-alkoxo-amide tripodal functionalization as shown by single crystal X-ray diffraction. Direct reaction of **1** in a 1:1 Fe^{2+}:POM ratio gives rise to a 1D polymer in compound **3**, whereas a 2:1 Fe^{2+}:POM ratio leads to a precipitate partially soluble in DMF, which leads to **2** after recrystallisation. These results confirm the versatility of the coordination chemistry of tris-alkoxo-amide tripodal functionalized POMs to obtain a great variety of structures ranging from 2D cationic networks in compound **2** or an amorphous polymer in

compound **3**. Further characterizations (Mössbauer spectroscopy, synchrotron techniques) or crystallization are needed to confirm the 1D polymeric structure of compound **3**. Two conclusions can be extracted from the structure of **2**: i) the excess of metal leads to coordination with the oxo groups of the POM and; ii) recrystallization in polar aprotic solvents such as DMF involves dissociation of the 1-bpp-metal coordination bond. A similar behavior has been observed in other functionalized POMs such as pyridyl-functionalized hexavanadates.[5]

Magnetic properties of **1** have shown that it presents a field-induced relaxation of magnetization due to magnetic anisotropy of Mn^{III}, as observed in other four mononuclear Mn^{III} complexes reported very recently. This is the first example of d-metal POM exhibiting this behavior reported in the literature. To our knowledge SIM behavior in POMs has only been found in POMs containing lanthanoids such as the $[Ln(W_5O_{18})_2]^{9-}$ POM series.[24] The similar behavior of the reference compound **4**, one of the simplest functionalized Anderson POM reported so far, and **2** and **3** confirms that this type of behavior is general for this type of structures. Furthermore, it shows that a high Jahn-Teller tetrahedral distortion as that of previous Mn^{III} complexes showing SIM behavior is not needed to obtain such behavior. This result opens the way for the preparation of hybrid POMs combining this property with other magnetic properties of interest. Thus, spin-crossover behavior could be expected if two 1-bpp ligands were coordinated to Fe^{II} as observed in compound **3**. However, the magnetic properties indicate that, in this case, Fe^{II} complexes remain in the LS state. Possible strategies to reach this goal are the use of other counterions or solvents as the spin transition of this type of complexes is very sensitive to the changes of packing and intermolecular interactions resulting from different counterion or solvent molecules. Other possibility is to decrease the ligand field by the introduction of substituents in the 1-bpp derivative. Finally, photomagnetic measurements of **3** are in progress to see if it is possible to induce by light irradiation the spin-crossover of the Fe^{II} in the hybrid POM (LIESST effect).

Notes and references

1 *(a)* M. T. Pope, *Comprehensive Coordination Chemistry II*, 2004, **4**, Elsevier Ltd, Oxford, UK, , pp. 635–678; *(b)* C. L. Hill, *Chem. Rev.,* 1998, **98**, 1 (Special issue: polyoxometalates); *(c)* J. M. Clemente-Juan, E. Coronado and A. Gaita-Ariño, *Chem. Soc. Rev.*, 2012, **41**, 7464.

2 C. Bosch-Navarro, B. Matt, G. Izzet, C. Romero-Nieto, K. Dirian, A. Raya, S. I. Molina, A. Proust, D. M. Guldi , C. Martí-Gastaldo and E. Coronado, *Chem. Sci.,* 2014, **5**, 4346.

3 *(a)* Y. Zhu, P. Yin, F. Xiao, D. Li, E. Bitterlich, Z. Xiao, J. Zhang, J. Hao, T. Liu, Y. Wang and Y. Wei, *J. Am. Chem. Soc.,* 2013, **135**, 17155-17160; *(b)* I. Bar-Nahum, H. Cohen and R. Neumann, *Inorg. Chem.,* 2003, **42**, 3677.

4 M. P. Santoni, G. S. Hanan and B. Hasenknopf, *Coord. Chem. Rev.,* 2014, **281**, 64.

5 J. W. Han, K. I. Hardcastle and C. L. Hill, *Eur. J. Inorg. Chem.*, 2006, 2598.

6 J. W. Han and C. L. Hill, *J. Am. Chem. Soc.,* 2007, **129**, 15094.

7 C. Allain, S. Favette, L. M. Chamoreau, J. Vaissermann, L. Ruhlmann and B. Hasenknopf, *Eur. J. Inorg. Chem.,* 2008, 3433.

8 C. Allain, D. Schaming, N. Karakostas, M. Erard, J.-P. Gisselbrecht, S. Sorgues, I. Lampre, L. Ruhlmann and B. Hasenknopf, *Dalton Trans.*, 2013, **42**, 2745.

9 I. Ahmed, R. Farha, Z. Huo, C. Allain, X. Wang, H. Xug, M. Goldmann, B. Hasenknopf and L. Ruhlmann, *Electrochim. Acta,* 2014, **110**, 726.

10 M. P. Santoni, A. K. Pal, G. S. Hanan, M. C. Tang, K. Venne, A. Furtos, P. Ménard-Tremblay, C. Malveau and B. Hasenknopf, *Chem. Commun.,* 2012, **48**, 200.

11 M. P. Santoni, A. K. Pal, G. S. Hanan and B. Hasenknopf, *Dalton Trans.*, 2014, **43**, 6990.

12 P. Yin, T. Li, R. S. Forgan, C. Lydon, X. Zuo, Z. N. Zheng, B. Lee, D. L. Long, L. Cronin and T. Liu, *J. Am. Chem. Soc.*, 2013, **135,** 13425.

13 M. P. Santoni, A. K. Pal, G. S. Hanan, A. Proust and B. Hasenknopf, *Inorg. Chem.*, 2011, **50**, 6737.

14 M. A. Halcrow, *Coord. Chem. Rev.,* 2009, **253**, 2493.

15 *(a)* T. Buchen, P. Gütlich, K. H. Sugiyarto and H. A. Goodwin, *Chem. Eur. J.*, 1996, **2,** 1134; *(b)* S. Marcen, L. Lecren, L. Capes, H. A. Goodwin and J. F. Létard, *Chem. Phys.*

Lett., 2002, **358**, 87; *(c)* G. Chastanet, C. A. Tovee, G. Hyett, M. A. Halcrow and J. F. Létard, *Dalton Trans.*, 2012, **41,** 4896.

16 M. A. Halcrow, *New J. Chem.*, 2014, **38**, 1868.

17 P. R. Marcoux, B. Hasenknopf, J. Vaissermann, P. Gouzerh, *Eur. J. Inorg. Chem.*, 2003, 2406.

18 J. Zhang, J. Hao, Y. Wei, F. Xiao, P. Yin and L. Wang, *J. Am. Chem. Soc.*, 2010, **132**, 14.

19 B. Hasenknopf, R. Delmont, P. Herson and P. Gouzerh, *Eur. J. Inorg. Chem.*, 2002, 1081.

20 *(a)* J. Vallejo, A. Pascual-Álvarez, J. Cano, I. Castro, M. Julve, F. Lloret, J. Krzystek, G. De Munno, D. Armentano, W. Wernsdorfer, R. Ruiz-García and E. Pardo, *Angew. Chem. Int. Ed.*, 2013, **52**, 14075; *(b)* R. Ishikawa, R. Miyamoto, H. Nojiri, B. K. Breedlove and M. Yamashita, *Inorg. Chem.*, 2013, **52**, 8300; *(c)* A. Grigoropoulos, M. Pissas, P. Papatolis, V. Psycharis, P. Kyritsis and Y. Sanakis, *Inorg. Chem.*, 2013, **52**, 12869; *(d)* G. A. Graig, J. J. Marbey, S. Hill, O. Roubeau, S. Parsons and M. Murrie, *Inorg. Chem.*, 2015, **54**, 13.

21 *(a)* J. Limburg, J. S. Vrettos, R. H. Crabtree, G. W. Brudvig, J. C. de Paula, A. Hassan, A. L. Barra, C. Duboc-Toia and M. N. Collomb, *Inorg. Chem.*, 2001, **40,** 1698; *(b)* C. Mantel, A. K. Hassan, J. Pécaut, A. Deronzier, M. N. Collomb and C. Duboc-Toia, *J. Am. Chem. Soc.*, 2003, **125**, 12337.

22 S. Stoll and A. Schweiger, *J. Magn. Reson.*, 2006, **178,** 42.

23 A. Abhervé, M. Clemente-León, E. Coronado, C. J. Gómez-Garcia and M. López-Jordà, *Dalton Trans.*, 2014, **43**, 9406.

24 *(a)* M. A. AlDamen, J. M. Clemente-Juan, E. Coronado, C. Martí-Gastaldo and A. Gaita-Ariño, *J. Am. Chem. Soc.*, 2008, **130**, 8874; *(b)* M. A. AlDamen, S. Cardona-Serra, J. M. Clemente-Juan, E. Coronado, A. Gaita-Ariño, C. Martí-Gastaldo, F. Luis and O. Montero, *Inorg. Chem.*, 2009, **48**, 3467; *(c)* M. J. Martínez-Pérez, S. Cardona-Serra, C. Schlegel, F. Moro, P. J. Alonso, H. Prima-García, J. M. Clemente-Juan, M. Evangelisti, A. Gaita-Ariño, J. Sesé, J. van Slageren, E. Coronado and F. Luis, *F. Phys. Rev. Lett.*, 2012, **108**, 247213.

Associated Content:

Electronic Supplementary Information (ESI)

Experimental section

General Remarks. $(C_{16}H_{36}N)_4\alpha$-$[Mo_8O_{26}]$,[1] bppCOOEt[2] and $(C_{16}H_{36}N)_3[MnMo_6O_{18}\{(OCH_2)_3CNH_2\}_2]$ **(4)**[3] were synthetized according to the literature methods. All other materials and solvents were commercially available and used without further purification.

Synthesis of TRIS-bpp. Under nitrogen atmosphere, bppCOOEt (181 mg, 0.64 mmol), $(HOCH_2)_3CNH_2$ (77 mg, 0.64 mmol) and K_2CO_3 (88 mg, 0.64 mmol) were suspended in dry dimethyl sulfoxide (DMSO) (5 mL) and stirred at room temperature for 18 h. The reaction mixture was then filtered, and the solvent removed by vacuum. The residue was dissolved in EtOH (3 mL) and the product precipitated by adding H_2O (25 mL). The white precipitate was filtered, washed with diethyl ether, and dried to give pure TRIS-bpp (87 mg, 38 %). ^{1}H NMR (d6-DMSO, 300 MHz): 8.99 (dd, J = 3, 0.75 Hz, 2H, H_{Im1}), 8.12 (s, 2H, H_{Pyr}), 7.92 (dd, J = 2, 0.75 Hz, 2H, H_{Im2}), 7.82 (br, 1H, H_{NH}), 6.67 (dd, J = 3, 2 Hz, 2H, H_{Im3}), 4.69 (t, J = 6 Hz, 3H, H_{OH}), 3.74 (d, J = 6 Hz, 6H, H_{CH2}).

Synthesis of $(C_{16}H_{36}N)_3[MnMo_6O_{24}(C_{16}H_{15}N_6O)_2]\cdot(C_4H_9NO)_2\cdot(H_2O)_{2.5}$ (1). $(C_{16}H_{36}N)_4\alpha$-$[Mo_8O_{26}]$ (150 mg, 0.07 mmol) and $Mn(CH_3COO)_3.2H_2O$ (27 mg, 0.10 mmol) were dissolved in dry dimethylacetamide (DMAc, 8mL). Then a solution of TRIS-bpp (87 mg, 0.24 mmol) in dry DMAc (3 mL) was added, and the mixture was heated at 80ºC for 18 h. The obtained orange solution was allowed to cool down. After two days, orange cubic crystals of **1** were obtained (177 mg, 98 %). ^{1}H NMR (d_6-DMSO, 300 MHz): 8.97 (d, J = 2.7 Hz, 4H, H_{Im1}), 8.09 (br, 4H, H_{Pyr}), 7.91 (d, J = 1.2 Hz, 4H, H_{Im2}), 6.65 (dd, J = 2.7, 1.2 Hz, 4H, H_{Im3}), 3.16 (m, 24H, H_{C1}), 1.56 (q, J = 7.5 Hz, 24H_{C2}), 1.31 (sx, J = 7.5 Hz, 24H_{C3}), 0.93 (t, J = 7.5 Hz, 36H_{C4}) (presence of 2 equiv. of DMAc confirmed by peaks at 1.96, 2.78 and 2.94 ppm). IR (KBr pellet, cm^{-1}): 2960 (νC-H, s), 2935 (νC-H, s), 2874

(ν C-H, s), 1670 (m), 1618 (m), 1570 (m), 1552 (sh), 1524 (m), 1483 (sh), 1462 (s), 1396 (ν C-H, s), 1362 (w), 1320 (w), 1288 (w), 1259 (w), 1207 (w), 1151 (w), 1111 (sh), 1097 (ν C-O, w), 1047 (m), 1036 (ν C-O, sh), 1030 (sh), 941 (ν Mo=O, vs), 922 (ν Mo=O, vs), 903 (ν Mo=O, vs), 789 (m), 760 (m), 667 (ν Mo-O-Mo, vs), 565 (m), 464 (m). Anal. Calcd for $(C_{16}H_{36}N)_3[MnMo_6O_{24}(C_{16}H_{15}N_6O)_2]\cdot(C_4H_9NO)_2\cdot(H_2O)_{2.5}$: C, 41.0; H, 6.3; N, 9.2 %. Found: C, 40.9; H, 5.8; N, 9.1 %.

Synthesis of $[Fe(H_2O)(C_3H_7NO)]_2[MnMo_6O_{24}(C_{16}H_{15}N_6O)_2](OH)\cdot(H_2O)$ (2). $(C_{16}H_{36}N)_3[MnMo_6O_{24}(C_{16}H_{15}N_6O)_2]\cdot(C_4H_9NO)_2\cdot(H_2O)_{2.5}$ (1) (25.8 mg, 0.01 mmol) was dissolved in acetonitrile (3 mL). A solution of $Fe(ClO_4)_2,xH_2O$ (5.1 mg, 0.02 mmol) in acetonitrile (3 mL) was added slowly, and the resulted mixture was stirring for 30 min at room temperature. The orange precipitate was filtered and recrystallized in dimethylformamide (10 mL). After three days, red crystals were obtained (0.8 mg, 4 %) IR (KBr pellet, cm^{-1}): 2922 (ν C-H, s), 2875 (ν C-H, s), 1654 (m), 1648 (m), 1628 (m), 1572 (m), 1528 (m), 1500 (m), 1460 (s), 1405 (ν C-H, s), 1327 (w), 1295 (w), 1274 (w), 1211 (s), 1173 (s), 1156 (w), 1098 (ν C-O, s), 1055 ((ν C-O, sh), 1025 (sh), 972 (s), 946 (ν Mo=O, vs), 925 (ν Mo=O, vs), 912 (ν Mo=O, vs), 796 (s), 765 (m), 668 (ν Mo-O-Mo, vs), 569 (m), 466 (m). Anal. Calcd for $[Fe(H_2O)(C_3H_7NO)]_2[MnMo_6O_{24}(C_{16}H_{15}N_6O)_2]\cdot(OH)\cdot(H_2O)$: C, 23.2; H, 2.6; N, 10.0 %. Found: C, 21.59; H, 3.62; N, 8.99 %.

Synthesis of $(C_{16}H_{36}N)[Fe(MnMo_6O_{24}(C_{16}H_{15}N_6O)_2)]\cdot(H_2O)_4$ (3). $(C_{16}H_{36}N)_3[MnMo_6O_{24}(C_{16}H_{15}N_6O)_2]\cdot(C_4H_9NO)_2\cdot(H_2O)_{2.5}$ (1) (12.9 mg, 0.005 mmol) was dissolved in dry acetonitrile (5 mL). A solution of $Fe(ClO_4)_2,xH_2O$ (1.3 mg, 0.005 mmol) in dry acetonitrile (500 µL) was added slowly, and the resulted mixture was stirring for 10 min at room temperature. The orange precipitate was centrifuged, washed with dry acetonitrile (5 mL), and dried under vacuum (4 mg, 40 %). IR (KBr pellet, cm^{-1}): 2958 (ν C-H, s), 2923 (ν C-H, s), 2872 (ν C-H, s), 1670 (m), 1624 (m), 1570 (m), 1527 (m), 1499 (sh), 1459 (s), 1400 (ν C-H, s), 1390 (w), 1363 (w), 1323 (w), 1264 (w), 1209 (w), 1169 (w), 1096 (ν C-O, w), 1052 (ν C-O, sh), 1026 (sh), 972 (s), 945 (ν Mo=O, vs), 922 (ν

Mo=O, vs), 903 (ν Mo=O, vs), 795 (m), 764 (m), 665 (ν Mo-O-Mo, vs), 567 (m), 462 (m). Anal. Calcd for $(C_{16}H_{36}N)[Fe(MnMo_6O_{24}(C_{16}H_{15}N_6O)_2)]\cdot(H_2O)_4$: C, 28.8; H, 3.7; N, 9.1 %. Found: C, 27.5; H, 2.5; N, 9.1 %. The bands at 1624, 1390, 1169 and 972 cm^{-1} could support the coordination of Fe^{II} to 1-bpp.

Physical measurements.

Infrared (IR) spectra were recorded in the solid state (KBr pellets) on a Nicolet Avatar 320 FTIR spectrometer in the 400-4000 cm^{-1} range. C, H and N elemental analyses were done on a CE Instruments EA 1110 CHNS Elemental analyser. The Mn:Mo and Fe:Mn:Mo ratios were measured on a Philips ESEM X230 scanning electron microscope equipped with an EDAX DX-4 microsonde. ^{1}H NMR spectra were acquired on a Bruker AVANCE DRX 300 spectrometer.

Single crystals of all compounds were mounted on glass fibers using a viscous hydrocarbon oil to coat the crystal and then transferred directly to the cold nitrogen stream for data collection. All reflection data were collected at 120 K for **1** and 180 K for **2** on a Supernova diffractometer (**1**) and on a Supernova Atlas Dual Source diffractometer (**2**) equipped with a graphite-monochromated Enhance (Mo) X-ray Source (λ = 0.7107 Å)**.** The CrysAlisPro program, Oxford Diffraction Ltd., was used for unit cell determinations and data reduction. Empirical absorption correction was performed using spherical harmonics, implemented in the SCALE3 ABSPACK scaling algorithm. Crystal structures were solved by direct methods with the SIR97 program,[4] and refined against all F^2 values with the SHELXL-2013 program,[5] using the WinGX graphical user interface.[6] All non-hydrogen atoms were refined anisotropically except as noted and hydrogen atoms were placed in calculated positions and refined isotropically with a riding model. Initial refinements revealed the presence of substantial volume of unresolvable solvent (DMF) molecules in **1**. The subroutine SQUEEZE from PLATON was used to remove the diffracting component of disordered solvents resulting in a void of ca. 741.5 $Å^3$ and 142 electrons/cell omitted. This corresponds to ca. 3 DMF molecules per unit cell. Crystallographic data are

summarized in Table 1. 0.5 mm glass capillaries were filled with polycrystalline samples of compound **1** and mounted and aligned on a Empyrean PANalytical powder diffractometer, using CuKα radiation (λ = 1.54177 Å). A total of 3 scans were collected at room temperature in the 2θ range 5-40^{o}.

Electrospray ionization mass spectrometry (ESI-MS). A Q-TOF Premier mass spectrometer with an orthogonal Z-spray electrospray source (Waters, Manchester, U.K.) was used. The temperature of the source block was set to 100 °C and the desolvation temperature to 120 °C. A capillary voltage of 3.3 kV was used in the negative scan mode, and the cone voltage was set to 5 V to control the extent of fragmentation of the identified species. TOF mass spectra were acquired in the W-mode operating at a resolution of ca. 15000 (fwhm). Mass calibration was performed using a solution of sodium iodide in isopropanol/water (50:50) from m/z 50 to 3000. Acetonitrile sample solutions were infused via syringe pump directly connected to the ESI source at a flow rate of 10 μL/min. The observed isotopic pattern of each compound perfectly matched the theoretical isotope pattern calculated from their elemental composition using the MassLynx 4.1 program.

Magnetic measurements were performed with a Quantum Design MPMS-XL-5 SQUID magnetometer on powdered polycrystalline samples. High-frequency EPR (HF-EPR) spectra (100 – 370 GHz) were recorded on a home-built spectrometer. Its microwave source is a 8 – 20 GHz signal generator (VDI) in combination with an amplifier–multiplier chain (VDI) to obtain the required frequencies. It features a quasi-optical bridge (Thomas Keating) and induction mode detection. The detector is a QMC magnetically tuned InSb hot electron bolometer. The sample is located in an Oxford Instruments 15/17T cryomagnet equipped with a variable temperature insert (1.5–300 K). The sample was measured as a 5 mm pressed pellet, which was mixed with eicosan (ratio 1:1 25 mg each). Spectral simulations were performed using the EasySpin 4.5.3 simulation software. A modulation amplitude of 80 mA (80 G) was used to modulate the magnetic field. Two temperature sensors allowed monitoring of the sample

temperature with high accuracy. The sample was investigated at different frequencies and temperatures (see Table S1). A linewidth of 120 mT (FWHM) was used. The powder spectrum is obtained using 91 orientations.

Table S1. High-frequency EPR spectra performed on compound **1**.

ν (GHz)	T (K)	Field range (T)
100	10	0-15
110	10	0-15
180	10	0-15
200	10	0-15
220	10	0-15
240	10	0-15
250	10	0-1
255	10	0-1
260	2, 5, 10, 20, 40	0-15
300	10	0-15
330	2, 5, 10, 20, 40	0-15
370	10	0-15

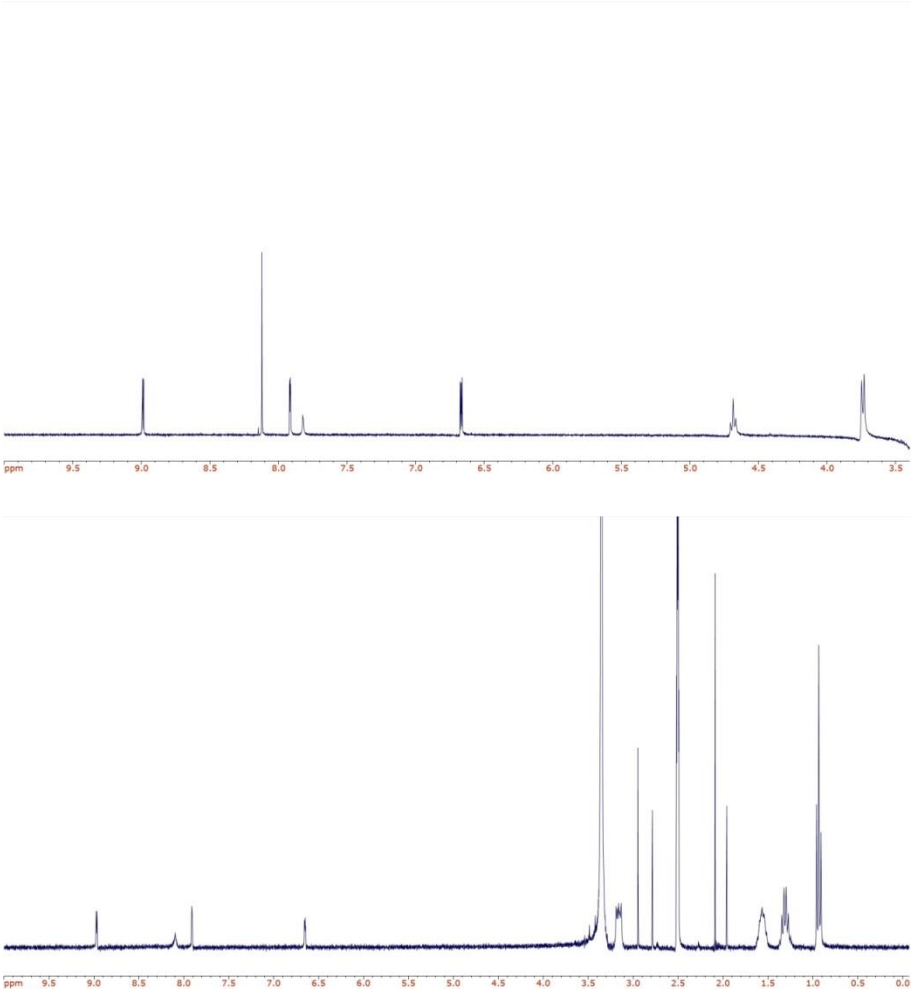

Figure S1. ^{1}H NMR spectra of TRIS-bpp (up) and **1** (bottom).

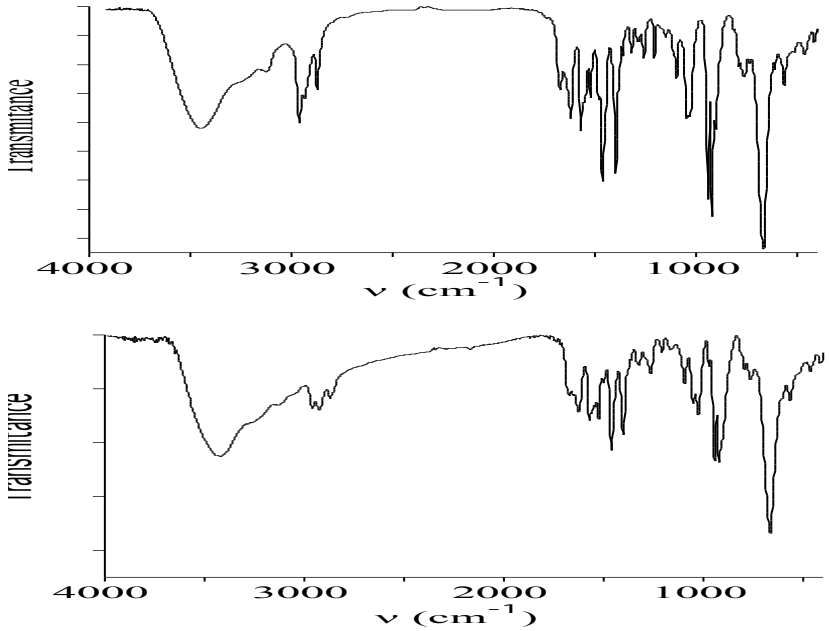

Figure S2. IR spectra of **1** (top) and **3** (bottom).

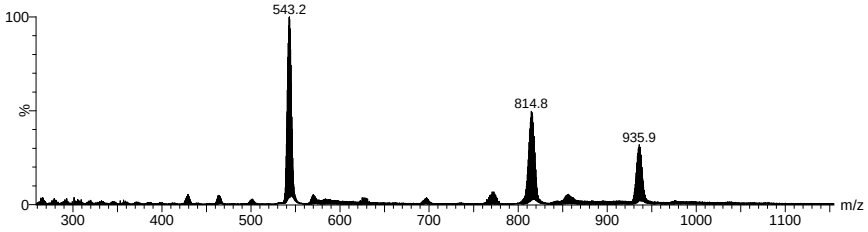

Figure S3. ESI mass spectrum of acetonitrile solutions of compound **1** recorded at Uc = 5 V.

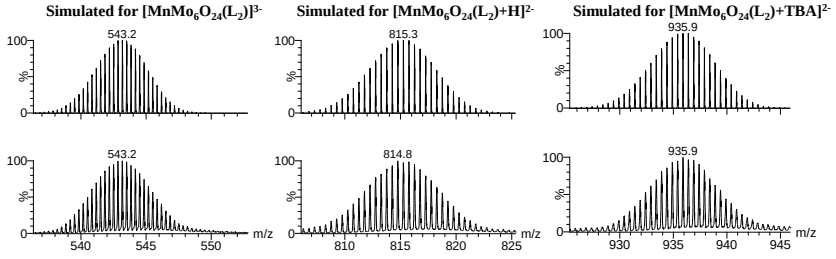

Figure S4. Simulated (top) and experimental (bottom) isotopic distribution for the identified species, $[\mathbf{1}]^{3-}$ (left), $[\mathbf{1} + H]^{2-}$ (center) and $[\mathbf{1} + TBA]^{2-}$ (right).

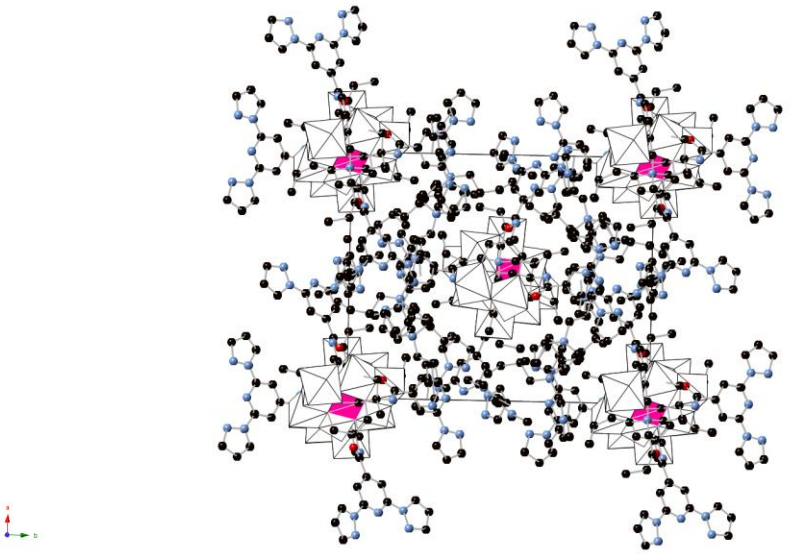

Figure S5. Projection of the structure of **1** in the *ab* plane. (Mn (pink), Mo (white), C (black), N (blue), O (red)). Hydrogen atoms have been omitted for clarity.

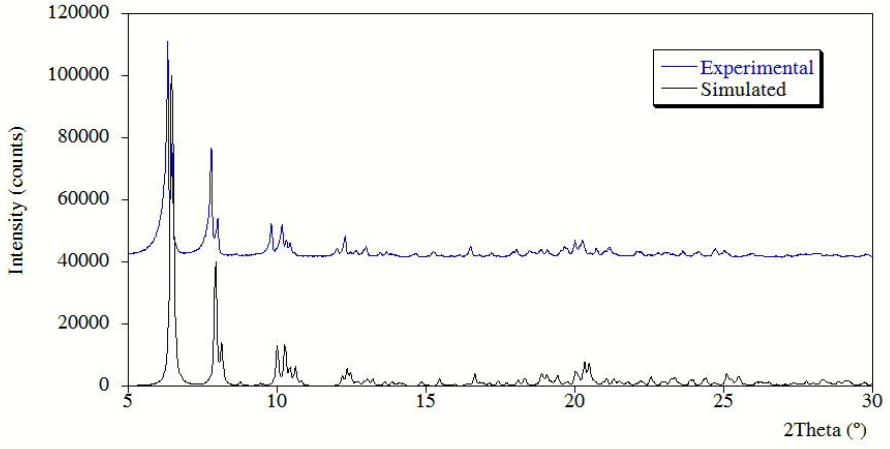

Figure S6. Experimental (top) and simulated (bottom) X-ray powder diffraction patterns of **1**.

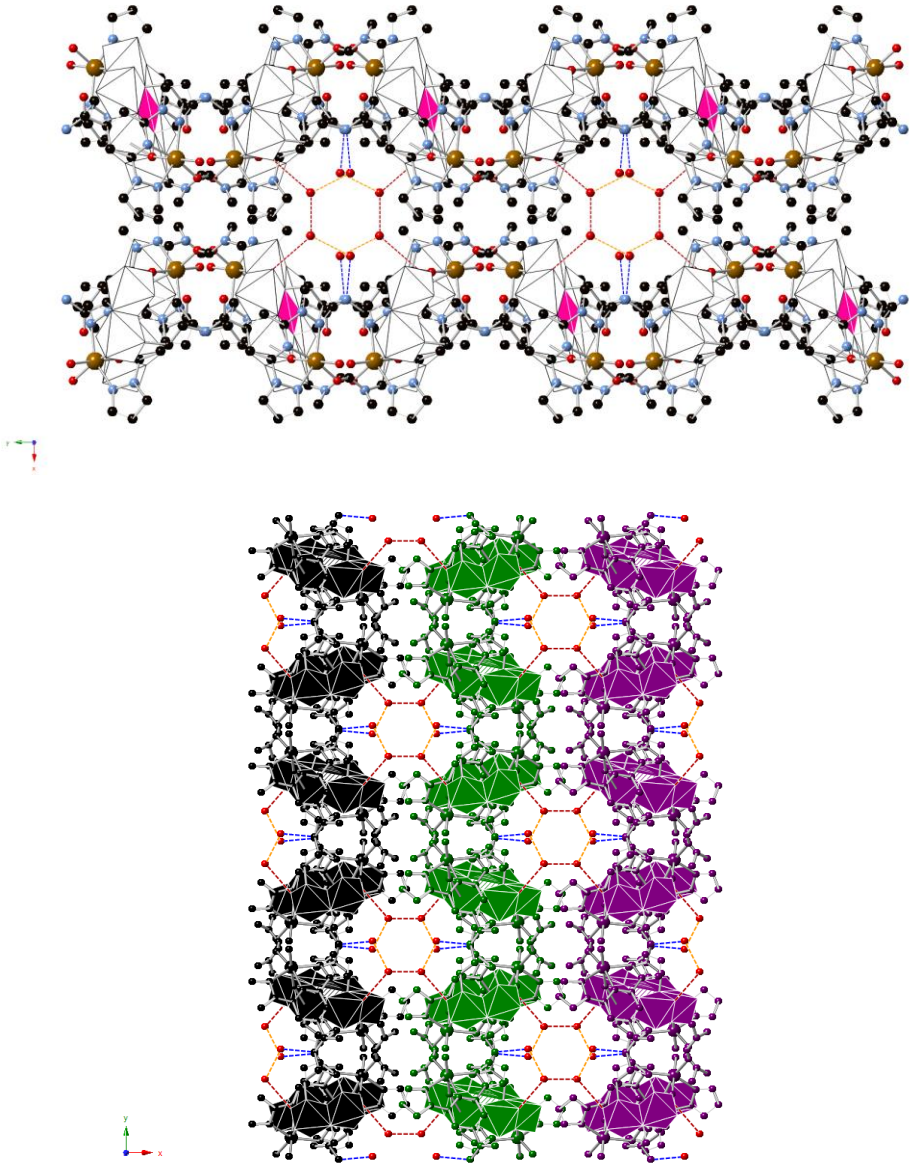

Figure S7. Projection of the structure of **2** in the *ab* plane. (Mn (pink), Mo (white), Fe (yellow), C (black), N (blue), O (red)) (top) and view of three covalently-bonded layers with different colors (bottom). Hydrogen atoms have been omitted for clarity. Dashed lines correspond to the hydrogen bonds. O200 is the OH^- group.

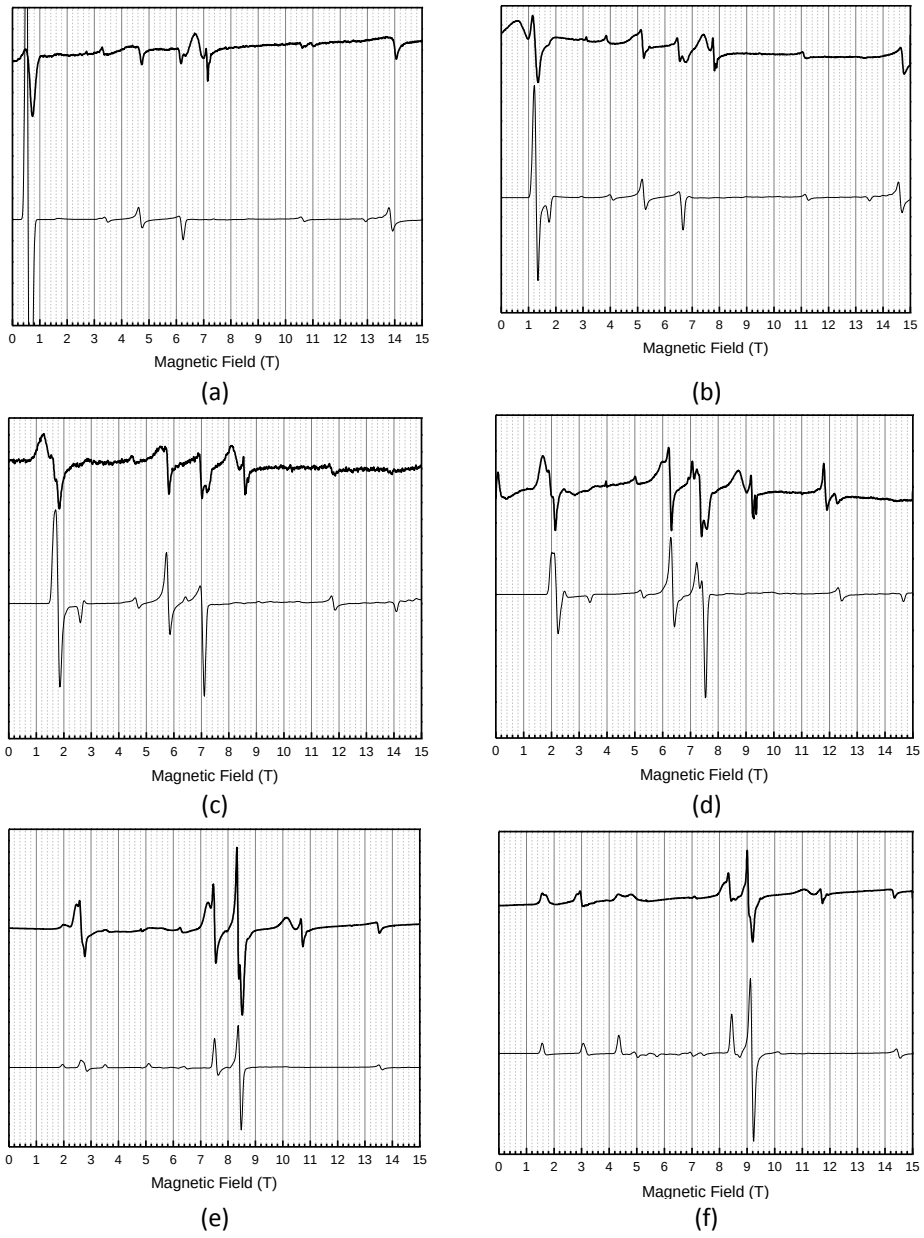

Figure S8. HF-EPR spectra of **1** (bold: experiment, thin: simulation) at 200 GHz (a), 220 GHz (b), 240 GHz (c), 260 GHz (d), 300 GHz (e) and 330 GHz (f) and 10 K. Note that the strong signals at 6.8 T (a), 7.6 T (b), 8.3 T (c), 9 T (d), 10.5 T (e) and 11.4 T (f) are at g = 2 and caused by some impurity.

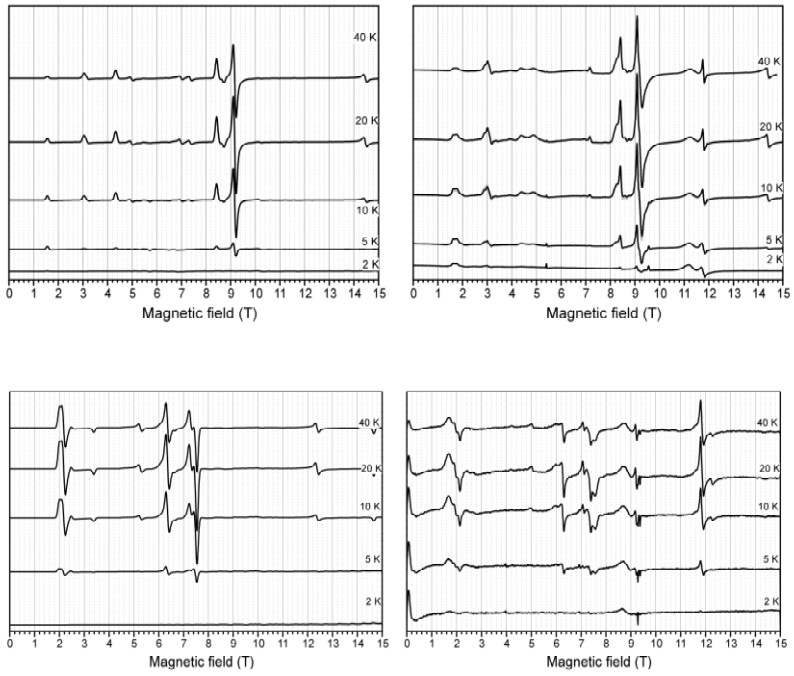

Figure S9. Temperature dependence of the HF-EPR spectra of **1**.The left figures show the simulations for 330 GHz (upper) and 260 GHz (lower). The right figures show the experimental data for the same frequencies.

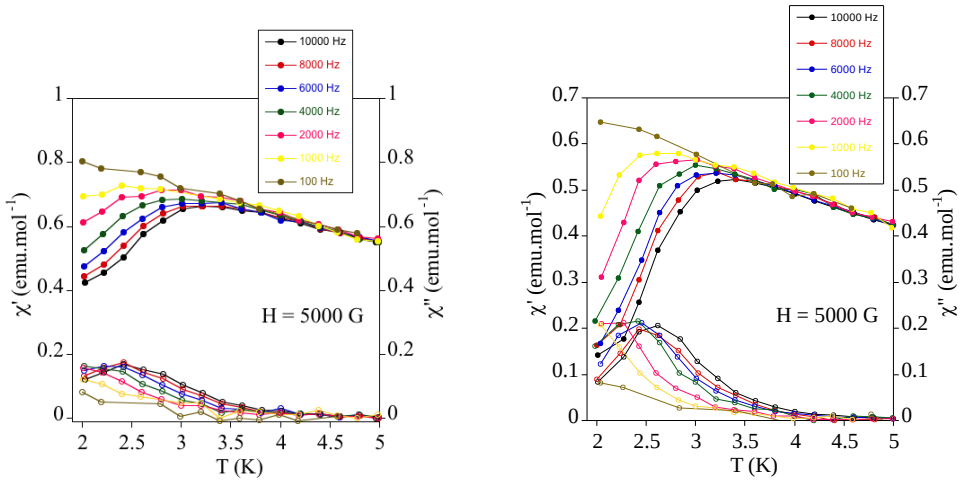

Figure S10. Temperature dependence of the in-phase AC susceptibility (χ_m') (filled symbols) and the out-of-phase AC susceptibility (χ_m") (empty symbols) of **3** (left) and **4** (right) under an applied field of 0.5 T.

The calculated values of the pre-exponential factor and the activation energy (τ_0 = 4.8 10^{-8} s and E_a = 15.4 cm^{-1}) from the fitting to an Arrhenius law for **4** measured at 0.5 T are consistent with those of other Mn^{III} complexes showing this behavior.

---

[1] M. Filowitz, R. K. C. Ho, W. G. Klemperer and W. Shum, *Inorg. Chem.*, 1979, **18**, 93.

[2] T. Vermonden, D. Branowska, A. T. M. Marcelis and E. J. R. Sudhölter, *Tetrahedron*, 2003, **59**, 5039.

[3] P. R. Marcoux, B. Hasenknopf, J. Vaissermann and P. Gouzerh, *Eur. J. Inorg. Chem.*, 2003, 2406.

[4] A. Altomare, M. C. Burla, M. Camalli, G. L. Cascarano, C. Giacovazzo, A. Guagliardi, A. G. G. Moliterni, G. Polidori and R. Spagna, *J. Appl. Cryst.*, 1999, **32**, 115.

[5] G. M. Sheldrick, *Acta Cryst.*, 2008, **A64,** 112.

[6] L. J. Farrugia, *J. Appl. Cryst.*, 2012, **45**, 849.

One-Dimensional and Two-Dimensional Anilate-Based Magnets with Inserted Spin-Crossover Complexes

Chapter 4

Inorganic Chemistry

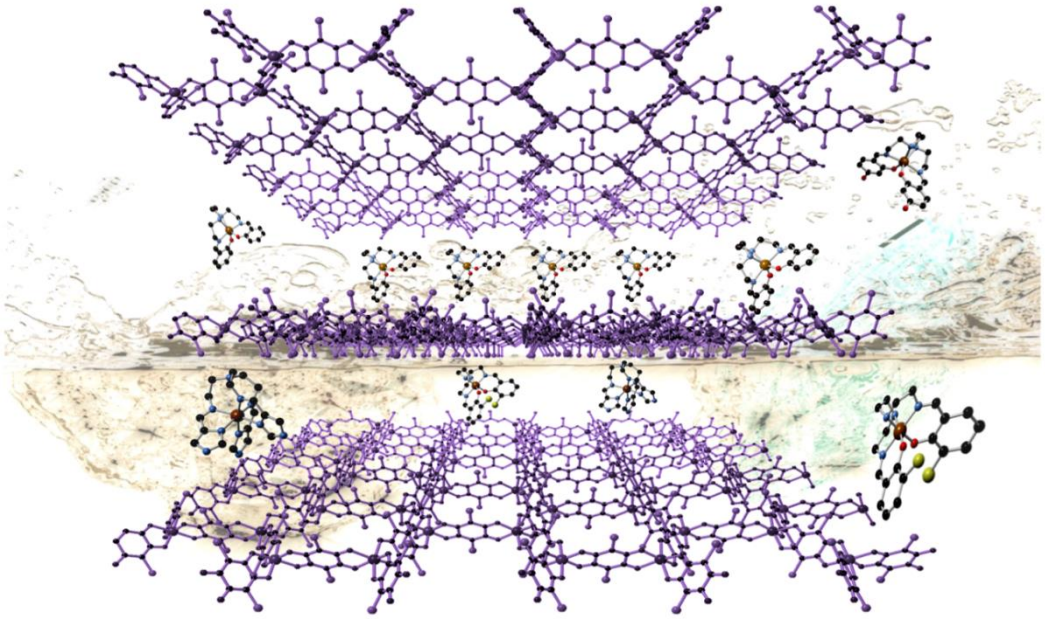

Abhervé, A., Clemente-León, M., Coronado, E., Gómez-García, C. J., Verneret, M. *Inorg. Chem.* **2014**, *53*, 12014-12026.

Chapter 4. One-Dimensional and Two-Dimensional Anilate-Based Magnets with Inserted Spin-Crossover Complexes

Abstract

The syntheses, structures and magnetic properties of a family of bimetallic anilate-based compounds with inserted spin-crossover cationic complexes are reported. The structures of **1**-**4** present a two-dimensional anionic network formed by Mn^{II} and Cr^{III} ions linked through anilate ligands with inserted $[Fe^{III}(sal_2\text{-trien})]^+$ (**1**), $[Fe^{III}(4\text{-OH-sal}_2\text{-trien})]^+$ (**2**), $[Fe^{III}(sal_2\text{-epe})]^+$ (**3**) or $[Fe^{III}(5\text{-Cl-sal}_2\text{-trien})]^+$ (**4**) complexes. The structure of **5** is formed by anionic $[Mn^{II}Cl_2Cr^{III}(Cl_2An)_3]^{3-}$ chains surrounded by $[Fe^{II}(tren(imid)_3)]^{2+}$, Cl^-, and solvent molecules. The magnetic properties indicate that **1**-**4** undergo a long-range ferrimagnetic ordering at *ca.* 10 K. On the other hand, the inserted Fe^{III} cations remain in the LS (in **4**) or HS state (in **1**, **2** and **3**). In the case of **5**, half of the inserted Fe^{II} cations undergo a complete and gradual spin crossover from 280 to 90 K that coexists with a magnetic ordering below 2.5 K.

Introduction

Multifunctionality is one of the most appealing topics in chemical science. A rational approach to design hybrid multifunctional materials consists of the controlled assembly of two functional networks incorporating two properties or contributing synergistically to the appearance of new physical phenomena.[1] Among the later class of materials, those responding to an external stimulus are attracting considerable interest in view of their potential applications as chemical switches, memory or molecular sensors.[2] In this context, two-network compounds formed by a magnetic lattice and a switchable molecular component are promising candidates for the preparation of responsive magnetic materials.

Spin-crossover complexes are particularly suitable as switchable molecular components because they represent one of the best examples of molecular bistability. These molecular complexes change their spin state from LS to HS configurations under an external stimulus such as temperature, light irradiation, or pressure.[3] As this is accompanied by changes in the molecular size, the spin-crossover process should act as an internal pressure in the hybrid material, and therefore, it might affect the long-range magnetic ordering in the extended magnetic network.

Bimetallic oxalate-bridged compounds have been thoroughly used as magnetic lattice of multifunctional magnetic materials. They are formed by polymeric anionic networks $[M^{II}M^{III}(ox)_3]^-$ (ox = oxalate) with magnetic ions linked through bis-bidentate bridging oxalate ligands. The use of different charge-compensating molecular cations, which template the network formation, has provided many examples of multifunctional materials,[4] combining the long-range magnetic ordering of the oxalate network with paramagnetism,[5] photochromism,[6] electrical conductivity,[7] proton conductivity,[8] ferroelectricity,[9] chirality,[10] or single-molecule magnet behavior from the cation.[11] Fe^{II} and Fe^{III} spin-crossover cationic complexes have been used for the growth of two-dimensional (2D) and three-dimensional (3D) bimetallic oxalate-based magnets in the search of responsive magnetic materials.[12] Fe^{II} spin-crossover complexes have led to the growth of 3D bimetallic oxalate-based compounds, which present magnetic properties very sensitive to the changes in size of the inserted cation, although the inserted Fe^{II} complexes do not present a clear spin-crossover behavior.[12g,13] The most interesting results were obtained for the family of compounds $[Fe^{III}(sal_2\text{-trien})][Mn^{II}Cr^{III}(ox)_3]\cdot G$ (G= CH_2Cl_2, $CHBr_3$, CH_2Br_2 and $CHCl_3$, H_2Sal_2-trien = *N,N'*-disalicylidenetriethylene-tetramine, see Scheme 1) formed by alternating layers of a 2D oxalate-based network, $[Fe^{III}(sal_2\text{-trien})]^+$ complexes and solvent molecules.[12b,e,h] They show that the confinement of spin crossover cations into extended networks induce an unexpected property, a photoinduced spin-crossover transition of the inserted complex (LIESST effect), something very unusual for Fe^{III} complexes. Unfortunately, the photo-induced spin conversion of the inserted Fe^{III} complex has a

negligible influence on the magnetic behavior of the 2D oxalate network as the magnetic ordering of this type of network is not sensitive to the change in size of the inserted cation.

Motivated by the interesting results obtained with bimetallic oxalate-based networks, we have attempted the use of larger bis-bidentate bridging ligands as the 2,5-dihydroxy-1,4-benzoquinone dianion derivatives of formula $C_6O_4X_2^{2-}$ (X_2An^{2-}; X = Cl or Br, see Scheme 2). These ligands, which show coordination modes similar to the oxalate ligand, present additional advantages: (i) they are easy to modify or functionalize by simply changing the X group; (ii) they present higher ordering temperatures, T_c's; (iii) their bigger size may enable the introduction of a larger library of cations in order to prepare multifunctional molecular materials. The first example of this kind, obtained by our group, is the family of layered ferrimagnets $A[M^{II}M^{III}(X_2An)_3]\cdot G$ (A = $[(H_3O)(phz)_3]^+$ (phz = phenazine) or NBu_4^+; X = H, Cl, Br, I; G = water or acetone) with T_c ranging from 5.5 to 11.0 K and which, depending on the X substituent, can be porous and/or chiral.[14a]

In this work, we explore the use of the Fe^{III} complexes, $[Fe^{III}(sal_2\text{-trien})]^+$, $[Fe^{III}(4\text{-OH-}sal_2\text{-trien})]^+$, $[Fe^{III}(sal_2\text{-epe})]^+$, and $[Fe^{III}(5\text{-Cl-}sal_2\text{-trien})]^+$ derivatives, and the Fe^{II} complex, $[Fe^{II}(tren(imid)_3)]^{2+}$ (Scheme 1) for the preparation of multifunctional compounds based on the anilate-based network in the search of new compounds combining spin-crossover and magnetic ordering. The first results of this strategy are reported in this paper.

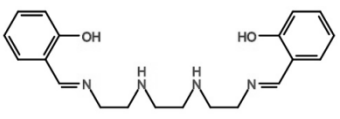

$H_2(sal_2\text{-trien})$

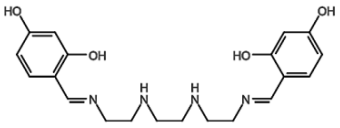

$H_2(4\text{-OH-}sal_2\text{-trien})$

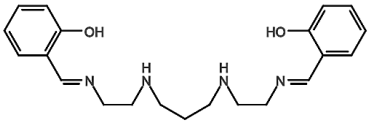

$H_2(sal_2\text{-epe})$

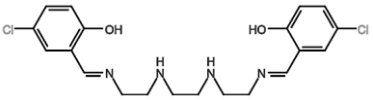

$H_2(5\text{-Cl-}sal_2\text{-trien})$

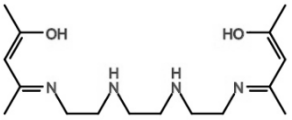

$H_2(acac_2\text{-trien})$

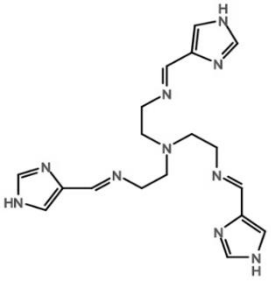

$Tren(imid)_3$

Scheme 1. Ligands of the Fe^{III} and Fe^{II} complexes.

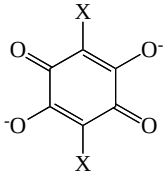

X_2An^{2-}; X = Cl or Br

Scheme 2. 2,5- dihydroxy-1,4-benzoquinone dianion derivatives used in this work.

Experimental Section

General Remarks. The Fe^{III} complexes[15,16] and $[Fe^{II}(tren(imid)_3)](BF_4)_2$ were prepared according to literature methods.[17] $[(n\text{-}Bu)_4N]_3[Cr^{III}(X_2An)_3]$ (X=Cl, Br) was prepared by a modification of the literature method.[14] All other materials and solvents were commercially available and used without further purification.

Synthesis of $[NBu_4]_3[Cr^{III}(Cl_2An)_3]$ and $[NBu_4]_3[Cr^{III}(Br_2An)_3]$. An aqueous solution (10 mL) of $CrCl_3 \cdot 6H_2O$ (400 mg, 1.5 mmol) was added dropwise to an aqueous solution (30 mL) of H_2Cl_2An or H_2Br_2An (5 mmol), NaOH (400 mg, 10 mmol), and NBu_4Br (1.6 g, 5 mmol). After 30 min at 70 °C, the mixture was allowed to cool to room temperature and extracted three times with 75 mL of CH_2Cl_2. The CH_2Cl_2 solution was dried with Na_2SO_4, filtered, rotoevaporated to dryness, and crystallized in dimethylformamide to give red shiny crystals after 2 weeks.

Synthesis of $[Fe^{III}(sal_2\text{-trien})][Mn^{II}Cr^{III}(Cl_2An)_3] \cdot (CH_2Cl_2)_{0.5} \cdot (CH_3OH) \cdot (H_2O)_{0.5} \cdot (CH_3CN)_5$ (1), $[Fe^{III}(4\text{-OH-}sal_2\text{-trien})][Mn^{II}Cr^{III}(Cl_2An)_3] \cdot$(solvate) (2), $[Fe^{III}(sal_2\text{-epe})][Mn^{II}Cr^{III}(Br_2An)_3] \cdot (CH_3CN)_4 \cdot$(solvate) (3), $[Fe^{III}(5\text{-Cl-}sal_2\text{-trien})][Mn^{II}Cr^{III}(Br_2An)_3] \cdot (CH_2Cl_2) \cdot (CH_3OH) \cdot (H_2O)_4 \cdot (CH_3CN)_{1.5} \cdot$(solvate) (4) and $[Fe^{II}(tren(imid)_3)]_2[Mn^{II}Cl_2Cr^{III}(Cl_2An)_3]Cl \cdot (CH_3OH) \cdot (CH_2Cl_2)_3 \cdot (CH_3CN)_{0.5}$ (5). Crystals of these compounds were obtained by slow diffusion of two solutions. The first solution was prepared by dissolving $MnCl_2 \cdot 4H_2O$ (12 mg, 0.06 mmol) and the Fe^{III} complexes (0.06 mmol) in 6 mL of a 9:1 dichloromethane/methanol mixture ($[Fe^{III}(sal_2\text{-trien})](PF_6)$ (32 mg) for **1**, $[Fe^{III}(4\text{-OH-}sal_2\text{-trien})]Cl$ (27 mg) for **2**, $[Fe^{III}(sal_2\text{-epe})](ClO_4)$ (31 mg) for **3** and $[Fe^{III}(5\text{-Cl-}sal_2\text{-trien})](PF_6)$ (38 mg) for **4**). In the case of **5**, it is necessary to dissolve first the $[Fe^{II}(tren(imid)_3)](BF_4)_2$ complex (73 mg, 0.12 mmol) in 6 mL of a 2:1 dichloromethane/methanol mixture and then add $MnCl_2 \cdot 4H_2O$ (12 mg, 0.06 mmol). The second solution was obtained by dissolving $[NBu_4]_3[Cr^{III}(Cl_2An)_3]$ (84 mg, 0.06 mmol, for **1**, **2** and **5**) or $[NBu_4]_3[Cr^{III}(Br_2An)_3]$ (100 mg, 0.06 mmol, for **3** and **4**) in 6 mL of acetonitrile. After 2-4 weeks, black prismatic single crystals suitable for X-ray crystal analysis were obtained. Yields: 6.8% (**1**), 6.8% (**2**), 7.4% (**3**), 5.4% (**4**) and 11.1% (**5**). These yields could be improved by diffusing the two solutions for longer times. Anal. Calcd for $C_{38.5}H_{37}Cl_7CrFeMnN_4O_{20}$ (**1**) (with 0.5 dichloromethane molecule and 6 water molecules per formula in the structure due to desolvation and rehydratation): C, 35.6; H, 3.1; N, 4.4%. Found: C, 35.9; H, 2.9; N, 4.4%. Anal. Calcd for $C_{38}H_{56}Cl_6CrFeMnN_4O_{32}$ (**2**) (with 16 water molecules per formula in the structure due to partial desolvation): C,

31.3; H, 3.9; N, 3.8%. Found: C, 31.4; H, 3.5; N, 4.3%. Anal. Calc. for $C_{39}H_{26}Br_6CrFeMnN_4O_{14}$ (**3**) (with no solvent molecules in the structure due to complete desolvation): C, 33.1; H, 1.8; N, 4.0%. Found: C, 32.4; H, 2.0; N, 4.0%. Anal. Calcd for $C_{43}H_{40.5}Br_6Cl_4CrFeMnN_{5.5}O_{19}$ (**4**): C, 30.0; H, 2.4; N, 4.5%. Found: C, 30.7; H, 2.1; N, 3.7%. Anal. Calcd for $C_{58}H_{55.5}Cl_{13}CrFe_2MnN_{20.5}O_{13}$ (**5**): C, 36.1; H, 2.9; N, 14.9%. Found: C, 35.5; H, 1.7; N, 14.1%. IR (KBr pellet) for **1**: 1624 (s), 1590 (sh), 1506 (vs), 1398 (w), 1359 (vs), 1305 (sh), 1007 (m), 835 (m) cm^{-1}. IR (KBr pellet) for **2**: 1625 (s), 1542 (sh), 1516 (vs), 1400 (m), 1360 (vs), 1007 (m), 849 (m) cm^{-1}. IR (KBr pellet) for **3**: 1623 (s), 1540 (sh), 1509 (sh), 1491 (vs), 1400 (m), 1351 (vs), 989 (m), 817 (m) cm^{-1}. IR (KBr pellet) for **4**: 1629 (s), 1517 (sh), 1491 (vs), 1401 (m), 1352 (vs), 990 (m), 817 (m) cm^{-1}. IR (KBr pellet) for **5**: 1635 (vs), 1533 (vs), 1507 (sh), 1401 (m), 1356 (vs), 1005 (m), 848 (m) cm^{-1}.

Structural Characterization. Single crystals of all compounds were mounted on glass fibers using a viscous hydrocarbon oil to coat the crystal and then transferred directly to the cold nitrogen stream for data collection. All reflection data were collected at 120 K for **1**-**4** and at 120 and 220 K for **5** on a Supernova diffractometer equipped with a graphite-monochromated Enhance (Mo) X-ray Source (λ = 0.7107 Å). The CrysAlisPro program, Oxford Diffraction Ltd., was used for unit cell determinations and data reduction. Empirical absorption correction was performed using spherical harmonics, implemented in the SCALE3 ABSPACK scaling algorithm. Crystal structures were solved by direct methods with the SIR97 program[18] and refined against all F^2 values with the SHELXL-2013 program[19] using the WinGX graphical user interface.[20] All non-hydrogen atoms were refined anisotropically except as noted, and hydrogen atoms were placed in calculated positions and refined isotropically with a riding model. Data collection and refinement statistics are collected in Tables 1 and 2. The structure of **5** at 220 K showed a weak diffraction due to the loss of CH_2Cl_2 solvent molecules from the structure. As a result of this weak diffraction, it was not possible to refine anisotropically C atoms from $[Fe^{II}(tren(imid)_3)]^{2+}$ complexes. Furthermore, this caused a smaller number of CH_2Cl_2 molecules in the structure solved at 220 K compared with that solved at 120 K (Table 2). The subroutine SQUEEZE from PLATON[21] was used to

calculate and remove the diffracting component of disordered solvents in **2**, **3** and **4**, resulting in a void of ca. 5383 $Å^3$ and 1537 electrons/cell for **2**, in two voids of ca. 314 $Å^3$ and ca. 90 electrons/cell plus six smaller voids of less than 41 $Å^3$ and 7 electrons/cell for **3**, and two voids of ca. 307 $Å^3$ and 96 electrons/cell plus four smaller voids of less than 54 $Å^3$ and 20 electrons/cell for **4**. This corresponds to ca. 23 H_2O molecules per asymmetric unit for **2**, ca. 2 CH_3CN molecules per asymmetric unit for **3**, and 1 CH_3OH + 2 CH_3CN molecules per asymmetric unit for **4**. The CH_3OH molecule from the smallest voids of **4** has been included in the formula of the compound in Table 2 and Supporting Information (see cif file). CCDC-998895 to 998898, 1003585, and 1004948 contain the supplementary crystallographic data for this paper. These data can be obtained free of charge from The Cambridge Crystallographic Data Centre via www.ccdc.cam.ac.uk/data_request/cif. Glass capillaries (0.5 mm) were filled with polycrystalline samples of the compounds and mounted and aligned on a Empyrean PANalytical powder diffractometer, using Cu Kα radiation (λ = 1.54177 Å). A total of two scans were collected at room temperature in the 2θ range 5-40°.

Physical Measurements. Magnetic measurements were performed with a Quantum Design MPMS-XL-5 SQUID magnetometer in the 2 to 300 K temperature range with an applied magnetic field of 0.1 T on polycrystalline samples. The AC measurements were performed in the temperature range of 2-15 K at different frequencies with an oscillating magnetic field of 0.395 mT. The magnetization and hysteresis studies were performed between 5 and -5 K T, cooling the samples at zero field. Infrared (IR) spectra were recorded on a FTIR 320 Nicolet spectrometer. C, H, and N elemental analyses were measured on a CE Instruments EA 1110 CHNS Elemental analyzer. The Fe/Mn/Cr/Cl and Fe/Mn/Cr/Br/Cl ratios were measured with a Philips ESEM X230 scanning electron microscope equipped with an EDAX DX-4 microsonde.

Table 1. Crystallographic data for compounds **1, 2** and **3**.

Compound	**1**	**2**	**3**
Empirical formula	$C_{49.5}H_{40}Cl_7CrFeMnN_9O_{15.5}$	$C_{38}H_{24}Cl_6CrFeMnN_4O_{16}$	$C_{47}H_{26}Br_6CrFeMnN_8O_{14}$
Formula weight	1419.84	1168.10	1569.01
Crystal color	Black	Black	Black
Crystal size	0.2×0.08×0.04	0.10×0.08×0.06	0.16×0.08×0.06
Temperature (K)	120(2)	120(2)	120(2)
Wavelength (Å)	0.71073	0.71073	0.71073
Crystal system, *Z*	Monoclinic, 4	Hexagonal, 3	Monoclinic, 4
Space group	*C* 222_1	*P* 6_122	*P* $2_1/c$
a (Å)	12.9780(6)	13.7059(2)	14.1383(7)
b (Å)	24.8692(12)	13.7059(2)	22.3075(10
c (Å)	21.9676(9)	66.2433(10)	23.4765(11
α (deg)	90	90	90
ß (deg)	90	90	103.200(5)
γ (deg)	90	120	90
V (Å^3)	7090.1(6)	10776.7(4)	7208.6(6)
ρ_{calc} (Mg/m^3)	1.330	1.081	1.446
μ(Mo Kα) (mm^{-1})	0.852	0.791	3.899
θ range (deg)	2.916-27.597	3.205-25.081	2.892-26.048
Reflns collected	81831	180425	117721
Independent reflns (R_{int})	8183 (0.1702)	7375 (0.2011)	7113 (0.2088)
L. S. parameters, *p*/ restraints, *r*	355 / 1	223 / 0	659 / 24
Absolute structure parameter	0.076(19)	0.19(10)	
$R1(F)$,[a] $I > 2\sigma(I)$	0.0935	0.1354	0.1505
$wR2(F^2)$,[b] all data	0.2815	0.3273	0.4105
$S(F^2)$,[c] all data	1.029	0.827	1.011

[a] $R1(F) = \Sigma||F_O|-|F_C||/\Sigma|F_O|$; [b] $wR2(F^2) = [\Sigma w(F_O^2-F_C^2)^2/\Sigma wF_O^4]^{1/2}$; [c] $S(F^2) = [\Sigma w(F_O^2-F_C^2)^2/(n+r-p)]^{1/2}$

Table 2. Crystallographic data for compounds **4, 5** at 120 K and **5** at 220 K.

Compound	**4**	**5** (120 K)	**5** (220 K)
Empirical formula	$C_{43}H_{40.5}Br_6Cl_4CrFeMnN_{5.5}O_{19}$	$C_{59}H_{59.5}Cl_{15}CrFe_2MnN_{20.5}O_{13}$	$C_{58}H_{55.5}Cl_{13}CrFe_2MnN_{20.5}O_{13}$
Formula weight	1722.32	2014.16	1927.22
Crystal color	Black	Black	Black
Crystal size	0.16×0.09×0.06	0.11×0.09×0.07	0.12×0.09×0.06
Temperature (K)	120(2)	120(2)	220(2)
Wavelength (Å)	0.71073	0.71073	0.71073
Crystal system, *Z*	Monoclinic, 4	Triclinic, 2	Triclinic, 2
Space group	*P* 2_1/c	*P*-1	*P*-1
a (Å)	13.9066(8)	13.2167(3)	13.2687(6)
b (Å)	23.1892(9)	16.2053(4)	16.5753(4)
c (Å)	22.7189(13)	20.2599(5)	20.3252(7)
α (deg)	90	97.796(2)	98.056(3)
ß (deg)	101.422(6)	97.354(2)	98.056(3)
γ (deg)	90	95.928(2)	95.922(3)
V (Å^3)	7181.4(7)	4231.55(18)	4347.9(3)
ρ_{calc} (Mg/m^3)	1.552	1.581	1.472
μ(Mo Kα) (mm^{-1})	4.066	1.148	1.054
θ range (deg)	2.985-26.427	2.955-27.502	2.849-26.483
Reflns collected	113316	62029	69165
Independent reflns (R_{int})	7832 (0.2296)	19299 (0.0887)	7112 (0.1373)
L. S. parameters, *p*/ restraints, *r*	706 / 0	1048 / 0	817 / 8
*R*1(*F*),[a] $I > 2\sigma(I)$	0.1618	0.0812	0.1101
*wR*2(F^2),[b] all data	0.4331	0.2649	0.3631
S(F^2),[c] all data	1.064	1.037	1.031

[a] $R1(F) = \Sigma||F_O|-|F_C||/\Sigma|F_O|$; [b] $wR2(F^2) = [\Sigma w(F_O^2-F_C^2)^2/\Sigma wF_O^4]^{1/2}$; [c] $S(F^2) = [\Sigma w(F_O^2-F_C^2)^2/(n+r-p)]^{1/2}$

Results and Discussion

Synthesis. The compounds of formula $[Fe^{III}(sal_2\text{-}trien)][Mn^{II}Cr^{III}(Cl_2An)_3]\cdot(CH_2Cl_2)_{0.5}\cdot(CH_3OH)\cdot(H_2O)_{0.5}\cdot(CH_3CN)_5$ (**1**), $[Fe^{III}(4\text{-}OH\text{-}sal_2\text{-}trien)][Mn^{II}Cr^{III}(Cl_2An)_3]\cdot(solvate)$ **(2)**, $[Fe^{III}(sal_2\text{-}epe)][Mn^{II}Cr^{III}(Br_2An)_3]\cdot(CH_3CN)_4\cdot(solvate)$ (**3**), $[Fe^{III}(5\text{-}Cl\text{-}sal_2\text{-}trien)][Mn^{II}Cr^{III}(Br_2An)_3]\cdot(CH_2Cl_2)\cdot(CH_3OH)\cdot(H_2O)_4\cdot(CH_3CN)_{1.5}\cdot(solvate)$ **(4)** and $[Fe^{II}(tren(imid)_3)]_2[Mn^{II}Cl_2Cr^{III}(Cl_2An)_3]Cl\cdot(CH_3OH)\cdot(CH_2Cl_2)_3\cdot(CH_3CN)_{0.5}$ **(5)** have been prepared and characterized. The method to prepare these anilate-based compounds differs from that used to prepare oxalate-based compounds with similar templating cations.[12] Oxalate-based compounds were obtained in most cases by the slow diffusion of a solution of the Fe^{III} or Fe^{II} complex into a solution containing the precursors of the oxalate network almost free of other counterions. This was possible thanks to the use of the Ag^+ salt of the $[Cr^{III}(ox)_3]^{3-}$ complex and $MnCl_2$ which enables the removal of Ag^+ and Cl^- counterions by precipitation of AgCl. In the case of the anilate-based compounds, a similar strategy could not be used due to poor stability of the Ag^+ salts of $[Cr^{III}(X_2An)_3]^{3-}$ complexes. $[NBu_4]^+$ salts of $[Cr^{III}(Cl_2An)_3]^{3-}$ and $[Cr^{III}(Br_2An)_3]^{3-}$ were chosen instead because they can be obtained with a high degree of purity, something very important for the crystallization of the compounds. On the other hand, because the mixture of $[NBu_4]_3[Cr^{III}(Cl_2An)_3]$ or $[NBu_4]_3[Cr^{III}(Br_2An)_3]$ and $MnCl_2$ in the same solvent gives rise to a fast precipitation of the 2D compound, $[NBu_4][Mn^{II}Cr^{III}(X_2An)_3]$ (X = Cl or Br), the two precursors of the anilate-based network were dissolved in different solvents. The best results were obtained mixing $MnCl_2$ with the Fe^{III} or Fe^{II} complex in methanol/dichloromethane and slowly diffusing this solution into an acetonitrile solution of $[(n\text{-}Bu)_4N]_3[Cr^{III}(Cl_2An)_3]$ or $[(n\text{-}Bu)_4N]_3[Cr^{III}(Br_2An)_3]$. Other solvent mixtures with the same templating cations (chloroform in the place of dichloromethane or methanol in the place of acetonitrile) gave rise to other phases with a similar structure that will be reported in future works. In the case of **5**, it was necessary to dissolve the Fe^{II} complex first in the methanol/dichloromethane mixture and then add the $MnCl_2\cdot4H_2O$ salt. The excess of Mn^{2+} resulting from an addition of the Fe^{II} complex to a

methanol solution of $MnCl_2 \cdot 4H_2O$ gives rise to the partial substitution of Fe^{II} by Mn^{II} in the tren(imid)$_3$ complex of the final compound. This was not observed in the other compounds of this paper. Furthermore, in contrast to **1**, **2**, **3** and **4**, the Cl^- anions from $MnCl_2$ in **5** are coordinated to Mn^{II} and act as counterions. The use of other Mn^{II} salts to avoid the presence of Cl^- in the structure did not result in suitable crystals for X-ray diffraction. The composition of crystals of these compounds was checked by elemental analysis and microanalysis. C, H and N elemental analyses show differences with respect to the calculated values using the formulas obtained from X-ray diffraction data at 120 K, in the case of **1**, **2** and **3**. These differences may be explained by the loss of solvent molecules when the crystals are extracted from the mother liquor at room temperature. Indeed, a good coincidence between experimental and calculated values is obtained by decreasing the number of solvent molecules in these three structures (see above). Moreover in the case of **1**, the low nitrogen and carbon contents could indicate rehydration with water. Thermal gravimetry analysis should be performed to clarify this point, but it was not possible due to the small amount of sample available. Microanalysis shows a Fe/Mn/Cr/Cl ratio close to 1:1:1:7 for **1**, 1:1:1:6 for **2**, and 2/1/1/9 for **5**, a Fe/Mn/Cr/Br ratio close to 1:1:1:6 for **3**, and a Fe/Mn/Cr/Cl/Br ratio close to 1:1:1:3:6 for **4**. The results obtained for compound **5** indicate that CH_2Cl_2 solvent molecules observed in the crystal structure are lost after extracting the crystals from the mother liquor.

Structures. The structures of all compounds have been solved by single-crystal X-ray diffraction. The structures of **1**, **2**, **3** and **4** consist of bimetallic anionic layers with a 2D bimetallic X_2An (X=Cl or Br) network of formula $[Mn^{II}Cr^{III}(X_2An)_3]^-$ with inserted Fe^{III} cationic complexes and solvent molecules. The bimetallic anilate layer presents in these four compounds the well-known honeycomb structure, which is similar to that found for other extended oxalate or anilate-based networks.[14a] It consists in a hexagonal layer where the Cr^{III} and Mn^{II} ions occupy alternating vertices of the hexagons and are linked through X_2An bridges in such a way that each Mn^{II} is surrounded by three neighboring Cr^{III} and vice versa. This contrasts with the oxalate-

based compounds obtained with similar Fe^{III} cationic complexes that may present either 2D or 3D structures, depending of the substituent of the sal_2-trien ligand.[12] In this work, three types of 2D structures have been obtained that present a similar 2D anilate-based network. Still, important differences in the packing of the Fe^{III} complexes and solvent molecules placed between these layers have been observed. They crystallize in orthorhombic (**1**), monoclinic (**3** and **4**) and hexagonal (**2**) space groups. A consequence of the replacement of oxalate by the larger bis-bidentate bridging X_2An^{2-} ligands is the presence of pores in the structures, which are filled with solvent molecules. Often these molecules are disordered. This has given rise to weak diffraction and quick loss of crystallinity due to fast evaporation of solvent molecules especially in compounds **2**, **3** and **4**. As a result of this, powder X-ray diffraction patterns of **1**, **2**, **3** and **4** do not show clear peaks. In contrast to the 2D compounds obtained with $[Fe^{III}(sal_2\text{-trien})]^+$ and derivatives, the use of the Fe^{II} complex, $[Fe^{II}(tren(imid)_3)]^{2+}$ results in the formation of an anionic chain in compound **5**. This chain is formed by $[Cr^{III}(Cl_2An)_3]^{3-}$ complexes bonded to two Mn^{II} ions through two bis-bidentate chloranilate bridges, whereas the third chloranilate is a terminal one. The octahedral coordination of Mn^{II} ions is completed with two chloride ions in cis. This type of structure has been found for other oxalate-based[4] and homometallic anilate-based compounds,[22] but it is the first time that it is obtained for heterometallic anilate-based networks. Again, the bimetallic oxalate-based compound obtained with the same complex presents a different structure, a very irregular 3D oxalate network with coexistence of bis(bidentate) and terminal oxalate ligands and solvent methanol molecules linked to heptacoordinated Mn^{II} ions.[12g] It seems that $[Fe^{II}(tren(imid)_3)]^{2+}$ favors the presence of terminal oxalate or anilate ligands due to the formation of hydrogen bonds beween the NH groups from imidazole ligands and the two oxygens of the terminal oxalate or anilate ligand (see below). The powder X-ray diffraction pattern of **5** presents some differences with respect to the theoretical one obtained from single crystal X-ray diffraction data at 120 or 220 K, which may be attributed to the loss of solvent molecules (CH_2Cl_2) after extracting the crystals from the mother liquor

already shown by micronalysis (see above and Figure S1 in the Supporting Information, SI).

Structure of $[Fe^{III}(sal_2\text{-trien})][Mn^{II}Cr^{III}(Cl_2An)_3]\cdot(CH_2Cl_2)_{0.5}(CH_3OH)(H_2O)_{0.5}(CH_3CN)_5$ (1). This compound crystallizes in the orthorhombic chiral space group $C222_1$. The structure is formed by bimetallic anionic sheets in the *ab* plane of formula $[Mn^{II}Cr^{III}(Cl_2An)_3]^-$ alternating with layers of $[Fe^{III}(sal_2\text{-trien})]^+$ cations (Figure 1). Acetonitrile, water, methanol or dichloromethane solvent molecules occupy the holes between cationic and anionic layers.

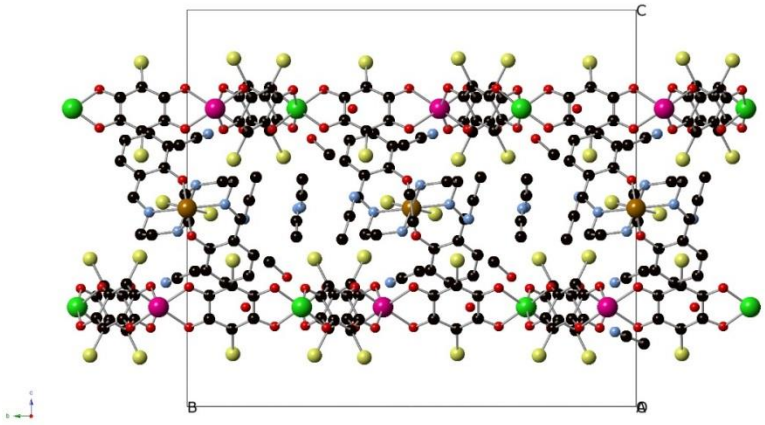

Figure 1. Projection of **1** in the *bc* plane. (Fe (brown), Cr (green), Mn (pink), C (black), N (blue), O (red), Cl (yellow). Hydrogen atoms have been omitted for clarity.

The anionic layer presents the honeycomb structure mentioned above (Figure 2). The Mn^{II} and Cr^{III} are localized and clearly distinguishable as they present different bond distances with anilate ligands. Thus, there is one crystallographically independent Mn, with an occupancy of 0.5 and Mn–O bond lengths in the range 2.136(8)-2.168(8) Å, and one crystallographically independent Cr, with an occupancy of 0.5 and Cr-O bond lengths in the range 1.975(8)-1.984(8) Å. These are typical Cr-O and Mn-O bond lengths. The neighboring metal centers of these layers present alternated chirality as usual for this type of 2D networks. In the crystal of **1** used to solve the structure, all the

Cr^{III} ions adopt a Δ-configuration, whereas all the Mn^{II} adopt the Λ-one. Therefore, the configuration of each metal ion is preserved in the neighboring anilate layers. Because we have started from a racemic mixture of $[Cr(Cl_2An)_3]^{3-}$, crystals of the two enantiomers are expected to be obtained. A similar behavior has been observed in other 2D oxalate and anilate structures.[8a,12c,f,14a] The chirality of the $[Fe^{III}(sal_2\text{-trien})]^+$ cations may be responsible of this first-order spontaneous resolution through chiral recognition between one of the enantiomers of $[Cr(Cl_2An)_3]^{3-}$ and $[Fe^{III}(sal_2\text{-trien})]^+$. In agreement to this, the crystallographically independent $[Fe^{III}(sal_2\text{-trien})]^+$ complex placed between the anilate layers adopts a Λ-configuration and interacts through several short contacts (see below) with the Cl_2An^{2-} ligands linked to Cr^{III} from the upper and lower layers, which adopt the opposite configuration. As expected, given the larger size of the $[Fe^{III}(sal_2\text{-trien})]^+$ cation, the interlayer distance in **1** (10.98 Å), is significantly longer than those observed in the other anilate-based 2D compounds with $[(H_3O)(phz)_3]^+$ (in the range 9.03-9.21 Å) or NBu_4^+ cations (8.42 Å).[14a] This longer interlayer distance and the displacement of consecutive layers in the *ab* plane (due to the *C*-type unit cell) implies that the minimum distance between metals of different layers (11.423 Å) is also significantly longer than those found in the other anilate-based 2D compounds with NBu_4^+ (9.69 Å, where the layers are also displaced) or $[(H_3O)(phz)_3]^+$ cations (9.03-9.21 Å, where the layers are eclipsed).[14a] Albeit, this shortest metal-metal distance in **1** (11.423 Å) is similar to that observed in the compounds obtained by insertion of $[Fe^{III}(sal_2\text{-trien})]^+$ cations and derivatives into 2D bimetallic oxalate-based networks (11.609-12.807 Å).[12] A second consequence of the displacement of the consecutive layers is the formation of channels along the *c* axis (Figure S2 in SI) that are occupied by solvent molecules.

The cationic layer intercalated between these anilate layers is formed by a crystallographically independent $[Fe^{III}(sal_2\text{-trien})]^+$ complex with an occupancy of 0.5 and solvent molecules. $[Fe^{III}(sal_2\text{-trien})]^+$ complexes are between two Mn atoms from the upper and lower anilate-based networks (Figures 2 and S2 in the SI). The longer axis of the molecule is approximately perpendicular to the anilate-based layers with

the atoms of the two phenolate rings of the complex parallel to one of the anilate ring of the two neighboring layers. Fe^{III} complexes present a very distorted octahedral symmetry. SHAPE calculations show that the coordination geometry around Fe falls along the minimal distortion path between a perfect octahedron and a perfect trigonal prism with a deviation of less than 10 %.[23] The generalized coordinate between the two ideal polyhedra is 50.1 %. This indicates that the geometry of the $[Fe^{III}(sal_2\text{-trien})]^+$ complexes is intermediate between a trigonal prism and an octahedron. It seems that the insertion of these cations into anilate-based networks induces a larger distortion of the octahedral geometry compared with their insertion into 2D oxalate-based networks, as the maximum values of trigonal prismacity of 2D oxalate-base compounds with similar complexes are always lower than 41 %.[12h] Average Fe-N and Fe-O bond lengths are 2.172(10) and 1.918(8) Å, which are in the range of those obtained for other HS Schiff base complexes, in agreement with magnetic properties (see below). The higher size of Cl_2An^{2-} ligand compared to the oxalate one gives rise to important differences in the packing of the spin-crossover cation compared to that observed in 2D oxalate-based compounds. Thus, in contrast to oxalate-based compounds, the spin-crossover cations are well isolated from each other as there are not intermolecular contacts between $[Fe^{III}(sal_2\text{-trien})]^+$ complexes belonging to the same layer. This is due to the fact that the size of the hexagons in the anilate-based layers is twice that of the oxalate-based ones. On the contrary, the $[Fe^{III}(sal_2\text{-trien})]^+$ complexes present numerous intermolecular interactions with the anilate-based network and solvent molecules. In particular, they present π-π stacking interactions between phenolate groups from $[Fe^{III}(sal_2\text{-trien})]^+$ complexes and the anilate ligands of the two neighboring layers. Thus, the two phenolate groups from $[Fe^{III}(sal_2\text{-trien})]^+$ complexes lie parallel to a Cl_2An^{2-} ligand of the upper and lower layer and present short C-C intermolecular distances (distance between the centroids of the two rings 3.475 Å). Furthermore, they present short contacts between their NH groups and Cl and O atoms from the upper and lower anilate-based layers (Figure S3 in the SI).

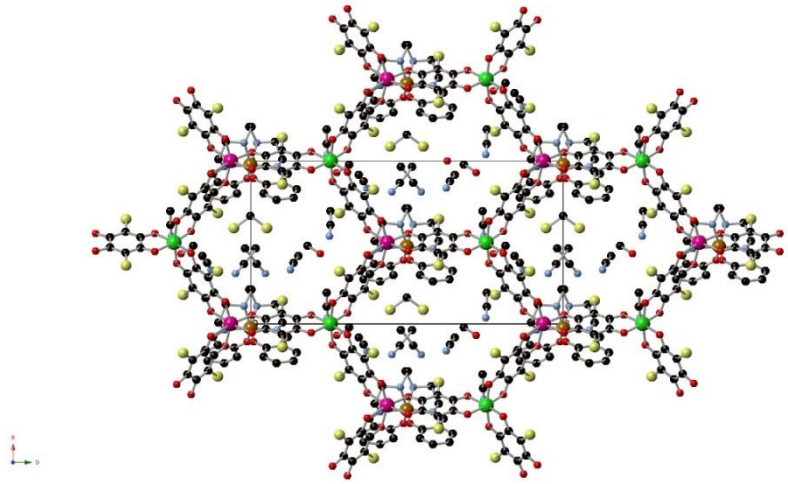

Figure 2. Projection of **1** in the *ab* plane showing one anionic layer and one cationic layer. (Fe (brown), Cr (green), Mn (pink), C (black), N (blue), O (red) Cl (yellow)). Hydrogen atoms have been omitted for clarity.

Structure of $[Fe^{III}(4\text{-OH-sal}_2\text{-trien})][Mn^{II}Cr^{III}(Cl_2An)_3]\cdot$(solvate) (**2**). This compound crystallizes in the hexagonal chiral space group $P6_122$. The structure is formed by bimetallic anionic sheets in the *ab* plane alternating along the *c* direction with layers containing $[Fe^{III}(4\text{-OH-sal}_2\text{-trien})]^+$ complexes and disordered solvent molecules (Figure 3).

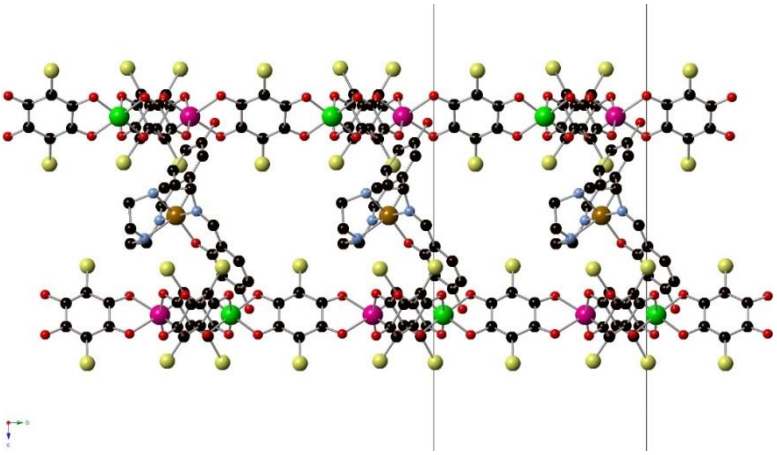

Figure 3. Projection of **2** in the *bc* plane. (Fe (brown), Cr (green), Mn (pink), C (black), N (blue), O (red), Cl (yellow)). Hydrogen atoms have been omitted for clarity.

The anionic layer presents the hexagonal honeycomb layer of the previous compound. There is one crystallographically independent Mn^{II} and Cr^{III}, which are localized and distinguishable (M-O bond lengths 2.122(11)-2.221(11) and 1.929(11)-2.035(12) Å, respectively). Mn and Cr present an occupancy of 0.5 as they are in a special position (2-fold axis). As shown in **1**, the configuration of each metal ion is preserved in the neighboring anilate layers. Thus, in the crystal used to solve the structure all the Cr^{III} ions adopt a Δ-configuration, whereas all the Mn^{II} ions adopt the Λ-one. $[Fe^{III}(4\text{-OH-sal}_2\text{-trien})]^+$ complex placed between the anilate layers adopts a Λ-configuration and interacts through several short contacts (see below) with two $\{Cr(Cl_2An)_3\}$ units from the upper and lower neighboring layers, which adopt the opposite configuration (Figure S4 in the SI). The minimum distance between metals of different layers is 11.060 Å, which is similar to that of compounds **1**, **3**, and **4**. As observed in **1**, the anilate-based layers in **2** are alternated.

The cationic layer intercalated between these anilate layers is formed by a crystallographically independent $[Fe^{III}(4\text{-OH-sal}_2\text{-trien})]^+$ complex with an occupancy of 0.5 due to the presence of a 2-fold axis, which runs from the Fe atom to a point placed in the middle of the central ethylene arm of the complex, and disordered solvent molecules. Average Fe-N and Fe-O bond lengths are 2.143(13) and 1.939(13) Å. These values are in the range of those obtained for other HS Schiff base complexes.[12] This contrasts with the LS state found in the $[Fe^{III}(4\text{-OH-sal}_2\text{-trien})]ClO_4$ precursor in the temperature range 2-300 K.[16] These complexes lie with their long axis almost perpendicular to the anilate network. As in **1**, the two phenolate groups lie parallel to a Cl_2An^{2-} ligand of the upper and lower layers with short C-C intermolecular distances (distance between the centroids of the two rings 3.440 Å) (Figure S4 in the SI). Furthermore, they present short contacts between their NH groups and Cl and O atoms from the upper and lower anilate-based layers. The generalized coordinate calculated with SHAPE[23] program is around 50 %. This indicates that the geometry of the $[Fe^{III}(4\text{-OH-sal}_2\text{-trien})]^+$ complexes is intermediate between a trigonal prism and an octahedron as in **1,** confirming that the intermolecular interactions of these cations

with two anilate layers may be the cause of the large distortion of the octahedral geometry. $[Fe^{III}(4\text{-OH-sal}_2\text{-trien})]^+$ complexes belonging to the same layer do not present intermolecular contacts, but interestingly and in contrast to compounds **1**, **3** and **4**, they form hydrogen-bonds with two $[Fe^{III}(4\text{-OH-sal}_2\text{-trien})]^+$ complexes of neighboring layers. This is a consequence of the large size of the hexagonal channels of the anilate-based anionic network that allows a high degree of penetration of the inserted cation. The lateral view of the structure (Figure 4) shows that the hydroxy groups from $[Fe^{III}(4\text{-OH-sal}_2\text{-trien})]^+$ complexes penetrate the anilate-based network, allowing the formation of hydrogen bonds with the $[Fe^{III}(4\text{-OH-sal}_2\text{-trien})]^+$ complexes from the upper and lower cationic layers. This gives rise to helical chains of $[Fe^{III}(4\text{-OH-sal}_2\text{-trien})]^+$ complexes (Figure 4) linked through hydrogen-bond interactions running along the *c* axis. This type of interactions has never been found in oxalate-based compounds. Finally, another consequence of the larger size of X_2An^{2-} ligands compared to the oxalate ones is the presence of holes in the structure surrounding the $[Fe^{III}(4\text{-OH-sal}_2\text{-trien})]^+$ complexes that are occupied by disordered solvent molecules and that could not be modelled (see Experimental Section and cif files). Indeed, crystals of **2** lose solvent very quickly when they are extracted from their mother liquor. Projection of the structure along the *bc* plane shows the presence of channels along the *a* axis that could be filled with different guest molecules (Figure 3). Thus, these compounds present a void volume of ca. 5383 $Å^3$ (ca. 50 % of the unit cell volume), where solvent molecules could be absorbed, opening the way to the synthesis of new porous magnets.

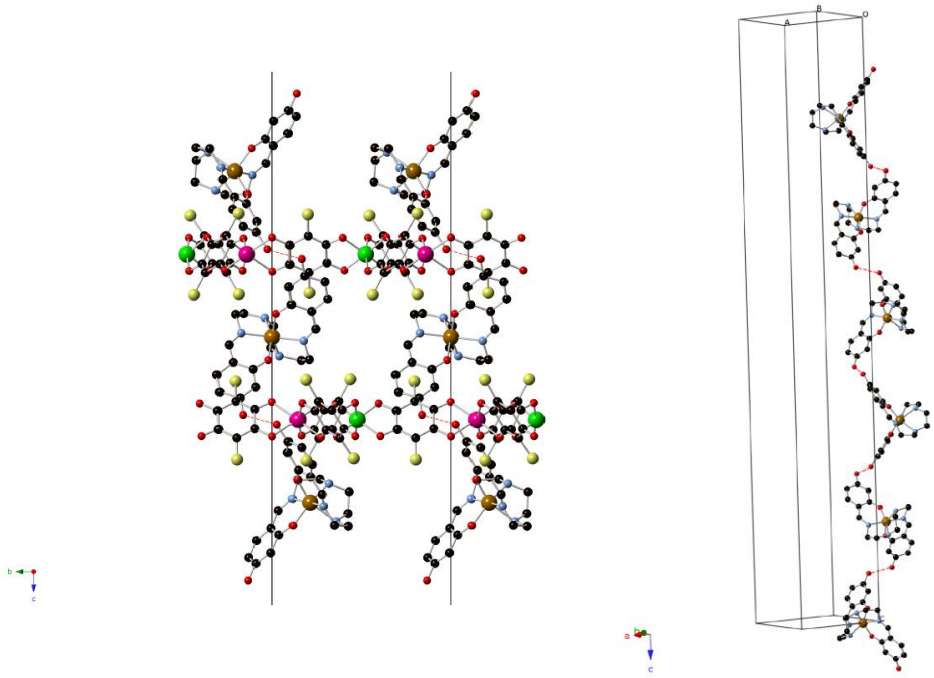

Figure 4. Projection of **2** in the *bc* plane showing the hydrogen bonds between $[Fe^{III}(4\text{-OH-sal}_2\text{-trien})]^+$ complexes from different layers (left). Helical chain of $[Fe^{III}(4\text{-OH-sal}_2\text{-trien})]^+$ complexes from different layers linked through hydrogen bonds (red dashed lines) (right). (Fe (brown), Cr (green), Mn (pink), C (black), N (blue), O (red), Cl (yellow)). Hydrogen atoms have been omitted for clarity.

Structure of $[Fe^{III}(sal_2\text{-epe})][Mn^{II}Cr^{III}(Br_2An)_3]\cdot(CH_3CN)_4$(solvate) (3) and $[Fe^{III}(5\text{-Cl-sal}_2\text{-trien})][Mn^{II}Cr^{III}(Br_2An)_3]\cdot(CH_2Cl_2)(CH_3OH)(H_2O)_4(CH_3CN)_{1.5}$(solvate) (4). The two compounds crystallize in the monoclinic space group $P2_1/c$. Their structure consists of 2D bimetallic $[MnCr(Br_2An)_3]^-$ layers in the *ab* plane with a honeycomb structure similar to that observed in compounds **1** and **2**, alternating with $[Fe^{III}(sal_2\text{-epe})]^+$ (in **3**) or $[Fe^{III}(5\text{-Cl-sal}_2\text{-trien})]^+$ (in **4**) cations and solvent molecules (Figure 5).

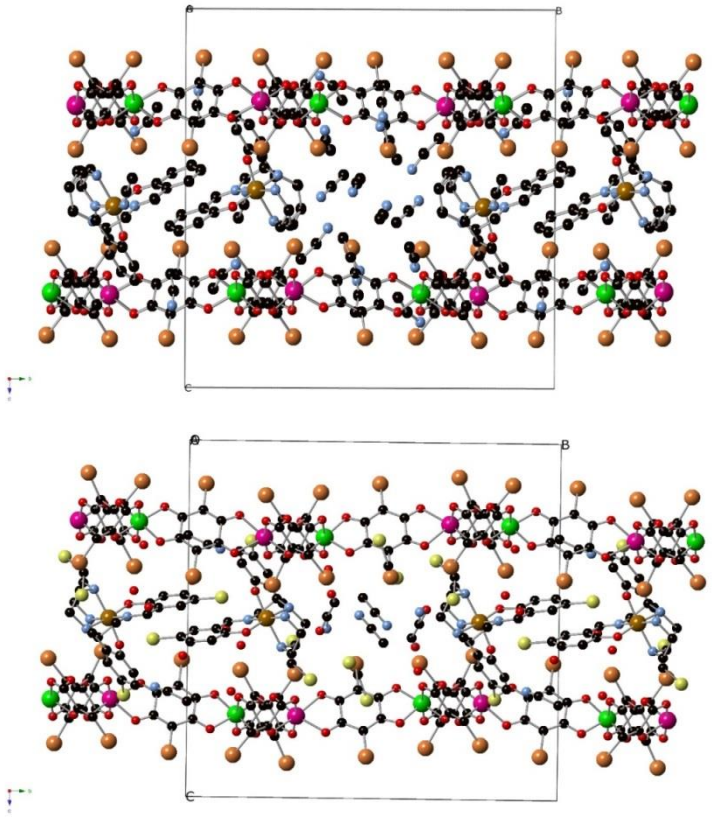

Figure 5. Projections of **3** (up) and **4** (down) in the *bc* plane. (Fe (brown), Br (orange), Cr (green), Mn (pink), C (black), N (blue), O (red), Cl (yellow)). Hydrogen atoms have been omitted for clarity.

In **4**, there is one crystallographically independent Mn^{II} and Cr^{III}, which are localized and distinguishable (M–O bond lengths 2.126(13)-2.206(16) Å and 1.961(15)-2.000(15) Å, respectively). Due to the presence of an inversion center located between the anilate-based layers, Mn and Cr ions from consecutive layers present opposite configurations. In contrast, the M-O bond lengths of the two crystallographically independent metal atoms of the anilate-based network in **3** (in the range 2.007(16)-2.127(15) Å) are intermediate between those expected for Mn-O and Cr-O bonds indicating a higher degree of disorder. The minimum distance between metals of

different layers is 11.919 Å for **3** and 11.557 Å for **4**, similar to those observed in compounds **1** and **2**. The anilate-based layers in **3** and **4** are also alternated.

The $[Fe^{III}(sal_2\text{-epe})]^+$, or $[Fe^{III}(5\text{-Cl-sal}_2\text{-trien})]^+$ complexes, and disordered solvent molecules occupying the space between the layers present a different packing to that shown in compounds **1** and **2**. Thus, two neighboring Fe^{III} complexes present several intermolecular interactions that involve the two phenolate rings (π-π stacking interactions between the two aromatic rings and two C-H$\cdots\pi$ or C-Cl$\cdots\pi$ interactions). These dimers of $[Fe^{III}(sal_2\text{-epe})]^+$ or $[Fe^{III}(5\text{-Cl-sal}_2\text{-trien})]^+$ complexes are well isolated from other Fe^{III} complexes, although they present numerous intermolecular interactions with solvent molecules and with the anilate-based layers. In contrast to **1** and **2**, only one of the two phenolate groups of the cations present π-π stacking interactions with the Br_2An^{2-} groups from the anilate-based layer as the other one is involved in the intermolecular interactions with a neighboring $[Fe^{III}(sal_2\text{-epe})]^+$ or $[Fe^{III}(5\text{-Cl-sal}_2\text{-trien})]^+$ complex as mentioned above (Figure S5 in the SI). $[Fe^{III}(sal_2\text{-epe})]^+$ and $[Fe^{III}(5\text{-Cl-sal}_2\text{-trien})]^+$ complexes present a distorted octahedral geometry with average Fe-N and Fe-O bond lengths of 2.122(18) and 1.939(16) Å for **3** and 1.98(2) and 1.854(18) Å for **4**. These bond lenghts indicate that the Fe ions in **3** are in the HS state, whereas those in **4** are in the LS one, in agreement with magnetic measurements (see below). SHAPE calculations[23] show that the coordination geometry around the Fe ion in **3** and **4** is closer to a perfect octahedron than that of compounds **1** and **2** (the generalized coordinate between a perfect octahedron and a perfect trigonal prism is 30.3 % for **3** and 14.3 % for **4**). These values are similar to those reported for similar complexes inserted into oxalate-based networks taking into account that HS complexes, as those of **3**, normally present a higher trigonal distortion.[12h] The higher trigonal distortion of **1** and **2** (with generalized coordinates of ca. 50 %) may be related to the distortions generated by the π-π intermolecular interactions between the Fe^{III} complexes and two anilate rings of two neighboring layers. Finally, the structures of **3** and **4** present numerous voids that are occupied by disordered solvents. Some of them could not be modelled (see Experimental Section

and cif files). Indeed, crystals of **3** and **4** lose solvent very quickly when they are out of the mother liquor.

Structure of $[Fe^{II}(tren(imid)_3)]_2[Mn^{II}Cl_2Cr^{III}(Cl_2An)_3]Cl\cdot(CH_3OH)(CH_2Cl_2)_3(CH_3CN)_{0.5}$ (5). This compound crystallizes in the triclinic space group *P*-1. It is formed by anionic $[Mn^{II}Cl_2Cr^{III}(Cl_2An)_3]^{3-}$ chains running along the *a* axis surrounded by $[Fe^{II}(tren(imid)_3)]^{2+}$, Cl^-, and solvent molecules (acetonitrile, methanol, or dichloromethane). These bimetallic anionic chains contain one crystallographically independent Cr and Mn with characteristic Mn-O and Cr-O distances (2.164(4)-2.370(4) Å for Mn1 and 1.950(4)-1.993(4) Å for Cr1). Furthermore, Mn is linked to two Cl^- anions in cis at 2.3823(19) and 2.4258(19) Å. These chains are formed by $[Cr^{III}(Cl_2An)_3]^{3-}$ complexes bonded to two Mn^{II} ions through two bis-bidentate chloranilate bridges while the third chloranilate is a terminal one (see Figure 6). At the same time, the Mn^{II} ions are coordinated to two chelating bis(bidentate) chloranilate bridges from two neighboring $[Cr^{III}(Cl_2An)_3]^{3-}$ complexes and to two chloride ion in cis (see Figure 6). These chains are formed by Mn and Cr ions of opposite chirality building a zigzag alternating arrangement of complexes. Due to the centrosymmetric space group, chains of both chiralities are observed in the structure related by an inversion center. $[Fe^{II}(tren(imid)_3)]^{2+}$ complexes, Cl^- anions, and solvent molecules surround these chains (Figure 6). $[Mn^{II}Cl_2Cr^{III}(Cl_2An)_3]^{3-}$ chains are in close contact with a neighboring one through halogen-halogen interactions[24] involving a Cl atom from Cl_2An ligand (Cl1) with minimum Cl···Cl interchain distances of 3.130 Å (Figure S6 in the SI). The shortest distance between metals of neighboring chains is 8.445 Å. These chains present numerous short contacts with free Cl^- anions, $[Fe^{II}(tren(imid)_3)]^{2+}$ complexes, and solvent molecules.

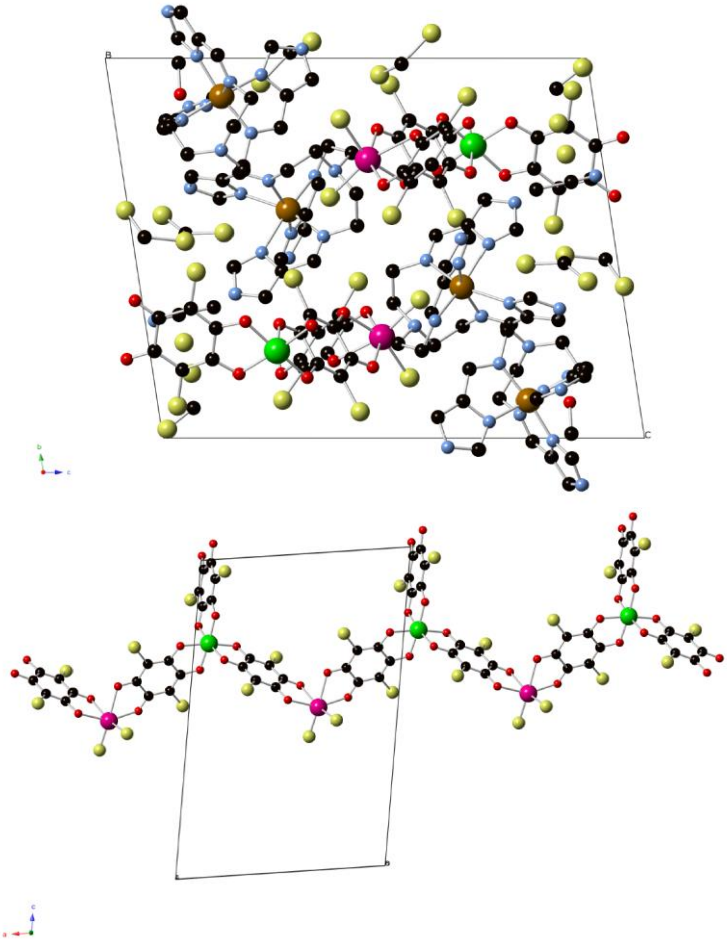

Figure 6. Projection of **5** in the *bc* plane (up). $[Mn^{II}Cl_2Cr^{III}(Cl_2An)_3]^{3-}$ chains in the structure of **5** (down). (Fe (brown), Cr (green), Mn (pink), C (black), N (blue), O (red), Cl (yellow)). Hydrogen atoms have been omitted for clarity.

$[Fe^{II}(tren(imid)_3)]^{2+}$ complexes, Cl^- anions, and solvent molecules are intercalated in the holes between these chains. There are two crystallographically independent $[Fe^{II}(tren(imid)_3)]^{2+}$ complexes in which Fe exhibits a distorted octahedral coordination environment involving six N donor atoms of the hexadentate Schiff base: three Fe-N(imine) and three Fe-N(imidazolyl) bonds. The average Fe–N distances of the two complexes (1.988(6) Å for the complex with Fe1 and 2.213(5) Å for the complex with

Fe2) are close to the ones expected for LS (Fe1) and HS (Fe2).[17] These distances indicate that at 120 K, the temperature of the structural resolution, half of the Fe^{II} complexes are in the HS state in agreement with magnetic measurements of the dry samples, see below. On the other hand, average Fe–N distances of the two complexes in the structure of another crystal solved at 220 K (2.162(10) Å for the complex with Fe1 and 2.235(8) Å for the complex with Fe2), are close to the expected ones for HS Fe^{II}. Furthermore, changes in the unit cell of this crystal indicate a shortening of *b* axis from 220 to 120 K, whereas the *a* and *c* axes remain almost constant (Figure S7 in the SI). At the same time, the unit cell volume decreases gradually from 220 to 120 K. All these changes are more important in the spin-crossover region (see below) from 220 to 140 K, indicating that they are associated with the change of spin state of half of the $[Fe^{II}(tren(imid)_3)]^{2+}$ complexes. It was not possible to solve the structure at 300 K due to the loss of crystallinity.

NH groups from two of the three imidazole ligands linked to Fe1 form hydrogen bonds with the Cl^- anion and a methanol molecule. In the same way, two of the three NH groups of $tren(imid)_3$ linked to Fe2 form hydrogen-bonds with the two oxygens of the terminal chloranilate ligand of Cr and the Cl^- anion. These hydrogen bonds between a terminal Cl_2An ligand and the NH groups of $[Fe^{II}(tren(imid)_3)]^{2+}$ could explain the coexistence of terminal and bridging Cl_2An ligands in this structure as they may compete with the coordination to a metal. This has also been observed in the bimetallic oxalate-based compounds obtained with $[Fe^{II}(tren(imid)_3)]^{2+}$.[12g] Cl^- anions occupy the holes between the $[Fe^{II}(tren(imid)_3)]^{2+}$ cations. As mentioned above, they form two hydrogen bonds with NH groups from two neighboring $[Fe^{II}(tren(imid)_3)]^{2+}$ complexes.

Finally, there are numerous holes that are occupied by acetonitrile, methanol, and dichloromethane solvent molecules, which are disordered in some cases.

Magnetic properties. Magnetic properties of **2** were measured for crystals of this compound in contact with the mother liquor to avoid the fast loss of solvent

molecules. The magnetic properties of the other four compounds were measured in freshly filtered samples. The product of the molar magnetic susceptibility times the temperature ($\chi_M T$) of the four 2D compounds is shown in Figure 7. It presents at 300 K a value close to 11.1 cm^3 K mol^{-1} for **1**, **2**, and **3**, and 8.3 cm^3 K mol^{-1} for **4**. These values are close to the expected ones for non-interacting Mn^{II} and Cr^{III} plus the contribution of a HS Fe^{III} ion (10.6 cm^3 K mol^{-1} for g = 2) in the case of **1**, **2**, and **3**, although the lower value found in **4** indicates that most of the Fe^{III} are in the LS state (expected value around 6.8 cm^3 K mol^{-1}). When the temperature is lowered, $\chi_M T$ of the four compounds shows a continuous decrease reaching a minimum value at 19.2 K (8.0 cm^3 K mol^{-1}) for **1**, 24.0 K (8.5 cm^3 K mol^{-1}) for **2**, 20.0 K (8.1 cm^3 K mol^{-1}) for **3**, and 18.5 K (5.9 cm^3 K mol^{-1}) for **4** followed by a sharp increase at lower temperatures with maxima between 6 and 9 K. The decrease of $\chi_M T$ with the temperature may be attributed to antiferromagnetic Mn-Cr interactions mediated through the X_2An^{2-} bridges, as observed in $[NBu_4]^+$ and $[(H_3O)(phz)_3]^+$ salts containing similar $[Mn^{II}Cr^{III}(X_2An)_3]^-$ layers (X = Cl, Br, I and H).[14a] Since the ground spin states of Cr^{III} and Mn^{II} are different (3/2 and 5/2, respectively), this interaction leads to an antiferromagnetic coupling that results in a $\chi_M T$ minimum, followed by an increase of $\chi_M T$ below ca. 18-22 K, and finally by a ferrimagnetic long range ordering at low temperatures for the four compounds. Furthermore, structural data may help to understand the contribution of the spin crossover to the observed decrease of $\chi_M T$. Thus, as the Fe-N and Fe-O bond lenghts of **1**, **2**, and **3** at 120 K indicate that the Fe^{III} ions are HS at this temperature, we conclude that only a small fraction of Fe^{III} ions in **1**, **2**, and **3** undergo spin crossover from 300 to 120 K. An additional proof of the absence of a significant spin-crossover transition in these three compounds is the linear behavior of the χ_M^{-1} versus T curve in the 50-300 K temperature range. This plot can be fitted to a Curie-Weiss law ($\chi_M^{-1} = (T - \theta)/C$) leading to Weiss constants, θ = -20.0 K for **1**, θ = -15.1 K for **2**, and θ = -13.1 K for **3,** which are close to those of other 2D $Mn^{II}Cr^{III}$ anilate-based networks.[14a] In the case of compound **4**, Fe-N and Fe-O bond lengths at 120 K indicate that the Fe^{III} complex is predominantly LS at this temperature. Therefore, the $\chi_M T$ value of **4** at 300 K and the approximately

constant difference of $\chi_M T$ of **1**, **2**, and **3** with respect to that of **4**, indicate that most of the Fe^{III} ions of this compound are in the LS state from 300 to 120 K. An additional proof of the absence of a significant spin-crossover in **4** is the linear behavior of the χ_M^{-1} versus *T* curve in the 50-300 K temperature range (θ value of -13.5 K). Mössbauer measurements are needed to confirm the LS/HS Fe^{III} ratios of these compounds with the temperature, but they could not be performed due to the small amount of sample available.

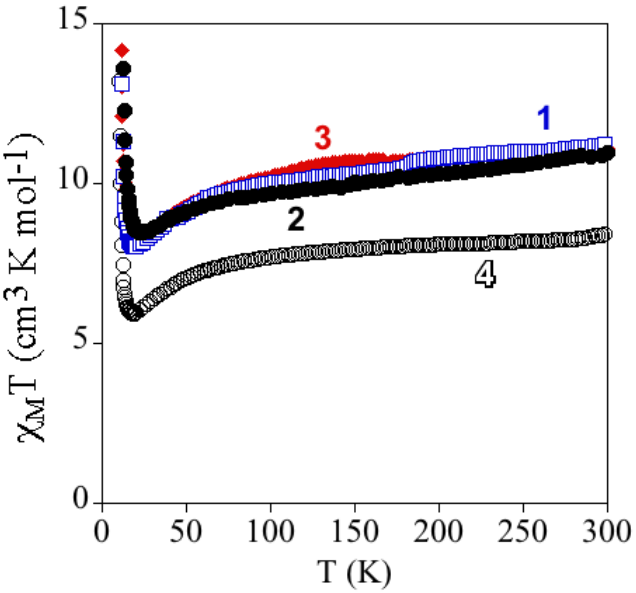

Figure 7. Temperature dependence of the product of the molar magnetic susceptibility times the temperature ($\chi_M T$) of **1** (empty blue squares), **2** (full circles), **3** (full red diamonds), and **4** (empty circles) with an applied field of 0.1 mT.

The confirmation of the long-range order and a more accurate determination of the ordering temperatures can be obtained from the susceptibility measurements performed with an alternating magnetic field (AC susceptibility). These measurements show a frequency-independent peak in the in-phase molar susceptibility (χ_M') and out-of-phase molar susceptibility (χ_M") of the four 2D compounds (Figure 8). In the case of **1**, the χ_M" is very weak and only appears at the lowest frequencies (1 and 10 Hz). On

the contrary, **2**, **3** and **4** show clear frequency-independent peaks in χ_M' and χ_M'' (Figure 8). In some cases, secondary peaks appear at lower temperatures that could be explained by formation of magnetic domains and domain-wall movement, as in the oxalate-based networks.[12] The ordering temperature, T_c, determined as the temperature at which χ_M'' becomes nonzero is ca. 10 K for **1**, 10.4 K for **2**, 10.2 K for **3**, and 9.8 K for **4**. These T_c values are much higher than those found for the $[NBu_4]^+$ and $[(H_3O)(phz)_3]^+$ salts containing similar $[Mn^{II}Cr^{III}(Cl_2An)_3]^-$ or $[Mn^{II}Cr^{III}(Br_2An)_3]^-$ layers (5.5 and 6.3 K),[14a] in contrast to oxalate-based 2D compounds, where T_c remains constant for a given 2D $[M^{II}M^{III}(C_2O_4)_3]^-$ lattice, independently of the inserted cation. We can, therefore, conclude that the magnetic coupling and, accordingly, the ordering temperatures of these heterometallic 2D anilate-based networks are much more sensitive to the changes of the inserted cations than the corresponding oxalate ones. The possible reasons to explain this effect are the presence of intermolecular interactions between the anilate ligands and Fe^{III} complexes (π-π interactions and NH···O and NH···Cl/Br interactions mentioned above), which are not observed in $[NBu_4]^+$ and $[(H_3O)(phz)_3]^+$ salts containing similar $[Mn^{II}Cr^{III}(Cl_2An)_3]^-$ or $[Mn^{II}Cr^{III}(Br_2An)_3]^-$ layers. Some of these interactions could result in an increase of the Mn^{II}-Cr^{III} coupling constant through the anilate ligand and, accordingly, of T_c. In fact, these exchange interactions have shown to be very sensitive to small electronic changes introduced in the anilate bridge. Thus, in the series $(NBu_4)[MnCr(X_2An)_3]$, a change in the electron density in the anilate ring by changing X from Cl to H has resulted in an increase of T_c from 5.5 K up to 11.0 K.[14a] Interestingly, this modulation of T_c with the inserted cation (or even with solvent molecules), besides the already observed modulation with X,[14a] represents an additional advantage of the anilate-based networks compared with the oxalate ones.

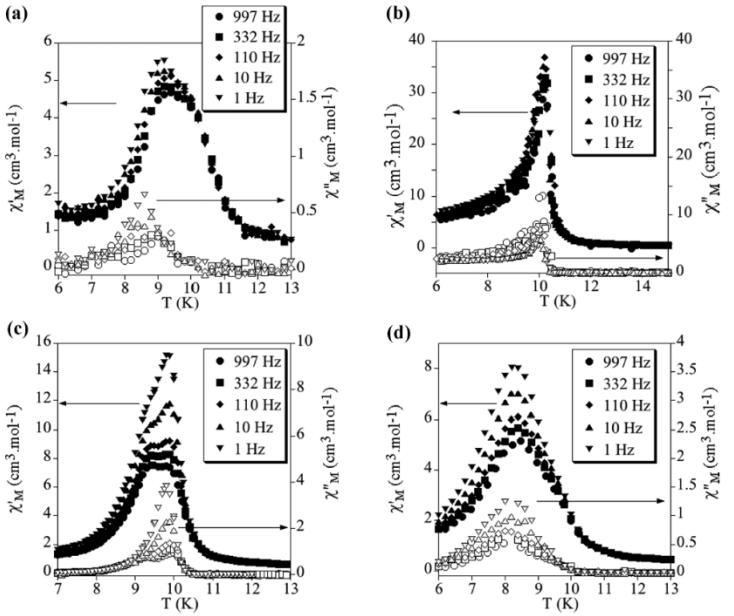

Figure 8. Temperature dependence of the in-phase AC susceptibility (χ') (filled symbols) and the out-of-phase AC susceptibility (χ'') of **1** (a), **2** (b), **3** (c), and **4** (c).

The ferrimagnetic nature of the long-range ordering is confirmed by the isothermal magnetization measurements at 2 K that show a sharp increase of the magnetization at low fields that becomes more gradual at higher fields (Figure 9). At low fields (H < 0.2 T), the magnetizations of the four compounds increase with high slope reaching values in the range 1.4-1.6 μ_B at H = 0.1 T (inset in Figure 9). At higher fields, the magnetization of the four compounds shows a gradual and nonlinear increase, which is higher in the case of **1, 2**, and **3** (7.1 μ_B for **1**, 6.3 μ_B for **2** and 7.2 μ_B for **3** at 5 T) than in **4** (4.0 μ_B at 5 T). These values are still far from saturation. The magnetization at lower fields is close to the expected value for a ferrimagnetic $Mn^{II}Cr^{III}$ network (M_s = 5 μ_B - 3 μ_B = 2 μ_B, possibly reduced by spin-canting effects in the anilate network). The gradual nonlinear increase observed at higher fields may be due to the contribution of the paramagnetic Fe^{III} plus the result of the competition between the antiferromagnetic couplings and the Zeeman interaction with the external magnetic field. The higher increase in **1**, **2**, and **3** compared to that in **4** indicates that most of the

Fe^{III} of **1**, **2**, and **3** are in the HS state, whereas those of **4** are in the LS state at 2 K, in agreement with susceptibility measurements. These isothermal magnetization measurements also provide an additional proof of the magnetic ordering exhibited by these compounds because they present hysteresis below the ordering temperatures with coercive fields of ca. 35 mT for **1**, 87 mT for **2**, 10 mT for **3**, and 66 mT for **4** (Figure 9).

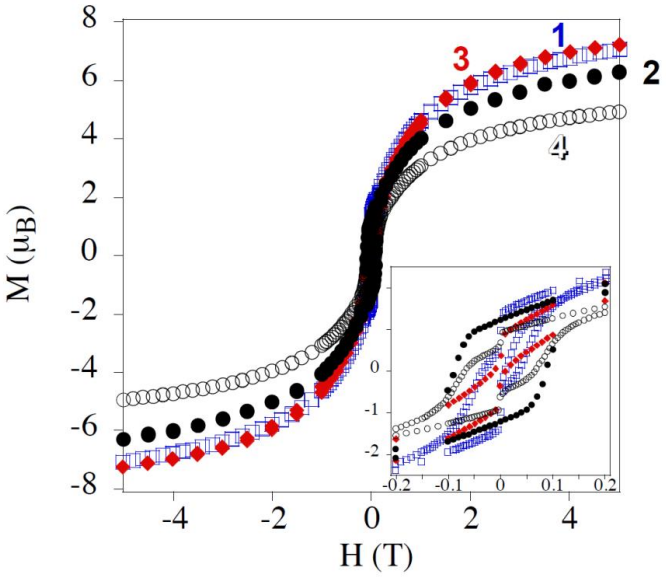

Figure 9. Isothermal magnetization at 2 K of **1** (empty blue squares), **2** (full circles), **3** (full red diamonds), and **4** (empty circles).

The $\chi_M T$ of **5** is shown in Figure 10. It presents at 300 K a value of 11.2 cm^3 K mol^{-1}. This value is close to the expected one for non-interacting Mn^{II} and Cr^{III} plus the contribution of two HS Fe^{II} ion (12.25 cm^3 K mol^{-1} for g = 2) in agreement with crystal structure at 220 K, which suggests that most of the Fe^{II} are in the HS. From 280 to 100 K, $\chi_M T$ shows a continuous decrease reaching a value of 8.4 cm^3 K mol^{-1} at 100 K. The decrease of $\chi_M T$ in this range of temperature (≈ 3 cm^3 K mol^{-1}) corresponds to the expected one for the spin-crossover of half of the Fe^{II}. This is supported by the structural data at 120 K, which indicate that 50 % of Fe^{II} are in the HS at this

temperature (see above). At lower temperatures, $\chi_M T$ presents a gradual decrease that becomes very abrupt below 50 K to reach a minimum at 4.8 K followed by a sharp increase at lower temperatures. This behavior may be attributed to the antiferromagnetic Mn-Cr interactions mediated through the X_2An^{2-} bridges within the chains, as observed in the other compounds in this paper. This is supported by the magnetic data of other Mn^{II}-Cr^{III} chains of similar structure to that of **5** with diamagnetic counterions, obtained very recently by us, that show a very gradual decrease of $\chi_M T$ from 300 K (6.3 cm^3 K mol^{-1}) to 100 K (6.1 cm^3 K mol^{-1}) and an abrupt decrease below 50 K with a minimum at 6 K (2.5 cm^3 K mol^{-1}) followed by a sharp increase at lower temperatures.[25]

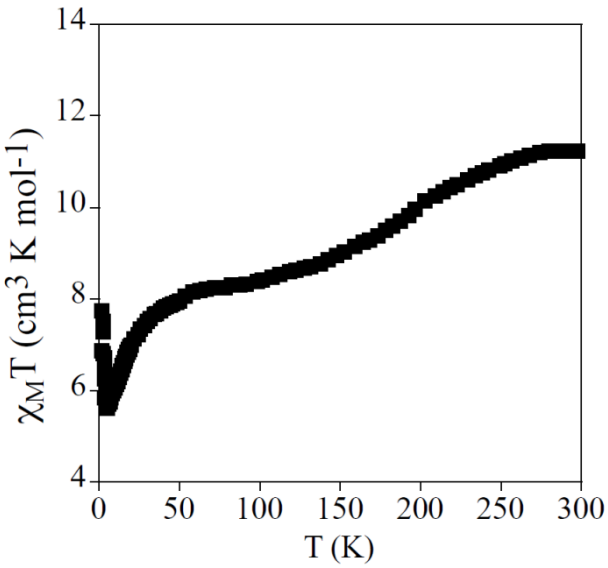

Figure 10. Temperature dependence of the product of the molar magnetic susceptibility times the temperature ($\chi_M T$) of **5** with an applied field of 0.1 mT.

AC measurements show a frequency-independent peak in χ_M' and χ_M'' at temperatures below 2.6 K (Figure 11). This indicates that the compound presents a magnetic long-range ordering below this temperature. The lack of frequency dependence of the AC peaks excludes a single-chain magnet (SCM) behavior.

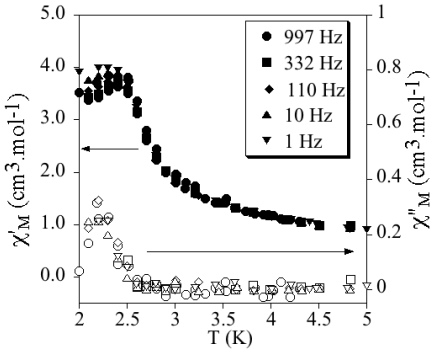

Figure 11. Temperature dependence of the in-phase AC susceptibility (χ') (filled symbols) and the out-of-phase AC susceptibility (χ'') of **5**.

The ferrimagnetic nature of the long range ordering is confirmed by the isothermal magnetization measurements at 2 K that show a sharp increase of the magnetization at low fields (1.5 μ_B at H = 0.2 T) that becomes more gradual at higher fields (Figure S8 in the SI). As in the four previous compounds, the magnetization at lower fields is close to the expected value for a ferrimagnetic $Mn^{II}Cr^{III}$ network (M_s = 5 μ_B - 3 μ_B = 2 μ_B), while the gradual nonlinear increase observed at higher fields may be due to the contribution of the paramagnetic HS Fe^{II}. The hysteresis loop does not show a measurable coercive field. Therefore, this compound behaves as a soft magnet. The magnetic ordering must be the result of the ferromagnetic interchain interactions, induced by dipolar interactions and also by a possible superexchange pathway that can work through the halogen-halogen interchain interactions (see above). The synthesis of other compounds with a similar structure (replacement of $[Fe^{II}(tren(imid)_3)]^{2+}$ by diamagnetic complexes or of Cl_2An by Br_2An) is in progress in order to understand the role played by spin-crossover complexes and X_2An ligands in the interchain interactions.

Conclusion

Five novel compounds formed by $[Fe^{III}(sal_2\text{-trien})]^+$, $[Fe^{III}(5\text{-Cl-sal}_2\text{-trien})]^+$, $[Fe^{III}(sal_2\text{-epe})]^+$, $[Fe^{III}(4\text{-OH-sal}_2\text{-trien})]^+$ and $[Fe^{II}(tren(imid)_3)]^{2+}$ and anionic bimetallic

coordination polymers based on the anilate ligand have been prepared and characterized. Two-dimensional anilate-based networks with a honeycomb structure have been obtained with the $[Fe^{III}(sal_2\text{-trien})]^+$ complex and derivatives (compounds **1**-**4**), whereas a one-dimensional (1D) anilate-based network has been obtained with $[Fe^{II}(tren(imid)_3)]^{2+}$ (compound **5**).

The first consequence of the replacement of oxalate by anilate ligands for $[Fe^{III}(sal_2\text{-trien})]^+$ and derivatives is that the formation of 2D compounds is favored when the larger anilate ligands are used. With oxalate ligands, one obtains either 2D or 3D networks, depending on the substituent of sal_2-trien. A second consequence is that, due to the larger size of anilate ligands, the distances between the Fe^{III} complexes inserted between the anilate layers are larger. This leads in some cases to the absence of intermolecular interactions between the spin-crossover complexes belonging to the same layer (**1** and **2**) or to the presence of isolated dimers of Fe^{III} complexes (**3** and **4**). Furthermore, this results in the presence of large voids filled with disordered solvent molecules. Finally, a third consequence of the substitution of oxalate by anilate is the presence of π-π stacking interactions between the anilate ligands and the phenolate rings of the spin-crossover complexes, which is not observed in the oxalate-based compounds. These π-π interactions, more important in compounds **1** and **2**, lead to a larger trigonal distortion of the octahedral geometry of Fe^{III} in these compounds. The rigidity imposed by π-π stacking with the anilate ligands and the lack of intermolecular interactions between the Fe^{III} complexes may be at the origin of the absence of a significant spin-crossover in the 2D compounds. Thus, the magnetic properties indicate that most of the inserted Fe^{III} cations remain in their HS (**1**, **2**, and **3)** or LS state (**4).** At the same time the anilate network presents a ferrimagnetic ordering at ca. 10 K, which is significantly higher than the ordering temperatures obtained for oxalate networks with the same metal ions (ca. 5 K) or for 2D anilate networks with other templating cations (ca. 6 K for $[NBu_4]^+$ and $[(H_3O)(phz)_3]^+$ salts). Notice that the presence of pores in these structures and the chiral character of some of them could lead to new

functionalities, in addition to the magnetic ordering such as solvent adsorption, proton conduction or chirality.

The preparation of anilate-based compounds combining spin-crossover and magnetic ordering has been achieved with the use of $[Fe^{II}(tren(imid)_3)]^{2+}$ complex, which do not present spin-crossover in bimetallic oxalate-based compounds.[12g] Compound **5** presents a 1D anionic anilate-based network surrounded by $[Fe^{II}(tren(imid)_3)]^{2+}$ complexes, Cl^- anions, and solvent molecules. The main difference with the previous series of 2D compounds is that the spin-crossover complexes do not show π-π stacking interactions with the anilate ligands and present numerous intermolecular contacts among them. As a result of this, **5** shows coexistence of spin crossover of half of the Fe^{II} complexes from 280 to 100 K and a ferrimagnetic coupling within the chains that gives rise to a magnetic ordering below 2.6 K. Photomagnetic measurements are in progress to study the possible effect of a photoinduced spin crossover in the magnetic properties of the anilate-based network in the search for a magnetic responsive material.

Finally, an additional advantage provided by this type of networks that remains to be explored is the functionalization of the anilate ligands with substituents leading to strong intermolecular interactions between the ferrimagnetic network and the spin-crossover complex or even covalent bonding between the two networks in order to enhance the interactions between them and to improve their responsive character.

Acknowledgments.

We thank the EU (SPINMOL ERC Adv. Grant), the Spanish MINECO (CTQ-2011-26507, and MAT2011-22785) and the Generalitat Valenciana (Prometeo and ISIC-Nano programs) for financial support. The authors also thank J. M. Martínez-Agudo and Dr. G. Agustí-López, University of Valencia, for magnetic characterization.

Notes and References.

[1] (a) Coronado E.; Day, P. *Chem. Rev.* **2004**, *104*, 5419-5448. (b) Coronado, E.; Martí-Gastaldo, C.; Navarro-Moratalla, E.; Ribera, A.; Blundell S. J.; Baker, P. J. *Nat. Chem.* **2010**, *2*, 1031-1036. (c) Coronado, E.; Martí-Gastaldo, C.; Navarro-Moratalla, E.; Burzuri, E.; Camon, E.; Luis, F. *Adv. Mater.* **2011**, *23*, 5021-5026. (d) Bourzami, R.; Eyele-Mezui, S.; Delahaye, E.; Drillon, M.; Rabu, P.; Parizel, N.; Choua, S.; Turek, P.; Rogez, G. *Inorg. Chem.* **2014**, *53*, 1184-1194.

[2] Coronado, E.; Mínguez Espallargas, G. *Chem. Soc. Rev.* **2013**, *42*, 1525-1539.

[3] See for general reviews: (a) Eds. Gütlich, P. and Goodwin, H.A. Spin Crossover in Transition Metal Compounds, *Topics in Current Chemistry*, Springer Verlag, Berlin-Heidelberg-New York, 2004, vols. *233-235*. (b) Ed. Halcrow, M. A. Spin-Crossover Materials: Properties and Applications, Wiley, New York, 2013.

[4] Clemente-León, M.; Coronado, E.; Martí-Gastaldo C.; Romero, F. M. *Chem. Soc. Rev.* **2011**, *40*, 473-497.

[5] (a) Clemente-León, M.; Galán-Mascarós, J. R.; Gómez-García, C. J. *Chem. Commun.* **1997**, 1727-1728. (b) Coronado, E.; Galán-Mascarós, J. R.; Gómez-García, C. J.; Martínez-Agudo, J. M. *Adv. Mater.* **1999**, *11*, 558-561. (c) Coronado, E.; Galán-Mascarós, J. R.; Gómez-García, C. J.; Ensling, J.; Gutlich, *Chem. Eur. J.* **2000**, *6*, 552-563.

[6] (a) Bénard, S.; Yu, P.; Audière, J. P.; Rivière, E.; Clèment, R.; Ghilhem, J.; Tchertanov, L.; Nakatami, K. *J. Am. Chem. Soc.* **2000**, *122*, 9444-9454. (b) Aldoshin, S. M.; Sanina, N. A.; Minkin, V. I.; Voloshin, N. A.; Ikorskii, V. N.; Ovcharenko, V. I.; Smirnov, V. A.; Nagaeva, N. K. *J. Mol. Struct.* **2007**, *826*, 69-74.

[7] (a) Coronado, E.; Galán-Mascarós, J. R.; Gómez-García C. J.; Laukhin, V. *Nature* **2000**, *408*, 447-449. (b) Alberola, A.; Coronado, E.; Galán-Mascarós, J. R.; Giménez-Saiz, C.; Gómez-García, C. J. *J. Am. Chem. Soc.* **2003**, *125*, 10774-10775. (c) Galán-Mascarós, J. R.; Coronado, E.; Goddard, P. A.; Singleton, J.; Coldea, A. I.; Wallis, J. D.; Coles S. J.; Alberola, A. *J. Am. Chem. Soc.* **2010**, *132*, 9271-9273. (d) Coronado, E.; Galán-Mascarós, J. R.; Gómez-García, C. J.; Martínez-Ferrero, E.; Van Smaalen, S. *Inorg. Chem.* **2004**, *43*, 4808-4810. (d) Zhang, B.; Zhang, Y.; Zhu, D. *Chem. Commun.* **2012**, *48*, 197-199.

[8] (a) Okawa, H.; Shigematsu, A.; Sadakiyo, M.; Miyagawa, T.; Yoneda, K.; Ohba, M.; Kitagawa, H. *J. Am. Chem. Soc.* **2009**, *131*, 13516-13522. (b) Pardo, E.; Train, C.; Contard, G.; Boubekeur, K.; Fabelo O.; Liu, H.; Dkhil, B.; Lloret, F.; Nakagawa, K.; Tokoro, H.; Ohkoshi, S. –I.; Verdaguer, M. *J. Am. Chem. Soc.* **2011**, *133*, 15328-15331. (c) Sadayiko, M.; Okawa, H.; Shigematsu, A.; Ohba, M.; Yamada, T.; Kitagawa, H. *J. Am. Chem. Soc.* **2012**, *134*, 5472-5475. (d) Okawa, H.; Sadakiyo, M.; Yamada, T.; Maesato, M.; Ohba, M.; Kitagawa, H. *J. Am. Chem. Soc.* **2013**, *135*, 2256-2262.

[9] (a) Endo, T.; Akutagawa, T.; Noro, S. I.; Nakamura, T. *Dalton Trans.* **2011**, *40*, 1491-1496. (b) Pardo, E.; Train, C.; Liu, H.; Chamoreau, L.-M.; Dkhil, B.; Boubekeur, K.; Lloret, F.; Nakatani, K.; Tokoro, H.; Ohkoshi, S.-i.; Verdaguer, M. *Angew. Chem. Int. Ed*. **2012**, *51*, 8356-8360.

[10] (a) Andrés, R.; Gruselle, M.; Malézieux, B.; Verdaguer, M.; Vaissermann, J.; *Inorg. Chem.* **1999**, *38*, 4637-4646. (b) Andrés, R.; Brissard, M.; Gruselle, M.; Train, C.; Vaissermann, J.; Malézieux, B.; Jamet, J. P.; Verdaguer, M. *Inorg. Chem.* **2001**, *40*, 4633-4640. (c) Clemente-León, M.; Coronado, E.; Dias, J. C.; Soriano-Portillo, A.; Willett, R. D. *Inorg. Chem.* **2008**, *47*, 6458-6463. (d) Train, C.; Gheorghe, R.; Krstic, V.; Chamoreau, L. M.; Ovanesyan, N. S.; Rikken, G. L. J. A.; Gruselle M.; Verdaguer, M. *Nat. Mater.* **2008**, *7*, 729-734. (e) Train, C.; Nuida, T.; Gheorghe, R.; Gruselle, M.; Ohkoshi, S. *J. Am. Chem. Soc.* **2009**, *131*, 16838-16843. (f) Gruselle, M.; Li, Y.; Ovanesyan, N.; Markhaev, V.; Shilov, G.; Mushenok, F.; Train, C.; Aldoshin, S. *Chirality* **2013**, *25*, 444-448.

[11] Clemente-León, M.; Coronado, E.; Gómez-García, C. J.; López-Jordà, M.; Camón, A.; Repollés, A.; Luis, F. *Chem. Eur. J*. **2014**, *20*, 1669-1676.

[12] (a) Clemente-León, M.; Coronado, E.; Giménez-López, M. C.; Soriano-Portillo, A.; Waerenborgh, J. C.; Delgado, F. S.; Ruiz-Pérez, C. *Inorg. Chem.* **2008**, *47*, 9111-9120. (b) Clemente-León, M.; Coronado, E.; López-Jordà, M.; Mínguez Espallargas, G.; Soriano-Portillo, A.; Waerenborgh, J. C. *Chem. Eur. J*. **2010**, *16*, 2207-2219. (c) Clemente-León, M.; Coronado, E.; López-Jordà, M. *Dalton Trans.* **2010**, *39*, 4903-4910. (d) Clemente-León, M.; Coronado, E.; López-Jordà, M.; Waerenborgh, J. C. *Inorg. Chem.* **2011**, *50*, 9122-9130. (e) Clemente-León, M.; Coronado, E.; López-Jordà, M.; Desplanches, C.; Asthana, S.; Wang, H.; Létard, J.-F. *Chem. Sci.* **2011**, *2*, 1121-1127. (f) Clemente-León, M.; Coronado, E.; López-Jordà, M. *Eur. J. Inorg. Chem.* **2013**, 2013, 753-762. (g) Ben Djamâa, A.; Clemente-León, M.; Coronado, E.; López-Jordà, M. *Polyhedron* **2013**, *64*, 142-150. (h) Clemente-León, M.; Coronado, E.; López-Jordà, M.; Waerenborgh, J. C.; Desplanches, C.; Wang, H.; Létard, J.-F.; Hauser, A.; Tissot, A. *J. Am. Chem.* Soc. **2013**, *135*, 8655-8677.

[13] Coronado, E.; Galán-Mascarós, J. R.; Giménez-López, M. C.; Almeida, M.; Waerenborgh, J. C. *Polyhedron* **2007**, *26*, 1838-1844.

[14] (a) Atzori, M.; Benmansour, S.; Mínguez Espallargas, G.; Clemente-León, M.; Abhervé, A.; Gómez-Claramunt, P.; Coronado, E.; Artizzu, F.; Sessini, E.; Deplano, P.; Serpe, A.; Mercuri, M: L.; Gómez-García, C. J. *Inorg. Chem.* **2013**, *52*, 10031-10040. (b) Atzori, M.; Artizzu, F.; Sessini, E.; Marchiò, L.; Loche, D.; Serpe, A.; Deplano, P.; Concas, G.; Pop, F.; Avarvari, N.; Mercuri, M: L. *Dalton Trans.* **2014**, *43*, 7006-7019.

[15] (a) Tweedle, M. F.; Wilson L. J. *J. Am. Chem. Soc*. **1976**, *98*, 4824-4834. (b) Griffin, M.; Shakespeare, S.; Shepherd, H. J.; Harding, C. J.; Létard, J. F.; Desplanches, C.; Goeta, A.

E.; Howard, J. A. K.; Powell, A. K.; Mereacre, V.; Garcia, Y.; Naik, A. D.; Müller-Bunz, H.; Morgan, G. G. *Angew. Chem. Int. Ed.* **2011**, *50*, 896-900.

[16] Nemec, I.; Herchel, R.; Salitros, I.; Trávnícek, Z.; Moncol, J.; Fuess, H.; Ruben, M.; Linert, W. *CrystEngComm* **2012**, *14*, 7015-7024.

[17] Sunatsuki, Y.; Ohta, H.; Kojima, M.; Ikuta, Y.; Goto, Y.; Matsumoto, N.; Iijima, S.; Akashi, H.; Kaizaki, S.; Dahan, F.; Tuchagues, J. -P. *Inorg. Chem.* **2004**, *43*, 4154-4171.

[18] Altomare, A.; Burla, M. C.; Camalli, M.; Cascarano, G. L.; Giacovazzo, C.; Guagliardi, A.; Moliterni, A. G. G.; Polidori, G.; Spagna, R. *J. Appl. Cryst*. **1999**, *32*, 115-119.

[19] Sheldrick, G. M. *Acta Cryst.* **2008**, *A64***,** 112-122.

[20] Farrugia, L. J. *J. Appl. Cryst.* **2012**, *45*, 849-854.

[21] Spek, A.L *J.Appl.Cryst.* **2003**, *36*, 7-13.

[22] (a) Kitagawa, S.; Kawata, S. *Coord. Chem. Rev.* **2002**, *224*, 11-34. (b) Michaelides, A.; Papadimitriou, C. D.; Plakatouras, J. C.; Skoulika, S.; Veltsistas, P. G. *Polyhedron* **2004**, *23*, 2587-2593. (c) Morikawa, S.; Yamada, T.; Kitagawa, H. *Chem. Lett.* **2009**, *38*, 654-655. d) Yamada, T.; Morikawa, S.; Kitagawa, H. *Bull. Chem. Soc. Jpn.* **2010**, *83*, 42-48.

[23] Llunell, M.; Casanova, D.; Cirera, J.; Bofill, J. M.; Alemany, P.; Alvarez, S.; Pinski, M.; Avnir. D. *SHAPE*, version 2.0; University of Barcelona, 2010.

[24] Mínguez Espallargas, G.; Brammer, L.; Allan, D. R.; Pulha, C. R.; Robertson, N.; Warren, J. E. *J. Am. Chem. Soc.* **2008**, *130,* 9058-9071.

[25] Abhervé, A.; Clemente-León, M.; Coronado, E.; Gómez-García, C. J. Unpublished results.

Associated Content:

Electronic Supplementary Information (ESI) for Inorganic Chemistry

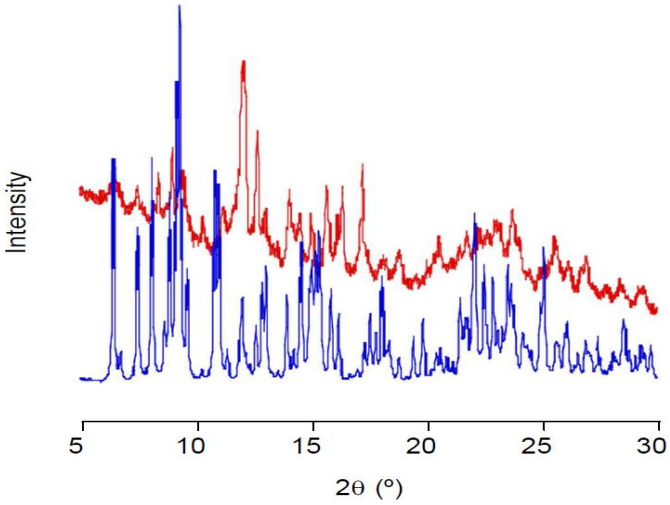

Figure S1. Powder X-ray diffraction pattern (red) and simulated one (blue) of **5** at room temperature.

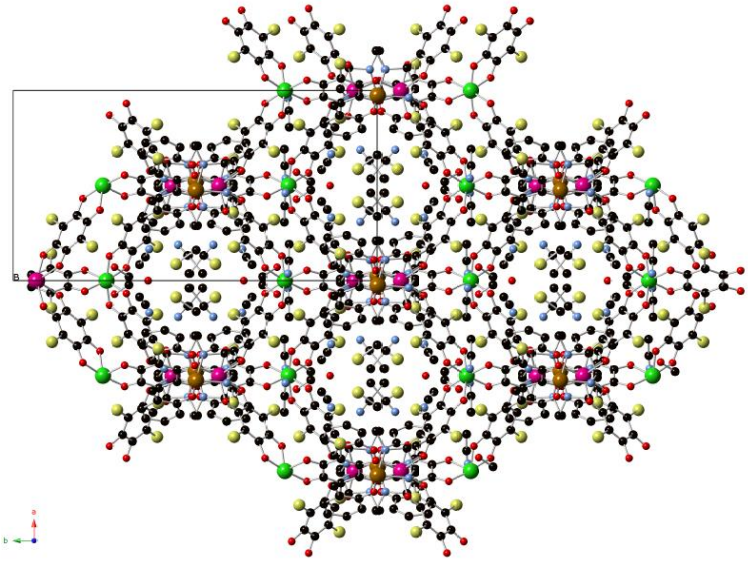

Figure S2. Projection of **1** in the *ab* plane. (Fe (orange), Cr (green), Mn (pink) C (black), N (blue), O (red), Cl (yellow)). Hydrogen atoms have been omitted for clarity.

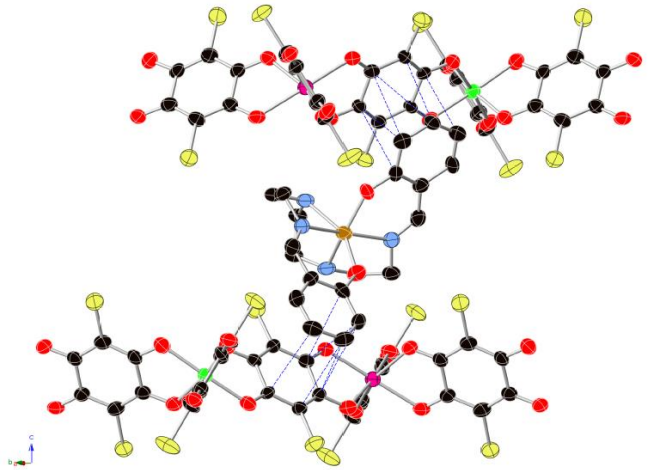

Figure S3. π-π stacking interactions (dashed blue lines) between $[Fe^{III}(sal_2\text{-trien})]^+$ complexes and the anilate layers in the structure of **1**. (Fe (brown), Cr (green), Mn (pink) C (black), N (blue), O (red), Cl (yellow)). Hydrogen atoms have been omitted for clarity.

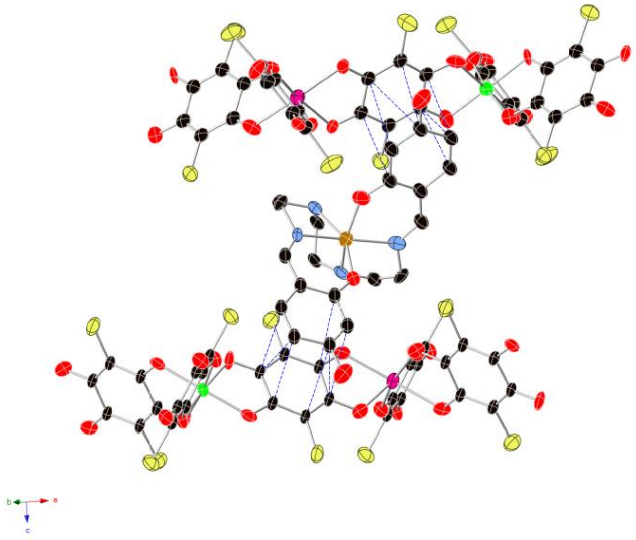

Figure S4. π-π stacking interactions (dashed blue lines) between $[Fe^{III}(4\text{-OH-}sal_2\text{-trien})]^+$ complexes and the anilate layers in the structure of **2**. (Fe (brown), Cr (green), Mn (pink) C (black), N (blue), O (red), Cl(yellow)). Hydrogen atoms have been omitted for clarity.

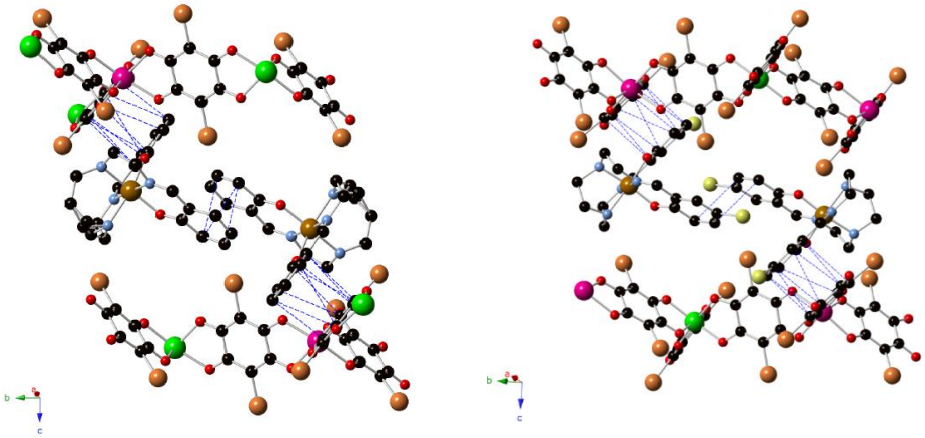

Figure S5. π-π stacking interactions (dashed blue lines) between Fe^{III} complexes and the anilate layers in **3** (up) and **4** (bottom). (Fe (brown), Br (orange), Cr (green), Mn (pink) C (black), N (blue), O (red), Cl (yellow)). Hydrogen atoms have been omitted for clarity.

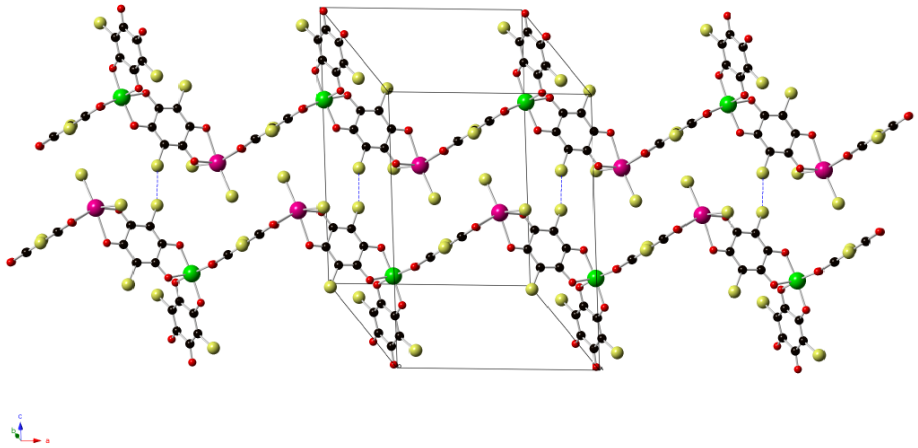

Figure S6. Cl···Cl contacts (dashed blue lines) between neighboring chains in **5** (Fe (brown), Cr (green), Mn (pink) C (black), N (blue), O (red), Cl (yellow)). Hydrogen atoms have been omitted for clarity.

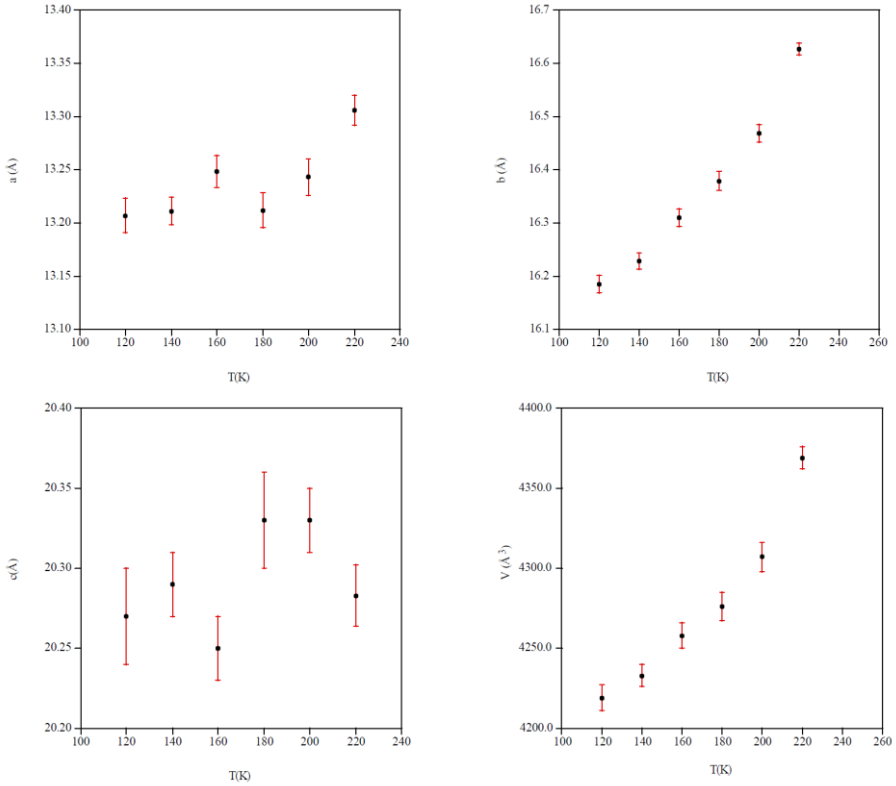

Figure S7. Changes of the unit cell parameters of a single crystal of **5** with the temperature.

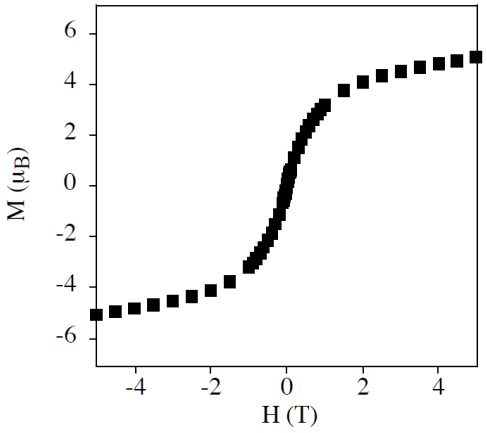

Figure S8. Isothermal magnetization at 2 K of **5**.

Exfoliation of 2D Anilate-Based Magnets with Inserted $[Fe^{III}(acac_2\text{-trien})]^+$ and $[Fe^{III}(sal_2\text{-trien})]^+$ Complexes

Chapter 5

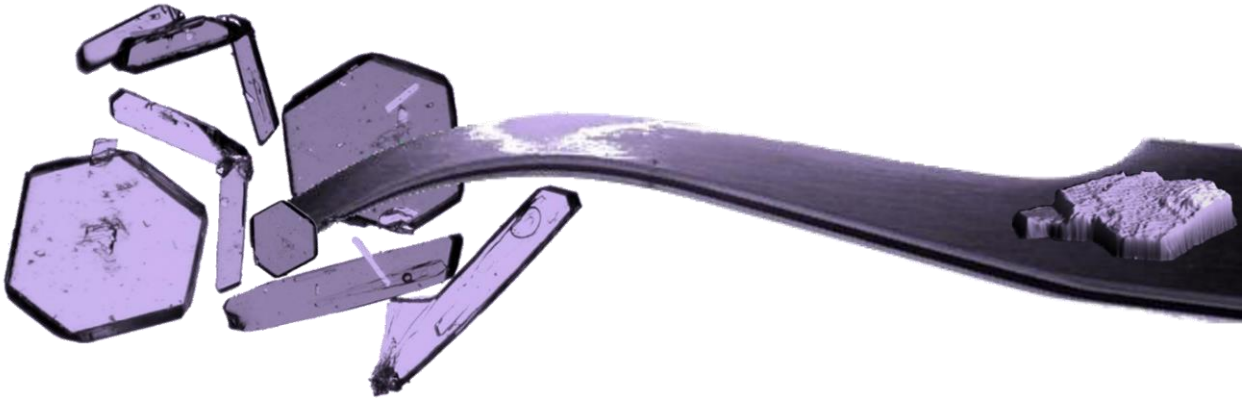

Chapter 5. Exfoliation of 2D Anilate-Based Magnets with Inserted $[Fe^{III}(acac_2\text{-trien})]^+$ and $[Fe^{III}(sal_2\text{-trien})]^+$ Complexes

Abstract

The syntheses, structures and magnetic properties of the compounds of formula $[Fe^{III}(acac_2\text{-trien})][Mn^{II}Cr^{III}(Cl_2An)_3]\cdot(CH_3CN)_2$ **(1),** $[Fe^{III}(acac_2\text{-trien})][Mn^{II}Cr^{III}(Br_2An)_3]\cdot(CH_3CN)_2$ **(2)** and $[Ga^{III}(acac_2\text{-trien})][Mn^{II}Cr^{III}(Br_2An)_3]\cdot(CH_3CN)_2$ **(3)** are reported. They present a 2D anionic network formed by Mn^{II} and Cr^{III} ions linked through anilate ligands with $[Fe^{III}(acac_2\text{-trien})]^+$ or $[Ga^{III}(acac_2\text{-trien})]^+$ cations placed into the hexagonal channels of the 2D network instead of the usual alternation of cationic and anionic layers of this type of compounds. The magnetic properties indicate that they undergo a long-range ferrimagnetic ordering at ca. 11 K while the inserted Fe^{III} cations remain in the HS state. **2** can be exfoliated in thin flakes with heights ranging from less than 2 nm (bilayer) by a micromechanical method (scotch-tape method). This method has also been applied successfully to exfoliate the 2D anilate-based compound $[Fe^{III}(sal_2\text{-trien})][Mn^{II}Cr^{III}(Cl_2An)_3]\cdot(CH_2Cl_2)_{0.5}\cdot(CH_3OH)\cdot(H_2O)_{0.5}\cdot(CH_3CN)_5$, (**4**), in which $[Fe^{III}(sal_2\text{-trien})]^+$ complexes are placed in between the anilate layers. A comparison of these results obtained from this micromechanical method with those obtained through a solvent mediated method is presented.

Introduction

The study of two-dimensional (2D) materials is one of the most appealing topics in chemical science. These materials have attracted increasing interest in the last few years due to their unique morphology and properties and their use in a variety of applications, such as electronics, gas storage or separation, catalysis and high performance sensors.[1] Top-down exfoliation approaches have been successfully

adopted for preparing nanosheets of many layered materials, which includes species such as graphite, layered silicates, titanates or perovskites together with chalcogenides and layered double hydroxides (LDHs). Many of these 2D materials have been exfoliated into individual nanosheets by different methods that involve intercalation and ion-exchange of the pristine layered materials, or simply by mechanical or solvent-mediated exfoliation.[2]

Multifunctional materials can display unprecedented combination of desirable physical properties, which could lead to new physical phenomena.[3] A rational approach to design hybrid multifunctional materials consists of the controlled assembly of two functional networks that possess different intrinsic functionalities and are combined into a single material. In many cases, this has been done by the insertion of different functional cations between anionic extended 2D networks providing a second property of interest. One of the main problems of this approach, however, is that the hybrid framework compounds obtained so far are largely micrometer-sized single crystals or polycrystalline powders, which are difficult to prepare as thin-film structures desirable for technological applications.[4] Although coordination polymers, which have an inherent 2D structure, are abundant, reports about their exfoliation into 2D nanostructures are scarce.[4,5] Indeed, they are limited to neutral coordination polymers with covalent connectivity in two dimensions and only weak van der Waals forces between the layers. These compounds have been exfoliated by solvent mediated methods, mostly based on the sonication of the crystals in different solvents.[6]

Oxalate-based extended networks of general formula $[M^{II}M^{III}(C_2O_4)_3]^-$ have attracted a lot of attention because their 2D anionic networks provide a magnetic functionality and are able to host a wide variety of functional cations. They have provided a rational synthesis of magnetic multifunctional materials.[7] Thus, the insertion of different cations has provided multifunctional materials combining the long-range magnetic ordering from the oxalate network with paramagnetism,[8]

photochromism,[9] electrical conductivity,[10] proton conductivity,[11,7a] ferroelectricity,[12] chirality,[13] spin-crossover,[14] or single-molecule magnet behavior from the cation.[15] Recently, we have extended this strategy to the larger anilate bis-bidentate bridging ligands, 2,5-dihydroxy-1,4-benzoquinone dianion and derivatives of formula $C_6O_4X_2^{2-}$ (X_2An^{2-}; X = Cl or Br, see Scheme 1). One of the advantages of this type of networks is that the bigger size of anilate ligands compared with oxalate ones may enable the introduction of a larger library of cations. The first examples of this kind were the compounds of formula $A[M^{II}M^{III}(X_2An)_3]\cdot G$ (A = $[(H_3O)(phz)_3]^+$ (phz = phenazine), NBu_4^+ [16] and $[Fe^{III}(sal_2\text{-trien})]^+$ and derivatives,[17] X = H, Cl, Br, I; G = solvent) such as compound $[Fe^{III}(sal_2\text{-trien})][Mn^{II}Cr^{III}(Cl_2An)_3]\cdot(CH_2Cl_2)_{0.5}\cdot(CH_3OH)\cdot(H_2O)_{0.5}\cdot(CH_3CN)_5$, (**4**). They are layered 2D ferrimagnets with Curie temperature, T_c, ranging from 5.5 to 11.0 K.

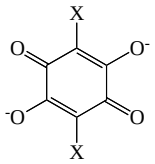

X_2An^{2-}; X = Cl or Br

Scheme 1. 2,5- dihydroxy-1,4-benzoquinone dianion derivatives used in this work.

In this work, we have explored the use of smaller cations for the growth of anilate-based magnetic networks in the search of new structures and properties. In particular, we have used the Fe^{III} complex with the hexadentate ligand derived from a *ß*-diketone and triethylenetetramine, $H_2(acac_2\text{-trien})$ (Scheme 2) as templating cation. Besides its smaller size, $[Fe^{III}(acac_2\text{-trien})]X$ (X = Br, I, PF_6, and BPh_4) complexes have shown gradual spin-crossover in solution and also in the solid state in the BPh_4^- salt and, hence, could be a source of spin-crossover in the final compound.[18]

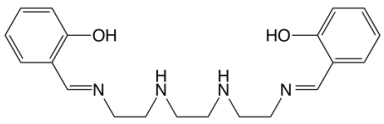

$H_2(sal_2\text{-trien})$

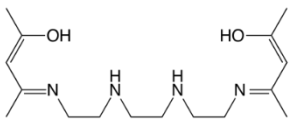

$H_2(acac_2\text{-trien})$

Scheme 2. Ligands of the Fe^{III} complexes.

We report the preparation of the compounds of formula $[Fe^{III}(acac_2\text{-trien})][Mn^{II}Cr^{III}(Cl_2An)_3]\cdot(CH_3CN)_2$ **(1),** $[Fe^{III}(acac_2\text{-trien})][Mn^{II}Cr^{III}(Br_2An)_3]\cdot(CH_3CN)_2$ **(2)** and $[Ga^{III}(acac_2\text{-trien})][Mn^{II}Cr^{III}(Br_2An)_3]\cdot(CH_3CN)_2$ **(3)**. In these three compounds the reduction in size of the templating cation gives rise to a novel 2D anilate-based structure in which the $[Fe^{III}(acac_2\text{-trien})]^+$ or $[Ga^{III}(acac_2\text{-trien})]^+$ complexes are inserted into the hexagonal channels of the network and not between the layers as in the 2D oxalate or anilate-based compounds reported so far. Interestingly, one of these compounds, **2**, can be exfoliated into nanosheets by mechanical methods (scotch-tape method). This method has also been used to exfoliate a compound in which $[Fe^{III}(sal_2\text{-trien})]^+$ cations are placed between the anionic layers of the 2D network (**4**). Furthermore, the exfoliation of **2** and **4** by solvent-mediated methods is reported. These results open the way for exfoliating layered materials of magnetic coordination polymers leading to the first examples of atomically-thin magnetic layers reported in coordination chemistry.

Results and discussion

Synthesis

The method to prepare the two compounds is similar to that used to prepare other 2D anilate-based networks of Fe^{III} Schiff-base complexes.[17] The best results were obtained using a methanol/chloroform (**1**) or methanol/dichloromethane (**2** and **3**) mixture to dissolve the Fe^{III} or Ga^{III} complex and Mn^{2+} salt, and acetonitrile to dissolve the anilate precursor. The chemical composition of these compounds, checked by microanalysis, shows a Fe/Mn/Cr/Cl (**1**), Fe/Mn/Cr/Br (**2**) or Ga/Mn/Cr/Br (**3**) ratio of 1/1/1/6. Elemental analyses confirm the purity of these samples, although the lower content of N and C in **1** could indicate the partial evaporation of acetonitrile solvent molecules after extracting the crystals from the mother liquor.

Structure

1, **2** and **3** crystallize in the monoclinic space group *C*2/c. The structure is formed by anionic 2D anilate-based layers in the *ab* plane of formula **[**$Mn^{II}Cr^{III}(Cl_2An)_3]^-$ (**1**) or **[**$Mn^{II}Cr^{III}(Br_2An)_3]^-$ (**2** and **3**) with the well-known honeycomb structure, which is similar to that of the previous anilate-based compounds such as **4** (Figure 1 and S1 in the Supporting Information, SI).[16,17] It consists in a hexagonal layer where the Cr^{III} and Mn^{II} ions occupy alternating vertices of the hexagons and are linked through X_2An bridges in such a way that each Mn^{II} is surrounded by three neighboring Cr^{III} and vice versa. It contains crystallographically independent Mn and Cr ions with occupancies of 0.5 and characteristic Mn-O and Cr-O distances (see SI). The bridged Mn^{II} and Cr^{III} present the opposite chirality as usual in this type of honeycomb structures. Due to the centrosymmetric character of the structure, Mn^{II} and Cr^{III} from neighboring layers present the opposite configuration. These layers are alternated due the *C*-type unit cell that gives rise to two possible dispositions of the neighboring layers (Figure S2 in the SI).

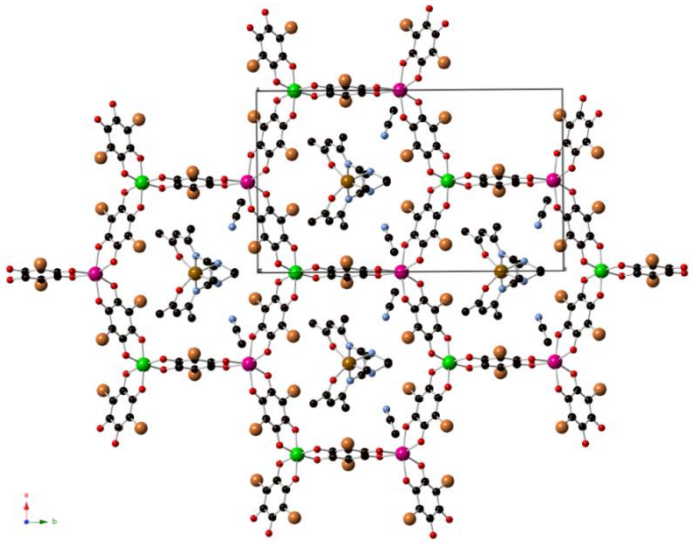

Figure 1. Projection of **2** in the *ab* plane (Fe (brown), Cr (green), Mn (pink) C (black), N (blue), O (red), Br (orange)). Hydrogen atoms have been omitted for clarity.

The main novelty of these structures is that the $[Fe^{III}(acac_2\text{-trien})]^+$ or $[Ga^{III}(acac_2\text{-trien})]^+$ templating cations are inserted into the hexagons of the 2D anilate-based network and not between the layers as in the previous oxalate or anilate-based 2D compounds. Thus, the center of the hexagons is occupied by a crystallographically independent $[Fe^{III}(acac_2\text{-trien})]^+$ or $[Ga^{III}(acac_2\text{-trien})]^+$ complex with an occupancy of 0.5 (Figure 1 and S1 in the SI). This gives rise to an important decrease of the interlayer separation between the anilate-based layers (Figure 2 and S3 in the SI) with minimum distances between metals of neighboring layers (7.39 Å for **1**, 7.53 Å for **2** and 7.57 Å for **3**) much smaller than those of 2D compounds with NBu_4^+ (9.69 Å), $[(H_3O)(phz)_3]^+$ cations (9.03-9.21 Å) or $[Fe^{III}(sal_2\text{-trien})]^+$ and derivatives (11.06-11.92 Å).[16,17] A second consequence of the smaller size of $[Fe^{III}(acac_2\text{-trien})]^+$ complexes is the absence of pores in the structures. These pores are present in most of the structures obtained with $[Fe^{III}(sal_2\text{-trien})]^+$ and derivatives and, as they are filled with disordered solvent molecules, give rise to problems in the structural resolution, which are not present in **1**, **2** and **3** as they present less space available for disordered solvent molecules. In the present case, the hexagonal channels of the honeycomb anilate-based network are filled by $[Fe^{III}(acac_2\text{-trien})]^+$ complexes. Interestingly, these anilate-based layers with inserted $[Fe^{III}(acac_2\text{-trien})]^+$ complexes interact with each other only via van der Waals interactions. Thus, in **2**, the shortest contacts between neighboring layers involve Br atoms from Br_2An ligand with Br atoms and CH_2 and CH_3 groups from $[Fe^{III}(acac_2\text{-trien})]^+$ complexes of neighboring layers. The weak nature of these interactions is critical for the exfoliation of these layers (see below).[4]

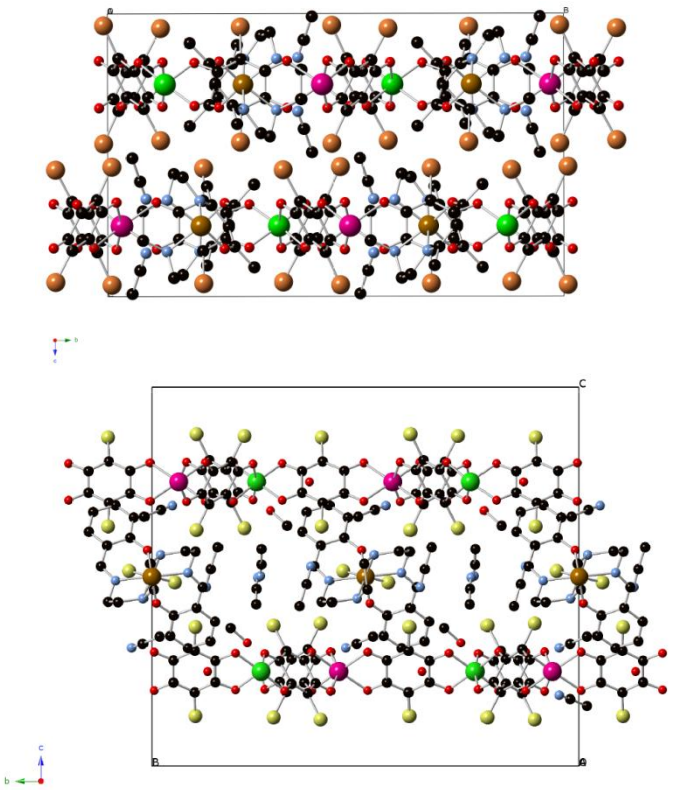

Figure 2. Projection of **2** (top) and **4** (bottom) in the *bc* plane (Fe (brown), Cr (green), Mn (pink) C (black), N (blue), O (red), Br (orange), Cl (yellow)). Hydrogen atoms have been omitted for clarity.

$[Fe^{III}(acac_2\text{-trien})]^+$ complexes present a distorted octahedral geometry with Fe-N and Fe-O distances and N/O-Fe-N/O angles (see SI) similar to those of other high-spin $[Fe^{III}(sal_2\text{-trien})]^+$ or $[Fe^{III}(acac_2\text{-trien})]^+$ complexes.[18a] This indicates that at the temperature of the structural resolution (120 K), Fe^{III} complexes are in the HS state in agreement with the magnetic properties (see below). $[Fe^{III}(acac_2\text{-trien})]^+$ or $[Ga^{III}(acac_2\text{-trien})]^+$ complexes present numerous short contacts with the anilate ligands of the same layer. On the other hand, they are well-isolated by the anilate-based layer. Finally, acetonitrile solvent molecules occupy the holes between these layers and form hydrogen-bonds with the NH groups of $[Fe^{III}(acac_2\text{-trien})]^+$ or $[Ga^{III}(acac_2\text{-trien})]^+$.

Furthermore, they present short contacts with O and C atoms from X_2An ligands. Powder X-ray diffraction patterns of **2** and **3** at 300 K confirm the structure obtained from single crystal X-ray diffraction experiments (Figure S4 in the SI). In the case of **1**, the small amount of sample available prevented us to carry out powder X-ray diffraction experiments.

Magnetic properties

The product of the molar magnetic susceptibility times the temperature ($\chi_M T$) of **1**, **2** and **3** is shown in Figure 3. It presents at 300 K a value of 9.3 cm^3 K mol^{-1} for **1** and 9.5 cm^3 K mol^{-1} for **2**, which is close to the expected value for non-interacting Mn^{II} and Cr^{III} plus the contribution of a HS Fe^{III} ion (10.6 cm^3 K mol^{-1} for g = 2). Furthermore, it is ~3.7 cm^3 K mol^{-1} higher than that of the reference compound **3**, which contains a diamagnetic $[Ga^{III}(acac_2\text{-trien})]^+$ in the place of $[Fe^{II}(acac_2\text{-trien})]$ (5.7 cm^3 K mol^{-1}). When the temperature is lowered, $\chi_M T$ shows a continuous decrease reaching a minimum at ca. 23 K of 6.0 cm^3 K mol^{-1} for **1,** 6.3 cm^3 K mol^{-1} for **2** and 3.4 cm^3 K mol^{-1} for **3** followed by a sharp increase at lower temperatures with a maximum at ca. 8.8 K. The decrease of $\chi_M T$ with the temperature may be attributed to antiferromagnetic Mn-Cr interactions mediated through the X_2An^{2-} bridges, as observed in $[NBu_4]^+$, $[(H_3O)(phz)_3]^+$ or $[Fe^{III}(salt_2\text{-trien})]^+$ salts containing similar $[Mn^{II}Cr^{III}(X_2An)_3]^-$ layers (X = Cl, Br, I and H).[16,17] Since the ground spin states of Cr^{III} and Mn^{II} are different (3/2 and 5/2, respectively), this interaction leads to an antiferromagnetic coupling that results in a $\chi_m T$ minimum, followed by an increase of $\chi_m T$ below ca. 23 K, and finally by a ferrimagnetic long range ordering at low temperatures for the three compounds. A comparison of the magnetic behavior observed in **1** and **2** with that observed in the reference compound **3** shows that the difference of χT values stays almost constant in the range 300-25 K, confirming that in **1** and **2** the Fe^{III} is HS.

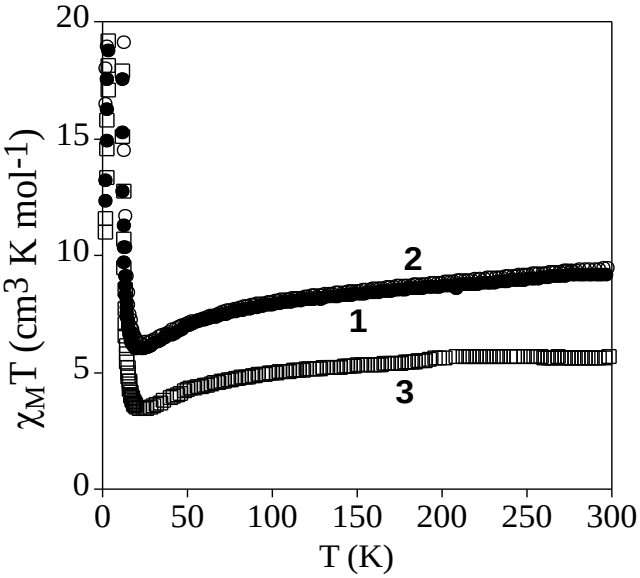

Figure 3. Temperature dependence of the product of the molar magnetic susceptibility times the temperature ($\chi_m T$) of **1** (full circles), **2** (empty circles) and **3** (empty squares) with an applied field of 0.1 mT.

The confirmation of the long-range order and a more accurate determination of the ordering temperatures are obtained from the susceptibility measurements performed with an alternating magnetic field (AC susceptibility). These measurements show a frequency-independent peak in the in phase molar susceptibility (χ_M') and out of phase molar susceptibility (χ_M'') for the three compounds (Figure 4). The T_c, determined as the temperature at which χ_M'' becomes non-zero, is 10.8 K for **1**, 11.4 K for **2** and 11.6 K for **3**. These T_c values are close to those found for $[Mn^{II}Cr^{III}(Cl_2An)_3]^-$ or $[Mn^{II}Cr^{III}(Br_2An)_3]^-$ salts of $[Fe^{III}(salt_2\text{-trien})]^+$ and derivatives.[16,17]

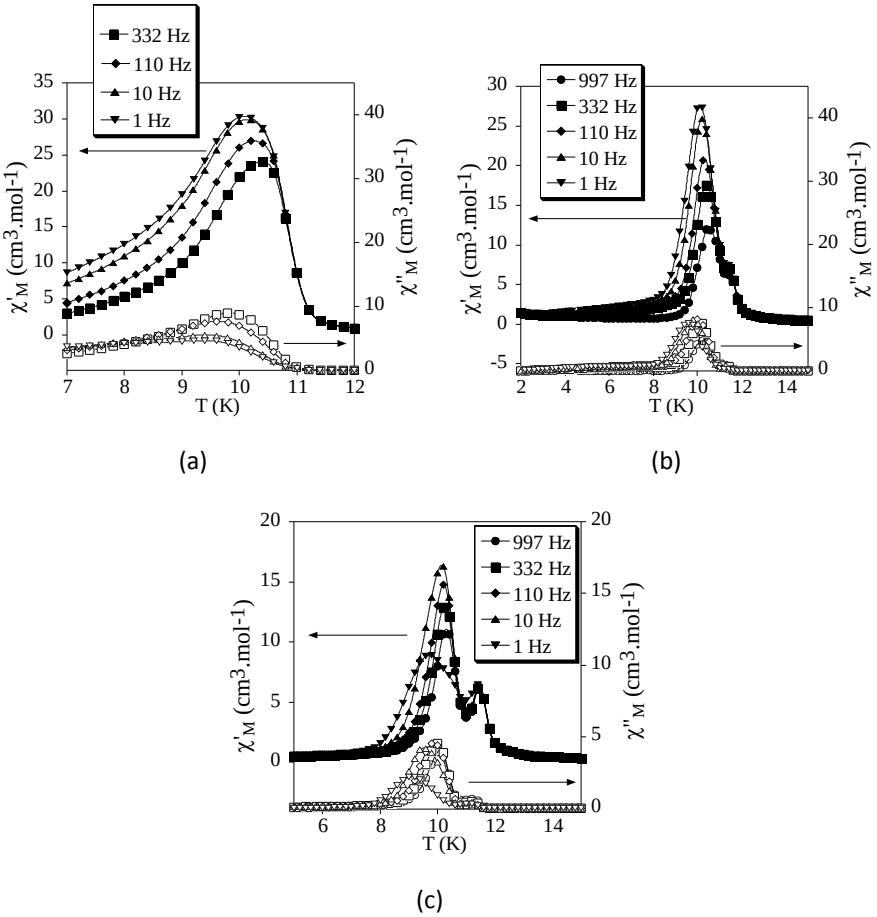

Figure 4. Temperature dependence of the in-phase AC susceptibility (χ') (filled symbols) and the out-of-phase AC susceptibility (χ'') of **1** (a), **2** (b) and **3** (c).

The ferrimagnetic nature of the long range ordering is confirmed by the isothermal magnetization measurements at 2 K that show a sharp increase of the magnetization at low fields that becomes more gradual at higher fields (Figure S5 in the SI). At low fields (H < 0.2 T), the magnetization of the three compounds increases with a high slope reaching values in the range 1.2-1.7 μ_B at H = 0.1 T (inset in Figure S5). At higher fields, the magnetization of **1** and **2** shows a gradual and nonlinear increase (5.1 μ_B for **1** and 5.0 μ_B for **2** at 5 T), while that of **3** tends to saturation at lower values (2.1 μ_B for **3** at 5 T). In **3**, this magnetization value is close to that

expected value for a ferrimagnetic $Mn^{II}Cr^{III}$ network ($M_s = 5\ \mu_B - 3\ \mu_B = 2\ \mu_B$). For **1** and **2**, the major contribution to the gradual nonlinear increase observed at higher fields is due to the contribution of the paramagnetic HS Fe^{III}. These isothermal magnetization measurements also provide an additional proof of the magnetic ordering exhibited by these compounds since they present hysteresis below the ordering temperatures with coercive fields of ca. 65 mT for **1**, 77 mT for **2** and 140 mT for **3** (inset in Figure S5).

Exfoliation

Scanning electron microscopy (SEM) images of bulk crystals of **2** suggest their layered character (Figure S6 in the SI). In order to exfoliate the layers, micromechanical and solvent-mediated methods were used. The same methods were applied to a compound with a similar 2D network but formed by alternating layers of the anilate-based network and a Fe^{III} complex of larger size. This is compound **4** from a previous work.[17]

To date, the micromechanical exfoliation (the so-called Scotch tape method) is the most efficient way to produce the cleanest, highly crystalline and atomically thin nanosheets of layered material.[19] To our knowledge it has never been applied to layered coordination polymers. In a typical mechanical exfoliation process, the 2D material is first peeled off from its bulk crystals by using adhesive Scotch tape. After the Scotch tape is removed, layers of the 2D material are left on the substrate. This method was applied to crystals of **2** and **4**. It produced flakes with different sizes and thicknesses randomly distributed over the substrate. Interestingly, a small fraction of them presents heights of a few nm. These thin flakes were indentified by the contrast difference between the flakes and the substrate in the color image obtained with an optical microscope (Figure 5 and S7 in the SI for **4**). These flakes were characterized by SEM and Atomic Force Microscopy (AFM). Microanalysis recorded during the SEM characterization shows a Fe/Mn/Cr/X (X=Br for **2** and Cl for **4**) ratio of 1/1/1/6 for the flakes, which is consistent with the initial composition of the crystals (Figure S8 in the SI). Unfortunately, it was not possible to evaluate the composition of the thinnest

flakes due to the low sensitivity of the SEM. SEM and AFM topography images revealed that the flakes of **2** and **4** display maximum lateral dimensions of several 5 and 10 µm, respectively, with well-defined edges and angles (Figures 5, S7 and S9 in the SI). Compound **4** shows rectangular flakes of larger size than those of compound **2**. The heights of the largest flakes of **2** and **4** are around 10-20 nm.

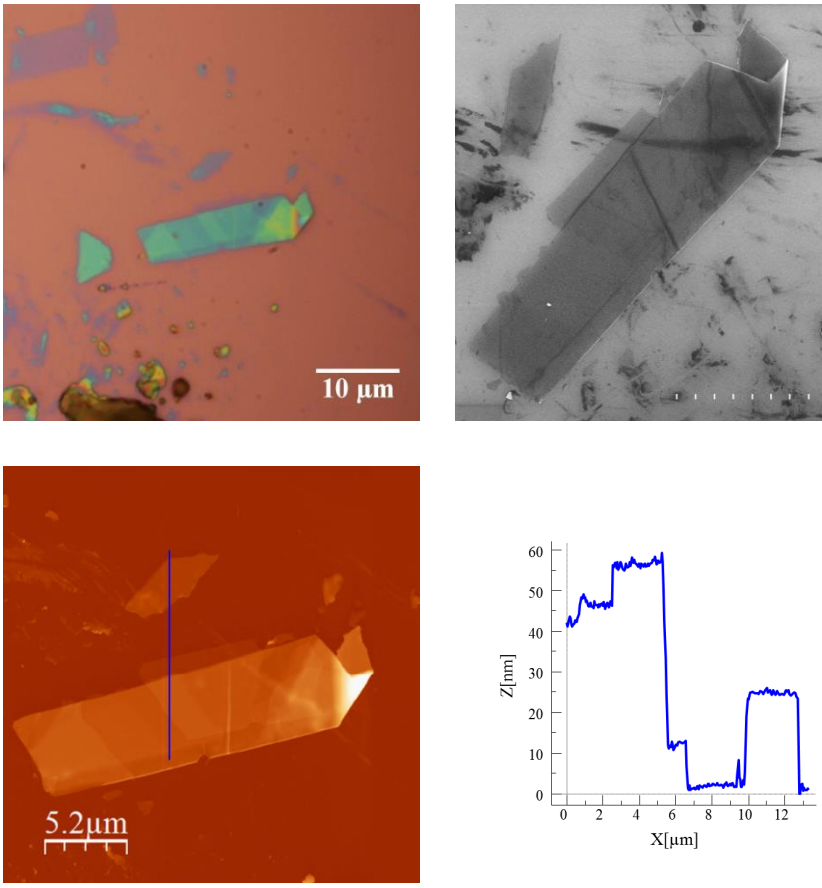

(a)

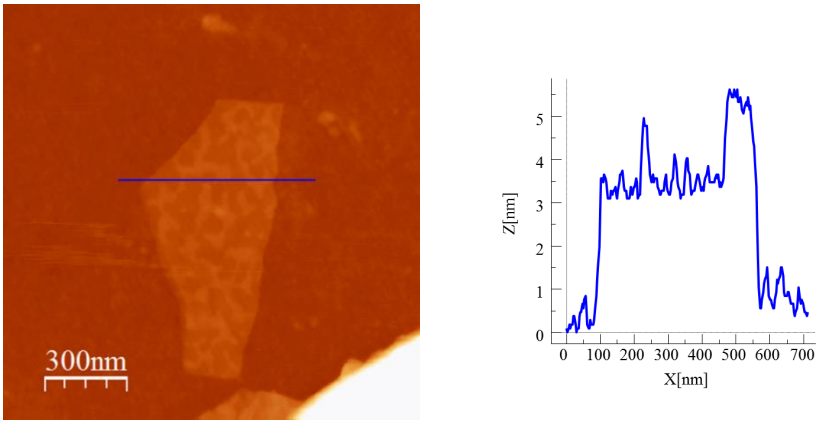

(b)

Figure 5. (a) Optical microscopy image (top left), SEM image (top right) and AFM image with height profile of a flake of **4** obtained by mechanical exfoliation on a 285 nm SiO_2/Si substrate taken in the same zone. (b) AFM image with height profile of a flake of **4**.

On the other hand, smaller nanosheets with heights of 2 nm in the case of **4**, and less than 2 nm in the case of **2**, were also found (Figures 5, 6, 7 and S9 in the SI). The layered nature of the two compounds is reflected by the presence of terraces with different heights. Comparison of the thickness of the thinnest nanosheets with the layer thickness calculated from single crystal X-ray diffraction data (0.74 nm for **2** and 1.10 nm for **4**) is consistent with the presence of bilayers of **2** and **4**.

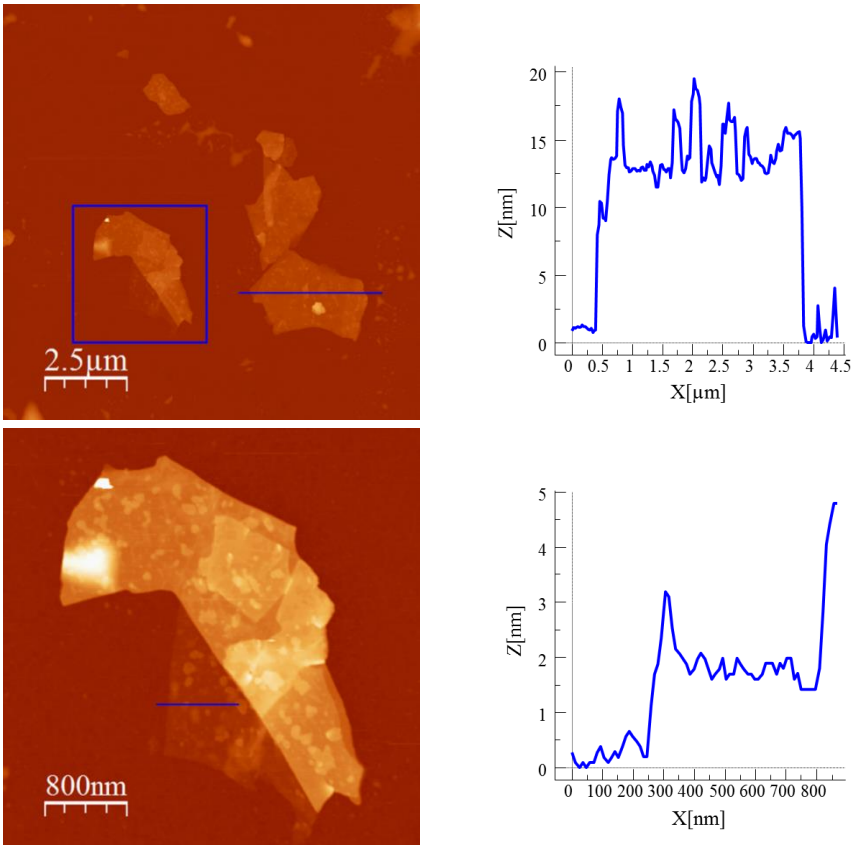

Figure 6. AFM images and height profiles of flakes of **2** obtained by mechanical exfoliation on a 285 nm SiO_2/Si substrate.

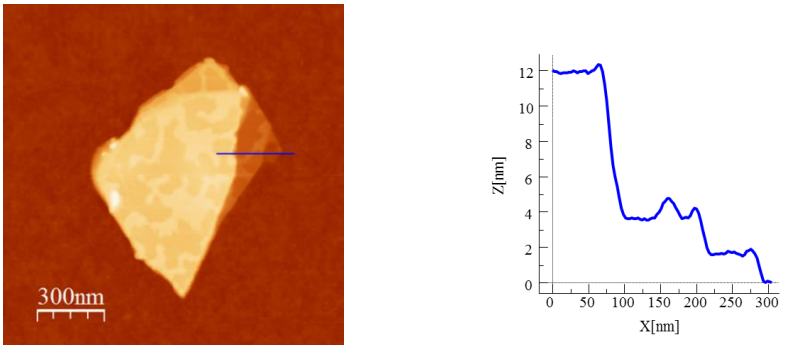

Figure 7. AFM image and height profile of a flake of **4** obtained by mechanical exfoliation on a 285 nm SiO_2/Si substrate. Three nanosheets of about 2, 4 and 12 nm are discernible.

In order to check if crystals of **2** and **4** could be exfoliated by solution methods, these crystals were immersed in acetone, ethanol or acetonitrile (1.0 mg in 1 mL) overnight and then ultrasonicated for 1 minute. In dimethylformamide, the compounds dissolved. The efficiency of the liquid exfoliation was confirmed by the observation of Tyndall light scattering of the colloidal suspension (Figure 8). The size of the exfoliated layers in the three dispersions of **2** was obtained from dynamic light scattering (DLS) and shows a narrow distribution centered around 270 nm in acetone, 290 nm in ethanol and 145 nm in acetonitrile.

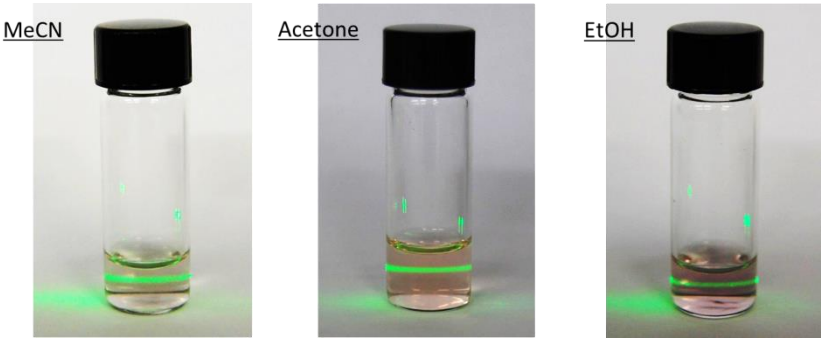

Figure 8. Tyndall effect of crystals of **2** after immersing in acetone, ethanol or acetonitrile (1.0 mg in 1 mL) overnight and then ultrasonicating for 1 minute.

For both compounds, the best results were obtained in ethanol. One drop of the ethanol suspensions were deposited on a grid for Transmission Electron Microscopy (TEM). TEM images confirm the presence of clusters of nanosheets with maximum lateral dimensions of 2 μm (Figures 9 and S10 in the SI). The chemical composition is confirmed by EDS analysis with a Fe/Mn/Cr/X (X=Br for **2** and Cl for **4**) ratio of 1/1/1/6 (Figure S10 in the SI). AFM images of nanosheets deposited on silicon substrates are shown in Figures 9, S11 and S12 in the SI. They show nanosheets with less well defined borders than those obtained by micromechanical exfoliation and lateral dimensions of a few hundred nm typically. In some cases, thicknesses lower than 5 nm are observed. These results demonstrate that the solvent mediated method is less efficient than the micromechanical one, as it has provided a lower degree of exfoliation for both

compounds and smaller lateral dimensions of the flakes (maximum of around 0.5 µm, compared to several µm with the micromechanical method). However, the solvent mediated method remains an interesting exfoliation process, as the suspension of the flakes in the organic solvent enables the deposition of the material on a greater variety of substrates and devices than the micromechanical one.

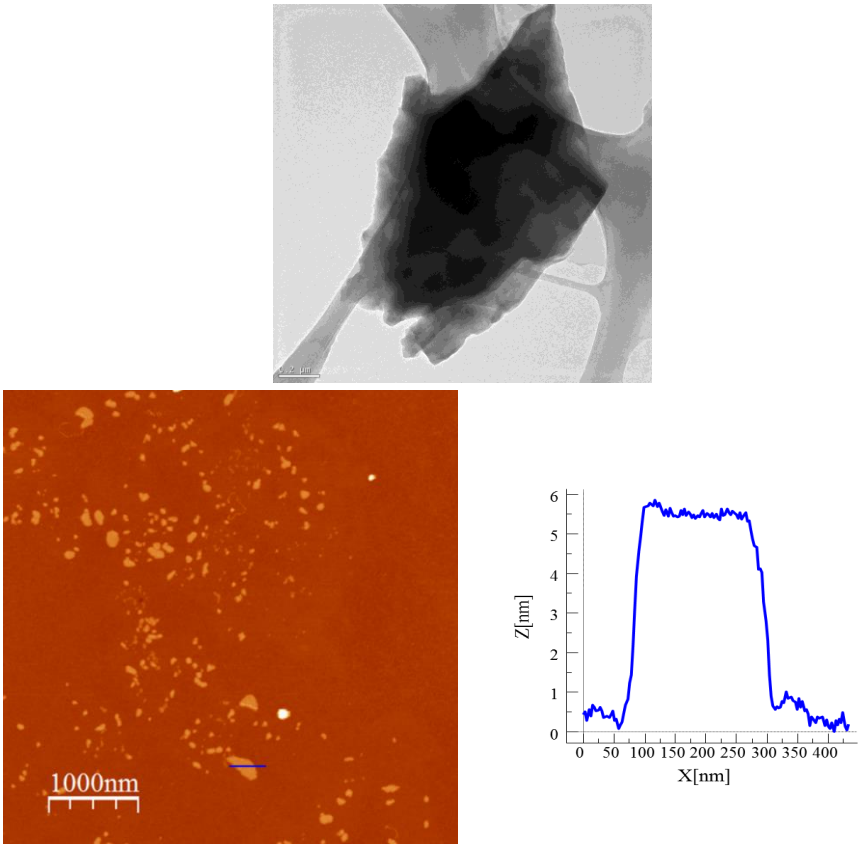

Figure 9. Exfoliation of **2** in ethanol. TEM image of a cluster of nanosheest (top). AFM image and height profile of a nanosheet deposited on a Si substrate (bottom).

Conclusions

Three novel compounds formed by $[Fe^{III}(acac_2\text{-trien})]^+$ or $[Ga^{III}(acac_2\text{-trien})]^+$ and anionic bimetallic coordination polymers based on the anilate ligand have been prepared and characterized. 2D anilate-based networks with a honeycomb structure have been obtained. The reduction of size of the $[Fe^{III}(acac_2\text{-trien})]^+$ or $[Ga^{III}(acac_2\text{-trien})]^+$ complex with respect to the templating cations used in previous compounds of this type has afforded a novel type of structure with the cations placed into the hexagonal channels of the 2D network instead of the usual alternation of cationic and anionic layers of this type of compounds. This has never been observed previously in oxalate or anilate-based 2D networks. This type of structure opens the way to the synthesis of a new type of multifunctional materials in which small templating cations are confined into the 1D channels defined by 2D anilate-based networks in close contact with the magnetic network. Indeed, preliminary results with other small templating cations such as NEt_3H^+ show the formation of a similar structure.[20] In **1**, **2** and **3** this results in an increase of the T_c (ca. 11 K) with respect to that of previous anilate-based compounds (ca. 10 K) but the spin-crossover of the inserted molecules is not favored by this confinement as $[Fe^{III}(acac_2\text{-trien})]^+$ complexes remain in the HS state. A possible strategy to overcome this problem could be the use of other derivatives of $[Fe^{III}(acac_2\text{-trien})]^+$ with withdrawing substituents such as Cl which favor low-spin population and therefore, spin-crossover.[18a] On the other hand, the confinement of small functional cations inside the hexagonal cavities of the honeycomb network provided by this type of structure could be a useful strategy for the introduction of other properties such as electric or proton conductivity in addition to the magnetic ordering of the anilate-based network. New properties could be expected thanks to formation of isolated chains of the cations in close contact with the magnetic network.

Another advantage of this type of networks is that the weak interaction between the layers of **2** enables its exfoliation by mechanical and suspension methods in flakes

formed by a few layers of the compound. Still, the presence of the cationic complexes inside the anionic anilate-based layers is not a necessary condition to achieve exfoliation as compound **4**, formed by alternated layers of the anilate-based network and bulkier $[Fe^{III}(sal_2\text{-trien})]^+$ complexes, can also be exfoliated by micromechanical and solvent mediated methods. We can conclude that the exfoliation of the anionic and cationic layers together is allowed even if they are well separated. For both **2** and **4**, the best results (larger and thinner flakes) are obtained with the micromechanical method, which to our knowledge, has not been used previously for the exfoliation of coordination polymers.

The exfoliation of **2** and **4** paves the way for new studies and applications such as characterization of the magnetic properties of a single magnetic layer by local probe microscopies (MFM, STM) or the processing of the flakes for magnetic devices. Furthermore, the exfoliation of compounds formed by an anionic network with an inserted cation opens the way to the preparation of nanosheets with combination of properties such as magnetic ordering and a second property of interest. This could not be possible with all coordination polymers exfoliated so far, which are formed by 2D neutral networks.

Notes and references

1 *(a)* R. Mas-Ballesté, C. Gómez-Navarro, J. Gómez-Herrero and F. Zamora, *Nanoscale*, 2011, **3**, 20; *(b)* G. Abellán, J. A. Carrasco, E. Coronado, J. Romero and M. Varela, *J. Mater. Chem. C*, 2014, **2**, 3723.

2 S. C. Junggeburth, L. Diehl, S. Werner, V. Duppel, W. Sigle and B. V. Lotsch, *J. Am. Chem. Soc.*, 2013, **135**, 6157.

3 *(a)* E. Coronado and P. Day, *Chem. Rev.*, 2004, **104**, 5419; *(b)* E. Coronado, C. Martí-Gastaldo, E. Navarro-Moratalla, A. Ribera, S. J. Blundell and P. J. Baker, *Nat. Chem.*, 2010, **2**, 1031; *(c)* E. Coronado, C. Martí-Gastaldo, E. Navarro-Moratalla, E. Burzuri, E. Camon and F. Luis, *Adv. Mater.,* 2011, **23**, 5021; *(d)* E. Coronado and G. Mínguez Espallargas, *Chem. Soc. Rev.,* 2013, **42**, 1525; *(e)* R. Bourzami, S. Eyele-Mezui, E. Delahaye, M. Drillon, P. Rabu, N. Parizel, S. Choua, P. Turek, and G. Rogez, *Inorg. Chem.,* 2014, **53**, 1184.

4 J. C. Tan, P. J. Saines, E. G. Bithell and A. K. Cheetham, *ACS Nano*, 2012, **6**, 615.

5 *(a)* T. Araki, A. Kondo and K. Maeda, *Chem. Commun.*, 2013, **49**, 552; (b) W. X. Nie, S. S. Bao, D. Zeng, L. R. Guo and L. M. Zheng, *Chem. Commun.*, 2014, **50**, 10622.

6 *(a)* R. B. Nielsen, K. O. Kongshaug and H. Fjellvag, *J. Mater. Chem.*, 2008, **18**, 1002. (b) P. Amo-Ochoa, L. Welte, R. González-Prieto, P. J. Sanz Miguel, C. J. Gómez-García, E. Mateo-Martí, S. Delgado, J. Gómez-Herrero and F. Zamora, *Chem. Commun.*, 2010, **46**, 3262; *(b)* P. Z. Li, Y. Maeda and Q. Xu, *Chem. Commun.*, 2011, **47**, 8436; *(c)* C. Martí-Gastaldo, J. E. Warren, K. C. Stylianou, N. L. O. Flack and M. J. Rosseinsky, *Angew. Chem. Int. Ed.*, 2012, **51**, 11044; *(d)* P. J. Saines, J. C. Tan, H. H. M. Yeung, P. T. Barton and A. K. Cheetham, *Dalton Trans.*, 2012, **41**, 8585; *(e)* P. J. Saines, M. Steinmann, J. C. Tan, H. H: M. Yeung, W. Li, P. T. Barton and A. K. Cheetham, *Inorg. Chem.*, 2012, **51**, 11198; *(f)* A. Kondo, C. C. Tiew, F. Moriguchi and K. Maeda, *Dalton Trans.*, 2013, **42**, 15267; *(g)* A. Gallego, C. Hermosa, O. Castillo, I. Berlanga, C. J. Gómez-García, E. Mateo-Martí, J. I. Martínez, F. Flores, C. Gómez-Navarro, J. Gómez-Herrero, S. Delgado and F. Zamora, *Adv. Mater.*, 2013, **25**, 2141; *(h)* P. J. Beldon, S. Tominaka, P. Singh, T. Saha Dasgupta, E. G. Bithell and A. K. Cheetham, *Chem. Commun.,* 2014, **50**, 3955-3957.

7 *(a)* M. Clemente-León, E. Coronado, C. Martí-Gastaldo and F. M. Romero, *Chem. Soc. Rev.,* 2011, **40**, 473; *(b)* C. Maxim, S. Ferlay, H. Tokoro, S. I. Ohkoshi and C. Train, *Chem. Commun.,* 2014, **50**, 5629.

8 *(a)* M. Clemente-León, J. R. Galán-Mascarós and C. J. Gómez-García, *Chem. Commun.*, 1997, 1727; *(b)* E. Coronado, J. R. Galán-Mascarós, C. J. Gómez-García and J. M.

Martínez-Agudo, *Adv. Mater.*, 1999, **11**, 558; *(c)* E. Coronado, J. R. Galán-Mascarós, C. J. Gómez-García, J. Ensling and P. Gütlich, *Chem. Eur. J.*, 2000, **6**, 552.

9 *(a)* S. Bénard, P. Yu, J. P. Audière, E. Rivière, R. Clèment, J. Ghilhem, L. Tchertanov and K. Nakatami, K. *J. Am. Chem. Soc.*, 2000, **122**, 9444; *(b)* S. M. Aldoshin, N. A. Sanina, V. I. Minkin, N. A. Voloshin, V. N. Ikorskii, V. I. Ovcharenko, V. A. Smirnov and N. K. Nagaeva, *J. Mol. Struct.*, 2007, **826**, 69.

10 *(a)* E. Coronado, J. R. Galán-Mascarós, C. J. Gómez-García and V. Laukhin, *Nature*, 2000, **408**, 447; *(b)* A. Alberola, E. Coronado, J. R. Galán-Mascarós, C. Giménez-Saiz and C. J. Gómez-García, *J. Am. Chem. Soc.*, 2003, **125**, 10774; *(c)* J. R. Galán-Mascarós, E. Coronado, P. A. Goddard, J. Singleton, A. I. Coldea, J. D. Wallis, S. J. Coles and A. Alberola, *J. Am. Chem. Soc.*, 2010, **132**, 9271; *(d)* E. Coronado, J. R. Galán-Mascarós, C. J. Gómez-García, E. Martínez-Ferrero and S. Van Smaalen, *Inorg. Chem.*, 2004, ***43***, 4808; *(e)* B. Zhang, Y. Zhang and D. Zhu, *Chem. Commun.,* 2012, **48**, 197.

11 *(a)* H. Okawa, A. Shigematsu, M. Sadakiyo, T. Miyagawa, K. Yoneda, M. Ohba and H. Kitagawa, *J. Am. Chem. Soc.*, 2009, **131**, 13516; *(b)* E. Pardo, C. Train, G. Contard, K. Boubekeur, O. Fabelo H. Liu, B. Dkhil, F. Lloret, K. Nakagawa, H. Tokoro, S.-I. Ohkoshi and M. Verdaguer, *J. Am. Chem. Soc.*, 2011, **133**, 15328; *(c)* M. Sadayiko, H. Okawa, A. Shigematsu, M. Ohba, T. Yamada and H. Kitagawa, *J. Am. Chem. Soc.*, 2012, **134**, 5472; *(d)* H. Okawa, M. Sadakiyo, T. Yamada, M. Maesato, M. Ohba and H. Kitagawa, *J. Am. Chem. Soc.,* 2013, **135**, 2256.

12 *(a)* T. Endo, T. Akutagawa, S. I. Noro and T. Nakamura, *Dalton Trans.*, 2011, **40**, 1491; *(b)* E. Pardo, C. Train, H. Liu, L.-M. Chamoreau, B. Dkhil, K. Boubekeur, F. Lloret, K. Nakatani, H. Tokoro, S.-I. Ohkoshi and M. Verdaguer, *Angew. Chem. Int. Ed*., 2012, **51**, 8356.

13 *(a)* R. Andrés, M. Gruselle, B. Malézieux, M. Verdaguer and J. Vaissermann, *Inorg. Chem.*, 1999, **38**, 4637; *(b)* R. Andrés, M. Brissard, M. Gruselle, C. Train, J. Vaissermann, B. Malézieux, J. P. Jamet and M. Verdaguer, *Inorg. Chem.*, 2001, **40**, 4633; *(c)* M. Clemente-León, E. Coronado, J. C. Dias, A. Soriano-Portillo and R. D. Willett, *Inorg. Chem.*, 2008, **47**, 6458; *(d)* C. Train, R. Gheorghe, V. Krstic, L. M. Chamoreau, N. S. Ovanesyan, G. L. J. A. Rikken, M. Gruselle and M. Verdaguer, *Nat. Mater.*, 2008, **7**, 729; *(e)* C. Train, T. Nuida, R. Gheorghe, M. Gruselle and S. Ohkoshi, *J. Am. Chem. Soc.*, 2009, **131**, 16838; *(f)* M. Gruselle, Y. Li, N. Ovanesyan, V. Markhaev, G. Shilov, F. Mushenok, C. Train and S. Aldoshin, *Chirality*, 2013, **25**, 444.

14 *(a)* M. Clemente-León, E. Coronado, M. C. Giménez-López, A. Soriano-Portillo, J. C. Waerenborgh, F. S. Delgado and C. Ruiz-Pérez, *Inorg. Chem.*, 2008, **47**, 9111; *(b)* M. Clemente-León, E. Coronado, M. López-Jordà, G. Mínguez Espallargas, A. Soriano-Portillo and J. C. Waerenborgh, *Chem. Eur., J*., 2010, **16**, 2207; *(c)* M. Clemente-León, E. Coronado and M. López-Jordà, *Dalton Trans.*, 2010, **39**, 4903; *(d)* M. Clemente-León, E.

Coronado, M. López-Jordà and J. C. Waerenborgh, *Inorg. Chem.*, 2011, **50**, 9122; *(e)* M. Clemente-León, E. Coronado, M. López-Jordà, C. Desplanches, S. Asthana, H. Wang and J.-F. Létard, *Chem. Sci.,* 2011, **2**, 1121; *(f)* M. Clemente-León, E. Coronado and M. López-Jordà, *Eur. J. Inorg. Chem.,* 2013, 753; *(g)* A. Ben Djamâa, M. Clemente-León, E. Coronado and M. López-Jordà, *Polyhedron*, 2013, **64**, 142; *(h)* M. Clemente-León, E. Coronado, M. López-Jordà, J. C. Waerenborgh, C. Desplanches, H. Wang, J.-F. Létard, A. Hauser and A. Tissot, *J. Am. Chem.* Soc., 2013, **135**, 8655.

15 M. Clemente-León, E. Coronado, C. J. Gómez-García, M. López-Jordà, A. Camón, A. Repollés and F. Luis, *Chem. Eur. J*., 2014, **20**, 1669.

16 M. Atzori, S. Benmansour, G. Mínguez Espallargas, M. Clemente-León, A. Abhervé, P. Gómez-Claramunt, E. Coronado, F. Artizzu, E. Sessini, P. Deplano, A. Serpe, M. L. Mercuri and C. J. Gómez-García, *Inorg. Chem.*, 2013, **52**, 10031.

17 A. Abhervé, M. Clemente-León, E. Coronado, C. J. Gómez-García and M. Verneret, *Inorg. Chem.*, 2014, **53**, 12014.

18 *(a)* P. J. van Koningsbruggen, Y. Maeda and H. Oshio, *Top. Curr. Chem.*, 2004, **233**, 259; *(b)* M. Nihei, T. Shiga, Y. Maeda and H. Oshio, *Coord. Chem. Rev.*, 2007, **251**, 2606.

19 *(a)* A. Castellanos-Gomez, E. Navarro-Moratalla, G. Mokry, J. Quereda, E. Pinilla-Cienfuegos, N. Agraït, H. S. J. van der Zant, E. Coronado, G. A. Steele and G. Rubio-Bollinger, *Nano Research*, 2013, **6(3)**, 191; *(b)* H. Li, J. Wu, Z. Yin and H. Zhang, *Acc. Chem. Res.*, 2014, **47**, 1067; *(c)* J. Yanan, J. Gao, W. Guo and L. Jiang, *Chem. Commun.*, 2014, **50**, 14149; *(d)* A. Castellanos-Gomez, M. Buscema, R. Molenaar, V. Singh, L. Janssen, H. S. J van der Zant and G. A Steele, *2D Materials 1*, 2014, 011002.

20 A. Abhervé, M. Clemente-León, E. Coronado and M. Palacios-Corella, *manuscript in preparation*.

Associated Content:

Electronic Supplementary Information (ESI)

Experimental Section

General Remarks: $[Fe^{III}(acac_2\text{-trien})]PF_6$ and $[Ga^{III}(acac_2\text{-trien})]PF_6$ were prepared according to literature methods.[1] $[(n\text{-}Bu)_4N]_3[Cr^{III}(X_2An)_3]$ (X=Cl, Br) were prepared as described in the literature.[2] All other materials and solvents were commercially available and used without further purification.

Syntheses: $[Fe^{III}(acac_2\text{-trien})][Mn^{II}Cr^{III}(Cl_2An)_3]\cdot(CH_3CN)_2$ (**1**), $[Fe^{III}(acac_2\text{-trien})][Mn^{II}Cr^{III}(Br_2An)_3]\cdot(CH_3CN)_2$ (**2**) and $[Ga^{III}(acac_2\text{-trien})][Mn^{II}Cr^{III}(Br_2An)_3]\cdot(CH_3CN)_2$ (**3**) were obtained by slow diffusion of two solutions. The first solution was prepared by dissolving $MnCl_2\cdot4H_2O$ (12 mg, 0.06 mmol) and $[Fe^{III}(acac_2\text{-trien})](PF_6)$ or $[Ga^{III}(acac_2\text{-trien})](PF_6)$ (0.06 mmol) in 6 mL of a 9:1 chloroform/methanol mixture (**1**) or 9:1 dichloromethane/methanol mixture (**2** and **3**). The second solution was obtained by dissolving $[NBu_4]_3[Cr^{III}(Cl_2An)_3]$ (84 mg, 0.06 mmol) (for **1**) or $[NBu_4]_3[Cr^{III}(Br_2An)_3]$ (100 mg, 0.06 mmol) (for **2** and **3**) in acetonitrile (6 mL). After 4 weeks, black prismatic single crystals suitable for X-ray crystal analysis were obtained. Anal. Calc. for $C_{38}H_{34}Cl_6CrFeMnN_6O_{14}$ (**1**): C, 38.9; H, 2.9; N, 7.2 %. Found: C, 35.3; H, 2.6; N, 4.6 %. Calc. for $C_{38}H_{34}Br_6CrFeMnN_6O_{14}$ (**2**): C, 31.7; H, 2.4; N, 5.8 %. Found: C, 31.6; H, 1.7; N, 5.4 %. Calc. for $C_{38}H_{34}Br_6CrGaMnN_6O_{14}$ (**3**): C, 31.4; H, 2.4; N, 5.8 %. Found: C, 28.9; H, 2.1; N, 4.2 %.

Structural Characterization: Single crystals of all compounds were mounted on glass fibres using a viscous hydrocarbon oil to coat the crystal and then transferred directly to the cold nitrogen stream for data collection. All reflection data were collected at 120 K on a Supernova diffractometer equipped with a graphite-monochromated Enhance (Mo) X-ray Source (λ = 0.71073 Å). The CrysAlisPro program, Oxford Diffraction Ltd., was used for unit cell determinations and data reduction. Empirical absorption correction was performed using spherical harmonics,

implemented in the SCALE3 ABSPACK scaling algorithm. Crystal structures were solved by direct methods with the SIR97 program,[3] and refined against all F^2 values with the SHELXL-2013 program,[4] using the WinGX graphical user interface.[5] All non-hydrogen atoms were refined anisotropically, and hydrogen atoms were placed in calculated positions and refined isotropically with a riding model. The details of data collection and structure refinements are provided in Table 1. 0.5 mm glass capillaries were filled with polycrystalline samples of 2 and 3 and mounted and aligned on a Empyrean PANalytical powder diffractometer, using CuKα radiation (λ = 1.54177 Å). A total of 3 scans were collected at room temperature in the 2θ range 5-40°.

Physical Measurements: Magnetic measurements were performed with a Quantum Design MPMS-XL-5 SQUID magnetometer in the 2 to 300 K temperature range with an applied magnetic field of 0.1 T on polycrystalline samples. The AC measurements were performed in the temperature range 2-15 K at different frequencies with an oscillating magnetic field of 0.395 mT. The magnetization and hysteresis studies were performed between 5 and -5 T, cooling the samples at zero field. C, H and N elemental analyses were measured on a CE Instruments EA 1110 CHNS Elemental analyzer. The M/Mn/Cr/X (M = Fe, Ga; X = Cl, Br) ratios and scanning electron microscopy (SEM) images were obtained with a Philips ESEM X230 scanning electron microscope equipped with an EDAX DX-4 microsonde.

Exfoliation:

Characterization of the nanosheets: High-resolution transmission electronic microscopy (TEM) measurements were performed on a TECNAI-F20 microscope operating at 200 kV. High-resolution SEM images were measured on a Hitachi S-4800 field emission scanning electron microscope. Comercial atomic force microscopes (Multimode SPM by Veeco and Nanotec Cervantes Full Mode AFM by Nanotec Electrónica S.L.) were employed for surface sample characterization. AFM was operated in tapping mode. Sharp silicon probes were purchased from Nanosensors (PPP-NCH-W; force constant: 10-130 N/m; resonance frequency: 204-497 kHz). Scan

rate was adjusted during the scanning of each image (usually below 1 Hz, 512 samples/line). AFM images were processed by using WSxM.[6]

	Mn-O distances	Cr-O distances
1	2.172(2)-2.186(2) Å	1.970(2)-1.974(2) Å
2	2.167(5)-2.177(5) Å	1.973(5)-1.985(5) Å
3	2.175(4)-2.183(4) Å	1.972(4)-1.983(4) Å

As usual for this type of complexes, the Fe/Ga–O distances are the shortest ones (1.939(3) Å for **1**, 1.949(5) Å for **2** and 1.949(5) for **3**), the Fe/Ga–N(amine) distances are the longest ones (2.172(3) Å for **1**, 2.186(6) Å for **2** and 2.140(5) Å for **3**), whereas the Fe/Ga–N(imine) bonds are intermediate (2.110(3) Å for **1**, 2.113(6) Å for **2** and 2.041(6) for **3**).

Table 1. Crystallographic data for compounds **1, 2** and **3**.

Compound	**1**	**2**	**3**
Empirical formula	$C_{38}H_{34}Cl_6CrFeMnN_6O_{14}$	$C_{38}H_{34}Br_6CrFeMnN_6O_{14}$	$C_{38}H_{34}Br_6CrGaMnN_6O_{14}$
Formula weight	1174.20	1440.91	1454.79
Crystal color	Black	Black	Purple
Crystal size	0.06×0.06×0.05	0.06×0.05×0.04	0.06×0.04×0.03
Temperature (K)	120(2)	120(2)	120(2)
Wavelength (Å)	0.71073	0.71073	0.71073
Crystal system, *Z*	Monoclinic, 4	Monoclinic, 2	Monoclinic, 4
Space group	*C* 2/*c*	*C* 2/*c*	*C* 2/*c*
a (Å)	14.2177(3)	14.1914(5)	14.1613(4)
b (Å)	22.9278(5)	23.0061(7)	23.0839(6)
c (Å)	14.5428(4)	14.7880(5)	14.8676(5)
α (°)	90	90	90
ß (°)	105.118(2)	104.703(3)	104.296(3)
γ (°)	90	90	90
V (Å^3)	4576.60(19)	4670.0(3)	4709.7(2)
ρ_{calc} (Mg/m^3)	1.704	2.041	2.052
μ($Mo_{K\alpha}$) (mm^{-1})	1.240	6.006	6.220
θ range (°)	3.028-26.394	2.968-26.405	2.969-26.380
Reflns collected	33850	35510	59295
Independent reflns (R_{int})	4679(0.0742)	4797(0.0779)	4825(0.1654)
L. S. parameters, *p*/ restraints, *r*	305 / 0	292 / 0	305 / 0
$R1(F)$,[a] $I > 2\sigma(I)$	0.0439	0.0617	0.0543
$wR2(F^2)$,[b] all data	0.1190	0.1770	0.1394
$S(F^2)$,[c] all data	1.057	1.063	1.003

[a] $R1(F) = \Sigma||F_O|-|F_C||/\Sigma|F_O|$; [b] $wR2(F^2) = [\Sigma w(F_O^2-F_C^2)^2/\Sigma wF_O^4]^{1/2}$; [c] $S(F^2) = [\Sigma w(F_O^2-F_C^2)^2/\Sigma n + r - p)]^{1/2}$

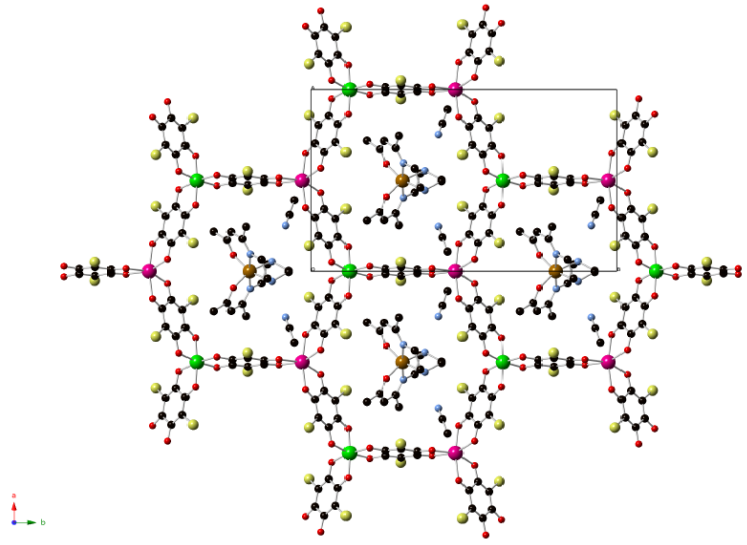

(a)

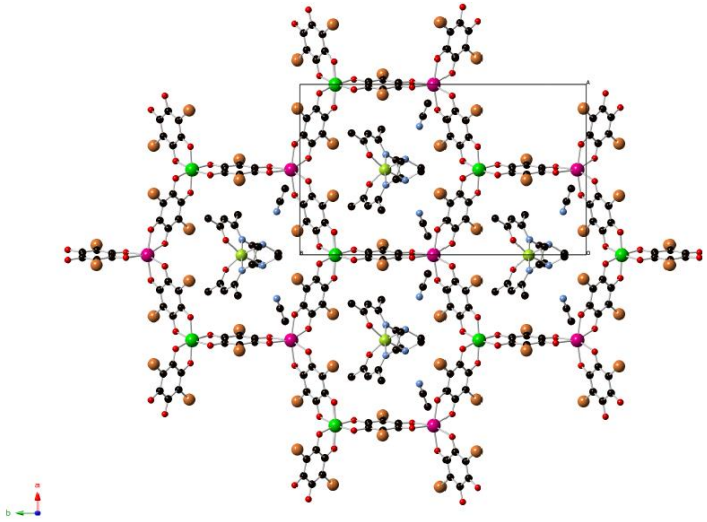

(b)

Figure S1. Projection of **1** (a) and **3** (b) in the *ab* plane (Fe (brown), Ga (olive green), Cr (green), Mn (pink) C (black), N (blue), O (red), Cl (yellow), Br (orange)). Hydrogen atoms have been omitted for clarity.

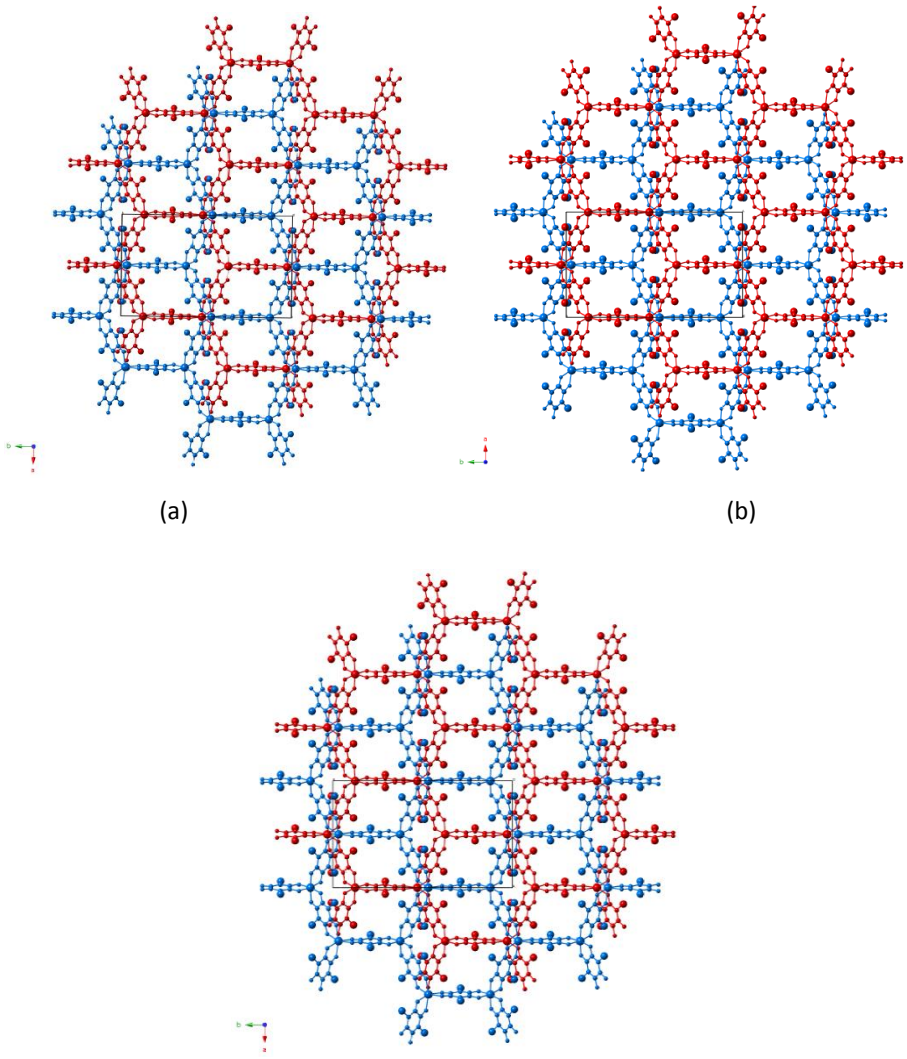

Figure S2. Projection, perpendicular to the layers, of two consecutive anionic layers of **1** (a), **2** (b) and **3** (c) showing their alternate packing.

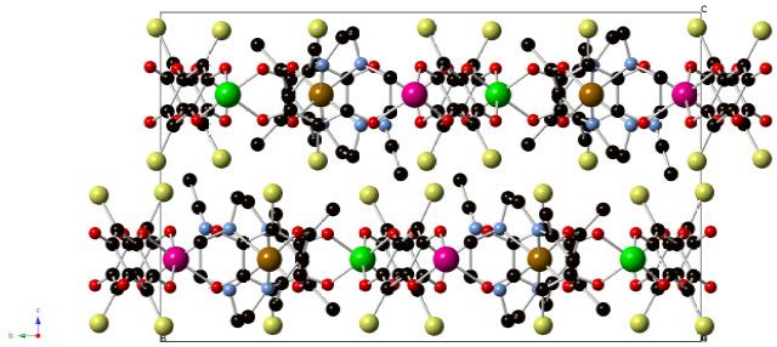

(a)

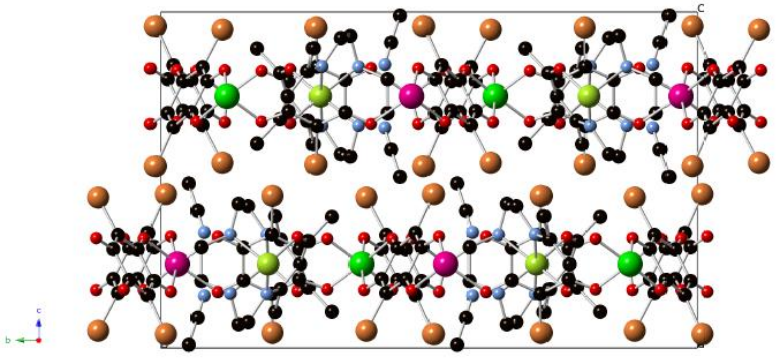

(b)

Figure S3. Projection of **1** (a) and **3** (b) in the *bc* plane (Fe (brown), Ga (olive green), Cr (green), Mn (pink) C (black), N (blue), O (red), Cl (yellow), Br (orange)). Hydrogen atoms have been omitted for clarity.

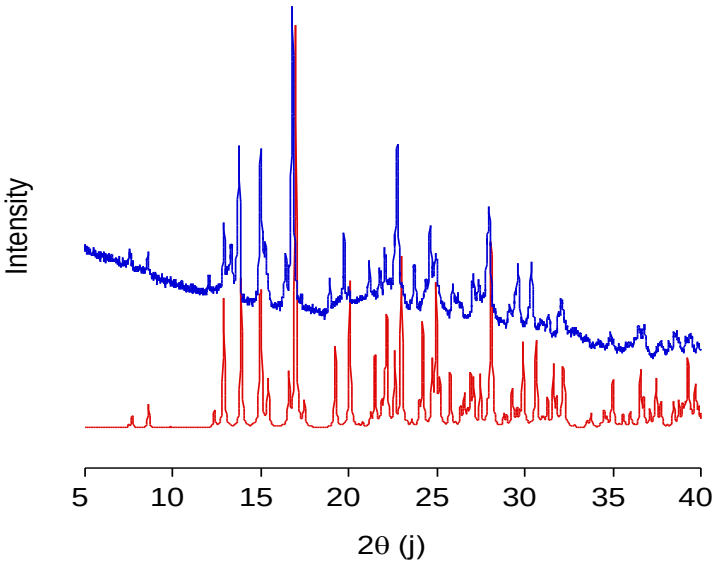

(a)

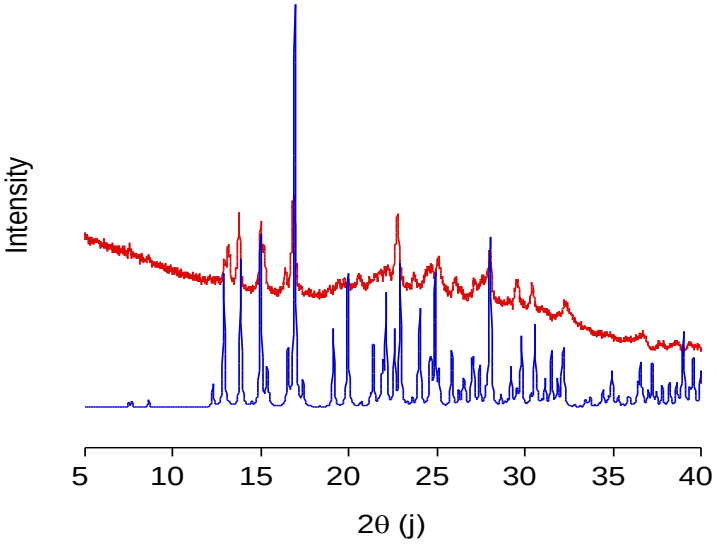

(b)

Figure S4. Powder X-ray diffraction pattern (top) and simulated pattern (bottom) of **2** (a) and **3** (b).

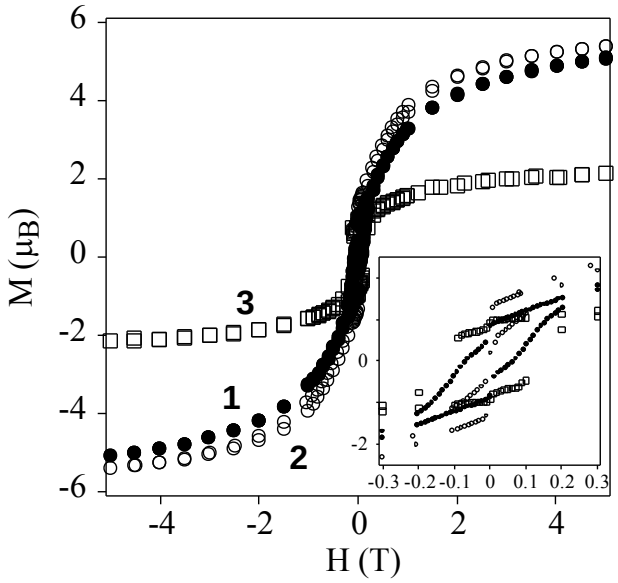

Figure S5. Isothermal magnetization at 2 K of **1** (full circles), **2** (empty circles) and **3** (empty squares).

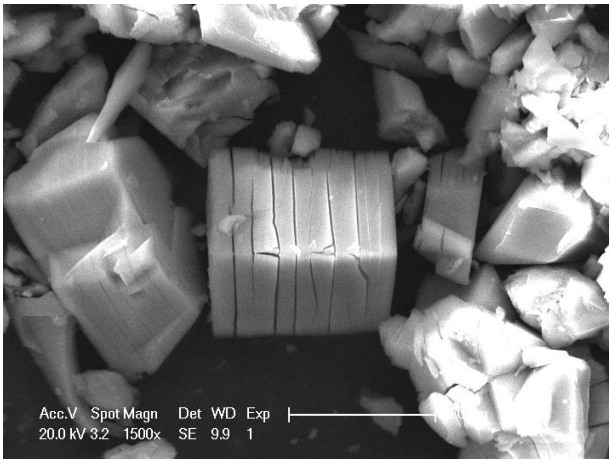

Figure S6. SEM image of bulk crystals of **2**.

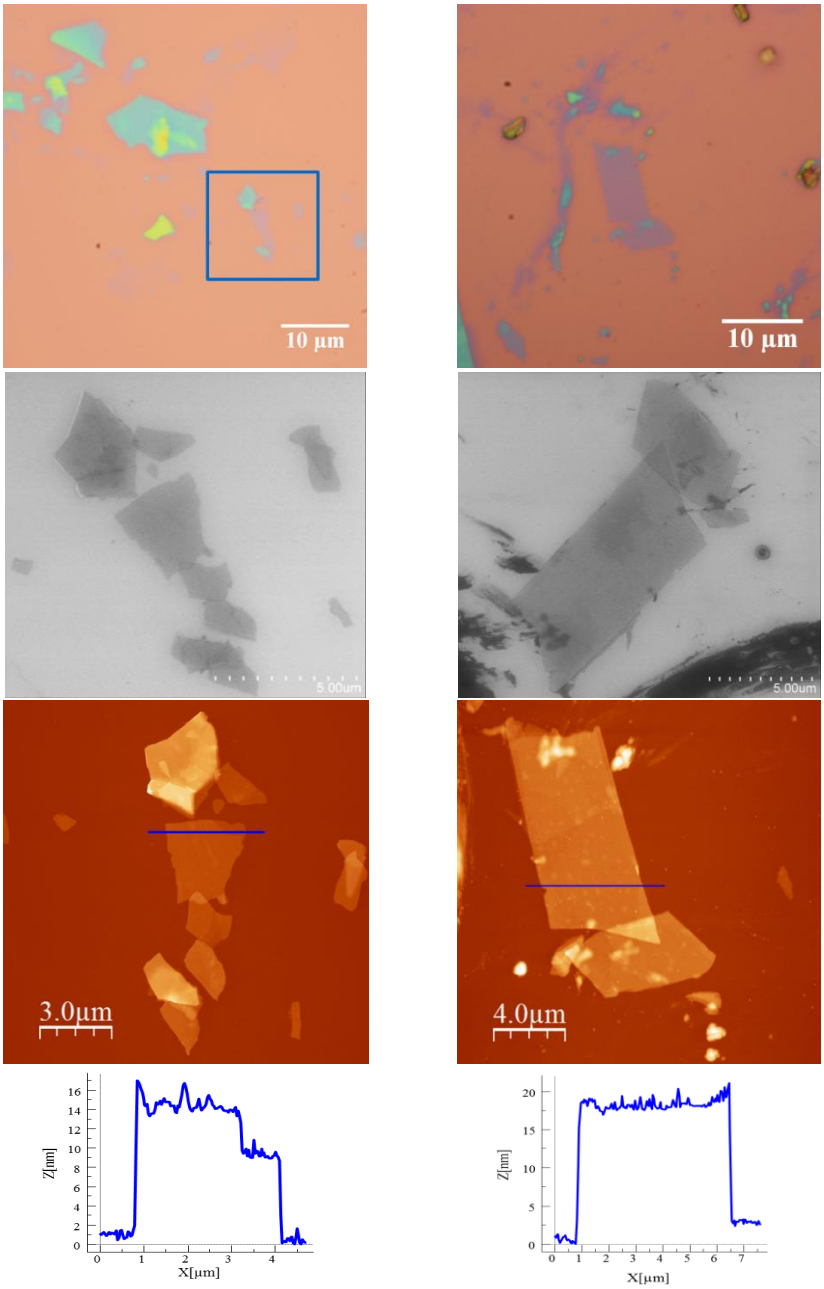

Figure S7. Optical microscopy images (top), SEM images (middle) and AFM images with height profiles (bottom) of flakes of **4** obtained by mechanical exfoliation on a 285 nm SiO_2/Si substrate taken in the same zone.

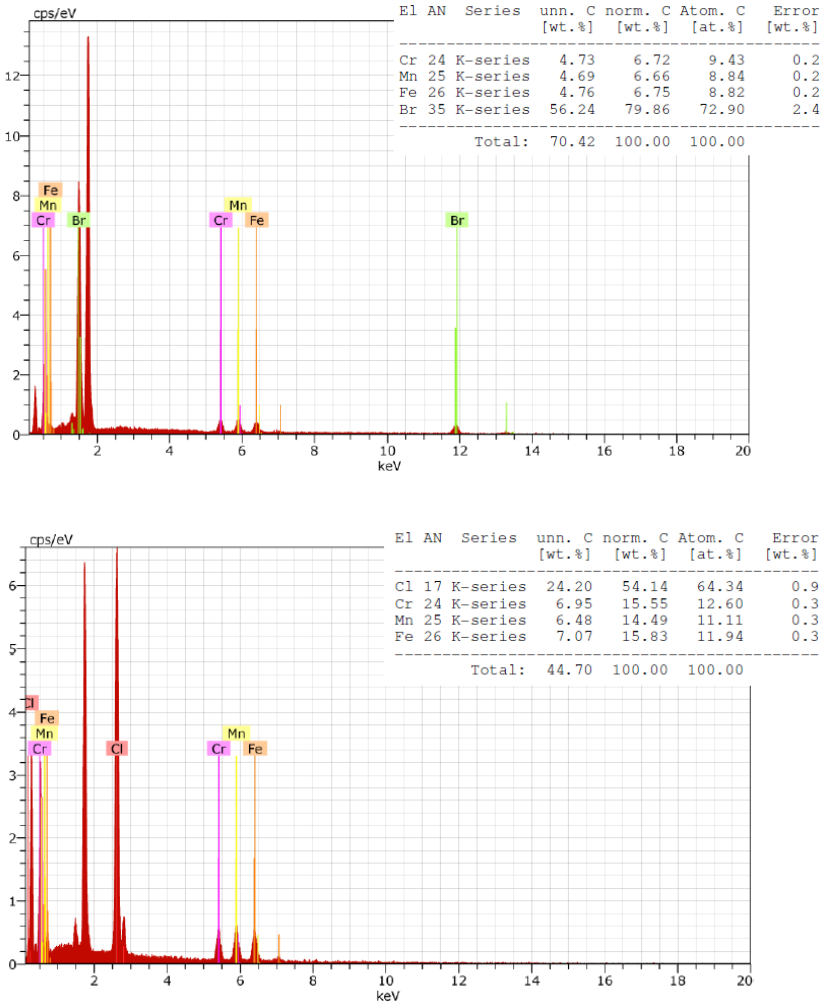

Figure S8. Microanalysis recorded during the SEM characterization of flakes of **2** (top) and **4** (bottom) obtained by mechanical exfoliation on a 285 nm SiO_2/Si substrate.

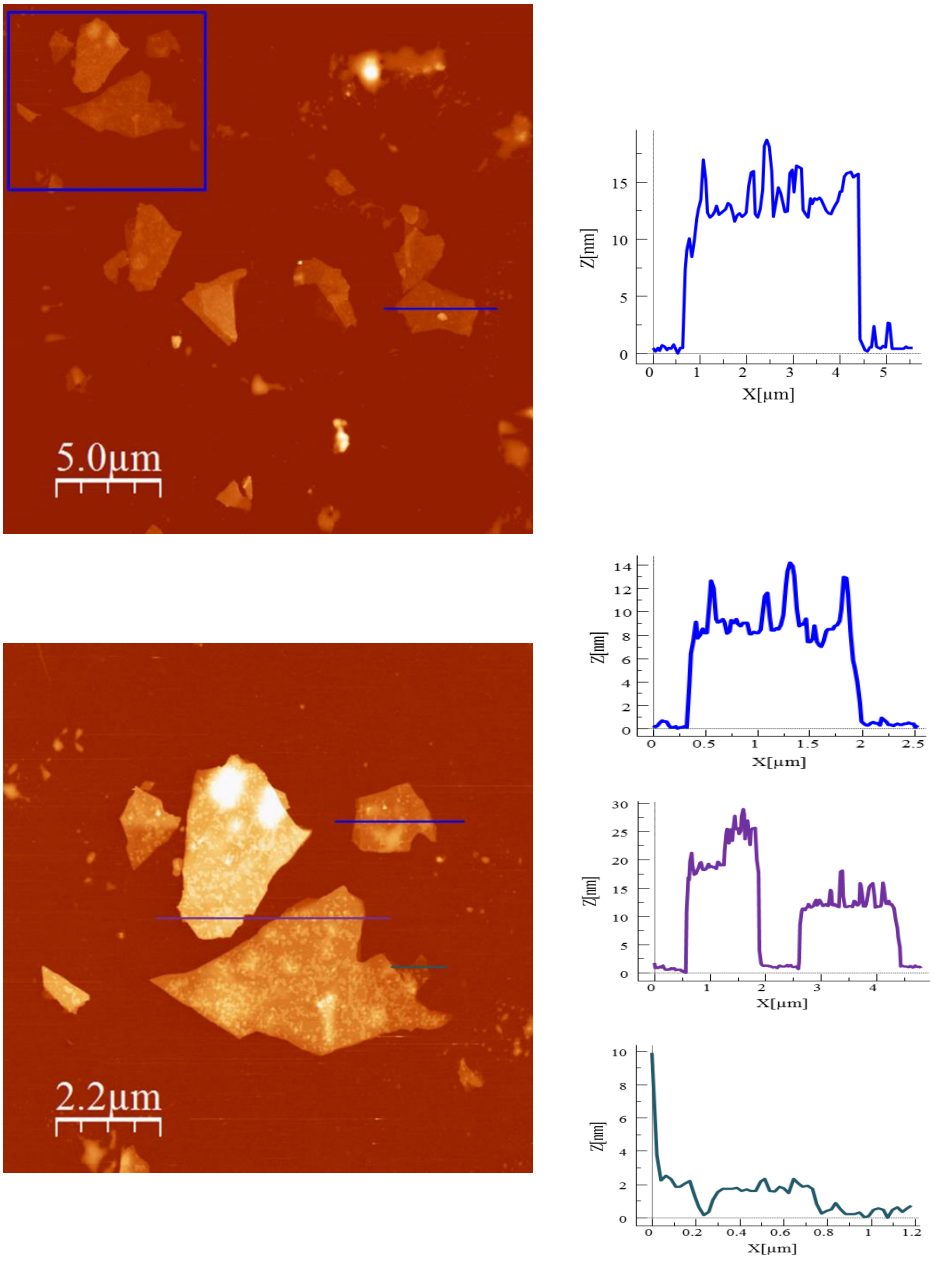

Figure S9. AFM images and height profiles of flakes of **2** obtained by mechanical exfoliation on a 285 nm SiO_2/Si substrate.

Element	Weight %	Atomic %
CrK	8.1	11.1
MnK	9.6	12.4
FeK	9.6	12.2
BrK	72.6	64.4
Total	100.0	100.0

Element	Net Inte.	Backgrd Inte.	Error	P/B
CrK	13.86	1.12	4.09	12.38
MnK	16.14	1.12	3.76	14.41
FeK	15.72	1.20	3.83	13.10
BrK	62.22	0.76	1.81	81.87

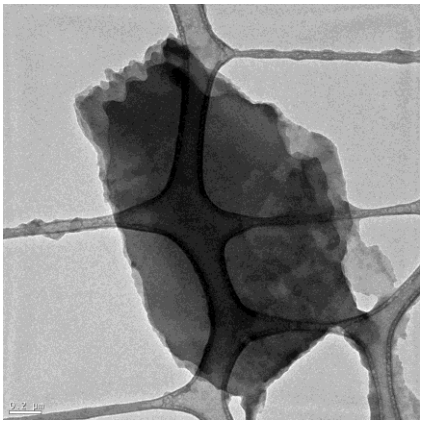

Element	Weight %	Atomic %
ClK	54.0	64.3
CrK	14.4	11.7
MnK	13.9	10.7
FeK	17.6	13.3
Total	100.0	100.0

Element	Net Inte.	Backgrd Inte.	Error	P/B
ClK	120.86	2.30	1.31	52.55
CrK	21.42	1.12	3.21	19.13
MnK	20.26	1.40	3.35	14.47
FeK	25.14	1.80	3.02	13.97

Figure S10. TEM images and EDS analysis of flakes of **2** (left) and **4** (right) obtained by solvent-mediated exfoliation in ethanol and deposited on a TEM grid.

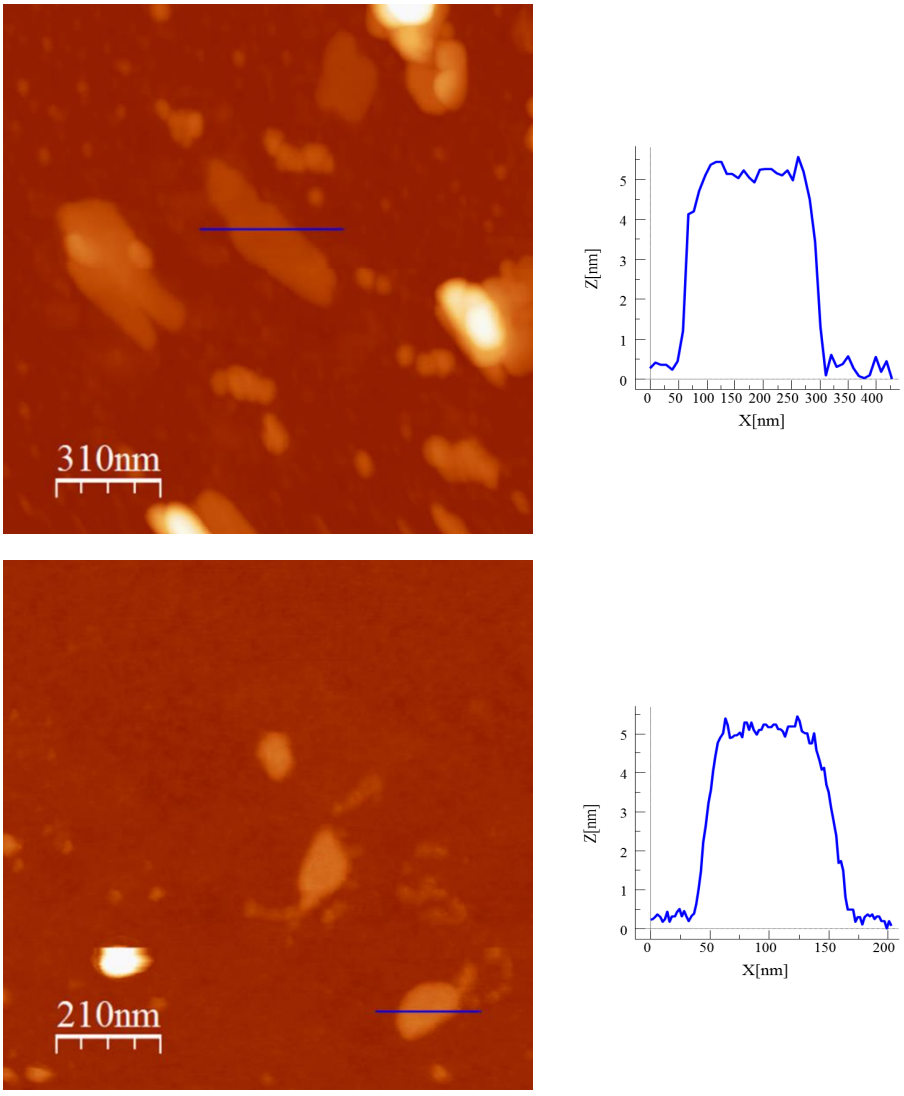

Figure S11. AFM images and height profiles of nanosheets of **2** exfoliated in ethanol and deposited on a Si substrate.

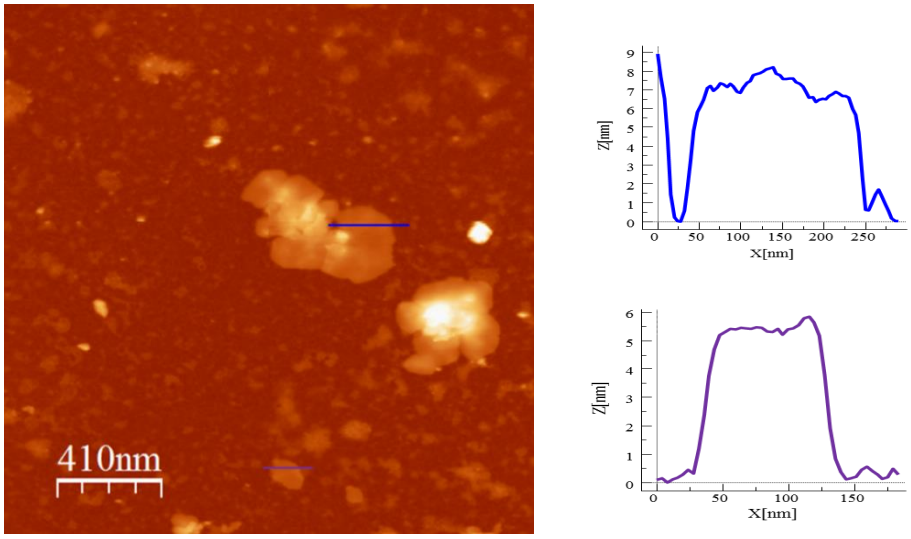

Figure S12. AFM image and height profiles of nanosheets of **4** exfoliated in ethanol and deposited on a Si substrate (bottom).

1 E. V. Dose, K. M. M. Murphy and L. J. Wilson, *Inorg. Chem.*, 1976, **15**, 2622.

2 A. Abhervé, M. Clemente-León, E. Coronado, C. J. Gómez-García and M. Verneret, *Inorg. Chem.*, 2014, **53**, 12014.

3 A. Altomare, M. C. Burla, M. Camalli, G. L. Cascarano, C. Giacovazzo, A. Guagliardi, A. G. G. Moliterni, G. Polidori and R. Spagna, *J. Appl. Cryst*., 1999, **32**, 115.

4 G. M. Sheldrick, *Acta Cryst.*, 2008, **A64,** 112.

5 L. J. Farrugia, *J. Appl. Cryst.,* 2012, **45**, 849.

6 I. Horcas, R. Fernández, J. M. Gómez-Rodríguez, J. Colchero, J. Gómez-Herrero and A. M. Baro, *Rev. Sci. Instrum.*, 2007, **78**, 013705.

Tuning the Nuclearity of Fe^{III} Polynuclear Clusters by using Tetradentate Schiff-Base Ligands

Chapter 6

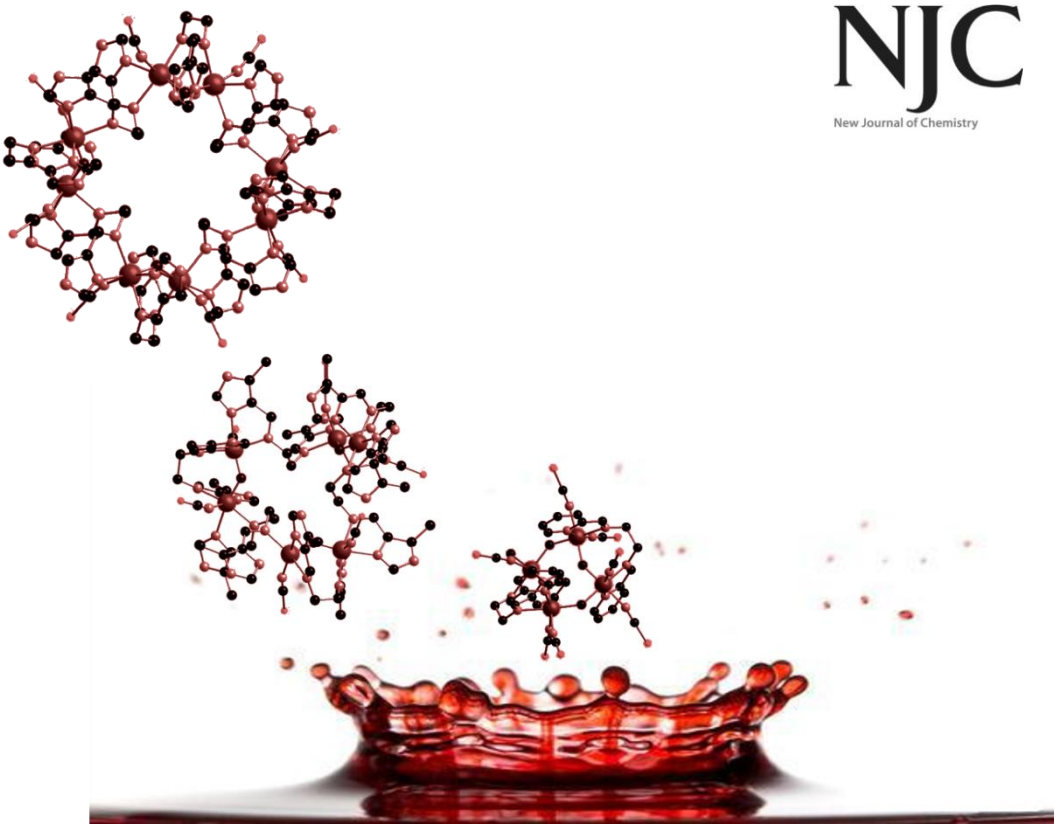

Abhervé, A., Clemente-Juan, J. M., Clemente-León, M., Coronado, E., Boonmak, J., Youngme, S. *New J. Chem.* **2014**, *38*, 2105-2113.

Chapter 6. Tuning the Nuclearity of Fe^{III} Polynuclear Clusters by using Tetradentate Schiff-Base Ligands

Abstract

Three novel octanuclear, hexanuclear and tetranuclear complexes of high-spin Fe^{III} ions were obtained by the reaction of *N,N*'-Bis-(1R-imidazol-4-ylmethylene)-ethane-1,2-diamine ligand (R= H, CH_3) and its derivatives with $Fe(ClO_4)_3 \cdot 6H_2O$ and KSCN. The tetradentate Schiff-base ligand acts as bis(bidentate) chelating bridge between two adjacent high-spin Fe^{III} centers. The presence of a methyl group in the imidazolyl substituent, the change of counterion or the replacement of imidazole by pyridine has a drastic effect in the nuclearity of the cluster. The magnetic properties of all compounds exhibit antiferromagnetic interactions *via* μ-oxo or μ-hydroxo pathways in Fe^{III} dimers.

Introduction

Self-assembly processes between organic ligands and metal ions may lead to the formation of functional supramolecular architectures exhibiting unusual properties[1,2] or interesting host–guest behaviors.[3] Imidazole and imidazolyl-containing ligands have been widely used in coordination chemistry due to their versatility in the preparation of polynuclear complexes, which are of interest in magnetochemistry, and in connection with the design of model compounds mimicking the core structures of active sites of some metalloproteins.[4] More recently, the use of flexible imidazole ligands have afforded the preparation of many coordination complexes with interesting topologies and functional properties such as ferroelectricity,[5] porosity, fluorescence[6] and chemisorption-induced magnetic properties.[7]

One of the most used strategies for the incorporation of imidazolyl moiety in ligands is the condensation of a diamine with an imidazolecarboxyaldehyde.[4]

Tridentate,[8] tetradentate[9,10] and hexadentate[11] Schiff base ligands have been prepared with this strategy. Reactions of these ligands with Fe^{II} have afforded many examples of mononuclear spin-crossover complexes. In the case of tetradentate imidazolyl ligands, mononuclear neutral ferrous complexes of formula $[FeL(NCS)_2]$ have been reported.[10]

The reaction of Fe^{III} with imidazolyl Schiff-base tetradentate ligands has been little explored. The preparation of high nuclearity species are often encountered in Fe^{III} chemistry due to the high charge-to-size ratio of Fe^{III} ion and the resulting propensity to form oxo bridges.[12] Polynuclear iron complexes raise interest as magnetic materials, such as single-molecule magnets (SMM),[13] but also due to their biological importance.[14]

Herein, we report that reaction of Fe^{III} with *N,N'*-Bis-(1R-imidazol-4-ylmethylene)-ethane-1,2-diamine and its derivatives (L_1 and L_2, Scheme 1), and NCS^- permit the preparation of a family of Fe^{III} ring cationic clusters. They are formed by Fe^{III}-O-Fe^{III} dimers bridged by the imidazolyl ligand in a bis(bidentate) mode. The number of Fe^{III}-O-Fe^{III} dimers of the cluster (four or three) and, therefore, its nuclearity (octanuclear or hexanuclear) can be controlled by changing the counterion or introducing a bulky substituent in the ligand. Furthermore, the related tetradentate pyridine ligand, L_3 (Scheme 1) leads to a tetranuclear neutral cluster. The magnetic properties of the three clusters are reported and discussed.

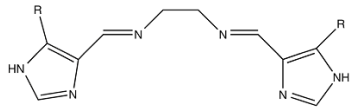

R = H (L_1), CH_3 (L_2)

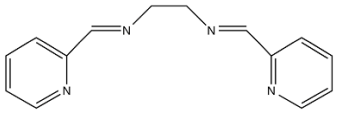

L_3

Scheme 1. Molecular structure of the ligands used in this work.

Experimental section

Syntheses. *N,N'*-Bis-(1-H-imidazol-4-ylmethylene)-ethane-1,2-diamine (L_1) was prepared by the reaction of 4-imidazolecarboxaldehyde (961 mg, 10.00 mmol) and ethylenediamine (334 µL, 5.00 mmol) in acetonitrile (100 mL) for 45 min at 353 K. *N,N'*-Bis-(1-CH_3-imidazol-4-ylmethylene)-ethane-1,2-diamine (L_2)[15] and N,N'-Bis-(pyridin-2-ylmethylene)-ethane-1,2-diamine (L_3) were prepared according to the literature method.[16] All other chemicals are commercially available and were used as received without further purification.

$[Fe_8(\mu\text{-}L_1)_8(\mu\text{-}O)_4(NCS)_8](ClO_4)_5(NCS)_3(H_2O)_6$ (1). KSCN (195 mg, 2 mmol) was added to a methanolic solution (20 mL) of $Fe(ClO_4)_3{\cdot}6H_2O$ (354 mg, 1 mmol). The solution was filtered and a solution of L_1 (216 mg, 1.00 mmol) in methanol (30 mL) was added to the filtrate. The mixture was stirred for 30 min at room temperature. The color of the mixture turned orange. Orange crystals of **1** suitable for X-ray crystal analysis were obtained by slow diffusion of diethyl ether into this solution. Anal. Calc. for $C_{91}H_{108}Cl_5Fe_8N_{59}O_{30}S_{11}$: C, 31.4; H, 3.1; N, 23.7; S, 10.1. Found: C, 31.7; H, 3.2; N, 22.9; S, 9.9 %. IR (selected peaks): 2051 (NCS), 1629 (imine) and 1090 (ClO_4^-) cm^{-1}.

$[Fe_6(\mu\text{-}L_2)_6(\mu\text{-}O)_3(NCS)_6](ClO_4)_2(NCS)_4(CH_3CH_2OCH_2CH_3)_{0.5}(H_2O)_{3.5}(CH_3OH)_{2.5}$ (2). Compound **2** was synthesized in a similar manner to that of compound **1** by using ligand L_2 (244 mg, 1 mmol) instead of L_1. Anal. Calc. for $C_{86.5}H_{118}Cl_2Fe_6N_{46}O_{17.5}S_{10}$: C, 37.0; H, 4.2; N, 22.9; S, 11.4. Found: C, 35.5; H, 3.8; N, 21.9; S, 10.9 %. IR (selected peaks): 2050 (NCS), 1629 (imine) and 1121 (ClO_4^-) cm^{-1}.

$[Fe_4(\mu\text{-}L_3)_2(\mu\text{-}OH)_2(\mu\text{-}OHO)(NCS)_7(OH_2)](H_2O)_2(CH_3CN)_{0.5}$ (3). Compound **3** was synthesized in a similar manner to that of compound **1** by using ligand L_3 (238 mg, 1 mmol) instead. The mixture was stirred for 1h at room temperature. The color solution turned to dark purple and then a brown solid was formed. The precipitate was filtered and recrystallized in acetonitrile. The solution was allowed to stand undisturbed at room temperature. After three days, red prismatic crystals of **3** were obtained. Anal.

Calc. for $C_{36}H_{38.5}Fe_4N_{15.5}O_{7.7}S_7$: C, 34.3; H, 3.1; N, 17.2; S, 17.7. Found: C, 35.0; H, 3.1; N, 17.3; S, 18.2 %. IR (selected peaks): 2030 (NCS), 1637 (imine) and 1400 ($\nu_{C=C}$) cm^{-1}.

$[Fe_6(\mu\text{-}L_1)_6(\mu\text{-}O)_3(NCS)_6](NO_3)_6(CH_3OH)_3(H_2O)$ (4). KSCN (195 mg, 2.00 mmol) was added to a solution of $Fe(NO_3)_3{\cdot}6H_2O$ (404 mg, 1.00 mmol) in methanol (20 mL). The solution was filtered and a solution of L_1 (216 mg, 1.00 mmol) in methanol (30 mL) was added to the filtrate. The mixture was stirred for 1h at room temperature. The color of the mixture turned orange. Orange crystals of **4** suitable for X-ray crystal analysis were obtained by diffusion of diethyl ether into the filtrate. The small amount of sample available prevented elemental analysis and powder X-ray diffraction measurements. IR (selected peaks): 2056 (NCS), 1632 (imine) and 1384 (NO_3^-) cm^{-1}.

$[Fe_6(\mu\text{-}L_2)_6(\mu\text{-}O)_3(NCS)_6](FeF_6)_{0.5}(NCS)_{4.5}(CH_3OH)_2$_(solvate) (5). KSCN (195 mg, 2.00 mmol) was added to a solution of $Fe(BF_4)_2{\cdot}6H_2O$ (338 mg, 1.00 mmol) in methanol (20 mL). Then a solution of L_2 (244 mg, 1.00 mmol) in methanol (30 mL) was added. The mixture was stirred for 1h at room temperature. The color of the mixture turned orange. Orange crystals of **5** suitable for X-ray crystal analysis were obtained by diffusion of diethyl ether into the filtrate. Anal. Calc. for $C_{84.5}H_{104}F_3Fe_{6.5}N_{46.5}O_5S_{10.5}$: C, 38.9; H, 4.0; N, 25.0; S, 12.9 (without disordered solvent molecules). Found: C, 36.4; H, 3.2; N, 23.2; S, 11.8 %. IR (selected peaks): 2049 (NCS), 1629 (imine) and 482 (FeF_6^{3-}) cm^{-1}.

X-Ray crystallography

Single crystals of compounds **1**-**5** were mounted on glass fibres using a viscous hydrocarbon oil to coat the crystal and then transferred directly to the cold nitrogen stream for data collection. All reflection data were collected at 120 K on a Supernova diffractometer equipped with a graphite-monochromated Enhance (Mo) X-ray Source (λ = 0.71073 Å). The CrysAlisPro program, Oxford Diffraction Ltd., was used for unit cell determinations and data reduction. Empirical absorption correction was performed using spherical harmonics, implemented in the SCALE3 ABSPACK scaling algorithm.

Crystal structures were solved by direct methods with the SIR97 program,[17] and refined against all F^2 values with the SHELXL-2013 program,[18] using the WinGX graphical user interface.[19a] All non-hydrogen atoms were refined anisotropically, and hydrogen atoms were placed in calculated positions and refined isotropically with a riding model. The details of data collection and structure refinements are provided in Table 1. In compounds **1** and **5,** the presence of disordered thiocyanate and solvent molecules gave rise to a very weak scattering. Initial refinements revealed the presence of substantial volume of unresolvable solvent (CH_3OH and H_2O) molecules in **5**. The subroutine SQUEEZE from PLATON[19b] was used to remove the diffracting component of disordered solvents resulting in a void of ca. 4163 $Å^3$ and 675 electrons/cell omitted. This corresponds to ca. 32 CH_3OH + 4 H_2O molecules per cell. In compound **3**, one thiocyanate anion coordinated to Fe3 is disordered over two sites and has been modelled with an occupancy of 70:30 ratio.

0.5 mm glass capillaries were filled with polycrystalline samples of **2** and **3** and mounted and aligned on a Empyrean PANalytical powder diffractometer, using CuKα radiation (λ = 1.54177 Å). A total of 3 scans were collected at room temperature in the 2θ range 5-30^o.

Physical measurements

C, H, N and S elemental analyses were measured on a CE Instruments EA 1110 CHNS Elemental analyzer. The Fe:S and Fe:S:Cl ratios were measured on a Philips ESEM X230 scanning electron microscope equipped with an EDAX DX-4 microsonde. Infrared spectra were recorded in the solid state (KBr pellets) on a Nicolet Avatar 320 FTIR spectrometer in the 400-4000 cm^{-1} range. ESI mass spectra were recorded on a Waters ZQ mass spectrometer using nitrogen as the drying and nebulising gas. The equipment was calibrated with appropriate standard samples. Magnetic measurements were performed with a Quantum Design MPMS-XL-5 SQUID magnetometer in the 2 to 300 K temperature range with an applied magnetic field of 0.1 T on polycrystalline samples. Mössbauer spectra were collected in transmission mode using a conventional

constant-acceleration spectrometer and a 50 mCi ^{57}Co source in a Rh matrix. The velocity scale was calibrated using α-Fe foil. The absorber was obtained by gently packing single crystals of **3** into a perspex holder. Isomer shifts (Table 2) are given relative to metallic α-Fe at room temperature.

Results

Syntheses

Reaction of $Fe(ClO_4)_3{\cdot}6H_2O$, Schiff-base ligand (L_1, L_2 or L_3) and KSCN in a 1:1:2 molar ratio in methanol leads to three Fe^{III} clusters with different nuclearities (8, 6 and 4) of formula $[Fe_8(\mu\text{-}L_1)_8(\mu\text{-}O)_4(NCS)_8](ClO_4)_5(NCS)_3$ (**1**), $[Fe_6(\mu\text{-}L_2)_6(\mu\text{-}O)_3(NCS)_6](ClO_4)_2(NCS)_4$ (**2**) and $[Fe_4(\mu\text{-}L_3)_2(\mu\text{-}OH)_2(\mu\text{-}OHO)(NCS)_7(OH_2)]$ (**3**), respectively. The 1:1 metal:ligand ratio of the syntheses is maintained in the final structure for compounds **1** and **2**, which contain the tetradentate imidazolyl ligands L_1 and L_2, but not in **3**, which contains the tetradentate pyridyl ligand L_3. In this last case, the structure presents a 2:1 metal:pyridyl ligand ratio. The complexes obtained with the imidazolyl ligands are soluble in methanol and were crystallized by slow diffusion with diethyl ether. Both **1** and **2** are cationic polynuclear complexes with NCS^- and ClO_4^- acting as counterions. In contrast, similar synthetic conditions with the pyridyl-based ligand, L_3, afforded the neutral compound, **3**, which precipitated in methanol and was obtained by recrystallization in acetonitrile. The use of other counterions in the Fe^{III} precursor salt such as NO_3^- with L_1 and BF_4^- or Cl^- with L_2 led in all cases to hexanuclear clusters with a similar structure to that of **2** (see compounds **4** and **5,** Figures S1 and S2 in the SI). In the case of BF_4^-, oxidation of Fe^{II} to Fe^{III} in air and decomposition of the anion gave rise to the presence of $[FeF_6]^{3-}$ counterions in the structure (see compound **5**, SI). Preliminary single crystal diffraction data of a compound obtained with L_2 and Cl^- show the presence of a hexamer with a similar structure to that found in **2**, **4** and **5**. However, due to the low quality of the data it was not possible to find a proper solution of the structure. Finally, powder X-ray diffraction patterns of **2** and **3** at 300 K

confirm the structure obtained from single X-ray diffraction experiments shown below (Figure S3 in the SI). X-ray diffraction patterns of **1** and **5** are not shown as powder samples of these compounds lost crystallinity very fast after filtering due to the loss of solvent. In the case of **4**, the small amount of sample available prevented the measurement of the powder X-ray diffraction. The composition of crystals of these compounds, checked by microanalysis, shows a Fe:S:Cl ratio close to 8:11:5 for **1**, and 6:10:2 for **2**, and a Fe:S ratio close to 4:7 for **3**, 6:6 for **4** and 6.5:10.5 for **5**.

Structure of $[Fe_8(\mu\text{-}L_1)_8(\mu\text{-}O)_4(NCS)_8](ClO_4)_5(NCS)_3(H_2O)_6$ (1)

1 crystallizes in tetragonal $I4_1cd$ space group. The structure is formed by an octanuclear cationic complex of formula $[Fe_8(\mu\text{-}L_1)_8(\mu\text{-}O)_4(NCS)_8]^{8+}$ (Figure 1), five perchlorate and three thiocyanate anions, and disordered lattice water molecules. The octanuclear, Fe_8, unit is formed from half of the molecule, which is crystallographically independent, through a 2-fold axis linking O1 and O3. Thus, it contains four crystallographically independent Fe^{III} atoms (Fe1-Fe4) and is composed by four $[Fe^{III}\text{–}O\text{–}Fe^{III}]^{4+}$ dimers. Four of the eight neutral tetradentate L_1 ligands connect the two Fe^{III} of the dimer in a bis(bidentate) chelating mode while the remaining four connect Fe^{III} belonging to different dimers in a similar way. Thus, each Fe^{III} center shows a distorted octahedral N_5O coordination to four nitrogen atoms from two chelating L_1 in cis-arrangement, one nitrogen atom from the NCS^-, and one oxygen atom from a μ-oxo (Figure 1). The Fe-N(imino) bond length distances range from 2.161(14) to 2.196(16) Å, while Fe-N(imidazolyl) ones range from 2.148(15) to 2.201(18) Å. In the axial position, the Fe-N(NCS^-) distances lie between 2.027(18) to 2.049(15) Å, Fe-O(oxo) are between 1.790(6) to 1.801(6) Å as normally observed for binuclear Fe^{III} complexes with a single oxygen bridge.[20] These distances are in good agreement with the expected ones for HS Fe^{III} centers. The imidazolyl NH groups in **1** present hydrogen bonds with disordered free NCS^- and ClO_4^- counterions and lattice water molecules. Two crystallographically equivalent ClO_4^- groups (with central atom Cl1) are close to the internal cavity of the Fe_8 cationic ring with numerous short

contacts with L_1 atoms. On the other hand, the second crystallographically independent ClO_4^- group (with central atom Cl2) occupies the space between Fe_8 cations and present numerous short contacts with L_1 atoms.

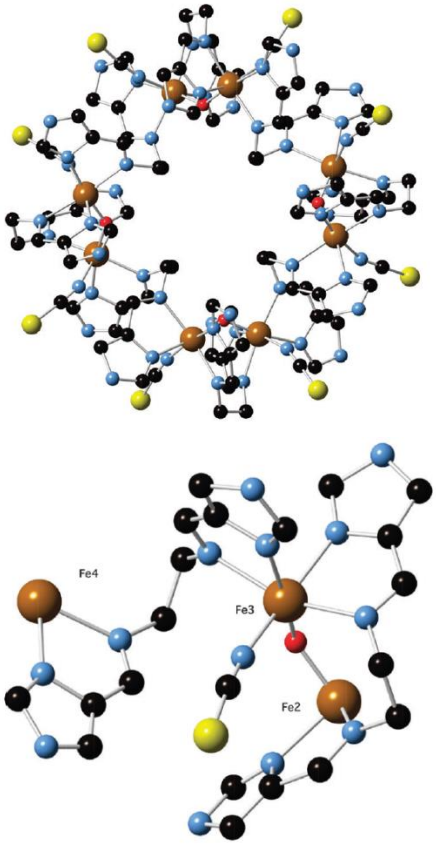

Figure 1. Molecular structure of the octanuclear $[Fe_8(\mu\text{-}L_1)_8(\mu\text{-}O)_4(NCS)_8]^{8+}$ complex of **1** (left) and view of the coordination sphere around Fe3 linked to an iron atom from the same dimer (Fe2) and another one from the neighboring dimer (Fe4) (right) (iron (brown), sulfur (yellow), oxygen (red), nitrogen (blue), carbon (black)).

Structure of $[Fe_6(\mu\text{-}L_2)_6(\mu\text{-}O)_3(NCS)_6](ClO_4)_2(NCS)_4(CH_3CH_2OCH_2CH_3)_{0.5}(H_2O)_{3.5}(CH_3OH)_{2.5}$ (2)

2 crystallizes in triclinic *P*-1 space group. The structure is formed by a hexanuclear complex cation of formula $[Fe_6(\mu\text{-}L_2)_6(\mu\text{-}O)_3(NCS)_6]^{6+}$ (Figure 2), two perchlorate and four thiocyanate anions, diethylether and disordered methanol and water molecules. The Fe_6 unit is formed by three $[Fe^{III}OFe^{III}]^{4+}$ dimers, six L_2 ligands and six NCS^- ligands. The L_2 ligands present the same intra or interdimer bis(bidentate) coordination mode between two Fe^{III} shown for compound **1**. Thus, each Fe^{III} center presents a N_5O coordination sphere to four nitrogen atoms from two chelating L_2 ligands, one nitrogen atom from the terminal NCS^- group, and one oxygen atom from an oxo group in a similar way as in compound **1**. The imidazolyl NH groups from L_2 ligands form hydrogen bonds with disordered free NCS^- counterions and lattice water and methanol molecules. The ClO_4^- groups present hydrogen bonds with the imidazolyl NH groups from L_2. One ClO_4^- group (with central atom Cl1) is very close to the internal cavity of the Fe_6 cationic ring with numerous short contacts with L_2 atoms. On the other hand, the second crystallographically independent ClO_4^- group (with central atom Cl3 with an occupancy of 0.5) is close to the opposite site of the internal cavity of the Fe_6 cationic ring. Finally, the third crystallographically independent ClO_4^- anion (with central atom Cl2 with an occupancy of 0.5) occupies the space between Fe_6 units.

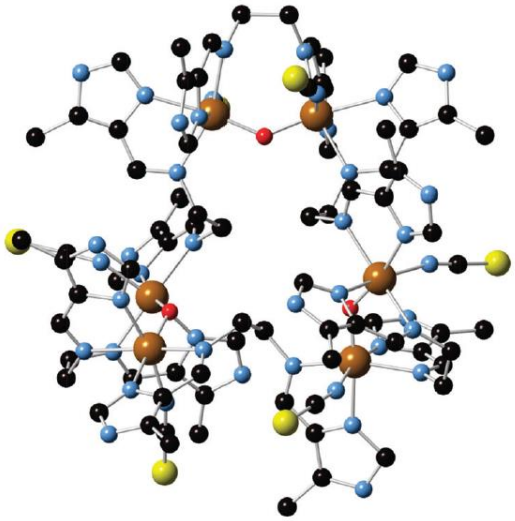

Figure 2. Molecular structure of the hexanuclear $[Fe_6(\mu\text{-}L_2)_6(\mu\text{-}O)_3(NCS)_6]^{6+}$ complex of **2** (iron (brown), sulfur (yellow), oxygen (red), nitrogen (blue), carbon (black)).

Structure of $[Fe_4(\mu\text{-}L_3)_2(\mu\text{-}OH)_3(\mu\text{-}O)(NCS)_7(OH_2)](H_2O)_2(CH_3CN)_{0.5}$ (3)

3 crystallizes in the monoclinic $P2_1/n$ space group. It is formed by a tetranuclear neutral complex of formula $[Fe_4(\mu\text{-}L_3)_2(\mu\text{-}OH)_3(\mu\text{-}O)(NCS)_7(OH_2)]$ and lattice water and acetonitrile solvent molecules, which are disordered in some cases. The neutral cluster is constructed from four crystallographically independent Fe^{III} ions (Fe1-Fe4) that lie at the corners of a very distorted rectangle (Figure 3). The $\mu\text{-}OH^-$ groups bridge Fe1/Fe2, Fe1/Fe3 and Fe3/Fe4 pairs (Figure 4), while Fe2/Fe4 pair is bridged by a $\mu\text{-}O^{2-}$. The Fe1/Fe3 and Fe2/Fe4 pairs are linked together by pyridyl-based L_3 ligands in bis(bidentate) chelating bridging mode. The distorted octahedral coordination of the four Fe^{III} ions is completed with two terminal NCS^- ligands with the exception of Fe4 which is coordinated to one terminal NCS^- ligand and one terminal water molecule (Figure 4). Therefore, three of the four Fe^{III} (Fe1, Fe2 and Fe3) present a N_4O_2 coordination sphere to two N(imine and pyridyl) from one L_3 ligand, two μ-O(hydroxo or oxo) and two $N(NCS^-)$, while the another one (Fe4) shows a N_3O_3 coordination sphere to two N (imine and pyridyl) from one L_3 ligand, one $N(NCS^-)$ and three μ-

O(hydroxo, oxo and terminal water molecule). The four Fe atoms are far to be coplanar and deviate from their best least-square plane by 0.267 (Fe1), -0.322 (Fe2), -0.286 (Fe3) and 0.341 (Fe4) Å. On the contrary, the four bridging oxygen atoms (O1 to O4) form a plane with a deviation of less than 0.006 Å from their best least-square plane.

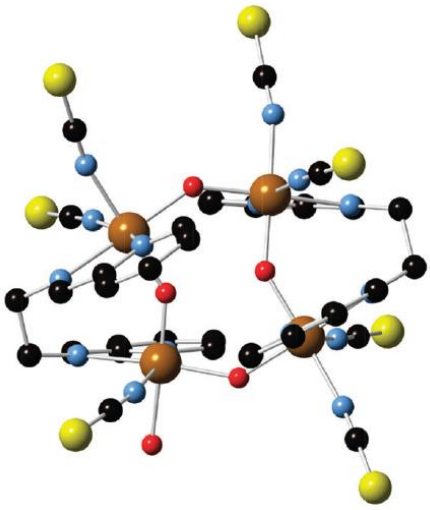

Figure 3. Molecular structure of the tetranuclear $[Fe_4(\mu\text{-}L_3)_2(\mu\text{-}OH)_3(\mu\text{-}O)(NCS)_7(H_2O)]$ complex of **3** (iron (brown), sulfur (yellow), oxygen (red), nitrogen (blue), carbon (black)).

The hydrogen atoms of the Fe_4 cluster were not crystallographically located. Given the absence of counterions and the fact that metal-ligand distances and Mössbauer spectroscopy (see below) indicate that the four metal centers are clearly HS Fe^{III}, charge considerations require that three of the four core oxygen are formally protonated. O1 and O4 atoms are protonated as evidenced by (i) their bond distances to Fe^{III} ions (mean Fe-O distance of 1.991(3) Å), which are typical of Fe^{III}-μ-(hydroxo) bonds,[21] and (ii) the short distance of these two atoms to lattice water molecules indicating the formation of hydrogen-bonds ($d_{O1\cdots O5W}$ = 2.880 Å and $d_{O4\cdots O2W}$ = 2.780 Å). The Fe-O distances of the remaining bridging oxygens (O2 and O3) are clearly differentiated suggesting a different protonation. Thus, Fe-O distances of O2 are 1.924(3) and 1.936(3) Å, which lie in the range to that found for other Fe^{III}-μ-(hydroxo)

bonds. In contrast, Fe-O distances of O3 (1.810(4) and 1.826(4) Å) are consistent with the formation of a Fe^{III}-μ-(oxo) bond (see above). Furthermore, the distance between O2 and O3 (2.551 Å) is consistent with the formation of a hydrogen bond between them (see Fig. 4). The significant difference of Fe-O distances indicating that the μ-oxo and μ-hydroxo can be considered as separate structural entities rather than a $(O\text{-}H\text{-}O)^{3-}$ unit.[22,23] Indeed, Fe_4 complexes with $(O\text{-}H\text{-}O)^{3-}$ units present shorter O···O distances ranging from 2.394 to 2.529 Å.[21,24] Finally, the presence of two protons in the terminal oxygen coordinated to Fe4 (O1W) is supported by the formation of two hydrogen bonds with one disordered lattice water/acetonitrile molecule and one S atom from a NCS^- group, as shown in Figure 4.

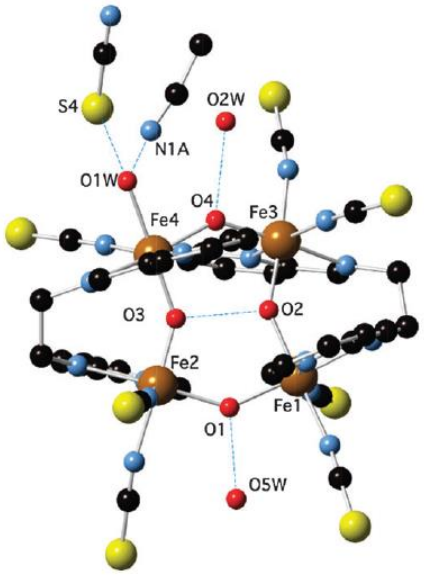

Figure 4. Intra- and intermolecular hydrogen-bonding of **3**.

Table 1. Crystallographic data for **1**, **2**, **3**, **4** and **5**.

Compound	**1**	**2**	**3**	**4**	**5**
Empirical formula	$C_{91}H_{108}Cl_5Fe_8N_{59}O_3$	$C_{86.5}H_{118}Cl_2Fe_6N_{46}$	$C_{36}H_{38.5}Fe_4N_{15.5}O_{7.7}$	$C_{69}H_{86}Fe_6N_{48}O_{25}S_6$	$C_{93.5}H_{142}F_3Fe_{6.5}N_{46.5}$
	$_0S_{11}$	$O_{17.5}S_{10}$	S_7		$O_{15}S_{10.5}$
Formula weight	3484.97	2808.69	1259.26	2513.21	2914.11
Crystal color	Red	Red	Red	Red	Red
Crystal size	0.2*0.07*0.05	0.06*0.06*0.02	0.15*0.11*0.10	0.23*0.10*0.05	0.33*0.11*0.07
Temperature (K)	120(2)	120(2)	120(2)	120(2)	120(2)
Wavelength (Å)	0.71073	0.71073	0.71073	0.71073	0.71073
Crystal system, *Z*	Tetragonal, 8	Monoclinic, 2	Monoclinic, 4	Orthorhombic, 4	Monoclinic, 4
Space group	$I4_1cd$	P-1	$P2_1/n$	Pbna	$C2/c$
a (Å)	28.5279(3)	17.1614(6)	20.2912(6)	15.5153(4)	45.2573(13)
b (Å)	28.5279(3)	17.3252(6)	11.7876(5)	25.8550(9)	27.5089(6)
c (Å)	41.3731(6)	24.4236(7)	22.1837(6)	26.6761(11)	28.4547(9)
α (°)	90.00	70.309(3)	90	90	90
b (°)	90.00	79.499(3)	98.084(3)	90	119.372(4)
γ (°)	90.00	77.344(3)	90	90	90
V (Å^3)	33671.1(9)	6624.3(4)	5253.3(3)	10701.1(6)	30871.7(18)
ρ_{calc} (Mg/m^3)	1.370	1.397	1.579	1.552	1.119
$\mu(Mo_{K\alpha})$ (mm^{-1})	0.960	0.910	1.422	0.999	0.791
θ range (°)	2.856-27.500	2.944-27.484	3.053-27.519	3.062-27.498	2.955-26.408
Reflns collected	178800	105489	28735	42210	260859
Independent reflns (R_{int})	8631 (0.1501)	14588 (0.1269)	8545 (0.0445)	5927 (0.0934)	16529 (0.13173)
L. S. parameters, *p*/ restraints, *r*	898 / 14	1479 / 7	651 / 3	683 / 31	1306 / 15
$R1(F)$,[a] $I > 2\sigma(I)$	0.1109	0.0968	0.0660	0.0826	0.1149
$wR2(F^2)$,[b] all data	0.3470	0.3045	0.1816	0.2527	0.3644
$S(F^2)$,[c] all data	1.012	1.053	1.028	1.027	1.082

[a] $R1(F) = \Sigma||F_O|-|F_C||/\Sigma|F_O|$; [b] $wR2(F^2) = [\Sigma w(F_O^2-F_C^2)^2/\Sigma wF_O^4]^{1/2}$; [c] $S(F^2) = [\Sigma w(F_O^2-F_C^2)^2/\Sigma n + r - p)]^{1/2}$

Electrospray

The behavior of the polynuclear Fe_6 cationic cluster of **2** in solution has been characterized by electrospray ionization mass spectrometry (ESI-MS). Figure S4 in the SI shows the ESI-MS (positive mode) analysis of a solution of **2** in methanol. The two most intense peaks appear at m/z values of 588.67 and 598.95 Da which correspond respectively to the $[Fe_6(\mu\text{-}L_2)_6(\mu\text{-}O)_3(NCS)_6](ClO_4)(NCS)^{4+}$ and $[Fe_6(\mu\text{-}L_2)_6(\mu\text{-}O)_3(NCS)_6](ClO_4)_2^{4+}$ species. The third most intense peak corresponds to a $[Fe(L_2)(NCS)]^+$ monomer that have been reduced by one electron. Finally, the remaining peaks could be assigned to Fe_6 units that have been reduced by one electron plus one ClO_4^- (574.05 Da), one ClO_4^- and SCN^- (784.68 Da) or two ClO_4^- (798.39). The charge of the species present in the spectrum has been unambiguously characterized by single ion recording (SIR) at the highest resolution of the spectrometer with monoisotopic peaks separated by 1/*z* Da. Figure S5 in the SI shows the isotopic distributions of the most intense peaks. As the majority of peaks arise from species in which the Fe_6 core remains intact, we can conclude that the cluster is preserved in solution.

Mössbauer spectrum of 3

Owing to the structural features exhibited by the Fe_4 clusters, four different iron sites and two sorts of bridging ligands ($\mu\text{-}OH^-$ and $\mu\text{-}O^{2-}$), it seemed to be of interest to study the Mössbauer spectrum of **3** (Figure 5). In order to satisfactorily fit this spectrum, it was necessary to consider nested quadrupole-split doublets, *i.e.* of very close isomer shift (IS), in line with a very similar N_4O_2 or N_3O_3 environment for all four iron sites, but significantly different quadrupole splittings (QS). The data may in principle be analyzed assuming two quadrupole-split doublets in a 1:1 ratio with fitting parameters shown in table 2. These parameters are typical of HS Fe^{III}. The quadrupole-split doublet with smaller QS value could be assigned to Fe1 and Fe3 as they exhibit very similar environments since both are linked to two $\mu\text{-}OH^-$ groups, whereas the one with larger QS could be assigned to Fe2 and Fe4, taking into account the more distorted octahedral coordination of Fe2 and Fe4 which contain shorter $Fe^{III}\text{-}\mu\text{-}O^{2-}$

bonds. Still, the Mössbauer spectrum of **3** could also be fitted to three doublets with a 2:1:1 ratio. This is not surprising given the low sensitivity of HS–Fe^{III} Mössbauer parameters to the coordination environment, and the similarities of the coordination spheres of the four sites.[22] In any case and for purposes of comparison, indicative parameters of the fitting to two doublets are summarized in Table 2.

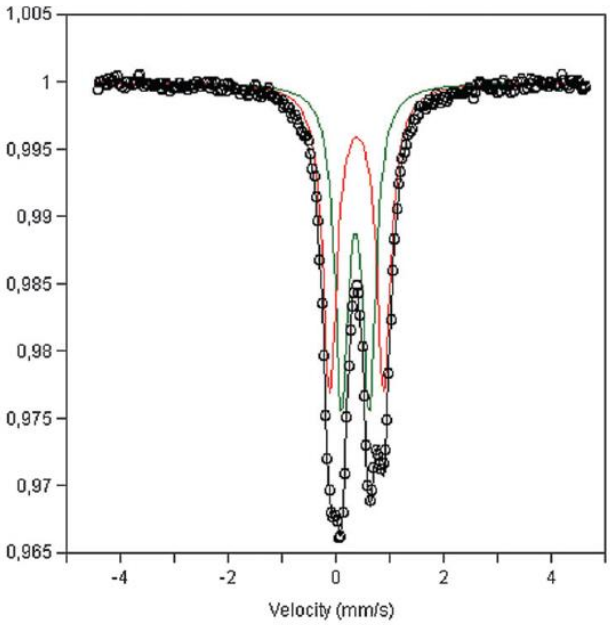

Figure 5. Room temperature Mössbauer spectrum of **3**. The lines over the experimental points are the sum of two doublets. The estimated parameters of these doublets are collected in Table 2.

Table 2. Estimated parameters from the Mössbauer spectrum of **3** taken at room temperature.

[a]	IS	QS	Γ	*I* (%)
	0.365	0.512	0.293	48.23
	0.393	1.003	0.319	51.77

[a] IS (mm s^{-1}) isomer shift relative to metallic Fe at 297K. QS (mm s^{-1}) quadrupole splitting of doublets; Γ (mm s^{-1}) half-width of the doublet peaks. *I* relative area. Estimated standard deviations are < 0.02 mm s^{-1} for IS, QS and Γ, and < 3 % for I.

Magnetic properties

The temperature dependence of the product of the molar magnetic susceptibility times the temperature (χT) of compounds **1** and **2** is shown in insets of Figure 6. The two compounds present a very similar behavior as expected from their structures. The χT values at 300 K (2.8 and 2.7 cm^3 K mol^{-1} for **1** and **2**, respectively) are significantly lower than theoretically expected for non-interacting HS Fe^{III} ions (35.00 and 26.25 cm^3 K mol^{-1} for 8 and 6 Fe^{III} ions with g = 2, respectively). The χT of both compounds decreases gradually almost linearly when temperature decreases down to 50 K and stays approximately constant (0.15 cm^3 K mol^{-1}) until 2 K which is an indication of strong antiferromagnetic interactions through $[Fe^{III}–O–Fe^{III}]^{4+}$ dimer with the ground state S = 0. The similar χT curves of both compounds indicate that the magnetic interactions through the bis(bidentate) L_1 or L_2 ligands are very weak and that the observed behavior should be attributed to strong intradimer antiferromagnetic interactions between Fe^{III} centers linked by μ-oxo. Indeed, it has been modeled using the isotropic spin-spin interaction by the Heisemberg-Dirac-Van Vleck Hamiltonian $H = -2JS_1S_2$, where $S_1 = S_2 = 5/2$.[25] To reproduce the data satisfactorily we had to consider a certain amount of a paramagnetic impurity (ρ, %). The best fit was obtained with the following parameters J = -119.2 cm-1, g = 2.00 and ρ = 0.903% for **1** (with R = 2.97×10^{-3}) and J = -110.5 cm^{-1}, g = 2.02 and ρ = 0.606% for **2** (with R = 2.82×10^{-4}). These parameters are similar to those found in other Fe^{III}-oxo dimers.[26]

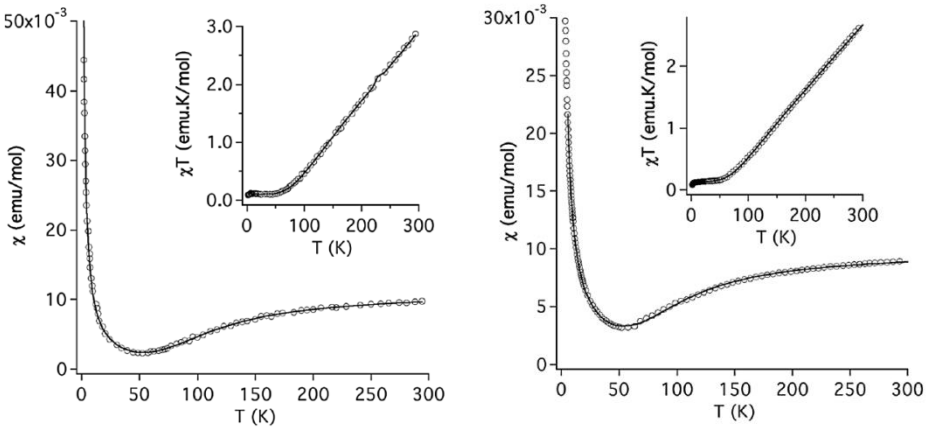

Figure 6. Plot of χ vs. T and $\chi_M T$ vs. T (insets) for **1** (left) and **2** (right). The susceptibility, χ, was measured under a 0.1 T magnetic field. The solid line is the best fit of the 2-300 K data.

χT of **3** decreases linearly from 5.6 cm^3 K mol^{-1} at 300 K to 0.05 cm^3 K mol^{-1} at 10 K, and stays approximately constant down to 2 K (see inset on Figure 7). The presence of four Fe^{III} linked by μ-OH^- or μ-O^{2-} ligands gives rise to a magnetic behavior, which indicates weaker antiferromagnetic interactions between S = 5/2 of the Fe^{III} than those found for **1** and **2**. Inspection of the molecular structure of **3** reveals that due to the lack of symmetry, four exchange interactions would be rigorously required for the interpretation of the magnetic properties.[21] A simplification considering only three type of interactions: $J_{12} = J_{34}$ corresponding to hydroxo bridge interactions through O1 and O4 oxygen atoms, J_{13} corresponding the other type of hydroxo bridge through O2 oxygen atom and finally J_{24} associated to oxo bridge through O3 oxygen atom. The best fitting to experimental data is obtained with the following parameters $J_{12} = J_{34}$ = -3.07 cm^{-1}, $J_{24} \approx J_{13}$ = -34.37 cm^{-1}, g = 2.00 and ρ = 0.5 % (with R = 3.54×10^{-4}). This fit is not very sensible to the J_{24}/J_{13} ratio. The dependence of the fit respect to them is shown on a two-dimensional plot of the error factor R on the values J_{24} and J_{13} (Figure 8). The minimum error region (R < 7.0×10^{-4}) has a banana shape where both Js can be interconverted and with limits at J_{13} = -27.5 cm^{-1} and J_{24} = -48.8 cm^{-1}. These parameters are similar to those found in related compounds.[21-23]

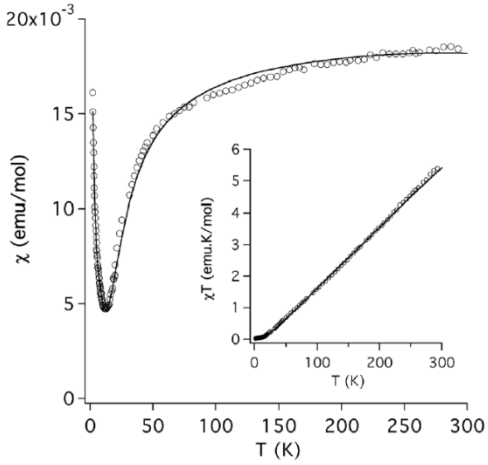

Figure 7. Plot of χ vs. T and $\chi_M T$ vs. T (insets) for **3**. The susceptibility, χ, was measured under a 0.1 T magnetic field. The solid line is the best fit of the 2-300 K data.

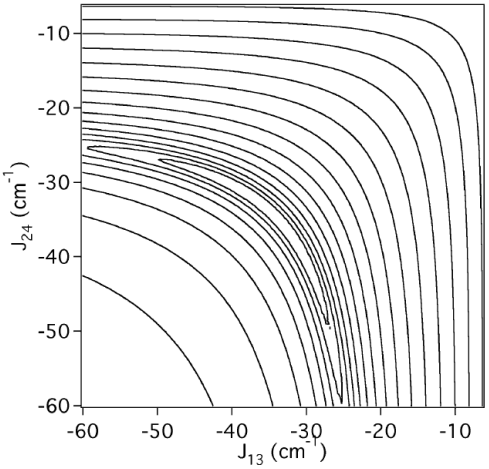

Figure 8. Surface error plot of χ_M vs. T as a function of J_{24} and J_{13} revealing a banana minima.

Discussion

The reactivity of Fe^{III} with tetradentate Schiff-base ligands derived from imidazole has been studied. In all cases the imidazolyl ligands coordinate to two Fe^{III} linked

through an oxo ligand in a bis(bidentate) chelating bridging mode instead of only tetradentate chelating mode observed for Fe^{II} systems with similar ligands. As a result of this, two novel polynuclear clusters with ring structures of eight and six Fe^{III} centers have been obtained in contrast to reactions of similar ligands with Fe^{II}, which lead to mononuclear complexes in all cases. In addition, we have observed that the presence of a methyl group in the imidazolyl substituent of L_2 or the change of counterion have a drastic effect in the nuclearity of the cluster. Thus, reaction of $Fe(ClO_4)_3 \cdot 6H_2O$ with L_1 gives rise to an octanuclear Fe^{III} cluster, but if the size of the counteranion is reduced (replacement of ClO_4^- by NO_3^- or Cl^-) or a methyl group is introduced in the ligand (replacement of L_1 by L_2), hexanuclear clusters are obtained in compounds **2**, **4** and **5**. A possible explanation is that ClO_4^- anions present the correct size and shape to template the growth of an octanuclear cluster. Indeed, two ClO_4^- anions in the structure of compound **1** are close to the center of the octanuclear cluster and present numerous short contacts with L_1 ligands of this octanuclear cluster. When the size of the anion is reduced or bulky methyl substituents are introduced in the ligand, the octanuclear cluster cannot be formed and templating of a hexanuclear cluster occurs as in compound **4** and compound with Cl^- mentioned above with L_1 or compounds **2** and **5** with L_2. In these two last compounds, ClO_4^- or FeF_6^{3-} anions do not enter in the internal cavity of the cluster as they present short contacts with at least two neighboring hexanuclear complexes. On the other hand, replacement of the imidizolyl units by pyridyl ones leads to a tetranuclear neutral cluster of **3**, in which Fe^{III} is in the HS state. ES-MS studies of methanol solutions of **2** show that the hexanuclear polynuclear complexes are preserved in solution as they form adducts with NCS^- and/or ClO_4^- counterions. This could open the way for possible applications of these clusters in solution or deposited onto surfaces.

The magnetic properties of the compounds of the octanuclear cluster of **1** and the hexanuclear cluster of **2** can be explained by the presence of four or three Fe^{III} dimers bridged by μ-oxo ligands that gives rise to antiferromagnetic interactions and to antiferromagnetic ground states. They could be modelled by using the isotropic spin-

spin interaction with similar parameters (J = -119.2 cm-1 for **1** and J = -110.5 cm^{-1} for **2**). The angular and distance dependence of J of oxo-bridged Fe^{III} dimers has been rationalized by Weihe and Güdel by using an angular and radial overlap model.[27] The similar J values of **1** and **2** are a consequence of the similar Fe-O distances (1.790(18) Å for **1** and 1.797(5) Å for **2**) and Fe-O-Fe angles (136.7(15)° for **1** and 133.2(5)° for **2**) that they present. These values are consistent with those obtained for Fe^{III}-oxo dimers with similar Fe-O lengths and Fe-O-Fe angles.[27] In the case of **3**, the presence of four Fe^{III} linked by μ-OH^- or μ-O^{2-} ligands gives rise to a different magnetic behavior with weaker antiferromagnetic interactions between S=5/2 of the Fe^{III} than those found for **1** and **2**. The magnetic properties could be modelled by a simplified model considering only three types of interactions: $J_{12} = J_{34}$ corresponding to hydroxo bridge interactions, J_{13} corresponding the other type of hydroxo bridge and J_{24} associated to oxo. The lower value of J_{24} of **3** compared to J values of **1** and **2** is consistent with the increase of Fe-O lengths (1.818(4) Å) and Fe-O-Fe angles (145.15(18)°) for **3**.[27] As expected, the O^{2-}-bridged pair (Fe2···Fe4) is much more strongly antiferromagnetically coupled than the OH^--bridged pairs.[23] The Fe1···Fe2 and Fe3···Fe4 couplings between hydroxo-bridged pairs are similar, as expected for similarities in distances and angles. J value of these two pairs ($J_{12} = J_{34}$ = -3.07 cm^{-1}) is weaker than that of the remaining hydroxo-bridged pair (J_{13} = -27.5 cm^{-1}) as expected on the basis of the smaller Fe-O-Fe angles (≈ 138° for Fe1-O1-Fe2 and Fe3-O4-Fe4 versus ≈ 145° for Fe1-O2-Fe3) and longer Fe-O distances (1.993(3) Å for Fe1-O1-Fe2 and 1.990(3) Å for Fe3-O4-Fe4 versus 1.930(3) Å for Fe1-O2-Fe3).[23]

Conclusions

Two novel interesting polynuclear clusters with ring structures of eight and six Fe^{III} centers have been obtained by reaction of Fe^{III} with tetradentate Schiff-base ligands derived from imidazole. In these compounds, the imidazolyl ligands coordinate to two Fe^{III} in a bis(bidentate) chelating bridging mode instead of only tetradentate chelating mode observed for Fe^{II} systems with similar ligands. In addition, the presence of a

methyl group in the imidazolyl substituent or the change of counterion allows controlling the nuclearity of the cluster (from eight to six). Replacement of the imidizolyl units by pyridyl ones leads to a tetranuclear neutral cluster. This cluster presents an unusual Fe_4 structure since the presence of the L_3 ligand imposes a non-planar arrangement of the four Fe^{III}.

From the point of view of the magnetic properties, the presence in these clusters of pairs of HS Fe^{III} ions bridged by μ-oxo or μ-hydroxo ligands gives rise to antiferromagnetic interactions and to antiferromagnetic ground states in all cases.

These results demonstrate that the reaction of Fe^{III} with tetradentate imidazolyl ligands is a suitable strategy to obtain new Fe^{III} polynuclear complexes with interesting topologies. Some small changes in the ligands such as replacement of NCS^- by CN^- could lead to a stronger ligand fields and perhaps to spin-crossover. Other interesting possibility could be the use of other metal ions with a higher magnetic axial anisotropy such as Mn^{III} or lanthanides.

Acknowledgements

Financial support from the European Union (Project HINTS and ERC Advanced Grant SPINMOL), the Spanish MINECO (Project Consolider-Ingenio in Molecular Nanoscience CSD2007-00010, and projects MAT2011-22785 and CTQ-2011-26507) and the Generalitat Valenciana (Prometeo and ISIC-NANO Programs) are gratefully acknowledged. The authors thank J. M. Martínez-Agudo and Dr. G. Agustí-López, University of Valencia, for magnetic characterisation and E. Tormos, University of Valencia, for ESI-MS measurements. Manfred Womes is acknowledged for the help with Mössbauer spectroscopy.

Notes and References

[1] M. D. Pluth, R. G. Bergman and K. N. Raymond, *Acc. Chem. Res.* 2009, **42**, 1650.

[2] H. T. Chifotides, I. D. Giles and K. R. Dunbar, *J. Am. Chem. Soc.* 2013, **135**, 3039.

[3] W. Meng, J. D. Clegg and J. R. Nitschke, *J. Am. Chem. Soc.* 2012, **51**, 1881.

[4] J. M. Domínguez-Vera, A. Rodríguez, R. Cuesta, R. Kivekäs and E. Colacio, *J. Chem. Soc., Dalton Trans.* 2002, 561.

[5] Y. Wang, F. –H.Zhao, A. -H. Shi, Y. -X. Che and J. -M. Zheng, *Inorg. Chem. Commun.* 2012, **20**, 23.

[6] J. Yao, Z. -D. Lu, Y, -Z. Li, J. -G. Lin, X. -Y. Duan, S. Gao, Q. -J. Meng and C. -S. Lu, *Cryst. Eng. Comm.* 2008, **10**, 1379.

[7] (a) Z. Su, M. Chen, T. A. Okamura, M. -S. Chen, S. -S. Chen and W. -Y. Sun, *Inorg. Chem.* 2011, **50**, 985*;* (b) E. Coronado, M. Giménez-Marqués, G. Mínguez Espallargas and L. Brammer, *Nat. Commun.* 2012, **3**, 828.

[8] (a) T. Sato, K. Nishi, S. Iijima, M. Kojima and N. Matsumoto, *Inorg. Chem.* 2009, **48**, 7211; (b) Y. Sunatsaki, R. Kawamoto, K. Fujita, H. Maruyama, T. Suzuki, H. Ishida, M. Kojima, S. Iijima and N. Matsumoto, *Coord. Chem. Rev.* 2010, **254**, 1871.

[9] (a) N. Bréfuel, S. Shova, J. Lipkowski and J. -P. Tuchagues, *Chem. Mater.* 2006, **18**, 5467; (b) N. Bréfuel, I. Vang, S. Shova, F. Dahan, J. -P. Costes and J. -P. Tuchagues, *Polyhedron* 2007, **26**, 1745; (c) N. Bréfuel, S. Shova and J. -P. Tuchagues, *Eur. J. Inorg. Chem.* 2007, 4326.

[10] N. Bréfuel, C. Duhayon, S. Shova and J. -P. Tuchagues, *Chem. Commun.* 2007, 5223.

[11] (a) Y. Sunatsuki, Y. Ikuta, N. Matsumoto, H. Ohta, M. Kojima, S. Iijima, S. Hayami, Y. Maeda, S. Kaizaki, F. Dahan and J. -P. Tuchagues, *Angew. Chem. Int. Ed.* 2003, **42**, 1614; (b) Y. Sunatsuki, H. Ohta, M. Kojima, Y. Ikuta, Y. Goto, N. Matsumoto, S. Iijima, H. Akashi, S. Kaizaki, F. Dahan and J. -P. Tuchagues, *Inorg. Chem.* 2004, **43**, 4154; (c) N. Bréfuel, S. Imatomi, H. Torigoe, H. Hagiwara, S. Shova, J. -F. Meunier, S. Bonhommeau, J. -P. Tuchagues and N. Matsumoto, *Inorg. Chem.* 2006, **45**, 8126; (d) N. Bréfuel, H. Watanabe, L. Toupet, J. Come, N. Matsumoto, E. Collet, K. Tanaka and J. -P. Tuchagues, *Angew. Chem. Int. Ed.* 2009, **48**, 9304; (e) N. Bréfuel, E. Collet, H. Watanabe, M. Kojima, N. Matsumoto, L. Toupet, K. Tanaka and J. -P. Tuchagues, *Chem. Eur. J.* 2010, **16**, 14060.

[12] R. Bagai, M. R. Daniels, K. A. Abboud and G. Christou, *Inorg. Chem.* 2008, **47**, 3318.

[13] D. Gatteschi, R. Sessoli and A. Cornia, *Chem. Commun.* 2000, 725.

[14] (a) X. Liu and E. C. Theil, *Acc. Chem. Res.* 2005, **38**, 167; (b) M. Faiella, C. Andreozzi, R. T. M. de Rosales, V. Pavone, O. Maglio, F. Nastri, W. F. DeGrado and A. Lombardi, *Nature Chem. Biol.* 2009, **5**, 882; (c) S. Friedle, E. Reisner and S. J. Lippard, *Chem. Soc. Rev.* 2010, **39**, 2768.

[15] F. J. LaRonde and M. A. Brook, *Inorg. Chim. Acta* 1999, **296**, 208.

[16] S. H. Rahaman, R. Ghosh, G. Mostafa and B. K. Ghosh, *Inorg. Chem. Commun.* 2005, **8**, 1137.

[17] A. Altomare, M. C. Burla, M. Camalli, G. L. Cascarano, C. Giacovazzo, A. Guagliardi, A. G. G. Moliterni, G. Polidori and R. Spagna, *J. Appl. Cryst*. 1999, **32**, 115.

[18] G. M. Sheldrick, *Acta Cryst.* 2008, **A64,** 112.

[19] (a) L. J. Farrugia, *J. Appl. Cryst.* 2012, **45**, 849; (b) A.L.Spek, *J.Appl.Cryst.* 2003, **36**, 7.

[20] K. Takahashi, Y. Nishida, Y. Maeda and S. Kida, *J. Chem. Soc., Dalton Trans.* 1985, 2375.

[21] A. K. Singh, W. Jacob, A. K. Boudalis, J. -P. Tuchagues and R. Mukherjee, *Eur. J. Inorg. Chem.* 2008, 2820.

[22] A. K. Boudalis, R. E. Aston, S. J. Smith, R. E. Mirams, M. J. Riley, G. Schenk, A. G. Blackman, L. R. Hanton and L. R. Gahan, *Dalton Trans.* 2007, 5132.

[23] T. C. Stamatatos, A. G. Christou, C. M. Jones, B. J. O'Callaghan, K. A. Abboud, T. A. O'Brien and G. Christou, *J. Am. Chem. Soc.* 2007, **129**, 9840.

[24] A. K. Boudalis, N. Latioti, G. A. Spyroulias, C. P. Raptopoulou, A. Terzis, V. Tangoulis and S. P. Perlepes, *J. Chem. Soc., Dalton Trans.* 2001, 955.

[25] M. Scarpellini, A. Neves, A. J. Bortoluzzi, I. Vencato, V. Drago, W. A. Ortiz and C. Zucco, *J. Chem. Soc., Dalton Trans.* 2001, 2616.

[26] (a) J. R. Hartman, R. L. Rardin, P. Chaudhuri, K. Pohl, K. Wieghardt, B. Nuber, J. Weiss, G. C. Papaefthymiou, R. B. Frankel and S. J. Lippard, *J. Am. Chem. Soc.* 1987, **109**, 7387; (b) U. Bossek, H. Hummel, T. Weyhermüller, E. Bill and K. Wieghardt, *Angew. Chem., Int. Ed. Engl.* 1995, **34**, 2642; (c) S. C. Payne and K. S. Hagen, *J. Am. Chem. Soc.* 2000, **122**, 6399.

[27] H. Weihe and H. U. Güdel, *J. Am. Chem. Soc.* 1997, **119**, 6539.

Associated Content:

Electronic Supplementary Information (ESI) for New Journal of Chemistry

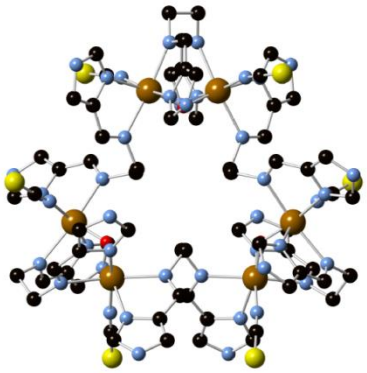

Figure S1. Molecular structure of an hexanuclear $[Fe_6(\mu\text{-}L_1)_6(\mu\text{-}O)_3(NCS)_6]^{6+}$ complex of $[Fe_6(\mu\text{-}L_1)_6(\mu\text{-}O)_3(NCS)_6](NO_3)_6(CH_3OH)_3(H_2O)$ (**4**) (iron (brown), sulfur (yellow), oxygen (red), nitrogen (blue), carbon (black)). The complex is generated from half of the molecule, which is crystallographically independent, through a 2-fold axis.

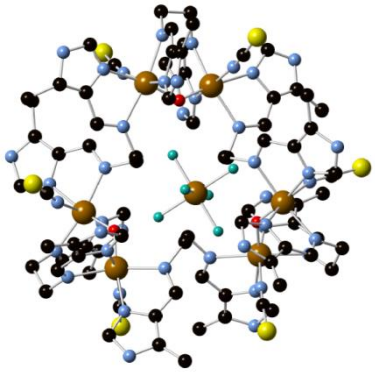

Figure S2. Molecular structure of an hexanuclear $[Fe_6(\mu\text{-}L_2)_6(\mu\text{-}O)_3(NCS)_6]^{6+}$ complex with a $[FeF_6]^-$ anion close to the center of the ring of $[Fe_6(\mu\text{-}L_2)_6(\mu\text{-}O)_3(NCS)_6](FeF_6)_{0.5}(NCS)_{4.5}(CH_3OH)_2$(solvate) (**5**) (iron (brown), sulfur (yellow), oxygen (red), nitrogen (blue), carbon (black), fluoride (green)). The FeF_6^{3-} complex is generated from half of the molecule, which is crystallographically independent, through a 2-fold axis linking F3, F4 and Fe7 atoms.

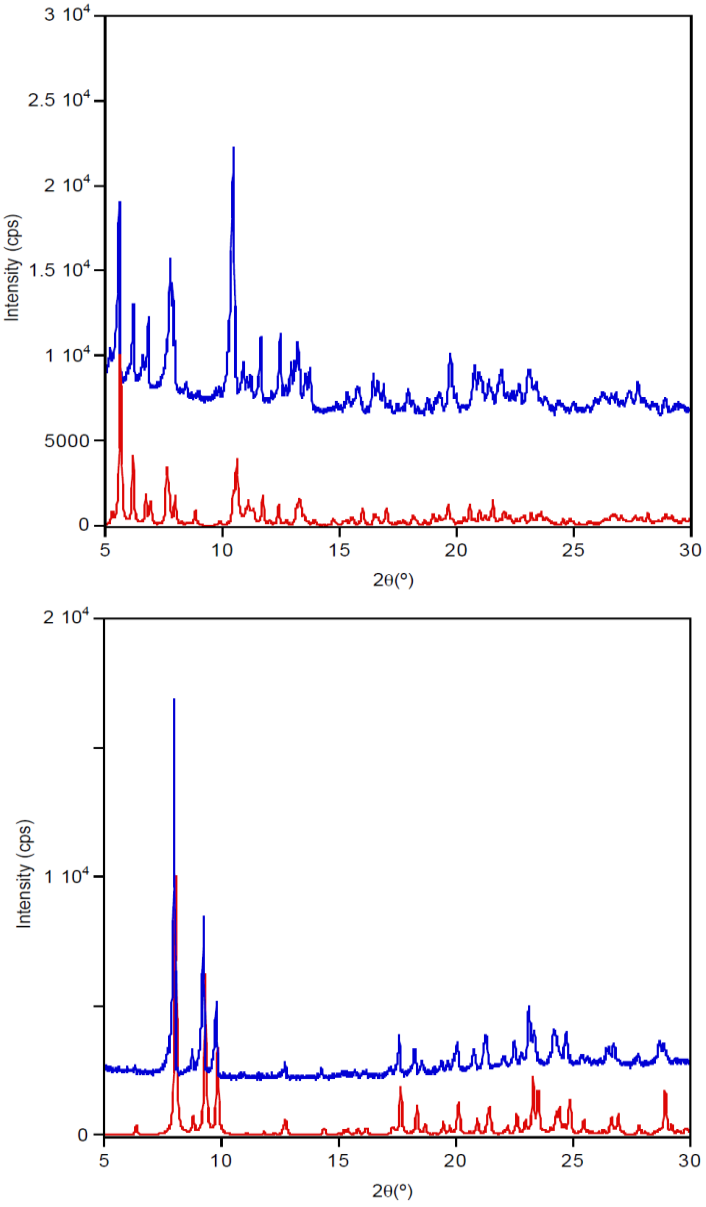

Figure S3. Powder X-ray diffraction patterns (blue) and simulated patterns (red) of **2** (top) and **3** (bottom).

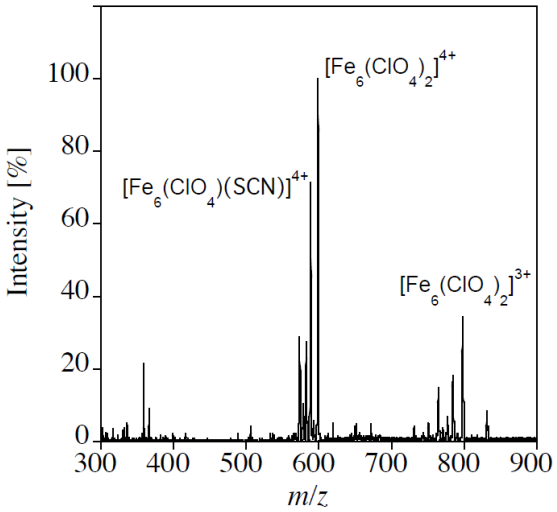

Figure S4. ES-MS of **2** in methanol.

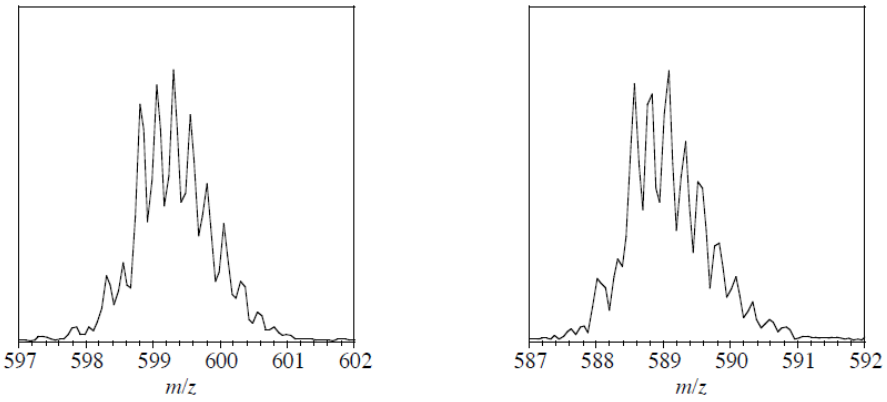

Figure S5. ES-MS of **2** in methanol (isotopic resolution of the most intense peaks).

Concluding Remarks and Perspectives

Chapter 7

Chapter 7. Concluding Remarks and Perspectives

As part of the research area in molecular materials, this thesis presents several strategies to prepare new multifunctional hybrid materials. Some relevant results have been obtained:

The reaction of Fe^{II} with the carboxylate derivative of 1-bpp ligand (bppCOOH) has afforded a new spin-crossover complex. The compound $[Fe^{II}(bppCOOH)_2](ClO_4)_2$ presents an abrupt spin transition at 383 K, due to strong intermolecular interactions via hydrogen bonding, and LIESST effect, with a T_{LIESST} of 60 K. This value of T_{LIESST} is much higher than expected for the family of Fe^{II} complexes based on the 1-bpp ligand. These results together with similar results obtained with the Fe^{II} complex of the carboxy-ester derivative of 1-bpp (bppCOOEt), $[Fe^{II}(bppCOOEt)_2](ClO_4)_2(H_2O)_2$, seems to indicate that very high $T_{1/2}$ may induce higher T_{LIESST} than those calculated from the data of compounds with lower $T_{1/2}$. More examples are needed to confirm this result. The presence of the carboxylate group at the pyridine ring allows the anchoring of the spin-crossover complex to metal-oxide surfaces, which is an essential step for the preparation of devices based on the spin-crossover phenomenon. Preliminary reflectivity IR and XPS results have confirmed that deposition of the complex on a surface is possible by simply immersing a glass substrate covered by Al_2O_3 into an acetonitrile solution of the complex. Synchrotron measurements are needed to calculate the HS/LS ratio with the temperature after deposition. On the other hand, deprotonation of the carboxylic acid and reaction with Fe^{III} has allowed the formation of the nonanuclear cluster $[Fe^{III}_3(\mu_3\text{-}O)(H_2O)_3(Fe^{II}(bppCOOH)(bppCOO))_6](ClO_4)_{13}\cdot((CH_3)CO)_6(H_2O)_{12.25}$, in which six partially deprotonated $[Fe^{II}(bppCOOH)_2]$ are linked by one of their carboxylate to a trimer of Fe^{III} ions. Finally, the deposition of $[Fe^{II}(bppCOOH)_2](ClO_4)_2$ on surfaces, and the study of the LIESST effect (structure and relaxation kinetics of the photoinduced metastable state) in the compounds $[Fe^{II}(bppCOOH)_2](ClO_4)_2$ and $[Fe^{II}(bppCOOEt)_2](ClO_4)_2(H_2O)_2$ will be described in a future report.

Derivatives of 1-bpp ligand have been incorporated into an Anderson POM in compound $(C_{16}H_{36}N)_3[MnMo_6O_{24}(C_{16}H_{15}N_6O)_2]\cdot(C_4H_9NO)_2(H_2O)_{2.5}$ (**1**) by using the well-known tris-alkoxo-amide tripodal functionalization. The structure of **1**, solved by single-crystal X-ray diffraction, consists of an Anderson POM with two terminal 1-bpp ligands. Direct reaction in a 1:1 Fe^{2+}:POM ratio gives rise to a 1D "amorphous" polymer in compound $(C_{16}H_{36}N)[Fe(MnMo_6O_{24}(C_{16}H_{15}N_6O)_2)]\cdot(H_2O)_4$ (**3**), whereas recrystallization in DMF of the precipitate obtained with a 2:1 Fe^{2+}:POM ratio induces the formation of compound $[Fe^{II}(H_2O)(C_3H_7NO)]_2[MnMo_6O_{24}(C_{16}H_{15}N_6O)_2](OH)\cdot(H_2O)(C_3H_7NO)_3$ (**2**). The structure of **2**, solved by single crystal X-ray diffraction, is formed by a 2D network, in which each $[MnMo_6O_{24}(C_{16}H_{15}N_6O)_2]^{3-}$ POM is linked to two Fe^{II} ions through the two 1-bpp ligands, while the two Fe^{II} ions are linked to a neighboring POM through an oxo ligand and to one DMF and one water solvent molecules. This gives rise to layers of $[Fe^{II}(H_2O)(C_3H_7NO)]_2[MnMo_6O_{24}(C_{16}H_{15}N_6O)_2]^+$ units with OH^- counterions. These results confirm the versatility of the coordination chemistry of tris-alkoxo-amide tripodal functionalized POMs to obtain a great variety of structures ranging from 2D cationic networks in compound **2** to amorphous 1D polymers in compound **3**. Attempts to crystallize the 1D polymeric compound, with Fe^{II} connected with two functionalized POMs through the tridentate 1-bpp ligand, have been unsuccessful as reactions with metals of this functionalized POM lead to insoluble polymers. The structure of **2** may indicate that the excess of metal lead to coordination with the oxo groups of the POM and the recrystallization in polar solvents such as DMF involves dissociation of the 1-bpp-metal coordination bond. More attempts to slow down the precipitation of the polymer in a 1:1 metal:POM ratio are needed by using slow diffusion techniques and other solvents. Magnetic properties of **1** have shown that it presents a field-induced relaxation of magnetization due to magnetic anisotropy of Mn^{III}, as observed in other mononuclear Mn^{III} complexes reported very recently. This is the first example of d-metal POM exhibiting SIM behavior reported in the literature. The similar behavior of **2**, **3** and the reference compound $(C_{16}H_{36}N)_3[MnMo_6O_{24}\{(OCH_2)_3CNH_2\}_2]$ (**4**), one of the

simplest functionalized Anderson POM reported so far, confirms that this type of behavior is general for this type of structures. This opens the way to the preparation of hybrid POMs combining this property with other magnetic properties of interest. For instance, spin-crossover behavior could be expected if two 1-bpp ligands were coordinated to Fe^{II} as observed in compound **3**. However, the magnetic properties indicate that Fe^{II} complexes remain in the LS state. Possible strategies to enhance spin transition of the Fe^{II} ions are the use of other counterions or solvents, as the spin transition of this type of complexes is very sensitive to the packing and intermolecular interactions in the bulk solid, induced by the nature of anions and solvent molecules or the introduction of substituents in the 1-bpp derivative.

A new family of compounds with spin-crossover complexes inserted into bimetallic anilate-based networks has been prepared and characterized. The insertion of $[Fe^{III}(sal_2\text{-trien})]^+$ and derivatives gave rise to extended 2D compounds of formula $[Fe^{III}(sal_2\text{-trien})][Mn^{II}Cr^{III}(Cl_2An)_3]\cdot(CH_2Cl_2)_{0.5}(CH_3OH)(H_2O)_{0.5}(CH_3CN)_5$, $[Fe^{III}(4\text{-OH-}sal_2\text{-trien})][Mn^{II}Cr^{III}(Cl_2An)_3]\cdot$(solvate), $[Fe^{III}(sal_2\text{-epe})][Mn^{II}Cr^{III}(Br_2An)_3]\cdot(CH_3CN)_4$(solvate) and $[Fe^{III}(5\text{-Cl-}sal_2\text{-trien})][Mn^{II}Cr^{III}(Br_2An)_3]\cdot(CH_2Cl_2)(CH_3OH)(H_2O)_4(CH_3CN)_{1.5}$(solvate). These four compounds present the well-known honeycomb structure, similar to that found for other extended oxalate or anilate-based networks. It is formed by $[Mn^{II}Cr^{III}(X_2An)_3]^-$ sheets in the *ab* plane alternating with layers of Fe^{III} cationic complexes. The magnetic properties of these compounds indicate that the Fe^{III} ions remain in their HS or LS state between 2 and 300 K. This absence of spin-crossover in the 2D network can be explained by the lack of intermolecular interactions between the Fe^{III} complexes in the large anilate-network, and by the rigidity of the ligand around the Fe^{III} ion, imposed by strong intermolecular contacts (π-π stacking) between the anilate ligand and the phenolate rings of the Fe^{III} complex. At the same time, the anilate network presents a ferrimagnetic long-range ordering at ca. 10 K in the four compounds, which is significantly higher than the ordering temperatures obtained for oxalate networks with the same metal ions (ca. 5 K) or for 2D anilate networks with other templating cations (ca. 6 K for $[NBu_4]^+$ and $[(H_3O)(phz)_3]^+$ salts). The use of the

Fe^{II} complex $[Fe^{II}(tren)imid_3)]^{2+}$ has led to the compound $[Fe^{II}(tren)imid_3)]_2[Mn^{II}Cl_2Cr^{III}(Cl_2An)_3]Cl\cdot(CH_3OH)(CH_2Cl_2)_3(CH_3CN)_{0.5}$. It presents a 1D anionic network, which is surrounded by two $[Fe^{II}(tren)imid_3)]^{2+}$ complexes, one Cl^- anion, and solvent molecules. In this compound, the intermolecular contacts between Fe^{II} cations, as well as the absence of π-π stacking between the cations and the anilate ligand, result in the spin transition of half of the Fe^{II} complexes between 280 and 100 K. Also, the bimetallic anilate network presents a magnetic long-range ordering below 2.6 K, as a result of the ferromagnetic interchain interactions. This is the first anilate-based compound combining spin-crossover and magnetic ordering. Photomagnetic measurements are in progress to study the effect of photoinduced spin-crossover on the magnetic properties of the anilate network.

Insertion of the smaller cationic complex $[Fe^{III}(acac_2\text{-trien})]^+$ in the anilate network has afforded a new type of structure, in which the Fe^{III} cation is inserted into the hexagonal cavities of the 2D anilate network, and not between the layers as in the previous 2D oxalate and anilate-based compounds. Magnetic characterization of the compounds $[Fe^{III}(acac_2\text{-trien})][Mn^{II}Cr^{III}(Cl_2An)_3]\cdot(CH_3CN)_2$ and $[Fe^{III}(acac_2\text{-trien})][Mn^{II}Cr^{III}(Br_2An)_3]\cdot(CH_3CN)_2$, and the diamagnetic reference $[Ga^{III}(acac_2\text{-trien})][Mn^{II}Cr^{III}(Br_2An)_3]\cdot(CH_3CN)_2$, shows an increase of the ordering temperature of the network (ca. 11K), but also an absence of spin-crossover, as the Fe^{III} cations remain in the HS state. This type of structures paves the way to the synthesis of a new type of multifunctional materials, in which new properties could be obtained thanks to the formation of isolated chains of cations in close contact with the magnetic network. Furthermore, the layered character of these compounds enables the exfoliation of the bulk crystals into nanosheets, by mechanical or solvent-assisted methods. The best results have been obtained with the micromechanical exfoliation (Scotch-tape method), which has not been used previously for the exfoliation of coordination polymers. This method has allowed the exfoliation of the compounds $[Fe^{III}(acac_2\text{-trien})][Mn^{II}Cr^{III}(Br_2An)_3]\cdot(CH_3CN)_2$, and $[Fe^{III}(sal_2\text{-trien})][Mn^{II}Cr^{III}(Cl_2An)_3]\cdot(CH_2Cl_2)_{0.5}(CH_3OH)(H_2O)_{0.5}(CH_3CN)_5$ previously described, which

is formed by alternating cationic and anionic layers, into nanosheets of about 2 nm of height and hundreds of nm of size. These two compounds can also be exfoliated by a solvent-assisted method, which is the method previously used to exfoliate neutral coordination polymers. Nanosheets of about 5 nm of thickness have been obtained after immersion and sonication in ethanol. The obtention of nanosheets of these two compounds opens a way for the delamination of 2D materials with more sophisticated structures than those exfoliated so far, and for the study and applications of single 2D nanosheets with combination of properties, such as magnetic ordering and spin-crossover. Finally, an interesting possibility derived from these structures could be the study of the properties of a single complex confined in the hexagonal cavities of the anilate-based network.

Finally, a new family of Fe^{III} polynuclear complexes based on tetradentate Schiff-base ligands has been reported. The nuclearity of the Fe^{III} cluster in the compounds $[Fe_8(\mu\text{-}L_1)_8(\mu\text{-}O)_4(NCS)_8](ClO_4)_5(NCS)_3$, $[Fe_6(\mu\text{-}L_2)_6(\mu\text{-}O)_3(NCS)_6](ClO_4)_2(NCS)_4$ and $[Fe_4(\mu\text{-}L_3)_2(\mu\text{-}OH)_2(\mu\text{-}OHO)(NCS)_7(OH_2)]$ have been tuned by small modification on the bis(bidentate) bridging ligand or the counter-ion. Magnetic characterization shows strong antiferromagnetic interactions and antiferromagnetic ground states in the three compounds, due to the presence of pairs of HS Fe^{III} ions bridged by μ-oxo or μ-hydroxo ligands. This work is a first step in the search of high-nuclearity compounds with interesting properties such as spin-crossover, which could be rise with stronger ligand fields, or single-molecule magnet behavior, by the use of metal ions with a higher magnetic axial anisotropy.

Resumen

El trabajo descrito en esta tesis se encuadra en el ámbito de los materiales moleculares. Presenta varias estrategias para preparar nuevos materiales híbridos multifuncionales.

Los complejos de transición de espín (SCO) constituyen uno de los ejemplos más espectaculares de biestabilidad molecular. En estos sistemas, las transiciones entre los estados de bajo espín (LS) y alto espín (HS) pueden estar inducidos por una variedad de estímulos externos (temperatura, presión o radiación electromagnética). Además de los interesantes aspectos fundamentales, este fenómeno es de interés creciente en el área de los materiales funcionales debido a las posibles aplicaciones en sensores, memorias o dispositivos de conmutación. Los sistemas SCO más estudiados están basados en complejos de Fe^{II} que presentan una transición de espín entre una configuración diamagnética (S = 0, LS) y una configuración paramagnética (S = 2, HS). Así, bajo condiciones experimentales específicas, el mismo compuesto se puede encontrar en dos estados, y así presentar diferentes comportamientos ópticos y magnéticos. Una interesante familia de compuestos de SCO son los complejos de Fe^{II} basados en el ligando 2,6-bis(pirazol-1-il)piridina (1-bpp). Este ligando se puede funcionalizar en su periferia con una gran variedad de sustituyentes. El cambio de estado de espín de estos materiales es por lo general muy abrupto y aparece con histéresis térmica cerca de la temperatura ambiente. Además, las sales de $[Fe^{II}(1\text{-}bpp)_2]^{2+}$ tienen la ventaja de tener la propiedad de transición de espín inducida por irradiación ("Light-Induced Excited Spin State Trapping", LIESST) a altas temperaturas, con tiempos de vida de los estados meta-estable fotoinducidos relativamente largos. La sustitución en el anillo piridina del ligando permite la inclusión de grupos funcionales en la periferia del complejo $[Fe^{II}(1\text{-}bpp)_2]^{2+}$, sin perturbar el comportamiento magnético del centro de Fe^{II}. Una mayoría de síntesis de derivados de 1-bpp sustituidos en la posición 4 de la piridina parten del ácido 2,6-dihidroxi-isonicotínico que, después de un paso de halogenación, puede ser fácilmente

convertido en el ácido 2,6-di(pirazol-1-il)piridina-4-carboxílico (bppCOOH). A partir del bppCOOH es relativamente fácil introducir otros grupos funcionales en la posición 4 del anillo piridínico. A pesar de que ésta es la ruta más común para funcionalizar el anillo de piridina del ligando 1-bpp, la formación de complejos de transición de espín de Fe^{II} con el ligando bppCOOH no había sido descrita hasta esta tesis.

La reacción del derivado carboxilato del 1-bpp (bppCOOH) con Fe^{II} ha dado lugar a la formación del nuevo complejo de transición de espín $[Fe^{II}(bppCOOH)_2](ClO_4)_2$ (Capítulo 2). Este complejo presenta una transición de espín abrupta con una $T_{1/2}$ de 383 K, debida a interacciones intermoleculares fuertes a través de enlaces de hidrógeno, y el efecto LIESST, con una T_{LIESST} de 60 K. Este valor de T_{LIESST} es mucho más alto que esperado para la familia de complejos de Fe^{II} basados en el ligando 1-bpp, y parece indicar que un alto valor de $T_{1/2}$ puede inducir un T_{LIESST} más alto que los calculados a partir de los datos de otros compuestos de 1-bpp con $T_{1/2}$ más bajos. Son necesarios más ejemplos con este tipo de comportamiento para confirmar este resultado. La presencia del grupo carboxilato en el anillo piridina puede permitir la deposición del complejo sobre superficies de óxidos metálicos, lo que constituye un paso esencial para la preparación de dispositivos basados en el fenómeno de transición de espín. Resultados preliminares de reflectividad IR y espectroscopía fotoelectrónica de rayos X (XPS) confirman la deposición del complejo sobre la superficie en un sustrato de vidrio cubierto por Al_2O_3, que ha sido sumergido durante toda una noche en una disolución del complejo en acetonitrilo. Serán necesarias medidas de sincrotrón para calcular la proporción de HS/LS con la temperatura de los complejos sobre la superficie. Por otra parte, es un interesante precursor para unir este complejo a clústeres de alto espín o redes magnéticas extendidas.

Los polioxometalatos (POMs) son clústeres aniónicos de óxidos metálicos con una gran diversidad de tamaños, nuclearidades y formas. El metal (M) es un metal de transición en un alto estado de oxidación, en general V(IV,V), Mo(VI) o W(VI).

Constituyen una amplia familia de compuestos con numerosas aplicaciones en catálisis, ciencia de materiales y medicina. Además tienen aplicaciones en magnetismo ya que han sido usados desde los años 1990 como sistemas modelos en el magnetismo molecular e incorporados como componentes magnéticos en materiales moleculares híbridos inorgánicos e orgánicos. En general, la combinación de componentes orgánicos e inorgánicos en un material es una estrategia atractiva para acceder nuevas propiedades. Recientemente, el interés de los POMs magnéticos se ha desplazado hacia el diseño de imanes unimoleculares (Single-Molecule Magnets, SMMs) y sus aplicaciones como "spin-qubits" moleculares en dispositivos para la nano-espintronica.

En esta tesis hemos intentado aprovechar las estrategias de síntesis de POMs híbridos ya conocidas para preparar un nuevo POM híbrido que pueda combinar las propiedades magnéticas del POM (imán unimolecular) con una propiedad adicional como la transición de espín (Capítulo 3). Los derivados del ligando 1-bpp se han incorporado en un POM de Anderson en el compuesto $(C_{16}H_{36}N)_3[MnMo_6O_{24}(C_{16}H_{15}N_6O)_2]\cdot(C_4H_9NO)_2(H_2O)_{2.5}$ (**1**) mediante el grupo funcional tripodal tris-alkoxo-amida. La estructura de **1**, resuelta por difracción de rayos X de monocristal, consiste en un POM de Anderson con dos ligandos 1-bpp terminales. La reacción directa con Fe^{II} en una proporción Fe^{2+}:POM 1:1 da lugar a un polímero unidimensional (1D) en el compuesto $(C_{16}H_{36}N)[Fe(MnMo_6O_{24}(C_{16}H_{15}N_6O)_2)]\cdot(H_2O)_4$ (**3**), mientras que la recristalización en dimetilformamida (DMF) del precipitado obtenido con una proporción Fe^{2+}:POM 2:1 da lugar a la formación del compuesto $[Fe^{II}(H_2O)(C_3H_7NO)]_2[MnMo_6O_{24}(C_{16}H_{15}N_6O)_2](OH)\cdot(H_2O)(C_3H_7NO)_3$ (**2**). La estructura de **2**, resuelta por difracción de rayos X de monocristal, consiste en una red 2D, en la que cada unidad $[MnMo_6O_{24}(C_{16}H_{15}N_6O)_2]^{3-}$ se coordina a dos iones de Fe^{II} a través de sus dos ligandos 1-bpp. Al mismo tiempo, los dos Fe^{II} se unen a otro POM vecino por un ligando oxo. Su coordinación octaédrica se completa con una molécula de DMF y otra de agua. Esto da lugar a la formación de capas de complejos $[Fe^{II}(H_2O)(C_3H_7NO)]_2[MnMo_6O_{24}(C_{16}H_{15}N_6O)_2]^+$ con contraiones OH^-. Estos resultados confirman la versatilidad de la química de coordinación de los POMs funcionalizados

con un grupo tripodal tris-alkoxo-amida para obtener una gran variedad de estructuras, desde redes catiónicas 2D en el compuesto **2** hasta polímeros amorfos 1D aniónicos en el compuesto **3**. Por el momento no han dado resultado todos los intentos de cristalizar el compuesto polimérico 1D, con el Fe^{II} unido por dos ligandos 1-bpp a dos POMs vecinos, ya que las reacciones de este POM funcionalizado con metales dan lugar a la rápida aparición de polímeros insolubles. La estructura de **2** parece indicar que un exceso de metal provoca la coordinación con los grupos oxo del POM, mientras que la recristalización en disolventes polares como DMF usada para obtener este compuesto implica seguramente la disociación del enlace de coordinación 1-bpp – metal y la coordinación del DMF. Un comportamiento similar ha sido observado antes en otros POMs funcionalizados como los hexavanadatos funcionalizados con el ligando piridil. Son necesarias más pruebas para ralentizar la precipitación del polímero en una proporción metal:POM 1:1, usando técnicas de difusión lenta u otros solventes. Las propiedades magnéticas de **1** han puesto de manifiesto que este compuesto presenta una relajación lenta de la magnetización con un campo aplicado que es debida a la anisotropía magnética del Mn^{III}, al igual que se ha observado en otros complejos mononucleares de Mn^{III} descritos muy recientemente en la bibliografía. Este compuesto es el primer POM con un metal del bloque *d* que presenta un comportamiento de Single-Ion Magnet (SIM). El comportamiento similar de **3** y del compuesto de referencia $(C_{16}H_{36}N)_3[MnMo_6O_{24}\{(OCH_2)_3CNH_2\}_2]$ (**4**), uno de los más POMs de Anderson funcionalizados más simples que se conocen, confirma que este tipo de comportamiento es general para este tipo de estructuras. Estos resultados demuestran que es posible preparar POMs híbridos que combinen esta propiedad con otras propiedades magnéticas de interés. Por ejemplo, la transición de espin del Fe^{II} podría aparecer si dos ligandos 1-bpp estuviesen coordinados al Fe^{II} como ocurre en el compuesto **3**. Sin embargo, las propiedades magnéticas de este compuesto indican que los complejos de Fe^{II} permanecen en el estado de LS. Posibles estrategias para solucionar este problema son el uso de otros contraiones o disolventes, ya que la

transición de espín de este tipo de complejos es muy sensible a las interacciones intermoleculares con los aniones y moléculas de disolvente, o la introducción de otros sustituyentes en el derivado del ligando 1-bpp.

La investigación de nuevos imanes a base molecular es un área muy activa desde el principio del magnetismo molecular en los años ochenta. En los últimos años, el interés se ha centrado en la preparación de redes magnéticas multifuncionales, ya que estos materiales proporcionan oportunidades únicas para el diseño de estructuras cristalinas con magnetismo cooperativo combinado con una segunda propiedad de interés. Muchos compuestos bimetálicos basados en el ligando oxalato han sido usados como redes magnéticas en materiales magnéticos multifuncionales. En la mayoría de los casos, esos compuestos presentan una red polimérica aniónica bidimensional (2D) en la cual los metales Mn^{II} y Cr^{III} presentan una quiralidad opuesta. La elección de los cationes permite la introducción de nuevas propiedades al sistema hibrido. De forma que las propiedades magnéticas cooperativas (ferro-, ferri- o antiferromagnetismo) de la red pueden coexistir con las propiedades electrónicas de los cationes. En este contexto, los cationes de transición de espín son buenos candidatos para la preparación de materiales magnéticos multifuncionales, ya que constituyen uno de los mejores ejemplos de biestabilidad molecular. Esto permitía la preparación de imanes modulables en los que se podría modificar el ordenamiento magnético de la red, aprovechando la posibilidad de inducir la transición de espín por la aplicación de un estímulo externo como la irradiación con luz o la presión. Se ha obtenido compuestos multifuncionales que presentan transición de espín y orden magnético por combinación de cationes de transición de espín de Fe^{III} basados en ligandos de base de Schiff ($H_2(sal_2\text{-trien})$ = *N*,*N*'-disalicilidenetrietileno-tetramina) con redes aniónicas de oxalatos. Recientemente, nuestro grupo ha explorado el cambio del ligando oxalato por los derivados del ligando 2,5-dihidroxi-1,4-benzoquinona de fórmula $C_6O_4X_2^{2-}$ (anilatos, X_2An^{2-}; X = Cl, Br or I) en redes bimetálicas. Estos ligandos,

que presentan modos de coordinación similares al ligando oxalato, presentan ventajas adicionales: (i) se pueden modificar o funcionalizar, simplemente cambiando el grupo X; (ii) presentan temperaturas de ordenamiento más altas; (iii) el mayor tamaño del anilato puede permitir la introducción de una mayor variedad de cationes en el objetivo de preparar materiales moleculares multifuncionales.

En esta tesis hemos explorado la inserción de cationes de transición de espín en redes bimetálicas basadas en el ligando anilato, para preparar y caracterizar una nueva familia de materiales magnéticos multifuncionales (Capítulo 4). La inserción de los cationes $[Fe^{III}(sal_2\text{-trien})]^+$ y derivados ha dado lugar a la formación de los compuestos extendidos 2D de fórmula $[Fe^{III}(sal_2\text{-trien})][Mn^{II}Cr^{III}(Cl_2An)_3]\cdot(CH_2Cl_2)_{0.5}(CH_3OH)(H_2O)_{0.5}(CH_3CN)_5$, $[Fe^{III}(4\text{-OH-}sal_2\text{-trien})][Mn^{II}Cr^{III}(Cl_2An)_3]\cdot$(solvato), $[Fe^{III}(sal_2\text{-epe})][Mn^{II}Cr^{III}(Br_2An)_3]\cdot(CH_3CN)_4$(solvato) y $[Fe^{III}(5\text{-Cl-}sal_2\text{-trien})][Mn^{II}Cr^{III}(Br_2An)_3]\cdot(CH_2Cl_2)(CH_3OH)(H_2O)_4(CH_3CN)_{1.5}$(solvato). Los cuatro compuestos híbridos están formados por capas aniónicas de $[Mn^{II}Cr^{III}(X_2An)_3]^-$ en el plano *ab*, que se alternan con capas de complejos catiónicos de Fe^{III}. La red de anilatos presenta la típica forma de panal de abeja, similar a las encontradas para otras redes de oxalatos o de anilatos. Las propiedades magnéticas de estos compuestos indican que los iones Fe^{III} permanecen en el estado de HS o LS entre 2 y 300 K. La ausencia de transición de espín puede ser debida a la ausencia de interacciones intermoleculares entre los complejos de Fe^{III}, que están más aislados que en las redes basadas en el ligando oxalato debido al mayor tamaño del ligando anilato, y a la rigidez del ligando alrededor del Fe^{III}, debido a interacciones intermoleculares fuertes (del tipo interacción π-π) entre el ligando anilato y los anillos del grupo fenolato del complejo de Fe^{III}. Por otro lado, la red de anilatos presenta un ordenamiento ferrimagnético de largo alcance con una temperatura critica (T_c) de 10 K en los cuatro compuestos, un valor mucho más alto que las obtenidas para redes de oxalatos con los mismos iones metálicos (sobre 5 K) o para las redes de anilatos 2D con otros cationes (sobre 6 K para los sales de $[NBu_4]^+$ y de $[(H_3O)(phz)_3]^+$). La inserción del complejo de Fe^{II} $[Fe^{II}(tren)imid_3)]^{2+}$ ha dado lugar a la formación del compuesto de formula

$[Fe^{II}(tren)imid_3)]_2[Mn^{II}Cl_2Cr^{III}(Cl_2An)_3]Cl\cdot(CH_3OH)(CH_2Cl_2)_3(CH_3CN)_{0.5}$. Este presenta una red aniónica 1D de fórmula $[Mn^{II}Cl_2Cr^{III}(Cl_2An)_3]^-$, rodeada por dos complejos de $[Fe^{II}(tren)imid_3)]^{2+}$, un anión Cl^-, y moléculas de disolvente. En este compuesto, los contactos intermoleculares entre cationes Fe^{II}, así como la ausencia de interacción π-π entre los cationes y el ligando anilato, inducen la transición de espín de la mitad de los complejos de Fe^{II} entre 280 y 100 K. Además, la red bimetálica de anilatos presenta un ordenamiento magnético de largo alcance por debajo de 2.6 K, como consecuencia de las interacciones ferromagnéticas entre las cadenas. Es el primer compuesto basado en el ligando anilato que combina la transición de espín y el ordenamiento magnético. Se prevé realizar medidas fotomagnéticas para estudiar el efecto de la transición de espín fotoinducida en las propiedades magnéticas de la red de anilatos

La inserción de un complejo catiónico más pequeño, $[Fe^{III}(acac_2\text{-trien})]^+$, en la red de anilatos ha permitido obtener un nuevo tipo de estructura, en la cual el catión de Fe^{III} esta insertado en las cavidades hexagonales de la red 2D de anilatos, en lugar de estar insertado entre las capas de anilatos como en los compuestos 2D de oxalatos y anilatos anteriores (Capítulo 5). La caracterización magnética de los compuestos $[Fe^{III}(acac_2\text{-trien})][Mn^{II}Cr^{III}(Cl_2An)_3]\cdot(CH_3CN)_2$ y $[Fe^{III}(acac_2\text{-trien})][Mn^{II}Cr^{III}(Br_2An)_3]\cdot(CH_3CN)_2$, y del compuesto de referencia con un catión diamagnético $[Ga^{III}(acac_2\text{-trien})][Mn^{II}Cr^{III}(Br_2An)_3]\cdot(CH_3CN)_2$, indica un aumento de la temperatura de ordenamiento de la red (sobre 11 K) con respecto a los compuestos del capítulo anterior, pero también una ausencia de transición de espín, ya que los cationes Fe^{III} permaneciendo en el estado de HS. Este tipo de estructuras abre la posibilidad de sintetizar un nuevo tipo de materiales multifuncionales, en los que la formación de cadenas aisladas de cationes en contacto con la red magnética podrían favorecer la aparición de nuevas propiedades. El carácter laminar de los compuestos 2D de anilatos obtenidos en este trabajo permite exfoliar estos polímeros de coordinación en nanocapas 2D, preparadas por métodos micromecánicos o en disolución.

El descubrimiento del grafeno ha despertado un gran interés en los materiales 2D en los últimos años. La gran variedad de materiales laminares conocidos permite la obtención de materiales exfoliados con muchas aplicaciones en la electrónica, fotonica, almacenamiento de energía, medicina, catálisis de hidrógeno, y recubrimientos óptico. Una estrategia para la exfoliación consiste en exponer el material laminar a ondas de ultrasonidos en un disolvente. Esas ondas generan burbujas de cavitación que colapsan y rompen los cristalitos laminares y producen nanocapas. Otro método para producir capas de espesor atómica a partir de un material laminar es la exfoliación micromecánica (conocido como el método de cinta adhesiva o "Scotch-tape"). Este método a pesar de la simplicidad permite obtener muestras de alta calidad. La eficacia y la sofisticación de estos métodos de exfoliación hacen de los materiales 2D una rama de investigación central de la nanotecnología en el siglo XXI que debería estar acompañada por una extensión del número de materiales laminares que se pueden exfoliar. Recientemente, se ha extendido la exfoliación a los polímeros de coordinación, ya que su versatilidad química para cambiar sus propiedades los hace muy atractivos para numerosas aplicaciones. Hasta el momento, la técnica micromecánica ha sido utilizada sólo para la deslaminación del grafito y de materiales inorgánicos 2D simples, como óxidos e hidróxidos metálicos o calcogenuros. La exfoliación micromecánica de arquitecturas 2D más sofisticadas como polímeros de coordinación y redes metalo-orgánicas (MOFs) todavía no ha aparecido en la bibliografía.

En esta tesis, hemos desarrollado por primera vez la exfoliación micromecánica y en disolución de compuestos multifuncionales basados en redes 2D de anilatos (Capítulo 5). Esto representa una novedad en tres aspectos; i) no son compuestos laminares 2D neutros como otros polímeros de coordinación exfoliados hasta ahora, ii) presentan estructuras más complejas que contienen dos subredes funcionales diferentes (redes de anilatos ferrimagnéticas y catión de transición de espín) y, iii) la

exfoliación mecánica ha sido usada por primera vez para un polímero de coordinación. La exfoliación mecánica es la que ha dado los mejores resultados. Este método ha permitido la exfoliación de los compuestos $[Fe^{III}(acac_2\text{-trien})][Mn^{II}Cr^{III}(Br_2An)_3]\cdot(CH_3CN)_2$ y $[Fe^{III}(sal_2\text{-trien})][Mn^{II}Cr^{III}(Cl_2An)_3]\cdot(CH_2Cl_2)_{0.5}(CH_3OH)(H_2O)_{0.5}(CH_3CN)_5$ en nanocapas de aproximadamente 2 nm de espesor y cientos de nm de tamaño. Estos dos compuestos también se pueden exfoliar con el método en disolución que da lugar a nanocapas de aproximadamente 5 nm de grosor después de suspender los cristales del compuesto en etanol durante una noche y exponer la suspensión a ultrasonidos durante 1 minuto. La obtención de nanocapas de estos dos compuestos abre una vía para la deslaminación de materiales 2D con estructuras más sofisticadas que los exfoliados hasta ahora, y para el estudio y aplicaciones de monocapas 2D con combinación de propiedades, como el ordenamiento magnético y la transición de espín. Finalmente, una posibilidad interesante con estas estructuras seria el estudio de las propiedades de un único complejo insertado en las cavidades hexagonales de la red de anilatos.

Por último, se ha sintetizado una nueva familia de complejos polinucleares de Fe^{III} basados en ligandos tetradentados de base de Schiff (*N*,*N*'-bis-(1R-imidazol-4-ilmetileno)-etano-1,2-diamina (R = H, CH_3) y derivados). La nuclearidad del clúster de Fe^{III} en los compuestos $[Fe_8(\mu\text{-}L_1)_8(\mu\text{-}O)_4(NCS)_8](ClO_4)_5(NCS)_3$, $[Fe_6(\mu\text{-}L_2)_6(\mu\text{-}O)_3(NCS)_6](ClO_4)_2(NCS)_4$ y $[Fe_4(\mu\text{-}L_3)_2(\mu\text{-}OH)_2(\mu\text{-}OHO)(NCS)_7(OH_2)]$ está controlada por el contraion o por pequeños cambios en el ligando puente bis-(bidentado). Las medidas magnéticas muestran la presencia de interacciones antiferromagnéticas fuertes y estados fundamentales antiferromagnéticos en los tres compuestos, debido a la presencia de pares de iones Fe^{III} de HS unidos por puentes μ-oxo o μ-hidroxo. Este trabajo es una primera etapa en la búsqueda de compuestos de alta nuclearidad con propiedades interesantes como la transición de espín, que podría aparecer con un campo de ligandos más fuerte, o el fenómeno de imán unimolecular, con iones metálicos con anisotropía magnética axial más alta.

Annexes

Publications or Scientific-Technical Documents

Due to internal policy, authors of the UIMM group appear in alphabetic order. If the article is fruit of collaboration with other groups, authors from the other groups appear afterwards in the order that they decide.

Published Articles

1. A. Abhervé, J. M. Clemente-Juan, M. Clemente-León, E. Coronado, J. Boonmak, S. Youngme.
"Tuning the nuclearity of iron(III) polynuclear clusters by using tetradentate Schiff-base ligands"
New Journal of Chemistry, 2014, *38*, 2105-2113. DOI: 10.1039/c3nj01516e

2. A. Abhervé, M. Clemente-León, E. Coronado, C. J. Gómez-García, M. López-Jordà.
"A spin-crossover complex based on a 2,6-bis(pyrazol-1-yl)pyridine (1-bpp) ligand functionalized with a carboxylate group"
Dalton Transactions, 2014, *43*, 9406-9409. DOI: 10.1039/c4dt00327f

3. A. Abhervé, M. Clemente-León, E. Coronado, C. J. Gómez-García, M. Verneret.
"One-Dimensional and Two-Dimensional Anilate-Based Magnets with Inserted Spin-Crossover Complexes"
Inorganic Chemistry, 2014, *53*, 12014-12026. DOI: 10.1021/ic5016803

Articles in Preparation

4. A. Abhervé, M. Clemente-León, E. Coronado, S. Mañas-Valero.
"Exfoliation of 2D anilate-based magnets with inserted $[Fe^{III}(acac_2\text{-trien})]^+$ and $[Fe^{III}(sal_2\text{-trien})]^+$ complexes"
In preparation

5. A. Abhervé, J. M. Clemente-Juan, M. Clemente-León, E. Coronado, M. Palacios-Corella, R. Marx, J. van Slageren.
"Field-Induced Slow Relaxation of Magnetization in Mn^{III} Anderson POMs and their Functionalization with 2,6-bis(pyrazol-1-yl)pyridine (1-bpp)"
In preparation

Article not included in this thesis

M. Atzori, S. Benmansour, G. Mínguez Espallargas, M. Clemente-León, A. Abhervé, P. Gómez-Claramunt, E. Coronado, F. Artizzu, E. Sessini, P. Deplano, A. Serpe, M. L. Mercuri, C. J. Gómez-García.
"A Family of Layered Chiral Porous Magnets Exhibiting Tunable Ordering Temperatures"
Inorganic Chemistry, 2013, *52*, 10031-10040. DOI: 10.1021/ic4013284

NJC

PAPER

Tuning the nuclearity of iron(III) polynuclear clusters by using tetradentate Schiff-base ligands†

Cite this: *New J. Chem.*, 2014, **38**, 2105

Alexandre Abhervé,[a] Juan Modesto Clemente-Juan,[a] Miguel Clemente-León,*[a] Eugenio Coronado,*[a] Jaursup Boonmak[b] and Sujittra Youngme[b]

Received (in Victoria, Australia) 2nd December 2013, Accepted 4th February 2014

DOI: 10.1039/c3nj01516e

www.rsc.org/njc

Three novel octanuclear, hexanuclear and tetranuclear complexes of high-spin Fe(III) ions were obtained by the reaction of the *N*,*N*′-bis-(1R-imidazol-4-ylmethylene)-ethane-1,2-diamine ligand (R = H, CH_3) and its derivatives with $Fe(ClO_4)_3{\cdot}6H_2O$ and KSCN. The tetradentate Schiff-base ligand acts as a bis(bidentate) chelating bridge between two adjacent high-spin Fe(III) centers. The presence of a methyl group in the imidazolyl substituent, the change of counterions or the replacement of imidazole by pyridine has a drastic effect on the nuclearity of the cluster. The magnetic properties of all compounds exhibit antiferromagnetic interactions *via* μ-oxo or μ-hydroxo pathways in Fe(III) dimers.

Introduction

Self-assembly processes between organic ligands and metal ions may lead to the formation of functional supramolecular architectures exhibiting unusual properties[1,2] or interesting host–guest behaviors.[3] Imidazole and imidazolyl-containing ligands have been widely used in coordination chemistry due to their versatility in the preparation of polynuclear complexes, which are of interest in magnetochemistry, and in connection with the design of model compounds mimicking the core structures of active sites of some metalloproteins.[4] More recently, the use of flexible imidazole ligands has enabled the preparation of many coordination complexes with interesting topologies and functional properties such as ferroelectricity,[5] porosity, fluorescence[6] and chemisorption-induced magnetic properties.[7]

One of the most used strategies for the incorporation of the imidazolyl moiety in ligands is the condensation of a diamine with an imidazolecarboxaldehyde.[4] Tridentate,[8] tetradentate[9,10] and hexadentate[11] Schiff base ligands have been prepared using this strategy. Reactions of these ligands with iron(II) have afforded many examples of mononuclear spin-crossover complexes. In the case of tetradentate imidazolyl ligands, mononuclear neutral ferrous complexes of formula $[FeL(NCS)_2]$ have been reported.[10]

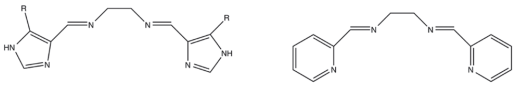

Scheme 1 Molecular structure of the ligands used in this work.

The reaction of iron(III) with imidazolyl Schiff-base tetradentate ligands has been little explored. The preparation of high nuclearity species are often encountered in iron(III) chemistry due to the high charge-to-size ratio of iron(III) ion and the resulting propensity to form oxo bridges.[12] Polynuclear iron complexes arouse interest as magnetic materials, such as single-molecule magnets (SMM),[13] but also due to their biological importance.[14]

Herein, we report that reaction of iron(III) with *N*,*N*′-bis-(1R-imidazol-4-ylmethylene)-ethane-1,2-diamine and its derivatives (L_1 and L_2, Scheme 1), and NCS^- permits the preparation of a family of Fe(III) ring cationic clusters. They are formed by Fe^{III}–O–Fe^{III} dimers bridged by the imidazolyl ligand in a bis(bidentate) mode. The number of Fe^{III}–O–Fe^{III} dimers in the cluster (four or three) and, therefore, its nuclearity (octanuclear or hexanuclear) can be controlled by changing the counterion or introducing a bulky substituent in the ligand. Furthermore, the related tetradentate pyridine ligand, L_3 (Scheme 1) leads to a tetranuclear neutral cluster. The magnetic properties of the three clusters are reported and discussed.

Experimental section

Syntheses

N,*N*′-Bis-(1-*H*-imidazol-4-ylmethylene)-ethane-1,2-diamine (L_1) was prepared by the reaction of 4-imidazolecarboxaldehyde

[a] *Instituto de Ciencia Molecular (ICMol), Universidad de Valencia, C/ Catedrático José Beltrán 2, 46980 Paterna, Spain. E-mail: miguel.clemente@uv.es, eugenio.coronado@uv.es; Fax: +34 963543273; Tel: +34 963544419*

[b] *Materials Chemistry Research Unit, Department of Chemistry and Center of Excellence for Innovation in Chemistry, Faculty of Science, Khon Kaen University, Khon Kaen 40002, Thailand*

† Electronic supplementary information (ESI) available: Structural views of **4** and **5**, powder X-ray diffraction patterns of **2** and **3** and ES-MS of **2** in methanol. CCDC 973767–973771. For ESI and crystallographic data in CIF or other electronic format see DOI: 10.1039/c3nj01516e

(961 mg, 10.00 mmol) and ethylenediamine (334 μL, 5.00 mmol) in acetonitrile (100 mL) for 45 min at 353 K. *N*,*N*′-Bis-(1-CH_3-imidazol-4-ylmethylene)-ethane-1,2-diamine (L_2)[15] and *N*,*N*′-bis-(pyridin-2-ylmethylene)-ethane-1,2-diamine (L_3) were prepared according to the literature method.[16] All other chemicals are commercially available and were used as received without further purification.

$[Fe_8(\mu\text{-}L_1)_8(\mu\text{-}O)_4(NCS)_8](ClO_4)_5(NCS)_3(H_2O)_6$ (1). KSCN (195 mg, 2.00 mmol) was added to a methanolic solution (20 mL) of $Fe(ClO_4)_3{\cdot}6H_2O$ (354 mg, 1.00 mmol). The solution was filtered and a solution of L_1 (216 mg, 1.00 mmol) in methanol (30 mL) was added to the filtrate. The mixture was stirred for 30 min at room temperature. The colour of the mixture turned orange. Orange crystals of **1** suitable for X-ray crystal analysis were obtained by slow diffusion of diethyl ether into this solution. Anal. calc. for $C_{91}H_{108}Cl_5Fe_8N_{59}O_{30}S_{11}$: C, 31.4; H, 3.1; N, 23.7; S, 10.1. Found: C, 31.7; H, 3.2; N, 22.9; S, 9.9%. IR (selected peaks): 2051 (NCS), 1629 (imine) and 1090 (ClO_4^-) cm^{-1}.

$[Fe_6(\mu\text{-}L_2)_6(\mu\text{-}O)_3(NCS)_6](ClO_4)_2(NCS)_4(CH_3CH_2OCH_2CH_3)_{0.5}(H_2O)_{3.5}(CH_3OH)_{2.5}$ (2). Compound **2** was synthesized in a similar manner to that of compound **1** by using ligand L_2 (244 mg, 1.00 mmol) instead of L_1. Anal. calc. for $C_{86.5}H_{118}Cl_2Fe_6N_{46}O_{17.5}S_{10}$: C, 37.0; H, 4.2; N, 22.9; S, 11.4. Found: C, 35.5; H, 3.8; N, 21.9; S, 10.9%. IR (selected peaks): 2050 (NCS), 1629 (imine) and 1121 (ClO_4^-) cm^{-1}.

$[Fe_4(\mu\text{-}L_3)_2(\mu\text{-}OH)_2(\mu\text{-}OHO)(NCS)_7(OH_2)](H_2O)_2(CH_3CN)_{0.5}$ (3). Compound **3** was synthesized in a similar manner to that of compound **1** by using ligand L_3 (238 mg, 1.00 mmol) instead. The mixture was stirred for 1 h at room temperature. The color of the solution turned dark purple and then a brown solid was formed. The precipitate was filtered and recrystallized in acetonitrile. The solution was allowed to stand undisturbed at room temperature. After three days, red prismatic crystals of **3** were obtained. Anal. calc. for $C_{36}H_{38.5}Fe_4N_{15.5}O_{7.7}S_7$: C, 34.3; H, 3.1; N, 17.2; S, 17.7. Found: C, 35.0; H, 3.1; N, 17.3; S, 18.2%. IR (selected peaks): 2030 (NCS), 1637 (imine) and 1400 ($\nu_{C=C}$) cm^{-1}.

$[Fe_6(\mu\text{-}L_1)_6(\mu\text{-}O)_3(NCS)_6](NO_3)_6(CH_3OH)_3(H_2O)$ (4). KSCN (195 mg, 2.00 mmol) was added to a solution of $Fe(NO_3)_3{\cdot}6H_2O$ (404 mg, 1.00 mmol) in methanol (20 mL). The solution was filtered and a solution of L_1 (216 mg, 1.00 mmol) in methanol (30 mL) was added to the filtrate. The mixture was stirred for 1 h at room temperature. The color of the mixture turned orange. Orange crystals of **4** suitable for X-ray crystal analysis were obtained by diffusion of diethyl ether into the filtrate. The small amount of sample available prevented elemental analysis and powder X-ray diffraction measurements. IR (selected peaks): 2056 (NCS), 1632 (imine) and 1384 (NO_3^-) cm^{-1}.

$[Fe_6(\mu\text{-}L_2)_6(\mu\text{-}O)_3(NCS)_6](FeF_6)_{0.5}(NCS)_{4.5}(CH_3OH)_2$_(solvate) (5). KSCN (195 mg, 2.00 mmol) was added to a solution of $Fe(BF_4)_2{\cdot}6H_2O$ (338 mg, 1.00 mmol) in methanol (20 mL). Then a solution of L_2 (244 mg, 1.00 mmol) in methanol (30 mL) was added. The mixture was stirred for 1 h at room temperature. The colour of the mixture turned orange. Orange crystals of **5** suitable for X-ray crystal analysis were obtained by diffusion of diethyl ether into the filtrate. Anal. calc. for $C_{93.5}H_{142}F_3Fe_{6.5}N_{46.5}O_{15}S_{10.5}$: C, 38.5; H, 4.9; N, 22.4; S, 11.5. Found: C, 36.4; H, 3.2; N, 23.2; S, 11.8%. IR (selected peaks): 2049 (NCS), 1629 (imine) and 482 (FeF_6^{3-}) cm^{-1}.

X-Ray crystallography

Single crystals of compounds **1–5** were mounted on glass fibres using a viscous hydrocarbon oil to coat the crystals and then transferred directly to the cold nitrogen stream for data collection. All reflection data were collected at 120 K on a SuperNova diffractometer equipped with a graphite-monochromated Enhance (Mo) X-ray source (λ = 0.71073 Å). The CrysAlisPro program, Oxford Diffraction Ltd., was used for unit cell determinations and data reduction. Empirical absorption correction was performed using spherical harmonics, implemented in the SCALE3 ABSPACK scaling algorithm. Crystal structures were solved by direct methods using the SIR97 program,[17] and refined against all F^2 values using the SHELXL-2013 program,[18] using the WinGX graphical user interface.[19a] All non-hydrogen atoms were refined anisotropically, and hydrogen atoms were placed in calculated positions and refined isotropically using a riding model. The details of data collection and structure refinements are provided in Table 1.‡ In compounds **1** and **5**, the presence of disordered thiocyanate and solvent molecules gave rise to a very weak scattering. Initial refinements revealed the presence of a substantial volume of unresolvable solvent (CH_3OH and H_2O) molecules in **5**. The subroutine SQUEEZE from PLATON[19b] was used to remove the diffraction component of disordered solvents resulting in two voids of *ca.* 4163 $Å^3$ and 675 electrons per cell plus eight smaller voids of less than 25 $Å^3$ and 5 electrons per cell omitted. This corresponds to *ca.* $9CH_3OH + 1H_2O$ molecules per asymmetric unit. In compound **3**, one thiocyanate anion coordinated to Fe3 is disordered over two sites and has been modelled with an occupancy ratio of 70 : 30.

0.5 mm glass capillaries were filled with polycrystalline samples of **2** and **3** and mounted and aligned on a Empyrean PANalytical powder diffractometer, using CuKα radiation (λ = 1.54177 Å). A total of 2 scans were collected at room temperature in the 2θ range 5–30°.

Physical measurements

C, H, N and S elemental analyses were done on a CE Instruments EA 1110 CHNS Elemental analyzer. The Fe : S and Fe : S : Cl ratios were measured on a Philips ESEM X230 scanning electron microscope equipped with an EDAX DX-4 microsonde. Infrared spectra were recorded in the solid state (KBr pellets) on a Nicolet Avatar 320 FTIR spectrometer in the 400–4000 cm^{-1} range. ESI mass spectra were recorded on a Waters ZQ mass spectrometer using nitrogen as the drying and nebulising gas. The equipment was calibrated with appropriate standard samples. Magnetic measurements were performed using a Quantum Design MPMS-XL-5 SQUID magnetometer in the 2 to 300 K temperature range with an applied magnetic field of 0.1 T on polycrystalline samples. Mössbauer spectra were collected in transmission mode using a conventional constant-acceleration spectrometer and a 50 mCi ^{57}Co source in a Rh matrix. The velocity

‡ CCDC 973767–973771.

Table 1 Crystallographic data for **1**, **2**, **3**, **4** and **5**

Compound	**1**	**2**	**3**	**4**	**5**
Empirical formula	$C_{91}H_{108}Cl_5Fe_8N_{59}O_{30}S_{11}$	$C_{86.5}H_{118}Cl_2Fe_6N_{46}O_{17.5}S_{10}$	$C_{36}H_{38.5}Fe_4N_{15.5}O_{7.7}S_7$	$C_{69}H_{86}Fe_6N_{48}O_{25}S_6$	$C_{93.5}H_{142}F_3Fe_{6.5}N_{46.5}O_{15}S_{10.5}$
Formula weight	3484.97	2808.69	1259.26	2513.21	2914.11
Crystal colour	Red	Red	Red	Red	Red
Crystal size	0.2 × 0.07 × 0.05	0.06 × 0.06 × 0.02	0.15 × 0.11 × 0.10	0.23 × 0.10 × 0.05	0.33 × 0.11 × 0.07
Temperature (K)	120(2)	120(2)	120(2)	120(2)	120(2)
Wavelength (Å)	0.71073	0.71073	0.71073	0.71073	0.71073
Crystal system, *Z*	Tetragonal, 8	Triclinic, 2	Monoclinic, 4	Orthorhombic, 4	Monoclinic, 8
Space group	$I4_1cd$	$P\bar{1}$	$P2_1/n$	*Pbna*	C2/*c*
a (Å)	28.5279(3)	17.1614(6)	20.2912(6)	15.5153(4)	45.2573(13)
b (Å)	28.5279(3)	17.3252(6)	11.7876(5)	25.8550(9)	27.5089(6)
c (Å)	41.3731(6)	24.4236(7)	22.1837(6)	26.6761(11)	28.4547(9)
α (°)	90.00	70.309(3)	90	90	90
β (°)	90.00	79.499(3)	98.084(3)	90	119.372(4)
γ (°)	90.00	77.344(3)	90	90	90
V (Å^3)	33671.1(9)	6624.3(4)	5253.3(3)	10701.1(6)	30871.7(18)
ρ_{calc} (Mg m^{-3})	1.370	1.397	1.579	1.552	1.251
μ ($Mo_{K\alpha}$) (mm^{-1})	0.960	0.910	1.422	0.999	0.803
θ range (°)	2.856–27.500	2.944–27.484	3.053–27.519	3.062–27.498	2.955–26.408
Reflns collected	178 800	105 489	28 735	42 210	260 859
Independent reflns (R_{int})	8631 (0.1501)	14 588 (0.1269)	8545 (0.0445)	5927 (0.0934)	16 529 (0.13173)
L. S. parameters, *p*/restraints, *r*	898/14	1479/7	651/3	683/31	1306/15
$R_1(F)$,[a] $I > 2\sigma(I)$	0.1109	0.0968	0.0660	0.0826	0.1149
$wR_2(F^2)$,[b] all data	0.3470	0.3045	0.1816	0.2527	0.3644
$S(F^2)$,[c] all data	1.012	1.053	1.028	1.027	1.082

[a] $R_1(F) = \Sigma||F_o| - |F_c||/\Sigma|F_o|$. [b] $wR_2(F^2) = [\Sigma w(F_o^2 - F_c^2)^2/\Sigma wF_o^4]^{1/2}$. [c] $S(F^2) = [\Sigma w(F_o^2 - F_c^2)^2/(n + r - p)]^{1/2}$.

Table 2 Estimated parameters from the Mössbauer spectrum of **3** taken at room temperature

[a]	IS	QS	Γ	I (%)
	0.365	0.512	0.293	48.23
	0.393	1.003	0.319	51.77

[a] IS (mm s^{-1}) isomer shift relative to metallic Fe at 297 K. QS (mm s^{-1}) quadrupole splitting of doublets; Γ (mm s^{-1}) half-width of the doublet peaks; I relative area. Estimated standard deviations are <0.02 mm s^{-1} for IS, QS and Γ, and $<3\%$ for I.

scale was calibrated using α-Fe foil. The absorber was obtained by gently packing single crystals of **3** into a perspex holder. Isomer shifts (Table 2) are given relative to metallic α-Fe at room temperature.

Results

Syntheses

Reaction of $Fe(ClO_4)_3{\cdot}6H_2O$, a Schiff-base ligand (L_1, L_2 or L_3) and KSCN in a 1 : 1 : 2 molar ratio in methanol leads to three Fe(III) clusters with different nuclearities (8, 6 and 4) of formula $[Fe_8(\mu\text{-}L_1)_8(\mu\text{-}O)_4(NCS)_8](ClO_4)_5(NCS)_3$ (**1**), $[Fe_6(\mu\text{-}L_2)_6(\mu\text{-}O)_3(NCS)_6]$-$(ClO_4)_2(NCS)_4$ (**2**) and $[Fe_4(\mu\text{-}L_3)_2(\mu\text{-}OH)_2(\mu\text{-}OHO)(NCS)_7(OH_2)]$ (**3**), respectively. The 1 : 1 metal : ligand ratio of the syntheses is maintained in the final structure for compounds **1** and **2**, which contain the tetradentate imidazolyl ligands L_1 and L_2, but not in **3**, which contains the tetradentate pyridyl ligand L_3. In this last case, the structure presents a 2 : 1 metal : pyridyl ligand ratio. The complexes obtained with the imidazolyl ligands are soluble in methanol and were crystallized by slow diffusion with diethyl ether. Both **1** and **2** are cationic polynuclear complexes with NCS^- and ClO_4^- acting as counterions. In contrast, similar synthetic conditions with the pyridyl-based ligand, L_3, afforded the neutral compound, **3**, which precipitated in methanol and was obtained by recrystallization in acetonitrile. The use of other counterions in the iron(III) precursor salt such as NO_3^- with L_1 and BF_4^- or Cl^- with L_2 led in all cases to hexanuclear clusters with a similar structure to that of **2** (see compounds **4** and **5**, Fig. S1 and S2, ESI†). In the case of BF_4^-, oxidation of Fe(II) to Fe(III) in air and decomposition of the anion gave rise to the presence of $[FeF_6]^{3-}$ counterions in the structure (see compound **5**, ESI†). Preliminary single crystal diffraction data for a compound obtained with L_2 and Cl^- show the presence of a hexamer with a similar structure to that found in **2**, **4** and **5**. However, due to the low quality of the data it was not possible to find a proper solution to the structure. Finally, powder X-ray diffraction patterns of **2** and **3** at 300 K confirm the structure obtained from single X-ray diffraction experiments shown below (see Fig. S3, ESI†). X-ray diffraction patterns of **1** and **5** are not shown as powder samples of these compounds lost crystallinity very fast after filtering due to the loss of solvent. In the case of **4**, the small amount of sample available prevented the measurement of the powder X-ray diffraction. The composition of crystals of these compounds, checked by microanalysis, shows a Fe : S : Cl ratio close to 8 : 11 : 5 for **1** and 6 : 10 : 2 for **2**, and a Fe : S ratio close to 4 : 7 for **3**, 6 : 6 for **4** and 6.5 : 10.5 for **5**.

Structure of $[Fe_8(\mu\text{-}L_1)_8(\mu\text{-}O)_4(NCS)_8](ClO_4)_5(NCS)_3(H_2O)_6$ (1). **1** crystallizes in the tetragonal $I4_1cd$ space group. The structure is formed by an octanuclear cationic complex of formula $[Fe_8(\mu\text{-}L_1)_8(\mu\text{-}O)_4(NCS)_8]^{8+}$ (Fig. 1), with five perchlorate and three thiocyanate anions, and disordered lattice water molecules.

The octanuclear, Fe_8, unit is formed from half of the molecule, which is crystallographically independent, through a 2-fold axis linking O1 and O3. Thus, it contains four crystallographically independent Fe(III) atoms (Fe1–Fe4) and is composed of four $[Fe^{III}–O–Fe^{III}]^{4+}$ dimers. Four of the eight neutral tetradentate L_1 ligands connect the two Fe(III) of the dimer in a bis(bidentate) chelating mode while the remaining four connect Fe(III) belonging to different dimers in a similar way. Thus, each Fe(III) center shows a distorted octahedral N_5O coordination to four nitrogen atoms from two chelating L_1 in a *cis*-arrangement, one nitrogen atom from the NCS^-, and one oxygen atom from a μ-oxo (Fig. 1). The Fe–N(imino) bond length distances range from 2.161(14) to 2.196(16) Å, while Fe–N(imidazolyl) ones range from 2.148(15) to 2.201(18) Å. In the axial position, the Fe–N(NCS^-) distances lie between 2.027(18) and 2.049(15) Å and Fe–O(oxo) between 1.790(6) and 1.801(6) Å as normally observed for binuclear Fe(III) complexes with a single oxygen bridge.[20] These distances are in good agreement with the expected ones for high-spin (HS) Fe(III) centres. The imidazolyl NH groups in **1** present hydrogen bonds with disordered free NCS^- and ClO_4^- counterions and lattice water molecules. Two crystallographically equivalent ClO_4^- groups

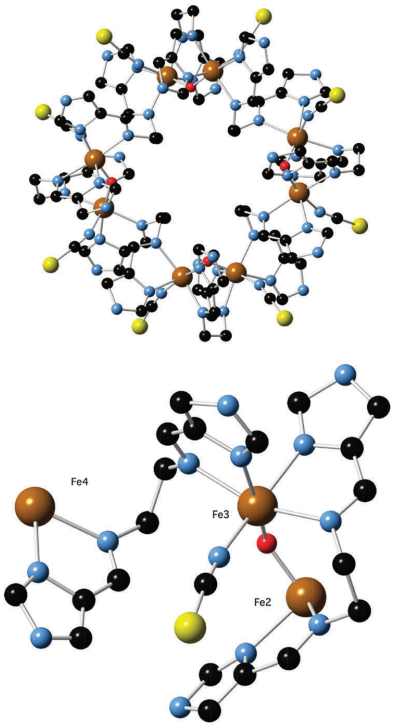

Fig. 1 Molecular structure of the octanuclear $[Fe_8(\mu\text{-}L_1)_8(\mu\text{-}O)_4(NCS)_8]^{8+}$ complex of **1** (top) and a view of the coordination sphere around Fe3 linked to an iron atom from the same dimer (Fe2) and another one from the neighboring dimer (Fe4) (bottom) (iron (brown), sulfur (yellow), oxygen (red), nitrogen (blue), and carbon (black)).

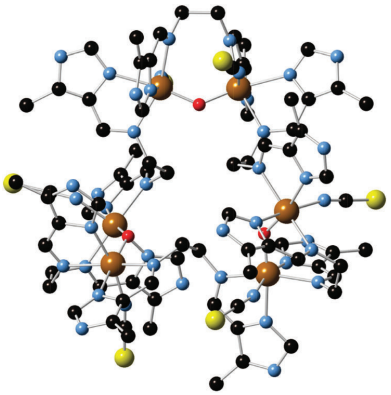

Fig. 2 Molecular structure of the hexanuclear $[Fe_6(\mu\text{-}L_2)_6(\mu\text{-}O)_3(NCS)_6]^{6+}$ complex of **2** (iron (brown), sulfur (yellow), oxygen (red), nitrogen (blue), and carbon (black)).

(with central atom Cl1) are close to the internal cavity of the Fe_8 cationic ring with numerous short contacts with L_1 atoms. On the other hand, the second crystallographically independent ClO_4^- group (with central atom Cl2) occupies the space between Fe_8 cations and presents numerous short contacts with L_1 atoms.

Structure of $[Fe_6(\mu\text{-}L_2)_6(\mu\text{-}O)_3(NCS)_6](ClO_4)_2(NCS)_4(CH_3CH_2OCH_2CH_3)_{0.5}(H_2O)_{3.5}(CH_3OH)_{2.5}$ (2). **2** crystallizes in the triclinic $P\bar{1}$ space group. The structure is formed by a hexanuclear complex cation of formula $[Fe_6(\mu\text{-}L_2)_6(\mu\text{-}O)_3(NCS)_6]^{6+}$ (Fig. 2), with two perchlorate and four thiocyanate anions, diethylether and disordered methanol and water molecules. The Fe_6 unit is formed by three $[Fe^{III}–O–Fe^{III}]^{4+}$ dimers, six L_2 ligands and six NCS^- ligands. The L_2 ligands present the same intra or interdimer bis(bidentate) coordination mode between two Fe(III) shown for compound **1**. Thus, each Fe^{III} center presents a N_5O coordination sphere to four nitrogen atoms from two chelating L_2 ligands, one nitrogen atom from the terminal NCS^- group, and one oxygen atom from an oxo group in a similar way as in compound **1**. The imidazolyl NH groups from L_2 ligands form hydrogen bonds with disordered free NCS^- counterions and lattice water and methanol molecules. The ClO_4^- groups present hydrogen bonds with the imidazolyl NH groups from L_2. One ClO_4^- group (with central atom Cl1) is very close to the internal cavity of the Fe_6 cationic ring with numerous short contacts with L_2 atoms. On the other hand, the second crystallographically independent ClO_4^- group (with central atom Cl3 with an occupancy of 0.5) is close to the opposite site of the internal cavity of the Fe_6 cationic ring. Finally, the third crystallographically independent ClO_4^- anion (with central atom Cl2 with an occupancy of 0.5) occupies the space between Fe_6 units.

Structure of $[Fe_4(\mu\text{-}L_3)_2(\mu\text{-}OH)_3(\mu\text{-}O)(NCS)_7(OH_2)](H_2O)_2(CH_3CN)_{0.5}$ (3). **3** crystallizes in the monoclinic $P2_1/n$ space group. It is formed by a tetranuclear neutral complex of formula $[Fe_4(\mu\text{-}L_3)_2(\mu\text{-}OH)_3(\mu\text{-}O)(NCS)_7(OH_2)]$ and lattice water and acetonitrile solvent molecules, which are disordered in some cases. The neutral cluster is constructed from four crystallographically independent Fe(III) ions (Fe1–Fe4) that lie at the corners of a very

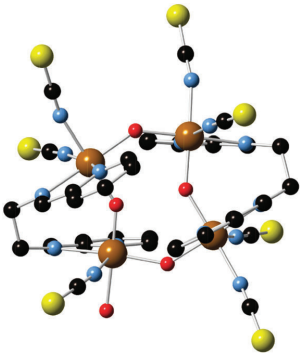

Fig. 3 Molecular structure of the tetranuclear $[Fe_4(\mu\text{-}L_3)_2(\mu\text{-}OH)_3(\mu\text{-}O)(NCS)_7(H_2O)]$ complex of **3** (iron (brown), sulfur (yellow), oxygen (red), nitrogen (blue), and carbon (black)).

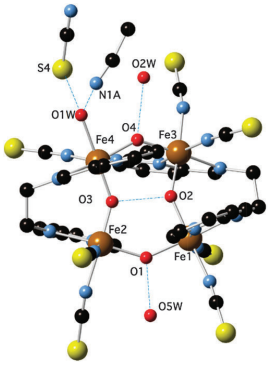

Fig. 4 Intra- and intermolecular hydrogen-bonding of **3**.

distorted rectangle (Fig. 3). The $\mu\text{-}OH^-$ groups bridge Fe1–Fe2, Fe1–Fe3 and Fe3–Fe4 pairs (Fig. 4), while the Fe2–Fe4 pair is bridged by a $\mu\text{-}O^{2-}$. The Fe1–Fe3 and Fe2–Fe4 pairs are linked together by pyridyl-based L_3 ligands in the bis(bidentate) chelating bridging mode. The distorted octahedral coordination of the four iron(III) ions is completed with two terminal NCS^- ligands with the exception of Fe4 which is coordinated to one terminal NCS^- ligand and one terminal water molecule (Fig. 4). Therefore, three of the four Fe(III) (Fe1, Fe2 and Fe3) present a N_4O_2 coordination sphere to two N (imine and pyridyl) from one L_3 ligand, two μ-O (hydroxo or oxo) and two N (NCS^-), while the other one (Fe4) shows a N_3O_3 coordination sphere to two N (imine and pyridyl) from one L_3 ligand, one N(NCS^-) and three μ-O (hydroxo, oxo and the terminal water molecule). The four iron atoms are far to be coplanar and deviate from their best least-square plane by 0.267 (Fe1), −0.322 (Fe2), −0.286 (Fe3) and 0.341 (Fe4) Å. In contrast, the four bridging oxygen atoms (O1 to O4) form a plane with a deviation of less than 0.006 Å from their best least-square plane.

The hydrogen atoms of the Fe_4 cluster were not crystallographically located. Given the absence of counterions and the fact that metal–ligand distances and Mössbauer spectroscopy (see below) indicate that the four metal centers are clearly HS Fe(III), charge considerations require that three of the four core oxygens are formally protonated. O1 and O4 atoms are protonated as evidenced by (i) their bond distances to Fe(III) ions (mean Fe–O distance of 1.991(3) Å), which are typical of Fe^{III}–μ-(hydroxo) bonds[21] and (ii) the short distance of these two atoms to lattice water molecules indicating the formation of hydrogen-bonds ($d_{O1\cdots O5W}$ = 2.880 Å and $d_{O4\cdots O2W}$ = 2.780 Å). The Fe–O distances of the remaining bridging oxygens (O2 and O3) are clearly differentiated suggesting a different protonation. Thus, Fe–O distances of O2 are 1.924(3) and 1.936(3) Å, which lie in the range found for other Fe^{III}–μ-(hydroxo) bonds. In contrast, Fe–O distances of O3 (1.810(4) and 1.826(4) Å) are consistent with the formation of a Fe^{III}–μ-(oxo) bond (see above). Furthermore, the distance between O2 and O3 (2.551 Å) is consistent with the formation of a hydrogen bond between them (see Fig. 4). The significant difference in Fe–O distances indicates that the μ-oxo and μ-hydroxo can be considered as separate structural entities rather than an $(O\text{–}H\text{–}O)^{3-}$ unit.[22,23] Indeed, Fe_4 complexes with $(O\text{–}H\text{–}O)^{3-}$ units present shorter O···O distances ranging from 2.394 to 2.529 Å.[21,24] Finally, the presence of two protons in the terminal oxygen coordinated to Fe4 (O1W) is supported by the formation of two hydrogen bonds with one disordered lattice water–acetonitrile molecule and one S atom from a NCS^- group, as shown in Fig. 4.

Electrospray ioinization mass spectrometry

The behaviour of the polynuclear Fe_6 cationic cluster of **2** in solution has been characterized by electrospray ionization mass spectrometry (ESI-MS). Fig. S4, ESI,† shows the ESI-MS (positive mode) analysis of a solution of **2** in methanol. The two most intense peaks appear at *m*/*z* values of 588.67 and 598.95 Da which correspond, respectively, to the $[Fe_6(\mu\text{-}L_2)_6(\mu\text{-}O)_3(NCS)_6](ClO_4)(NCS)^{4+}$ and $[Fe_6(\mu\text{-}L_2)_6(\mu\text{-}O)_3(NCS)_6](ClO_4)_2^{4+}$ species. The third most intense peak corresponds to a $[Fe(L_2)(NCS)]^+$ monomer that has been reduced by one electron. Finally, the remaining peaks could be assigned to Fe_6 units that have been reduced by one electron plus one ClO_4^- (574.05 Da), one ClO_4^- and SCN^- (784.68 Da) or two ClO_4^- (798.39). The charge of the species present in the spectrum has been unambiguously characterized by single ion recording (SIR) at the highest resolution of the spectrometer with monoisotopic peaks separated by 1/*z* Da. Fig. S5, ESI,† shows the isotopic distributions of the most intense peaks. As the majority of peaks arise from species in which the Fe_6 core remains intact, we can conclude that the cluster is preserved in solution.

Mössbauer spectrum of 3

Owing to the structural features exhibited by the Fe_4 clusters, four different iron sites and two sorts of bridging ligands ($\mu\text{-}OH^-$ and $\mu\text{-}O^{2-}$), it seemed to be of interest to study the Mössbauer spectrum of **3** (Fig. 5). In order to satisfactorily fit this spectrum, it was necessary to consider nested quadrupole-split doublets, *i.e.* of very close isomer shift (IS), in line with a very similar N_4O_2 or N_3O_3 environment for all four iron sites,

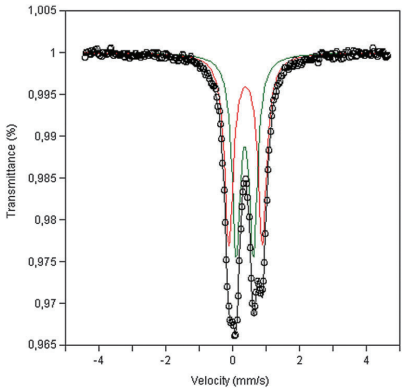

Fig. 5 Room temperature Mössbauer spectrum of **3**. The lines over the experimental points are the sum of two doublets. The estimated parameters of these doublets are collected in Table 2.

but significantly different quadrupole splittings (QS). The data may in principle be analyzed assuming two quadrupole-split doublets in a 1:1 ratio with fitting parameters shown in Table 2. These parameters are typical of HS Fe(III). The quadrupole-split doublet with a smaller QS value could be assigned to Fe1 and Fe3 as they exhibit very similar environments since both are linked to two μ-OH^- groups, whereas the one with larger QS could be assigned to Fe2 and Fe4, taking into account the more distorted octahedral coordination of Fe2 and Fe4 which contain shorter Fe^{III}–μ-O^{2-} bonds. Still, the Mössbauer spectrum of **3** could also be fitted to three doublets with a 2:1:1 ratio. This is not surprising given the low sensitivity of HS–Fe(III) Mössbauer parameters to the coordination environment, and the similarities of the coordination spheres of the four sites.[22] In any case and for purposes of comparison, indicative parameters of the fitting to two doublets are summarized in Table 2.

Magnetic properties

The temperature dependence of the product of the molar magnetic susceptibility and the temperature (χT) of compounds **1** and **2** is shown in insets of Fig. 6. The two compounds present a very similar behaviour as expected from their structures. The χT values at 300 K (2.8 and 2.7 cm^3 K mol^{-1} for **1** and **2**, respectively) are significantly lower than theoretically expected for non-interacting HS Fe(III) ions (35.00 and 26.25 cm^3 K mol^{-1} for 8 and 6 Fe(III) ions with $g = 2$, respectively). The χT of both compounds decreases gradually almost linearly when temperature decreases down to 50 K and stays approximately constant (0.15 cm^3 K mol^{-1}) until 2 K which is an indication of strong antiferromagnetic interactions of the $[Fe^{III}–O–Fe^{III}]^{4+}$ dimer with the ground state $S = 0$. The similar χT curves of both compounds indicate that the magnetic interactions of the bis(bidentate) L_1 or L_2 ligands are very weak and that the observed behavior should be attributed to strong intradimer antiferromagnetic interactions between Fe(III) centers linked by μ-oxo. Indeed, it has been

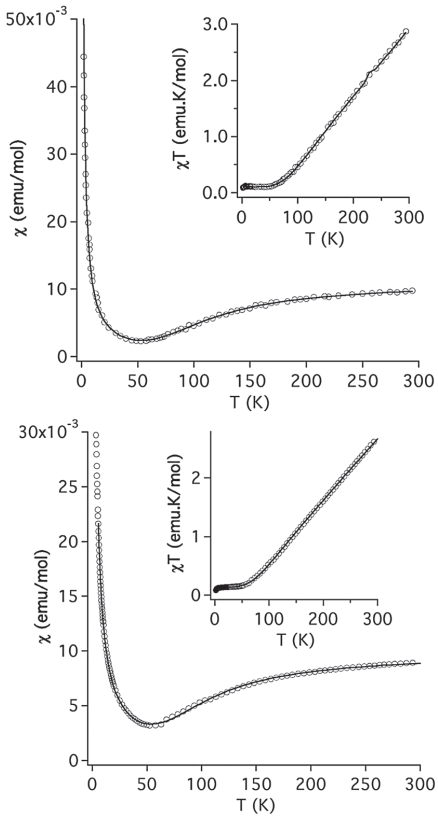

Fig. 6 Plot of χ *vs.* T and $\chi_m T$ *vs.* T (insets) for **1** (up) and **2** (down). The susceptibility, χ, was measured under a 0.1 T magnetic field. The solid line is the best fit of the 2–300 K data.

modeled using the isotropic spin–spin interaction by the Heisemberg–Dirac–Van Vleck Hamiltonian $H = -2JS_1S_2$, where $S_1 = S_2 = 5/2$.[25] To reproduce the data satisfactorily we had to consider a certain amount of a paramagnetic impurity (ρ, %). The best fit was obtained with the following parameters $J = -119.2$ cm^{-1}, $g = 2.00$ and $\rho = 0.903\%$ for **1** (with $R = 2.97 \times 10^{-3}$) and $J = -110.5$ cm^{-1}, $g = 2.02$ and $\rho = 0.606\%$ for **2** (with $R = 2.82 \times 10^{-4}$). These parameters are similar to those found in other Fe^{III}-oxo dimers.[26]

χT of **3** decreases linearly from 5.6 cm^3 K mol^{-1} at 300 K to 0.05 cm^3 K mol^{-1} at 10 K, and stays approximately constant down to 2 K (see the inset in Fig. 7). The presence of four Fe(III) linked by μ-OH^- or μ-O^{2-} ligands gives rise to a magnetic behavior, which indicates weaker antiferromagnetic interactions between $S = 5/2$ of the Fe(III) than those found for **1** and **2**. Inspection of the molecular structure of **3** reveals that due to the lack of symmetry, four exchange interactions would be rigorously required for the interpretation of the magnetic properties.[21] A simplification considering only three type of interactions: $J_{12} = J_{34}$ corresponding to hydroxo bridge

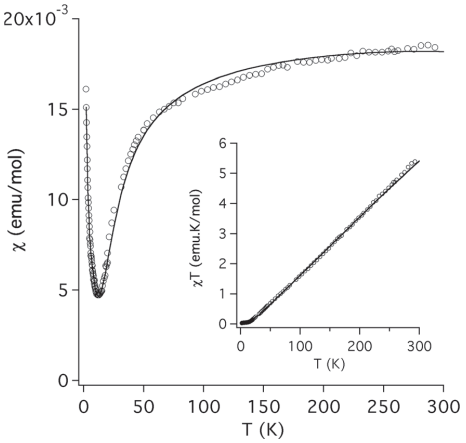

Fig. 7 Plot of χ *vs.* *T* and $\chi_m T$ *vs.* *T* (insets) for **3**. The susceptibility, χ, was measured under a 0.1 T magnetic field. The solid line is the best fit of the 2–300 K data.

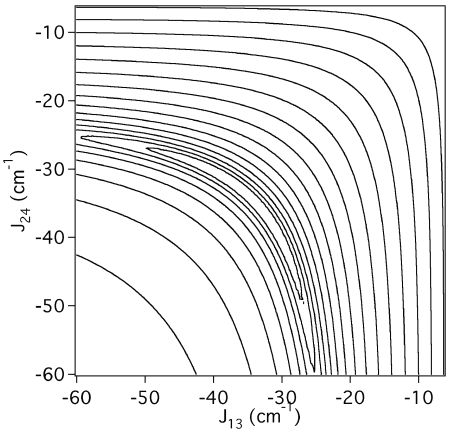

Fig. 8 Surface error plot of χ_m *vs.* *T* as a function of J_{24} and J_{13} revealing a banana minima.

interactions of O1 and O4 oxygen atoms, J_{13} corresponding to the other type of hydroxo bridge through the O2 oxygen atom and finally J_{24} associated with oxo bridge through the O3 oxygen atom. The best fitting to experimental data is obtained with the following parameters $J_{12} = J_{34} = -3.07$ cm^{-1}, $J_{24} \approx J_{13} = -34.37$ cm^{-1}, $g = 2.00$ and $\rho = 0.5\%$ (with $R = 3.54 \times 10^{-4}$). This fit is not very sensible to the J_{24}/J_{13} ratio. The dependence of the fit with respect to them is shown in a two-dimensional plot of the error factor R on the values J_{24} and J_{13} (see Fig. 8). The minimum error region ($R < 7.0 \times 10^{-4}$) has a banana shape where both *J*s can be interconverted and with limits at $J_{13} = -27.5$ cm^{-1} and $J_{24} = -48.8$ cm^{-1}. These parameters are similar to those found in related compounds.[21–23]

Discussion

The reactivity of iron(III) with tetradentate Schiff-base ligands derived from imidazole has been studied. In all cases the imidazolyl ligands coordinate to two iron(III) linked through an oxo ligand in a bis(bidentate) chelating bridging mode instead of only the tetradentate chelating mode observed for iron(II) systems with similar ligands. As a result of this, two novel polynuclear clusters with ring structures of eight and six iron(III) centers have been obtained in contrast to reactions of similar ligands with iron(II), which lead to mononuclear complexes in all cases. In addition, we have observed that the presence of a methyl group in the imidazolyl substituent of L_2 or the change of the counterion has a drastic effect on the nuclearity of the cluster. Thus, reaction of $Fe(ClO_4)_3 \cdot 6H_2O$ with L_1 gives rise to an octanuclear iron(III) cluster, but if the size of the counteranion is reduced (replacement of ClO_4^- by NO_3^- or Cl^-) or a methyl group is introduced in the ligand (replacement of L_1 by L_2), hexanuclear clusters are obtained in compounds **2**, **4** and **5**. A possible explanation is that ClO_4^- anions present the correct size and shape to template the growth of an octanuclear cluster. Indeed, two ClO_4^- anions in the structure of compound **1** are close to the center of the octanuclear cluster and present numerous short contacts with L_1 ligands of this octanuclear cluster. When the size of the anion is reduced or bulky methyl substituents are introduced in the ligand, the octanuclear cluster cannot be formed and templating of a hexanuclear cluster occurs as in compound **4** and compound with Cl^- mentioned above with L_1 or compounds **2** and **5** with L_2. In these two last compounds, ClO_4^- or FeF_6^{3-} anions do not enter into the internal cavity of the cluster as they present short contacts with at least two neighboring hexanuclear complexes. On the other hand, replacement of the imidazolyl units by pyridyl ones leads to a tetranuclear neutral cluster of **3**, in which iron(III) is in the HS state.

ES-MS studies of methanol solutions of **2** show that the hexanuclear polynuclear complexes are preserved in solution as they form adducts with NCS^- and/or ClO_4^- counterions. This could open the way for possible applications of these clusters in solution or deposited onto surfaces.

The magnetic properties of the compounds of the octanuclear cluster of **1** and the hexanuclear cluster of **2** can be explained by the presence of four or three iron(III) dimers bridged by μ-oxo ligands that give rise to antiferromagnetic interactions and to antiferromagnetic ground states. They could be modelled by using the isotropic spin–spin interaction with similar parameters ($J = -119.2$ cm^{-1} for **1** and $J = -110.5$ cm^{-1} for **2**). The angular and distance dependence of *J* of oxo-bridged iron(III) dimers has been rationalized by Weihe and Güdel by using an angular and radial overlap model.[27] The similar *J* values of **1** and **2** are a consequence of the similar Fe–O distances (1.790(18) Å for **1** and 1.797(5) Å for **2**) and Fe–O–Fe angles (136.7(15)° for **1** and 133.2(5)° for **2**) that they present. These values are consistent with those obtained for iron(III)-oxo dimers with similar Fe–O lengths and Fe–O–Fe angles.[27] In the case of **3**, the presence of four Fe(III) linked by μ-OH^- or μ-O^{2-} ligands gives rise to a different magnetic behavior with weaker antiferromagnetic interactions between $S = 5/2$ of the Fe(III) than those found

for **1** and **2**. The magnetic properties could be modelled by a simplified model considering only three types of interactions: $J_{12} = J_{34}$ corresponding to hydroxo bridge interactions, J_{13} corresponding to the other type of hydroxo bridge and J_{24} associated with oxo. The lower value of J_{24} of **3** compared to J values of **1** and **2** is consistent with the increase of Fe–O lengths (1.818(4) Å) and Fe–O–Fe angles (145.15(18)°) for **3**.[27] As expected, the O^{2-}-bridged pair (Fe2···Fe4) is much more strongly antiferromagnetically coupled than the OH^{-}-bridged pairs.[23] The Fe1···Fe2 and Fe3···Fe4 couplings between hydroxo-bridged pairs are similar, as expected for similarities in distances and angles. The J value of these two pairs ($J_{12} = J_{34} = -3.07$ cm^{-1}) is weaker than that of the remaining hydroxo-bridged pair ($J_{13} = -27.5$ cm^{-1}) as expected on the basis of the smaller Fe–O–Fe angles (~138° for Fe1–O1–Fe2 and Fe3–O4–Fe4 *versus* ~ 145° for Fe1–O2–Fe3) and longer Fe–O distances (1.993(3) Å for Fe1–O1–Fe2 and 1.990(3) Å for Fe3–O4–Fe4 *versus* 1.930(3) Å for Fe1–O2–Fe3).[23]

Conclusions

Three novel interesting polynuclear clusters with ring structures of eight and six Fe(III) centers have been obtained by reaction of iron(III) with tetradentate Schiff-base ligands derived from imidazole. In these compounds, the imidazolyl ligands coordinate to two Fe(III) in a bis(bidentate) chelating bridging mode instead of only the tetradentate chelating mode observed for Fe(II) systems with similar ligands. In addition, the presence of a methyl group in the imidazolyl substituent or the change of a counterion allows controlling the nuclearity of the cluster (from eight to six). Replacement of the imidazolyl units by pyridyl ones leads to a tetranuclear neutral cluster. This cluster presents an unusual Fe_4 structure since the presence of the L_3 ligand imposes a non-planar arrangement of the four Fe(III).

From the point of view of the magnetic properties, the presence in these clusters of pairs of HS Fe(III) ions bridged by μ-oxo or μ-hydroxo ligands gives rise to antiferromagnetic interactions and to antiferromagnetic ground states in all cases.

These results demonstrate that the reaction of iron(III) with tetradentate imidazolyl ligands is a suitable strategy to obtain new iron(III) polynuclear complexes with interesting topologies. Some small changes in the ligands such as replacement of NCS^{-} by CN^{-} could lead to stronger ligand fields and perhaps to spin-crossover. Another interesting possibility could be the use of other metal ions with a higher magnetic axial anisotropy such as Mn(III) or lanthanides.

Acknowledgements

Financial support from the European Union (Project HINTS and ERC Advanced Grant SPINMOL), the Spanish MINECO (Project Consolider-Ingenio in Molecular Nanoscience CSD2007-00010, and projects MAT2011-22785 and CTQ-2011-26507) and the Generalitat Valenciana (Prometeo and ISIC-NANO Programs) is gratefully acknowledged. The authors thank J. M. Martínez-Agudo and Dr G. Agustí-López, University of Valencia, for magnetic characterisation and E. Tormos, University of Valencia, for ESI-MS measurements. Manfred Womes is acknowledged for the help with Mössbauer spectroscopy.

Notes and references

1 M. D. Pluth, R. G. Bergman and K. N. Raymond, *Acc. Chem. Res.*, 2009, **42**, 1650.
2 H. T. Chifotides, I. D. Giles and K. R. Dunbar, *J. Am. Chem. Soc.*, 2013, **135**, 3039.
3 W. Meng, J. D. Clegg and J. R. Nitschke, *J. Am. Chem. Soc.*, 2012, **51**, 1881.
4 J. M. Domínguez-Vera, A. Rodríguez, R. Cuesta, R. Kivekäs and E. Colacio, *J. Chem. Soc., Dalton Trans.*, 2002, 561.
5 Y. Wang, F.-H. Zhao, A.-H. Shi, Y.-X. Che and J.-M. Zheng, *Inorg. Chem. Commun.*, 2012, **20**, 23.
6 J. Yao, Z.-D. Lu, Y.-Z. Li, J.-G. Lin, X.-Y. Duan, S. Gao, Q.-J. Meng and C.-S. Lu, *CrystEngComm*, 2008, **10**, 1379.
7 (*a*) Z. Su, M. Chen, T. A. Okamura, M.-S. Chen, S.-S. Chen and W.-Y. Sun, *Inorg. Chem.*, 2011, **50**, 985; (*b*) E. Coronado, M. Giménez-Marqués, G. Mínguez Espallargas and L. Brammer, *Nat. Commun.*, 2012, **3**, 828.
8 (*a*) T. Sato, K. Nishi, S. Iijima, M. Kojima and N. Matsumoto, *Inorg. Chem.*, 2009, **48**, 7211; (*b*) Y. Sunatsaki, R. Kawamoto, K. Fujita, H. Maruyama, T. Suzuki, H. Ishida, M. Kojima, S. Iijima and N. Matsumoto, *Coord. Chem. Rev.*, 2010, **254**, 1871.
9 (*a*) N. Bréfuel, S. Shova, J. Lipkowski and J.-P. Tuchagues, *Chem. Mater.*, 2006, **18**, 5467; (*b*) N. Bréfuel, I. Vang, S. Shova, F. Dahan, J.-P. Costes and J.-P. Tuchagues, *Polyhedron*, 2007, **26**, 1745; (*c*) N. Bréfuel, S. Shova and J.-P. Tuchagues, *Eur. J. Inorg. Chem.*, 2007, 4326.
10 N. Bréfuel, C. Duhayon, S. Shova and J.-P. Tuchagues, *Chem. Commun.*, 2007, 5223.
11 (*a*) Y. Sunatsuki, Y. Ikuta, N. Matsumoto, H. Ohta, M. Kojima, S. Iijima, S. Hayami, Y. Maeda, S. Kaizaki, F. Dahan and J.-P. Tuchagues, *Angew. Chem., Int. Ed.*, 2003, **42**, 1614; (*b*) Y. Sunatsuki, H. Ohta, M. Kojima, Y. Ikuta, Y. Goto, N. Matsumoto, S. Iijima, H. Akashi, S. Kaizaki, F. Dahan and J.-P. Tuchagues, *Inorg. Chem.*, 2004, **43**, 4154; (*c*) N. Bréfuel, S. Imatomi, H. Torigoe, H. Hagiwara, S. Shova, J.-F. Meunier, S. Bonhommeau, J.-P. Tuchagues and N. Matsumoto, *Inorg. Chem.*, 2006, **45**, 8126; (*d*) N. Bréfuel, H. Watanabe, L. Toupet, J. Come, N. Matsumoto, E. Collet, K. Tanaka and J.-P. Tuchagues, *Angew. Chem., Int. Ed.*, 2009, **48**, 9304; (*e*) N. Bréfuel, E. Collet, H. Watanabe, M. Kojima, N. Matsumoto, L. Toupet, K. Tanaka and J.-P. Tuchagues, *Chem.–Eur. J.*, 2010, **16**, 14060.
12 R. Bagai, M. R. Daniels, K. A. Abboud and G. Christou, *Inorg. Chem.*, 2008, **47**, 3318.
13 D. Gatteschi, R. Sessoli and A. Cornia, *Chem. Commun.*, 2000, 725.
14 (*a*) X. Liu and E. C. Theil, *Acc. Chem. Res.*, 2005, **38**, 167; (*b*) M. Faiella, C. Andreozzi, R. T. M. de Rosales, V. Pavone,

O. Maglio, F. Nastri, W. F. DeGrado and A. Lombardi, *Nat. Chem. Biol.*, 2009, **5**, 882; (*c*) S. Friedle, E. Reisner and S. J. Lippard, *Chem. Soc. Rev.*, 2010, **39**, 2768.
15 F. J. LaRonde and M. A. Brook, *Inorg. Chim. Acta*, 1999, **296**, 208.
16 S. H. Rahaman, R. Ghosh, G. Mostafa and B. K. Ghosh, *Inorg. Chem. Commun.*, 2005, **8**, 1137.
17 A. Altomare, M. C. Burla, M. Camalli, G. L. Cascarano, C. Giacovazzo, A. Guagliardi, A. G. G. Moliterni, G. Polidori and R. Spagna, *J. Appl. Crystallogr.*, 1999, **32**, 115.
18 G. M. Sheldrick, *Acta Crystallogr., Sect. A: Found. Crystallogr.*, 2008, **64**, 112.
19 (*a*) L. J. Farrugia, *J. Appl. Crystallogr.*, 2012, **45**, 849; (*b*) A. L. Spek, *J. Appl. Crystallogr.*, 2003, **36**, 7.
20 K. Takahashi, Y. Nishida, Y. Maeda and S. Kida, *J. Chem. Soc., Dalton Trans.*, 1985, 2375.
21 A. K. Singh, W. Jacob, A. K. Boudalis, J.-P. Tuchagues and R. Mukherjee, *Eur. J. Inorg. Chem.*, 2008, 2820.
22 A. K. Boudalis, R. E. Aston, S. J. Smith, R. E. Mirams, M. J. Riley, G. Schenk, A. G. Blackman, L. R. Hanton and L. R. Gahan, *Dalton Trans.*, 2007, 5132.
23 T. C. Stamatatos, A. G. Christou, C. M. Jones, B. J. O'Callaghan, K. A. Abboud, T. A. O'Brien and G. Christou, *J. Am. Chem. Soc.*, 2007, **129**, 9840.
24 A. K. Boudalis, N. Latioti, G. A. Spyroulias, C. P. Raptopoulou, A. Terzis, V. Tangoulis and S. P. Perlepes, *J. Chem. Soc., Dalton Trans.*, 2001, 955.
25 M. Scarpellini, A. Neves, A. J. Bortoluzzi, I. Vencato, V. Drago, W. A. Ortiz and C. Zucco, *J. Chem. Soc., Dalton Trans.*, 2001, 2616.
26 (*a*) J. R. Hartman, R. L. Rardin, P. Chaudhuri, K. Pohl, K. Wieghardt, B. Nuber, J. Weiss, G. C. Papaefthymiou, R. B. Frankel and S. J. Lippard, *J. Am. Chem. Soc.*, 1987, **109**, 7387; (*b*) U. Bossek, H. Hummel, T. Weyhermüller, E. Bill and K. Wieghardt, *Angew. Chem., Int. Ed. Engl.*, 1995, **34**, 2642; (*c*) S. C. Payne and K. S. Hagen, *J. Am. Chem. Soc.*, 2000, **122**, 6399.
27 H. Weihe and H. U. Güdel, *J. Am. Chem. Soc.*, 1997, **119**, 6539.

Dalton Transactions

COMMUNICATION

A spin-crossover complex based on a 2,6-bis(pyrazol-1-yl)pyridine (1-bpp) ligand functionalized with a carboxylate group†

Cite this: *Dalton Trans.*, 2014, **43**, 9406

Received 30th January 2014,
Accepted 13th March 2014

DOI: 10.1039/c4dt00327f

www.rsc.org/dalton

Alexandre Abhervé, Miguel Clemente-León,* Eugenio Coronado,* Carlos J. Gómez-García and Maurici López-Jordà

Combining Fe(II) with the carboxylate-functionalized 2,6-bis(pyrazol-1-yl)pyridine (bppCOOH) ligand results in the spin-crossover compound $[Fe(bppCOOH)_2](ClO_4)_2$ which shows an abrupt spin transition with a $T_{1/2}$ of *ca.* 380 K and a T_{LIESST} of 60 K due to the presence of a hydrogen-bonded linear network of complexes.

Spin crossover (SCO) complexes are one of the most spectacular examples of molecular bistability. In these systems low-spin (LS) to high-spin (HS) transitions can be triggered through a variety of external stimuli (*e.g.* temperature, pressure or electromagnetic radiation). In addition to the interesting fundamental aspects of this phenomenon, these systems are of growing interest in the area of functional materials due to their possible applications as sensors, memories or switching devices.[1] The most studied SCO systems are based on iron(II) complexes that undergo spin crossover between their diamagnetic LS (S = 0) and paramagnetic HS (S = 2) configurations.[2] The change of electronic configuration is accompanied by drastic changes in the optical and magnetic properties of these compounds.[3] Thus, under given experimental conditions, the same material can be found in two states exhibiting different optical and magnetic behaviours. Abrupt transformations with hysteretic behaviour are expected for systems with strong intermolecular interactions.

An interesting series of spin crossover compounds are bischelated iron(II) complexes of tridentate ligands based on 2,6-bis(pyrazol-1-yl)pyridine (1-bpp), which can be functionalized at its periphery with a variety of substituents.[4] The spin change in these materials is usually very abrupt and takes place with thermal hysteresis close to room temperature.[5] In addition, $[Fe(1\text{-}bpp)_2]^{2+}$ salts have the advantage of exhibiting spin-crossover induced by irradiation: light-induced excited spin state trapping effect (LIESST)[6] at high temperatures with relatively long lifetimes of the photoinduced metastable states.[7] Substitution on the pyridine ring allows functional groups to be included at the periphery of the $[Fe(1\text{-}bpp)_2]^{2+}$ centre without significantly perturbing the iron(II) centre.[8] This approach has afforded spin-crossover compounds with a variety of different pendant functionalities, coordination polymers or complexes for deposition on surfaces.[9–14] In an attempt to improve these results, we have added a carboxylate group to this ligand (bppCOOH, see Scheme 1). The well-known coordination capability of the carboxylate ligand could enable binding to metal ions or grafting on metal oxide surfaces, which are essential steps for the preparation of devices based on the spin-crossover phenomenon.[15] As a first step in this direction, herein we present the synthesis, and structural and magnetic characterization of the $[Fe^{II}(bppCOOH)_2](ClO_4)_2$ compound.

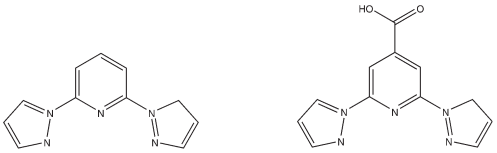

Scheme 1 Molecular structure of the 1-bpp (left) and bppCOOH (right) ligands.

Slow diffusion of diethyl ether on the mixture solution of $Fe(ClO_4)_2{\cdot}xH_2O$ and bppCOOH in a 1 : 2 molar ratio in acetone yielded crystals of compound $[Fe(bppCOOH)_2](ClO_4)_2$.

The structure of the compound was revealed by single crystal X-ray diffraction at 120 K and confirmed by the powder X-ray diffraction pattern (Fig. S1, ESI†). It crystallizes in a monoclinic crystal system with the centrosymmetric $C2/c$ space group. The asymmetric unit is composed of half of the $[Fe(bppCOOH)_2]^{2+}$ cation (Fig. 1) and one perchlorate anion. The central iron(II) ion of the complex is coordinated by six nitrogen atoms from two tridentate bppCOOH ligands with a

Instituto de Ciencia Molecular (ICMol), Universidad de Valencia, C/Catedrático José Beltrán 2, 46980 Paterna, Spain. E-mail: miguel.clemente@uv.es, eugenio.coronado@uv.es; Fax: +34 963543273; Tel: +34 963544419

†Electronic supplementary information (ESI) available: Experimental information: synthesis and structural and physical characterisation. X ray powder diffraction pattern of $[Fe^{II}(bppCOOH)_2](ClO_4)_2$ at 300 K, DSC curves and calculations and structural views of the structure. CCDC 977453. For ESI and crystallographic data in CIF or other electronic format see DOI: 10.1039/c4dt00327f

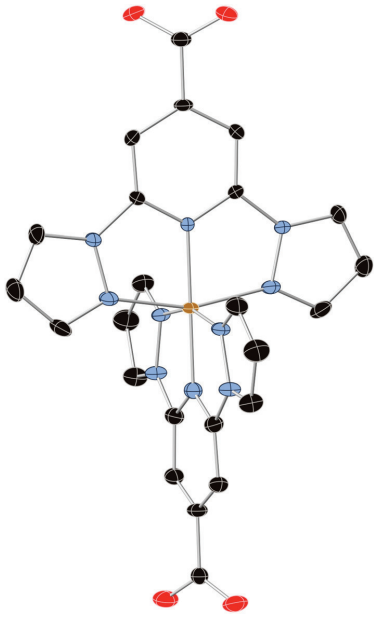

Fig. 1 X-ray structure of the complex $[Fe^{II}(bppCOOH)_2]^{2+}$ (C (black), N (blue), O (red) and Fe (yellow)) (hydrogen atoms omitted for clarity).

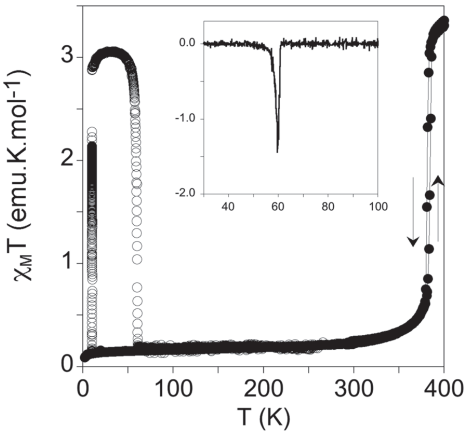

Fig. 3 Thermal variation of $\chi_M T$ for $[Fe^{II}(bppCOOH)_2](ClO_4)_2$. Full circles: data recorded in the cooling and heating modes without irradiation; empty circles: data recorded after irradiation at 10 K. The inset graph shows the temperature dependence of the first derivative of $\chi_M T$ with respect to the temperature.

distorted octahedral coordination geometry close to the ideal D_{2d} symmetry associated to a $[Fe(1\text{-}bpp)_2]^{2+}$ centre (*trans*-N(pyridyl)–Fe–N(pyridyl) angle (ϕ) of 180° and dihedral angle between the least squares planes of the two ligands (θ) of 87°). Fe–N bond lengths are in the range 1.888(4)–1.981(2) Å, typical of LS Fe–N lengths for this type of ligand.[9] Neighbouring $[Fe(bppCOOH)_2]^{2+}$ cations are linked through hydrogen bonds between the carboxylate groups ($d_{O1\cdots O3}$ = 2.671 Å, Fig. 2), forming a chain that runs along the *b* axis. These chains are linked through intermolecular interactions that involve the pyrazole groups and the carboxylate groups of neighbouring molecules giving rise to layers of complexes on the *bc* plane separated by layers of perchlorate anions (Fig. S2, ESI†). Finally, $[Fe(bppCOOH)_2]^{2+}$ complexes of neighbouring layers present short contacts involving CH groups of the pyrazole rings (Fig. S2, ESI†). The presence of the carboxylate groups causes packing which is different to that found in many salts of $[Fe(1\text{-}bpp)_2]^{2+}$ and derivatives. This is the so called "terpyridine embrace" crystal packing motif, a four-fold layer formed by π–π and edge-to-face C–X···π interactions between pyrazole groups of neighbouring molecules, which leads to a face-to-face configuration of the pyrazole groups with intermolecular distances of between 3.4 and 3.6 Å.[16] In contrast to this, in our compound the shortest intermolecular contacts of the pyrazole groups are with the carboxylate oxygen atoms of a complex belonging to a neighbouring chain (Fig. S2, ESI†).

The temperature dependence of the magnetic susceptibility of the compound was studied in heating and cooling modes. In the temperature range 2–370 K, the product of the molar magnetic susceptibility times the temperature, $\chi_M T$ (Fig. 3), shows a value close to 0, typical of a diamagnetic LS state (S = 0).

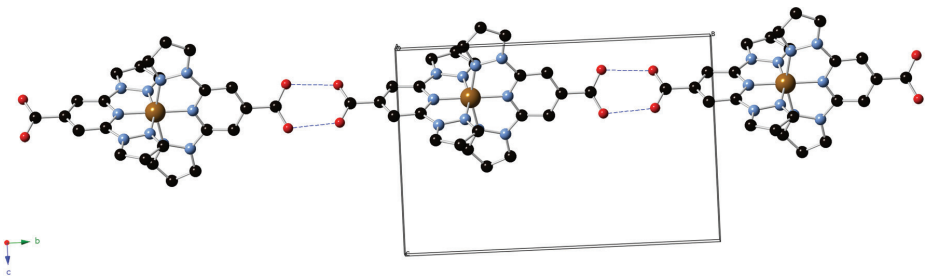

Fig. 2 Supramolecular 1D hydrogen-bonded chain structure of the complex $[Fe^{II}(bppCOOH)_2](ClO_4)_2$. The counter ions and hydrogen atoms are omitted for clarity.

Above this temperature, there is a sharp increase to a saturated HS value of 3.3 cm^3 K mol^{-1}, which corresponds to 100% of Fe(II) in the HS state (S = 2). This is consistent with the structure solved at 120 K which shows distances typical of LS Fe(II). The same behaviour is observed in heating and cooling modes with a small thermal hysteresis of 3 K ($T_{1/2}\uparrow$ = 384 K and $T_{1/2}\downarrow$ = 381 K, with $T_{1/2}$ = temperature of 50% HS → LS conversion). The presence of a thermal hysteresis loop clearly demonstrates the existence of a significant level of cooperativity probably due to the presence of intermolecular interactions mediated by the hydrogen-bonds between neighbouring $[Fe(bppCOOH)_2]^{2+}$ complexes. A similar cooperative behaviour has been observed for $[Fe^{II}(\mathbf{L})_2H](ClO_4)_3{\cdot}MeOH$ (**L** = 4′-(4‴-pyridyl)-1,2′:6′1″-bis(pyrazolyl)pyridine), which also contains hydrogen-bonded chains of complexes.[17] Finally, it is worth mentioning that the $T_{1/2}$ of this complex is noticeably higher than that of the unsubstituted 1-bpp Fe(II) complex (260 K)[18] but similar to that of other 1-bpp Fe(II) complexes with substituents in the fourth position of the pyridine ring[5,9,13,19,20] or 2,6-bis(pyrazol-3-yl)pyridine (3-bpp) Fe(II) complexes.[21]

In the heating mode the differential scanning calorimetry (DSC) measurement exhibited an endothermic peak centred at 383 K which corresponds to the LS to HS transition. Upon cooling a exothermic peak centred at 381 K was observed and could be assigned to the HS to LS transition, in good agreement with the magnetic measurements (Fig. S3 and Table S2, ESI†).

For the photomagnetic measurements the compound was irradiated with green light (λ = 532 nm, optical power 3.4 mW cm^{-2}) at 10 K in a SQUID magnetometer. A drastic increase of the magnetic signal was observed. After about two hours, the irradiation was switched off. The temperature was then increased at a rate of 0.3 K min^{-1} and the magnetic susceptibility recorded. The $\chi_M T$ value after irradiation was higher than the value recorded in the dark at temperatures below 60 K (see Fig. 3, empty circles). The fraction of Fe(II) photoconverted after irradiation was calculated to be 90%. The LIESST temperature (T_{LIESST}), defined as the minimum of the derivate of $\chi_M T$ with temperature, is 60 K. This value can be compared with those previously obtained for other 1-bpp compounds. Létard *et al.* have shown that a linear correlation between the thermal spin crossover temperature and T_{LIESST} holds generally for iron(II) complexes. In particular, for the Fe(1-bpp)$_2$ family, the two physical quantities may be related by the formula: $T_{LIESST} = T_0 - 0.3\ T_{1/2}$, with T_0 = 150 K.[7b,16] Taking $T_{1/2}$ = 382 K as the mean value of $T_{1/2}\uparrow$ and $T_{1/2}\downarrow$, a T_{LIESST} of 35.4 K is expected (well below the observed one of 60 K). Interestingly, the other Fe(1-bpp)$_2$ derivative with a high $T_{1/2}$ showing LIESST effect is the $[Fe(L)_2](BF_4)_2$ complex (L = 2,6-bis(4-iodopyrazol-1-yl)pyridine) with a reported $T_{1/2}$ > 360 K and an experimental T_{LIESST} of 54 K.[16] Therefore, there is a reasonable agreement between the data of the two compounds. Further studies needed to understand the photomagnetic behaviour of this compound (structure and relaxation kinetics of the photoinduced metastable state) are in progress.

In conclusion, we have demonstrated that the functionalization of the 1-bpp ligand with a carboxylate group is a suitable strategy for the preparation of new spin-crossover complexes. The presence of a carboxylate group linked to this spin-crossover complex makes it a useful synthon for the preparation of polynuclear metal complexes, polymers (metal–organic frameworks, MOFs) or for anchoring to metal-oxide surfaces/nanostructures. The preliminary results obtained by us show that some of these goals are possible. Thus, reaction of $[Fe(bppCOOH)_2]^{2+}$ complex with Fe^{3+} ions gives rise to a nonanuclear cluster formed by an iron trimer coordinated to six partially deprotonated $[Fe(bppCOOH)_2]^{2+}$ units. Furthermore X-ray photoelectron spectroscopy (XPS) measurements of a glass substrate covered with Al_2O_3 that has been immersed into an acetonitrile solution of $[Fe(bppCOOH)_2](ClO_4)_2$ confirm the deposition of the complex.

The authors thank the European Union (Project HINTS and ERC Advanced Grant SPINMOL), the Spanish MINECO (Project Consolider-Ingenio in Molecular Nanoscience CSD2007-00010, and projects MAT2011-22785 and CTQ-2011-26507) and the Generalitat Valenciana (Prometeo and ISIC-NANO Programs) for financial support. The authors also thank J. M. Martínez-Agudo and Dr G. Agustí-López, University of Valencia, for magnetic measurements.

Notes and references

1 (*a*) O. Kahn and C. Jay Martinez, *Science*, 1998, **279**, 44; (*b*) J. F. Létard, P. Guionneau and L. Goux-Capes, *Top. Curr. Chem.*, 2004, **235**, 221; (*c*) T. Mahfoud, G. Molnar, S. Cobo, L. Salmon, C. Thibault, C. Vieu, P. Demont and A. Bousseksou, *Appl. Phys. Lett.*, 2011, **99**, 053307; (*d*) D. Aravena and E. Ruiz, *J. Am. Chem. Soc.*, 2012, **134**, 777; (*e*) N. Baadji and S. Sanvito, *Phys. Rev. Lett.*, 2012, **108**, 217201.

2 See for general reviews: *Spin Crossover in Transition Metal Compounds, Topics in Current Chemistry*, ed. P. Gütlich and H. A. Goodwin, Springer Verlag, Berlin, Heidelberg, New York, 2004, vols. 233–235; *Spin-Crossover Materials: Properties and Applications*, ed. M. A. Halcrow, Wiley, 2013, ISBN: 978-1-119-99867-9.

3 P. Gütlich, A. Hauser and H. Spiering, *Angew. Chem., Int. Ed. Engl.*, 1994, **33**, 2024.

4 M. A. Halcrow, *Coord. Chem. Rev.*, 2005, **249**, 2880.

5 M. A. Halcrow, *Coord. Chem. Rev.*, 2009, **253**, 2493.

6 (*a*) S. Decurtins, P. Gütlich, C. P. Köhler, H. Spiering and A. Hauser, *Chem. Phys. Lett.*, 1984, **105**, 1; (*b*) S. Decurtins, P. Gütlich, K. M. Hasselbach, A. Hauser and H. Spiering, *Inorg. Chem.*, 1985, **24**, 2174.

7 (*a*) T. Buchen, P. Gütlich, K. H. Sugiyarto and H. A. Goodwin, *Chem. – Eur. J.*, 1996, **2**, 1134; (*b*) S. Marcen, L. Lecren, L. Capes, H. A. Goodwin and J. F. Létard, *Chem.*

Phys. Lett., 2002, **358**, 87; (*c*) G. Chastanet, C. A. Tovee, G. Hyett, M. A. Halcrow and J. F. Létard, *Dalton Trans.*, 2012, **41**, 4896.
8 T. D. Roberts, M. A. Little, L. J. K. Cook, S. A. Barrett, F. Tuna and M. A. Halcrow, *Polyhedron*, 2013, **64**, 4.
9 C. Rajadurai, O. Fuhr, R. Kruk, M. Ghafari, H. Hahn and M. Ruben, *Chem. Commun.*, 2007, 2636.
10 M. Nihei, L. Han and H. Oshio, *J. Am. Chem. Soc.*, 2007, **129**, 5312–5313.
11 C. A. Tovee, C. A. Kilner, S. A. Barrett, J. A. Thomas and M. A. Halcrow, *Eur. J. Inorg. Chem.*, 2010, 1007.
12 R. González-Prieto, B. Fleury, F. Schramm, G. Zoppellaro, R. Chandrasekar, O. Fuhr, S. Lebedkin, M. Kappes and M. Ruben, *Dalton Trans.*, 2011, **40**, 7564.
13 K. Takahashi, Y. Hasegawa, R. Sakamoto, M. Nishikawa, S. Kume, E. Nishibori and H. Nishihara, *Inorg. Chem.*, 2012, **51**, 5188.
14 M. S. Alam, M. Stocker, K. Gieb, P. Müller, M. Harvono, K. Student and A. Grohmann, *Angew. Chem., Int. Ed.*, 2010, **49**, 1159.
15 (*a*) C. Shen, M. Harvono, A. Grohmann, M. Buck, T. Weidner, N. Ballay and M. Zharkinov, *Langmuir*, 2008, **24**, 12883; (*b*) A. Bousseksou, G. Molnár, L. Salmon and N. Nicolazzi, *Chem. Soc. Rev.*, 2011, **40**, 3313.
16 R. Pritchard, H. Lazar, S. A. Barrett, C. A. Kilner, S. Asthana, C. Carbonera, J. F. Létard and M. A. Halcrow, *Dalton Trans.*, 2009, 6656.
17 C. Rajadurai, R. Kruk, F. Schramm, S. Brink, O. Fuhr, M. Ghafari, R. Kruk and M. Ruben, *Inorg. Chem.*, 2006, **45**, 10019.
18 J. M. Holland, J. A. McAllister, Z. Lu, C. A. Kilner, M. Thornton-Pett and M. A. Halcrow, *Chem. Commun.*, 2001, 577.
19 M. Nihei, T. Maeshima, Y. Kose and H. Oshio, *Polyhedron*, 2007, **26**, 1993.
20 I. Salitros, O. Fuhr, A. Eichhöfer, R. Kruk, J. Pavlik, L. Dlhán, R. Boca and M. Ruben, *Dalton Trans.*, 2012, **41**, 5163.
21 I. A. Gass, S. R. Batten, G. M. Forsyth, B. Moubaraki, C. J. Schneider and K. S. Murray, *Coord. Chem. Rev.*, 2011, **255**, 2058.

Inorganic Chemistry

Article

pubs.acs.org/IC

One-Dimensional and Two-Dimensional Anilate-Based Magnets with Inserted Spin-Crossover Complexes

Alexandre Abhervé, Miguel Clemente-León,* Eugenio Coronado,* Carlos J. Gómez-García, and Martin Verneret

Instituto de Ciencia Molecular (ICMol), Universidad de Valencia, Catedrático José Beltrán 2, 46980 Paterna, Spain

Supporting Information

ABSTRACT: The syntheses, structures, and magnetic properties of a family of bimetallic anilate-based compounds with inserted spin-crossover cationic complexes are reported. The structures of **1**−**4** present a two-dimensional anionic network formed by Mn(II) and Cr(III) ions linked through anilate ligands with inserted $[Fe^{III}(sal_2\text{-trien})]^+$ (**1**), $[Fe^{III}(4\text{-OH-sal}_2\text{-trien})]^+$ (**2**), $[Fe^{III}(sal_2\text{-epe})]^+$ (**3**), or $[Fe^{III}(5\text{-Cl-sal}_2\text{-trien})]^+$ (**4**) complexes. The structure of **5** is formed by anionic $[Mn^{II}Cl_2Cr^{III}(Cl_2An)_3]^{3-}$ chains surrounded by $[Fe^{II}(tren(imid)_3)]^{2+}$, Cl^-, and solvent molecules. The magnetic properties indicate that **1**−**4** undergo a long-range ferrimagnetic ordering at ca. 10 K. On the other hand, the inserted Fe(III) cations remain in the low-spin (in **4**) or high-spin state (in **1**, **2**, and **3**). In the case of **5**, half of the inserted Fe(II) cations undergo a complete and gradual spin crossover from 280 to 90 K that coexists with a magnetic ordering below 2.5 K.

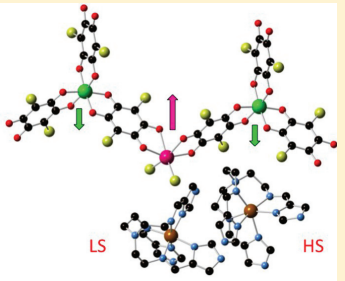

INTRODUCTION

Multifunctionality is one of the most appealing topics in chemical science. A rational approach to design hybrid multifunctional materials consists of the controlled assembly of two functional networks incorporating two properties or contributing synergistically to the appearance of new physical phenomena.[1] Among the later class of materials, those responding to an external stimulus are attracting considerable interest in view of their potential applications as chemical switches, memory or molecular sensors.[2] In this context, two-network compounds formed by a magnetic lattice and a switchable molecular component are promising candidates for the preparation of responsive magnetic materials.

Spin-crossover complexes are particularly suitable as switchable molecular components because they represent one of the best examples of molecular bistability. These molecular complexes change their spin state from low-spin (LS) to high-spin (HS) configurations under an external stimulus such as temperature, light irradiation, or pressure.[3] As this is accompanied by changes in the molecular size, the spin-crossover process should act as an internal pressure in the hybrid material, and therefore, it might affect the long-range magnetic ordering in the extended magnetic network.

Bimetallic oxalate-bridged compounds have been thoroughly used as magnetic lattice of multifunctional magnetic materials. They are formed by polymeric anionic networks $[M^{II}M^{III}(ox)_3]^-$ (ox = oxalate) with magnetic ions linked through bis-bidentate bridging oxalate ligands. The use of different charge-compensating molecular cations, which template the network formation, has provided many examples of multifunctional materials,[4] combining the long-range magnetic ordering of the oxalate network with paramagnetism,[5] photochromism,[6] electrical conductivity,[7] proton conductivity,[8] ferroelectricity,[9] chirality,[10] or single-molecule magnet behavior from the cation.[11] Fe(II) and Fe(III) spin-crossover cationic complexes have been used for the growth of two-dimensional (2D) and three-dimensional (3D) bimetallic oxalate-based magnets in the search of responsive magnetic materials.[12] Fe(II) spin-crossover complexes have led to the growth of 3D bimetallic oxalate-based compounds, which present magnetic properties very sensitive to the changes in size of the inserted cation, although the inserted Fe(II) complexes do not present a clear spin-crossover behavior.[12g,13] The most interesting results were obtained for the family of compounds $[Fe^{III}(sal_2\text{-trien})][Mn^{II}Cr^{III}(ox)_3]\cdot G$ (G = CH_2Cl_2, $CHBr_3$, CH_2Br_2, and $CHCl_3$, H_2 Sal_2-trien = *N*,*N*′-disalicylidenetriethylene-tetramine, see Scheme 1) formed by alternating layers of a 2D oxalate-based network, $[Fe^{III}(sal_2\text{-trien})]^+$ complexes and solvent molecules.[12b,e,h] They show that the confinement of spin-crossover cations into extended networks induce an unexpected property, a photoinduced spin-crossover transition of the inserted complex (LIESST effect), something very unusual for Fe(III) complexes. Unfortunately, the photo-induced spin conversion of the inserted Fe(III) complex has a negligible influence on the magnetic behavior of the 2D oxalate network as the magnetic ordering of this type of network is not sensitive to the change in size of the inserted cation.

Motivated by the interesting results obtained with bimetallic oxalate-based networks, we have attempted the use of larger bis-bidentate bridging ligands as the 2,5-dihydroxy-1,4-benzoquinone dianion derivatives of formula $C_6O_4X_2^{2-}$

Received: July 14, 2014
Published: October 28, 2014

dx.doi.org/10.1021/ic5016803 | *Inorg. Chem.* 2014, 53, 12014−12026

Scheme 1. Ligands of the Fe(III) and Fe(II) Complexes

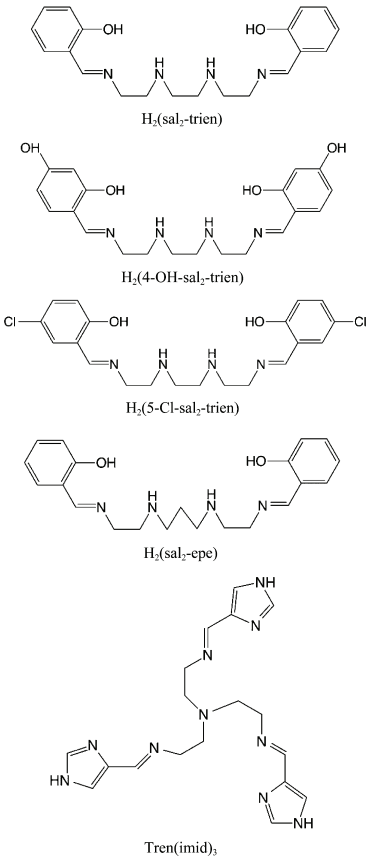

(X_2An^{2-}; X = Cl or Br, see Scheme 2). These ligands, which show coordination modes similar to the oxalate ligand, present additional advantages: (i) they are easy to modify or functionalize by simply changing the X group; (ii) they present higher ordering temperatures, T_c's; (iii) their bigger size may enable the introduction of a larger library of cations in order to prepare multifunctional molecular materials. The first example of this kind, obtained by our group, is the family of layered ferrimagnets $A[M^{II}M^{III}(X_2An)_3]\cdot G$ (A = $[(H_3O)(phz)_3]^+$ (phz = phenazine) or NBu_4^+; X = H, Cl, Br, I; G = water or acetone) with T_c ranging from 5.5 to 11.0 K and which, depending on the X substituent, can be porous and/or chiral.[14a]

Scheme 2. 2,5-Dihydroxy-1,4-benzoquinone Dianion Derivatives Used in This Work

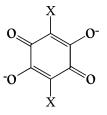

X_2An^{2-}; X = Cl or Br

In this work, we explore the use of the Fe(III) complexes, $[Fe^{III}(sal_2\text{-trien})]^+$, $[Fe^{III}(4\text{-OH-sal}_2\text{-trien})]^+$, $[Fe^{III}(sal_2\text{-epe})]^+$, and $[Fe^{III}(5\text{-Cl-sal}_2\text{-trien})]^+$ derivatives, and the Fe(II) complex, $[Fe^{II}(tren(imid)_3)]^{2+}$ (see Scheme 1) for the preparation of multifunctional compounds based on the anilate-based network in the search of new compounds combining spin-crossover and magnetic ordering. The first results of this strategy are reported in this paper.

EXPERIMENTAL SECTION

General Remarks. The Fe(III) complexes[15,16] and $[Fe^{II}(tren(imid)_3)](BF_4)_2$ were prepared according to literature methods.[17] $[(n\text{-}Bu)_4N]_3[Cr^{III}(X_2An)_3]$ (X═Cl, Br) was prepared by a modification of the literature method.[14] All other materials and solvents were commercially available and used without further purification.

Synthesis of $[NBu_4]_3[Cr^{III}(Cl_2An)_3]$ and $[NBu_4]_3[Cr^{III}(Br_2An)_3]$. An aqueous solution (10 mL) of $CrCl_3\cdot 6H_2O$ (400 mg, 1.5 mmol) was added dropwise to an aqueous solution (30 mL) of H_2Cl_2An or H_2Br_2An (5 mmol), NaOH (400 mg, 10 mmol), and NBu_4Br (1.6 g, 5 mmol). After 30 min at 70 °C, the mixture was allowed to cool to room temperature and extracted three times with 75 mL of CH_2Cl_2. The CH_2Cl_2 solution was dried with Na_2SO_4, filtered, rotoevaporated to dryness, and crystallized in dimethylformamide to give red shiny crystals after 2 weeks.

Synthesis of $[Fe^{III}(sal_2\text{-trien})][Mn^{II}Cr^{III}(Cl_2An)_3]\cdot(CH_2Cl_2)_{0.5}\cdot(CH_3OH)\cdot(H_2O)_{0.5}\cdot(CH_3CN)_5$ (1), $[Fe^{III}(4\text{-OH-sal}_2\text{-trien})][Mn^{II}Cr^{III}(Cl_2An)_3]\cdot$(solvate) (2), $[Fe^{III}(sal_2\text{-epe})][Mn^{II}Cr^{III}(Br_2An)_3]\cdot(CH_3CN)_4\cdot$(solvate) (3), $[Fe^{III}(5\text{-Cl-sal}_2\text{-trien})][Mn^{II}Cr^{III}(Br_2An)_3]\cdot(CH_2Cl_2)\cdot(CH_3OH)\cdot(H_2O)_4\cdot(CH_3CN)_{1.5}\cdot$(solvate) (4), and $[Fe^{II}(tren(imid)_3)]_2[Mn^{II}Cl_2Cr^{III}(Cl_2An)_3]Cl\cdot(CH_3OH)\cdot(CH_2Cl_2)_3\cdot(CH_3CN)_{0.5}$ (5). Crystals of these compounds were obtained by slow diffusion of two solutions. The first solution was prepared by dissolving $MnCl_2\cdot 4H_2O$ (12 mg, 0.06 mmol) and the Fe(III) complexes (0.06 mmol) in 6 mL of a 9:1 dichloromethane/methanol mixture ($[Fe^{III}(sal_2\text{-trien})](PF_6)$ (32 mg) for **1**, $[Fe^{III}(4\text{-OH-sal}_2\text{-trien})]Cl$ (27 mg) for **2**, $[Fe^{III}(sal_2\text{-epe})](ClO_4)$ (31 mg) for **3**, and $[Fe^{III}(5\text{-Cl-sal}_2\text{-trien})](PF_6)$ (38 mg) for **4**). In the case of **5**, it is necessary to dissolve first the $[Fe^{II}(tren(imid)_3)](BF_4)_2$ complex (73 mg, 0.12 mmol) in 6 mL of a 2:1 dichloromethane/methanol mixture and then add $MnCl_2\cdot 4H_2O$ (12 mg, 0.06 mmol). The second solution was obtained by dissolving $[NBu_4]_3[Cr^{III}(Cl_2An)_3]$ (84 mg, 0.06 mmol, for **1**, **2**, and **5**) or $[NBu_4]_3[Cr^{III}(Br_2An)_3]$ (100 mg, 0.06 mmol, for **3** and **4**) in 6 mL of acetonitrile. After 2−4 weeks, black prismatic single crystals suitable for X-ray crystal analysis were obtained. Yields: 6.8% (**1**), 6.8% (**2**), 7.4% (**3**), 5.4% (**4**), and 11.1% (**5**). These yields could be improved by diffusing the two solutions for longer times. Anal. Calcd for $C_{38.5}H_{37}Cl_7CrFeMnN_4O_{20}$ (**1**) (with 0.5 dichloromethane molecule and 6 water molecules per formula in the structure due to desolvation and rehydratation): C, 35.6; H, 3.1; N, 4.4%. Found: C, 35.9; H, 2.9; N, 4.4%. Anal. Calcd for $C_{38}H_{56}Cl_6CrFeMnN_4O_{32}$ (**2**) (with 16 water molecules per formula in the structure due to partial desolvation): C, 31.3; H, 3.9; N, 3.8%. Found: C, 31.4; H, 3.5; N, 4.3%. Anal. Calcd for $C_{39}H_{26}Br_6CrFeMnN_4O_{14}$ (**3**) (with no solvent molecules in the structure due to complete desolvation): C, 33.1; H, 1.8; N, 4.0%. Found: C, 32.4; H, 2.0; N, 4.0%. Anal. Calcd for $C_{43}H_{40.5}Br_6Cl_4CrFeMnN_{5.5}O_{19}$ (**4**): C, 30.0; H, 2.4; N, 4.5%. Found: C, 30.7; H, 2.1; N, 3.7%. Anal. Calcd for $C_{58}H_{55.5}Cl_{13}CrFe_2MnN_{20.5}O_{13}$ (**5**): C, 36.1; H, 2.9; N, 14.9%. Found: C, 35.5; H, 1.7; N, 14.1%. IR (KBr pellet) for **1**: 1624 (s), 1590 (sh), 1506 (vs), 1398 (w), 1359 (vs), 1305 (sh), 1007 (m), 835 (m) cm^{-1}. IR (KBr pellet) for **2**: 1625 (s), 1542 (sh), 1516 (vs), 1400 (m), 1360 (vs), 1007 (m), 849 (m) cm^{-1}. IR (KBr pellet) for **3**: 1623 (s), 1540 (sh), 1509 (sh), 1491 (vs), 1400 (m), 1351 (vs), 989 (m), 817 (m) cm^{-1}. IR (KBr pellet) for **4**: 1629 (s), 1517 (sh), 1491 (vs), 1401 (m), 1352 (vs), 990 (m), 817 (m) cm^{-1}. IR (KBr pellet) for **5**: 1635 (vs), 1533 (vs), 1507 (sh), 1401 (m), 1356 (vs), 1005 (m), 848 (m) cm^{-1}.

dx.doi.org/10.1021/ic5016803 | Inorg. Chem. 2014, 53, 12014−12026

Table 1. Crystallographic Data for Compounds 1, 2 and 3

compd	1	2	3
empirical formula	$C_{49.5}H_{40}Cl_7CrFeMnN_9O_{15.5}$	$C_{38}H_{24}Cl_6CrFeMnN_4O_{16}$	$C_{47}H_{26}Br_6CrFeMnN_8O_{14}$
fw	1419.84	1168.10	1569.01
cryst color	black	black	black
cryst size	0.2 × 0.08 × 0.04	0.10 × 0.08 × 0.06	0.16 × 0.08 × 0.06
temp (K)	120(2)	120(2)	120(2)
wavelength (Å)	0.71073	0.71073	0.71073
cryst syst, Z	monoclinic, 4	hexagonal, 3	monoclinic, 4
space group	$C\ 222_1$	$P\ 6_122$	$P\ 2_1/c$
a (Å)	12.9780(6)	13.7059(2)	14.1383(7)
b (Å)	24.8692(12)	13.7059(2)	22.3075(10)
c (Å)	21.9676(9)	66.2433(10)	23.4765(11)
α (deg)	90	90	90
ß (deg)	90	90	103.200(5)
γ (deg)	90	120	90
V (Å^3)	7090.1(6)	10776.7(4)	7208.6(6)
ρ_{calc}(Mg/m^3)	1.330	1.081	1.446
μ(Mo Kα) (mm^{-1})	0.852	0.791	3.899
θ range (deg)	2.916−27.597	3.205−25.081	2.892−26.048
reflns collected	81831	180425	117721
independent reflns (R_{int})	8183 (0.1702)	7375 (0.2011)	7113 (0.2088)
L. S. parameters, p/restraints, r	355/1	223/0	659/24
absolute structure parameter	0.076(19)	0.19(10)	
$R1(F)$,[a] $I > 2\sigma(I)$	0.0935	0.1354	0.1505
$wR2(F^2)$,[b] all data	0.2815	0.3273	0.4105
$S(F^2)$,[c] all data	1.029	0.827	1.011

[a] $R1(F) = \Sigma||F_0|-|F_C||/\Sigma|F_0|$; [b] $wR2(F^2) = [\Sigma w(F_0^2-F_C^2)^2/\Sigma wF_0^4]^{1/2}$; [c] $S(F^2) = [\Sigma w(F_0^2-F_C^2)^2/(n+r-p)]^{1/2}$.

Table 2. Crystallographic Data for Compounds 4, 5 at 120 K and 5 at 220 K

compd	4	5 (120 K)	5 (220 K)
empirical formula	$C_{43}H_{40.5}Br_6Cl_4CrFeMnN_{5.5}O_{19}$	$C_{59}H_{59.5}Cl_{15}CrFe_2MnN_{20.5}O_{13}$	$C_{58}H_{57.5}Cl_{13}CrFe_2MnN_{20.5}O_{13}$
fw	1722.32	2014.16	1927.22
cryst color	black	black	black
cryst size	0.16 × 0.09 × 0.06	0.11 × 0.09 × 0.07	0.12 × 0.09 × 0.06
temp (K)	120(2)	120(2)	120(2)
wavelength (Å)	0.71073	0.71073	0.71073
cryst syst, Z	monoclinic, 4	triclinic, 2	triclinic, 2
space group	$P\ 2_1/c$	P-1	P-1
a (Å)	13.9066(8)	13.2167(3)	13.2687(6)
b (Å)	23.1892(9)	16.2053(4)	16.5753(4)
c (Å)	22.7189(13)	20.2599(5)	20.3252(7)
α (deg)	90	97.796(2)	98.056(3)
ß (deg)	101.422(6)	97.354(2)	98.056(3)
γ (deg)	90	95.928(2)	95.922(3)
V (Å^3)	7181.4(7)	4231.55(18)	4347.9(3)
ρ_{calc} (Mg/m^3)	1.552	1.581	1.472
μ(Mo Kα) (mm^{-1})	4.066	1.148	1.054
θ range (deg)	2.985−26.427	2.955−27.502	2.849−26.483
reflns collected	113316	62029	69165
independent reflns (R_{int})	7832 (0.2296)	19299 (0.0887)	7112 (0.1373)
L. S. parameters, p/restraints, r	706/0	1048/0	817/8
$R1(F)$,[a] $I > 2\sigma(I)$	0.1618	0.0812	0.1101
$wR2(F^2)$,[b] all data	0.4331	0.2649	0.3631
$S(F^2)$,[c] all data	1.064	1.037	1.031

[a] $R1(F) = \Sigma||F_0|-|F_C||/\Sigma|F_0|$; [b] $wR2(F^2) = [\Sigma w(F_0^2-F_C^2)^2/\Sigma wF_0^4]^{1/2}$; [c] $S(F^2) = [\Sigma w(F_0^2-F_C^2)^2/(n+r-p)]^{1/2}$.

Structural Characterization. Single crystals of all compounds were mounted on glass fibers using a viscous hydrocarbon oil to coat the crystal and then transferred directly to the cold nitrogen stream for data collection. All reflection data were collected at 120 K for **1**−**4** and at 120 and 220 K for **5** on a Supernova diffractometer equipped with a graphite-monochromated Enhance (Mo) X-ray Source (λ = 0.7107 Å). The CrysAlisPro program, Oxford Diffraction Ltd., was used for unit cell determinations and data reduction. Empirical absorption correction was performed using spherical harmonics, implemented in the SCALE3 ABSPACK scaling algorithm. Crystal structures were

dx.doi.org/10.1021/ic5016803 | Inorg. Chem. 2014, 53, 12014−12026

solved by direct methods with the SIR97 program[18] and refined against all F^2 values with the SHELXL-2013 program[19] using the WinGX graphical user interface.[20] All non-hydrogen atoms were refined anisotropically except as noted, and hydrogen atoms were placed in calculated positions and refined isotropically with a riding model. Data collection and refinement statistics are collected in Tables 1 and 2. The structure of **5** at 220 K showed a weak diffraction due to the loss of CH_2Cl_2 solvent molecules from the structure. As a result of this weak diffraction, it was not possible to refine anisotropically C atoms from $[Fe^{II}(tren(imid)_3)]^{2+}$ complexes. Furthermore, this caused a smaller number of CH_2Cl_2 molecules in the structure solved at 220 K compared with that solved at 120 K (see Table 2). The subroutine SQUEEZE from PLATON[21] was used to calculate and remove the diffracting component of disordered solvents in **2**, **3**, and **4**, resulting in a void of ca. 5383 Å^3 and 1537 electrons/cell for **2**, in two voids of ca. 314 Å^3 and ca. 90 electrons/cell plus six smaller voids of less than 41 Å^3 and 7 electrons/cell for **3**, and two voids of ca. 307 Å^3 and 96 electrons/cell plus four smaller voids of less than 54 Å^3 and 20 electrons/cell for **4**. This corresponds to ca. 23 H_2O molecules per asymmetric unit for **2**, ca. 2 CH_3CN molecules per asymmetric unit for **3**, and 1 CH_3OH + 2 CH_3CN molecule per asymmetric unit for **4**. The CH_3OH molecule from the smallest voids of **4** has been included in the formula of the compound in Table 2 and Supporting Information (see cif file). CCDC-998895 to 998898, 1003585, and 1004948 contain the supplementary crystallographic data for this paper. These data can be obtained free of charge from The Cambridge Crystallographic Data Centre via www.ccdc.cam.ac.uk/data_request/cif. Glass capillaries (0.5 mm) were filled with polycrystalline samples of the compounds and mounted and aligned on a Empyrean PANalytical powder diffractometer, using Cu Kα radiation (λ = 1.54177 Å). A total of two scans were collected at room temperature in the 2θ range 5−40°.

Physical Measurements. Magnetic measurements were performed with a Quantum Design MPMS-XL-5 SQUID magnetometer in the 2 to 300 K temperature range with an applied magnetic field of 0.1 T on polycrystalline samples. The AC measurements were performed in the temperature range of 2−15 K at different frequencies with an oscillating magnetic field of 0.395 mT. The magnetization and hysteresis studies were performed between 5 and −5 K T, cooling the samples at zero field. Infrared (IR) spectra were recorded on a FTIR 320 Nicolet spectrometer. C, H, and N elemental analyses were measured on a CE Instruments EA 1110 CHNS Elemental analyzer. The Fe/Mn/Cr/Cl and Fe/Mn/Cr/Br/Cl ratios were measured with a Philips ESEM X230 scanning electron microscope equipped with an EDAX DX-4 microsonde.

RESULTS AND DISCUSSION

Synthesis. The compounds of formula $[Fe^{III}(sal_2\text{-trien})][Mn^{II}Cr^{III}(Cl_2An)_3]\cdot(CH_2Cl_2)_{0.5}\cdot(CH_3OH)\cdot(H_2O)_{0.5}\cdot(CH_3CN)_5$ (**1**), $[Fe^{III}(4\text{-OH-sal}_2\text{-trien})][Mn^{II}Cr^{III}(Cl_2An)_3]\cdot$(solvate) (**2**), $[Fe^{III}(sal_2\text{-epe})][Mn^{II}Cr^{III}(Br_2An)_3]\cdot(CH_3CN)_4\cdot$(solvate) (**3**), $[Fe^{III}(5\text{-Cl-sal}_2\text{-trien})][Mn^{II}Cr^{III}(Br_2An)_3]\cdot(CH_2Cl_2)\cdot(CH_3OH)\cdot(H_2O)_4\cdot(CH_3CN)_{1.5}\cdot$(solvate) (**4**), and $[Fe^{II}(tren(imid)_3)]_2\ [Mn^{II}Cl_2Cr^{III}(Cl_2An)_3]Cl\cdot(CH_3OH)\cdot(CH_2Cl_2)_3\cdot(CH_3CN)_{0.5}$ (**5**) have been prepared and characterized. The method to prepare these anilate-based compounds differs from that used to prepare oxalate-based compounds with similar templating cations.[12] Oxalate-based compounds were obtained in most cases by the slow diffusion of a solution of the Fe(III) or Fe(II) complex into a solution containing the precursors of the oxalate network almost free of other counterions. This was possible thanks to the use of the Ag^+ salt of the $[Cr^{III}(ox)_3]^{3-}$ complex and $MnCl_2$ which enables the removal of Ag^+ and Cl^- counterions by precipitation of AgCl. In the case of the anilate-based compounds, a similar strategy could not be used due to poor stability of the Ag^+ salts of $[Cr^{III}(X_2An)_3]^{3-}$ complexes. $[NBu_4]^+$ salts of $[Cr^{III}(Cl_2An)_3]^{3-}$ and $[Cr^{III}(Br_2An)_3]^{3-}$ were chosen instead because they can be obtained with a high degree of purity, something very important for the crystallization of the compounds. On the other hand, because the mixture of $[NBu_4]_3[Cr^{III}(Cl_2An)_3]$ or $[NBu_4]_3[Cr^{III}(Br_2An)_3]$ and $MnCl_2$ in the same solvent gives rise to a fast precipitation of the 2D compound, $[NBu_4][Mn^{II}Cr^{III}(X_2An)_3]$ (X = Cl or Br), the two precursors of the anilate-based network were dissolved in different solvents. The best results were obtained mixing $MnCl_2$ with the Fe(III) or Fe(II) complex in methanol/dichloromethane and slowly diffusing this solution into an acetonitrile solution of $[(n\text{-}Bu)_4N]_3[Cr^{III}(Cl_2An)_3]$ or $[(n\text{-}Bu)_4N]_3[Cr^{III}(Br_2An)_3]$. Other solvent mixtures with the same templating cations (chloroform in the place of dichloromethane or methanol in the place of acetonitrile) gave rise to other phases with a similar structure that will be reported in future works. In the case of **5**, it was necessary to dissolve the Fe(II) complex first in the methanol/dichloromethane mixture and then add the $MnCl_2\cdot4H_2O$ salt. The excess of Mn^{2+} resulting from an addition of the Fe(II) complex to a methanol solution of $MnCl_2\cdot4H_2O$ gives rise to the partial substitution of Fe(II) by Mn(II) in the tren(imid)$_3$ complex of the final compound. This was not observed in the other compounds of this paper. Furthermore, in contrast to **1**, **2**, **3**, and **4**, the Cl^- anions from $MnCl_2$ in **5** are coordinated to Mn(II) and act as counterions. The use of other Mn(II) salts to avoid the presence of Cl^- in the structure did not result in suitable crystals for X-ray diffraction. The composition of crystals of these compounds was checked by elemental analysis and microanalysis. C, H, and N elemental analyses show differences with respect to the calculated values using the formulas obtained from X-ray diffraction data at 120 K, in the case of **1**, **2**, and **3**. These differences may be explained by the loss of solvent molecules when the crystals are extracted from the mother liquor at room temperature. Indeed, a good coincidence between experimental and calculated values is obtained by decreasing the number of solvent molecules in these three structures (see above). Moreover in the case of **1**, the low nitrogen and carbon contents could indicate rehydration with water. Thermal gravimetry analysis should be performed to clarify this point, but it was not possible due to the small amount of sample available. Microanalysis shows a Fe/Mn/Cr/Cl ratio close to 1:1:1:7 for **1**, 1:1:1:6 for **2**, and 2:1:1:9 for **5**, a Fe/Mn/Cr/Br ratio close to 1:1:1:6 for **3**, and a Fe/Mn/Cr/Cl/Br ratio close to 1:1:1:3:6 for **4**. The results obtained for compound **5** indicate that CH_2Cl_2 solvent molecules observed in the crystal structure are lost after extracting the crystals from the mother liquor.

Structures. The structures of all compounds have been solved by single-crystal X-ray diffraction. The structures of **1**, **2**, **3**, and **4** consist of bimetallic anionic layers with a 2D bimetallic X_2An (X═Cl or Br) network of formula $[Mn^{II}Cr^{III}(X_2An)_3]$ with inserted Fe(III) cationic complexes and solvent molecules. The bimetallic anilate layer presents in these four compounds the well-known honeycomb structure, which is similar to that found for other extended oxalate or anilate-based networks.[14a] It consists in a hexagonal layer where the Cr(III) and Mn(II) ions occupy alternating vertices of the hexagons and are linked through X_2An bridges in such a way that each Mn(II) is surrounded by three neighboring Cr(III) and vice versa. This contrasts with the oxalate-based compounds obtained with similar Fe(III) cationic complexes that may present either 2D or 3D structures, depending on the substituent of the sal$_2$-trien ligand.[12] In this work, three types of 2D structures have been

dx.doi.org/10.1021/ic5016803 | Inorg. Chem. 2014, 53, 12014−12026

obtained that present a similar 2D anilate-based network. Still, important differences in the packing of the Fe(III) complexes and solvent molecules placed between these layers have been observed. They crystallize in orthorhombic (**1**), monoclinic (**3** and **4**), and hexagonal (**2**) space groups. A consequence of the replacement of oxalate by the larger bis-bidentate bridging X_2An^{2-} ligands is the presence of pores in the structures, which are filled with solvent molecules. Often these molecules are disordered. This has given rise to weak diffraction and quick loss of crystallinity due to fast evaporation of solvent molecules especially in compounds **2**, **3**, and **4**. As a result of this, powder X-ray diffraction patterns of **1**, **2**, **3**, and **4** do not show clear peaks. In contrast to the 2D compounds obtained with $[Fe^{III}(sal_2\text{-trien})]^+$ and derivatives, the use of the Fe(II) complex, $[Fe^{II}(tren(imid)_3)]^{2+}$, results in the formation of an anionic chain in compound **5**. This chain is formed by $[Cr^{III}(Cl_2An)_3]^{3-}$ complexes bonded to two Mn(II) ions through two bis-bidentate chloranilate bridges, whereas the third choranilate is a terminal one. The octahedral coordination of Mn(II) ions is completed with two chloride ions in cis. This type of structure has been found for other oxalate-based[4] and homometallic anilate-based compounds,[22] but it is the first time that it is obtained for heterometallic anilate-based networks. Again, the bimetallic oxalate-based compound obtained with the same complex presents a different structure, a very irregular 3D oxalate network with coexistence of bis(bidentate) and terminal oxalate ligands and solvent methanol molecules linked to heptacoordinated Mn(II) ions.[12g] It seems that $[Fe^{II}(tren(imid)_3)]^{2+}$ favors the presence of terminal oxalate or anilate ligands due to the formation of hydrogen bonds beween the NH groups from imidazole ligands and the two oxygens of the terminal oxalate or anilate ligand (see below). The powder X-ray diffraction pattern of **5** presents some differences with respect to the theorethical one obtained from single crystal X-ray diffraction data at 120 or 220 K, which may be attributed to the loss of solvent molecules (CH_2Cl_2) after extracting the crystals from the mother liquor already shown by micronalysis (see above and Figure S1 in the Supporting Information, SI).

Structure of $[Fe^{III}(sal_2\text{-trien})][Mn^{II}Cr^{III}(Cl_2An)_3]\cdot(CH_2Cl_2)_{0.5}\cdot(CH_3OH)\cdot(H_2O)_{0.5}\cdot(CH_3CN)_5$ (1). This compound crystallizes in the orthorhombic chiral space group $C222_1$. The structure is formed by bimetallic anionic sheets in the *ab* plane of formula $[Mn^{II}Cr^{III}(Cl_2An)_3]^-$ alternating with layers of $[Fe^{III}(sal_2\text{-trien})]^+$ cations (Figure 1). Acetonitrile, water, methanol, or dichloromethane solvent molecules occupy the holes between cationic and anionic layers.

The anionic layer presents the honeycomb structure mentioned above (Figure 2). The Mn(II) and Cr(III) are localized and clearly distinguishable as they present different bond distances with anilate ligands. Thus, there is one crystallographically independent Mn, with an occupancy of 0.5 and Mn−O bond lengths in the range of 2.136(8)−2.168(8) Å, and one crystallographically independent Cr, with an occupancy of 0.5 and Cr−O bond lengths in the range of 1.975(8)−1.984(8) Å. These are typical Cr−O and Mn−O bond lengths. The neighboring metal centers of these layers present alternated chirality as usual for this type of 2D networks. In the crystal of **1** used to solve the structure, all the Cr(III) ions adopt a Δ-configuration, whereas all the Mn(II) adopt the Λ-one. Therefore, the configuration of each metal ion is preserved in the neighboring anilate layers.

Because we have started from a racemic mixture of $[Cr(Cl_2An)_3]^{3-}$, crystals of the two enantiomers are expected

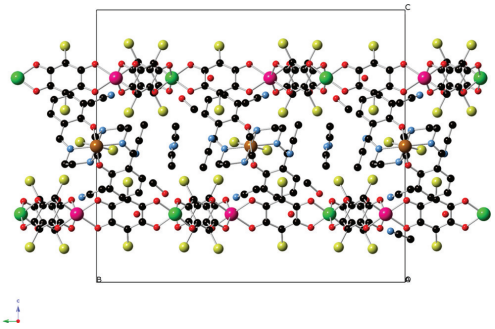

Figure 1. Projection of **1** in the *bc* plane. (Fe (brown), Cr (green), Mn (pink), C (black), N (blue), O (red), Cl (yellow). Hydrogen atoms have been omitted for clarity.

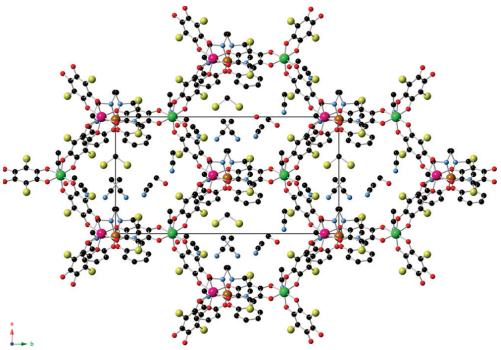

Figure 2. Projection of **1** in the *ab* plane showing one anionic layer and one cationic layer. (Fe (brown), Cr (green), Mn (pink), C (black), N (blue), O (red) Cl (yellow)). Hydrogen atoms have been omitted for clarity.

to be obtained. A similar behavior has been observed in other 2D oxalate and anilate structures.[8a,12c,f,14a] The chirality of the $[Fe^{III}(sal_2\text{-trien})]^+$ cations may be responsible of this first-order spontaneous resolution through chiral recognition between one of the enantiomers of $[Cr(Cl_2An)_3]^{3-}$ and $[Fe^{III}(sal_2\text{-trien})]^+$. In agreement with this, the crystallographically independent $[Fe^{III}(sal_2\text{-trien})]^+$ complex placed between the anilate layers adopts a Λ-configuration and interacts through several short contacts (see below) with the Cl_2An^{2-} ligands linked to Cr(III) from the upper and lower layers, which adopt the opposite configuration. As expected, given the larger size of the $[Fe^{III}(sal_2\text{-trien})]^+$ cation, the interlayer distance in **1** (10.98 Å), is significantly longer than those observed in the other anilate-based 2D compounds with $[(H_3O)(phz)_3]^+$ (in the range 9.03−9.21 Å) or NBu_4^+ cations (8.42 Å).[14a] This longer interlayer distance and the displacement of consecutive layers in the *ab* plane (due to the *C*-type unit cell) implies that the minimum distance between metals of different layers (11.423 Å) is also significantly longer than those found in the other anilate-based 2D compounds with NBu_4^+ (9.69 Å, where the layers are also displaced) or $[(H_3O)(phz)_3]^+$ cations (9.03−9.21 Å, where the layers are eclipsed).[14a] Albeit, this shortest metal−metal distance in **1** (11.423 Å) is similar to that

dx.doi.org/10.1021/ic5016803 | *Inorg. Chem.* 2014, 53, 12014−12026

observed in the compounds obtained by insertion of $[Fe^{III}(sal_2\text{-trien})]^+$ cations and derivatives into 2D bimetallic oxalate-based networks (11.609−12.807 Å).[12] A second consequence of the displacement of the consecutive layers is the formation of channels along the *c* axis (see Figure S2 in SI) that are occupied by solvent molecules.

The cationic layer intercalated between these anilate layers is formed by a crystallographically independent $[Fe^{III}(sal_2\text{-trien})]^+$ complex with an occupancy of 0.5 and solvent molecules. $[Fe^{III}(sal_2\text{-trien})]^+$ complexes are between two Mn atoms from the upper and lower anilate-based networks (see Figures 2 and S2 in the SI). The longer axis of the molecule is approximately perpendicular to the anilate-based layers with the atoms of the two phenolate rings of the complex parallel to one of the anilate ring of the two neighboring layers. Fe(III) complexes present a very distorted octahedral symmetry. SHAPE calculations show that the coordination geometry around Fe falls along the minimal distortion path between a perfect octahedron and a perfect trigonal prism with a deviation of less than 10%.[23] The generalized coordinate between the two ideal polyhedra is 50.1%. This indicates that the geometry of the $[Fe^{III}(sal_2\text{-trien})]^+$ complexes is intermediate between a trigonal prism and an octahedron. It seems that the insertion of these cations into anilate-based networks induces a larger distortion of the octahedral geometry compared with their insertion into 2D oxalate-based networks, as the maximum values of trigonal prismacity of 2D oxalate-base compounds with similar complexes are always lower than 41%.[12h] Average Fe−N and Fe−O bond lengths are 2.172(10) and 1.918(8) Å, which are in the range of those obtained for other HS Schiff base complexes, in agreement with magnetic properties (see below). The higher size of Cl_2An^{2-} ligand compared to the oxalate one gives rise to important differences in the packing of the spin-crossover cation compared to that observed in 2D oxalate-based compounds. Thus, in contrast to oxalate-based compounds, the spin-crossover cations are well isolated from each other as there are not intermolecular contacts between $[Fe^{III}(sal_2\text{-trien})]^+$ complexes belonging to the same layer. This is due to the fact that the size of the hexagons in the anilate-based layers is twice that of the oxalate-based ones. On the contrary, the $[Fe^{III}(sal_2\text{-trien})]^+$ complexes present numerous intermolecular interactions with the anilate-based network and solvent molecules. In particular, they present $\pi-\pi$ stacking interactions between phenolate groups from $[Fe^{III}(sal_2\text{-trien})]^+$ complexes and the anilate ligands of the two neighboring layers. Thus, the two phenolate groups from $[Fe^{III}(sal_2\text{-trien})]^+$ complexes lie parallel to a Cl_2An^{2-} ligand of the upper and lower layer and present short C−C intermolecular distances (distance between the centroids of the two rings 3.475 Å). Furthermore, they present short contacts between their NH groups and Cl and O atoms from the upper and lower anilate-based layers (Figure S3 in the SI).

Structure of $[Fe^{III}(4\text{-OH-}sal_2\text{-trien})][Mn^{II}Cr^{III}(Cl_2An)_3]\cdot$(solvate) (2). This compound crystallizes in the hexagonal chiral space group $P6_122$. The structure is formed by bimetallic anionic sheets in the *ab* plane alternating along the *c* direction with layers containing $[Fe^{III}(4\text{-OH-}sal_2\text{-trien})]^+$ complexes and disordered solvent molecules (Figure 3).

The anionic layer presents the hexagonal honeycomb layer of the previous compound. There is one crystallographically independent Mn(II) and Cr(III), which are localized and distinguishable (M-O bond lengths 2.122(11)-2.221(11) and 1.929(11)-2.035(12) Å, respectively). Mn and Cr present an

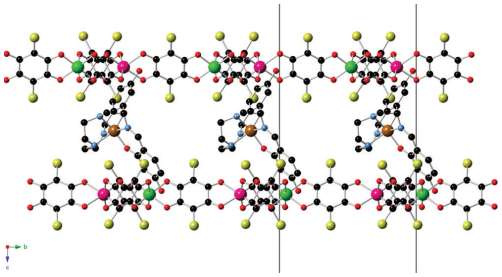

Figure 3. Projection of **2** in the *bc* plane. (Fe (brown), Cr (green), Mn (pink), C (black), N (blue), O (red), Cl (yellow)). Hydrogen atoms have been omitted for clarity.

occupancy of 0.5 as they are in a special position (2-fold axis). As shown in **1**, the configuration of each metal ion is preserved in the neighboring anilate layers. Thus, in the crystal used to solve the structure all the Cr^{III} ions adopt a Δ-configuration, whereas all the Mn^{II} ions adopt the Λ-one. $[Fe^{III}(4\text{-OH-}sal_2\text{-trien})]^+$ complex placed between the anilate layers adopts a Λ-configuration and interacts through several short contacts (see below) with two $\{Cr(Cl_2An)_3\}$ units from the upper and lower neighboring layers, which adopt the opposite configuration (Figure S4 in the SI). The minimum distance between metals of different layers is 11.060 Å, which is similar to that of compounds **1**, **3**, and **4**. As observed in **1**, the anilate-based layers in **2** are alternated.

The cationic layer intercalated between these anilate layers is formed by a crystallographically independent $[Fe^{III}(4\text{-OH-}sal_2\text{-trien})]^+$ complex with an occupancy of 0.5 due to the presence of a 2-fold axis, which runs from the Fe atom to a point placed in the middle of the central ethylene arm of the complex, and disordered solvent molecules. Average Fe−N and Fe−O bond lengths are 2.143(13) and 1.939(13) Å. These values are in the range of those obtained for other HS Schiff base complexes.[12] This contrasts with the LS state found in the $[Fe^{III}(4\text{-OH-}sal_2\text{-trien})]ClO_4$ precursor in the temperature range of 2−300 K.[16] These complexes lie with their long axis almost perpendicular to the anilate network. As in **1**, the two phenolate groups lie parallel to a Cl_2An^{2-} ligand of the upper and lower layers with short C−C intermolecular distances (distance between the centroids of the two rings 3.440 Å) (Figure S4 in the SI). Furthermore, they present short contacts between their NH groups and Cl and O atoms from the upper and lower anilate-based layers. The generalized coordinate calculated with the SHAPE[23] program is around 50%. This indicates that the geometry of the $[Fe^{III}(4\text{-OH-}sal_2\text{-trien})]^+$ complexes is intermediate between a trigonal prism and an octahedron as in **1**, confirming that the intermolecular interactions of these cations with two anilate layers may be the cause of the large distortion of the octahedral geometry. $[Fe^{III}(4\text{-OH-}sal_2\text{-trien})]^+$ complexes belonging to the same layer do not present intermolecular contacts, but interestingly and in contrast to compounds **1**, **3**, and **4**, they form hydrogen-bonds with two $[Fe^{III}(4\text{-OH-}sal_2\text{-trien})]^+$ complexes of neighboring layers. This is a consequence of the large size of the hexagonal channels of the anilate-based anionic network that allows a high degree of penetration of the inserted cation. The lateral view of the structure (Figure 4) shows that the hydroxy groups from $[Fe^{III}(4\text{-OH-}sal_2\text{-trien})]^+$ complexes penetrate the anilate-based

dx.doi.org/10.1021/ic5016803 | *Inorg. Chem.* 2014, 53, 12014−12026

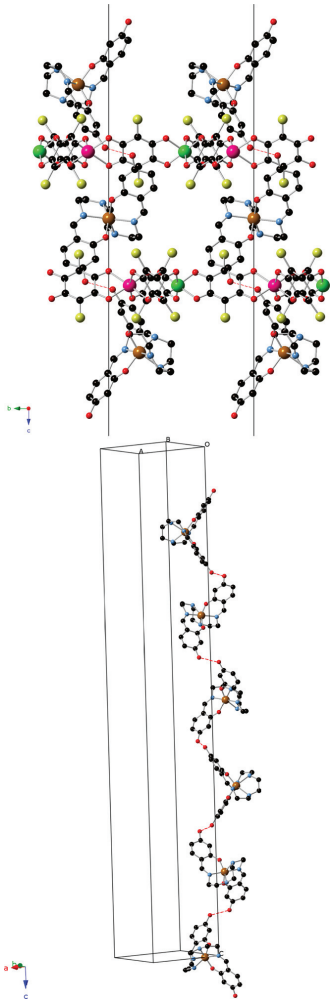

Figure 4. Projection of **2** in the *bc* plane showing the hydrogen bonds between $[Fe^{III}(4\text{-OH-sal}_2\text{-trien})]^+$ complexes from different layers (up). Helical chain of $[Fe^{III}(4\text{-OH-sal}_2\text{-trien})]^+$ complexes from different layers linked through hydrogen bonds (red dashed lines) (down). (Fe (brown), Cr (green), Mn (pink), C (black), N (blue), O (red), Cl (yellow)). Hydrogen atoms have been omitted for clarity.

network, allowing the formation of hydrogen bonds with the $[Fe^{III}(4\text{-OH-sal}_2\text{-trien})]^+$ complexes from the upper and lower cationic layers. This gives rise to helical chains of $[Fe^{III}(4\text{-OH-sal}_2\text{-trien})]^+$ complexes (Figure 4) linked through hydrogen-bond interactions running along the *c* axis. This type of interactions has never been found in oxalate-based compounds. Finally, another consequence of the larger size of X_2An^{2-} ligands compared to the oxalate ones is the presence of holes in the structure surrounding the $[Fe^{III}(4\text{-OH-sal}_2\text{-trien})]^+$ complexes that are occupied by disordered solvent molecules and that could not be modeled (see Experimental Section and cif files). Indeed, crystals of **2** lose solvent very quickly when they are extracted from their mother liquor. Projection of the structure along the *bc* plane shows the presence of channels along the *a* axis that could be filled with different guest molecules (Figure 3). Thus, these compounds present a void volume of ca. 5383 Å^3 (ca. 50% of the unit cell volume), where solvent molecules could be absorbed, opening the way to the synthesis of new porous magnets.

Structure of $[Fe^{III}(sal_2\text{-epe})][Mn^{II}Cr^{III}(Br_2An)_3]\cdot(CH_3CN_4\cdot$ (solvate) (3) and $[Fe^{III}(5\text{-Cl-sal}_2\text{-trien})][Mn^{II}Cr^{III}(Br_2An)_3]\cdot(CH_2Cl_2)\cdot(CH_3OH)\cdot(H_2O)_4\cdot(CH_3CN)_{1.5}\cdot$(solvate) (4). The two compounds crystallize in the monoclinic space group $P2_1/c$. Their structure consists of 2D bimetallic $[MnCr(Br_2An)_3]^-$ layers in the *ab* plane with a honeycomb structure similar to that observed in compounds **1** and **2**, alternating with $[Fe^{III}(sal_2\text{-epe})]^+$ (in **3**) or $[Fe^{III}(5\text{-Cl-sal}_2\text{-trien})]^+$ (in **4**) cations and solvent molecules (Figure 5).

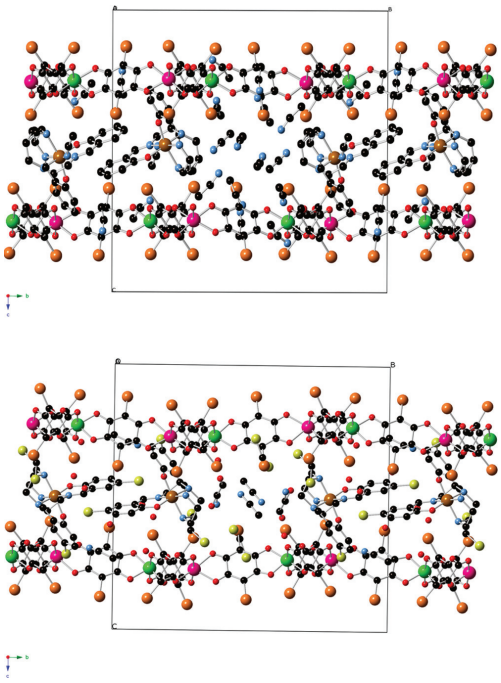

Figure 5. Projections of **3** (up) and **4** (down) in the *bc* plane. (Fe (brown), Br (orange), Cr (green), Mn (pink), C (black), N (blue), O (red), Cl (yellow)). Hydrogen atoms have been omitted for clarity.

In **4**, there is one crystallographically independent Mn(II) and Cr(III), which are localized and distinguishable (M−O bond lengths of 2.126(13)−2.206(16) Å and 1.961(15)−2.000(15) Å, respectively). Due to the presence of an inversion center located between the anilate-based layers, Mn and Cr ions from consecutive layers present opposite configurations. In contrast, the M−O bond lengths of the two crystallographically independent metal atoms of the anilate-based network in **3** (in the range of 2.007(16)−2.127(15) Å) are intermediate between those expected for Mn−O and Cr−O bonds indicating a higher

dx.doi.org/10.1021/ic5016803 | *Inorg. Chem.* 2014, 53, 12014−12026

degree of disorder. The minimum distance between metals of different layers is 11.919 Å for **3** and 11.557 Å for **4**, similar to those observed in compounds **1** and **2**. The anilate-based layers in **3** and **4** are also alternated.

The $[Fe^{III}(sal_2\text{-epe})]^+$, or $[Fe^{III}(5\text{-Cl-sal}_2\text{-trien})]^+$ complexes, and disordered solvent molecules occupying the space between the layers present a different packing to that shown in compounds **1** and **2**. Thus, two neighboring Fe(III) complexes present several intermolecular interactions that involve the two phenolate rings ($\pi-\pi$ stacking interactions between the two aromatic rings and two C−H···π or C−Cl···π interactions). These dimers of $[Fe^{III}(sal_2\text{-epe})]^+$ or $[Fe^{III}(5\text{-Cl-sal}_2\text{-trien})]^+$ complexes are well isolated from other Fe(III) complexes, although they present numerous intermolecular interactions with solvent molecules and with the anilate-based layers. In contrast to **1** and **2**, only one of the two phenolate groups of the cations present $\pi-\pi$ stacking interactions with the Br_2An^{2-} groups from the anilate-based layer as the other one is involved in the intermolecular interactions with a neighboring $[Fe^{III}(sal_2\text{-epe})]^+$ or $[Fe^{III}(5\text{-Cl-sal}_2\text{-trien})]^+$ complex as mentioned above (Figure S5 in the SI). $[Fe^{III}(sal_2\text{-epe})]^+$ and $[Fe^{III}(5\text{-Cl-sal}_2\text{-trien})]^+$ complexes present a distorted octahedral geometry with average Fe−N and Fe−O bond lengths of 2.122(18) and 1.939(16) Å for **3** and 1.98(2) and 1.854(18) Å for **4**. These bond lenghts indicate that the Fe ions in **3** are in the HS state, whereas those in **4** are in the LS one, in agreement with magnetic measurements (see below). SHAPE calculations[23] show that the coordination geometry around the Fe ion in **3** and **4** is closer to a perfect octahedron than that of compounds **1** and **2** (the generalized coordinate between a perfect octahedron and a perfect trigonal prism is 30.3% for **3** and 14.3% for **4**). These values are similar to those reported for similar complexes inserted into oxalate-based networks taking into account that HS complexes, as those of **3**, normally present a higher trigonal distortion.[12h] The higher trigonal distortion of **1** and **2** (with generalized coordinates of ca. 50%) may be related to the distortions generated by the $\pi-\pi$ intermolecular interactions between the Fe(III) complexes and two anilate rings of two neighboring layers. Finally, the structures of **3** and **4** present numerous voids that are occupied by disordered solvents. Some of them could not be modeled (see Experimental Section and cif files). Indeed, crystals of **3** and **4** lose solvent very quickly when they are out of the mother liquor.

Structure of $[Fe^{II}(tren(imid)_3)]_2[Mn^{II}Cl_2Cr^{III}(Cl_2An)_3]Cl\cdot(CH_3OH)\cdot(CH_2Cl_2)_3\cdot(CH_3CN)_{0.5}$ (5). This compound crystallizes in the triclinic space group *P*-1. It is formed by anionic $[Mn^{II}Cl_2Cr^{III}(Cl_2An)_3]^{3-}$ chains running along the *a* axis surrounded by $[Fe^{II}(tren(imid)_3)]^{2+}$, Cl^-, and solvent molecules (acetonitrile, methanol, or dichloromethane). These bimetallic anionic chains contain one crystallographically independent Cr and Mn with characteristic Mn−O and Cr−O distances (2.164(4)−2.370(4) Å for Mn1 and 1.950(4)−1.993(4) Å for Cr1). Furthermore, Mn is linked to two Cl^- anions in cis at 2.3823(19) and 2.4258(19) Å. These chains are formed by $[Cr^{III}(Cl_2An)_3]^{3-}$ complexes bonded to two Mn(II) ions through two bis-bidentate chloranilate bridges while the third chloranilate is a terminal one (see Figure 6). At the same time, the Mn(II) ions are coordinated to two chelating bis(bidentate) chloranilate bridges from two neighboring $[Cr^{III}(Cl_2An)_3]^{3-}$ complexes and to two chloride ion in cis (see Figure 6). These chains are formed by Mn and Cr ions of opposite chirality building a zigzag alternating arrangement of

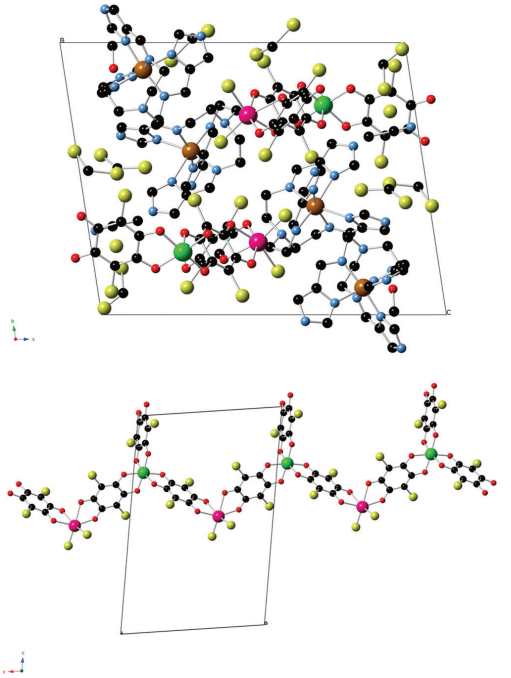

Figure 6. Projection of **5** in the *bc* plane (up). $[Mn^{II}Cl_2Cr^{III}(Cl_2An)_3]^{3-}$ chains in the structure of **5** (down). (Fe (brown), Cr (green), Mn (pink), C (black), N (blue), O (red), Cl (yellow)). Hydrogen atoms have been omitted for clarity.

complexes. Due to the centrosymmetric space group, chains of both chiralities are observed in the structure related by an inversion center. $[Fe^{II}(tren(imid)_3)]^{2+}$ complexes, Cl^- anions, and solvent molecules surround these chains (Figure 6). $[Mn^{II}Cl_2Cr^{III}(Cl_2An)_3]^{3-}$ chains are in close contact with a neighboring one through halogen−halogen interactions[24] involving a Cl atom from Cl_2An ligand (Cl1) with minimum Cl···Cl interchain distances of 3.130 Å (Figure S6 in the SI). The shortest distance between metals of neighboring chains is 8.445 Å. These chains present numerous short contacts with free Cl^- anions, $[Fe^{II}(tren(imid)_3)]^{2+}$ complexes, and solvent molecules.

$[Fe^{II}(tren(imid)_3)]^{2+}$ complexes, Cl^- anions, and solvent molecules are intercalated in the holes between these chains. There are two crystallographically independent $[Fe^{II}(tren(imid)_3)]^{2+}$ complexes in which Fe exhibits a distorted octahedral coordination environment involving six N donor atoms of the hexadentate Schiff base: three Fe−N(imine) and three Fe−N(imidazolyl) bonds. The average Fe−N distances of the two complexes (1.988(6) Å for the complex with Fe1 and 2.213(5) Å for the complex with Fe2) are close to the ones expected for LS (Fe1) and HS (Fe2).[17] These distances indicate that at 120 K, the temperature of the structural resolution, half of the Fe(II) complexes are in the HS state in agreement with magnetic measurements of the dry samples, see below. On the other hand, average Fe−N distances of the two complexes in the structure of another crystal solved at 220 K (2.162(10) Å for the complex with Fe1 and 2.235(8) Å for the

dx.doi.org/10.1021/ic5016803 | *Inorg. Chem.* 2014, 53, 12014−12026

complex with Fe2) are close to the expected ones for HS Fe(II). Furthermore, changes in the unit cell of this crystal indicate a shortening of *b* axis from 220 to 120 K, whereas the *a* and *c* axes remain almost constant (Figure S7 in the SI). At the same time, the unit cell volume decreases gradually from 220 to 120 K. All these changes are more important in the spin-crossover region (see below) from 220 to 140 K, indicating that they are associated with the change of spin state of half of the $[Fe^{II}(tren(imid)_3)]^{2+}$ complexes. It was not possible to solve the structure at 300 K due to the loss of crystallinity.

NH groups from two of the three imidazole ligands linked to Fe1 form hydrogen bonds with the Cl^- anion and a methanol molecule. In the same way, two of the three NH groups of $tren(imid)_3$ linked to Fe2 form hydrogen bonds with the two oxygens of the terminal chloranilate ligand of Cr and the Cl^- anion. These hydrogen bonds between a terminal Cl_2An ligand and the NH groups of $[Fe^{II}(tren(imid)_3)]^{2+}$ could explain the coexistence of terminal and bridging Cl_2An ligands in this structure as they may compete with the coordination to a metal. This has also been observed in the bimetallic oxalate-based compounds obtained with $[Fe^{II}(tren(imid)_3)]^{2+}$.[12g] Cl^- anions occupy the holes between the $[Fe^{II}(tren(imid)_3)]^{2+}$ cations. As mentioned above, they form two hydrogen bonds with NH groups from two neighboring $[Fe^{II}(tren(imid)_3)]^{2+}$ complexes.

Finally, there are numerous holes that are occupied by acetonitrile, methanol, and dichloromethane solvent molecules, which are disordered in some cases.

Magnetic Properties. Magnetic properties of **2** were measured for crystals of this compound in contact with the mother liquor to avoid the fast loss of solvent molecules. The magnetic properties of the other four compounds were measured in freshly filtered samples. The product of the molar magnetic susceptibility times the temperature ($\chi_m T$) of the four 2D compounds is shown in Figure 7. It presents at 300

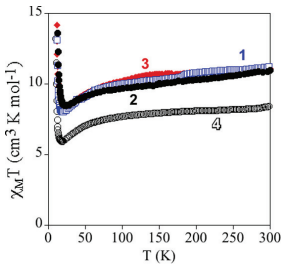

Figure 7. Temperature dependence of the product of the molar magnetic susceptibility times the temperature ($\chi_m T$) of **1** (empty blue squares), **2** (full circles), **3** (full red diamonds), and **4** (empty circles) with an applied field of 0.1 mT.

K a value close to 11.1 cm^3 K mol^{-1} for **1**, **2**, and **3**, and 8.3 cm^3 K mol^{-1} for **4**. These values are close to the expected ones for noninteracting Mn(II) and Cr(III) plus the contribution of a HS Fe(III) ion (10.6 cm^3 K mol^{-1} for $g = 2$) in the case of **1**, **2**, and **3**, although the lower value found in **4** indicates that most of the Fe(III) are in the LS state (expected value around 6.8 cm^3 K mol^{-1}). When the temperature is lowered, $\chi_m T$ of the four compounds shows a continuous decrease reaching a minimum value at 19.2 K (8.0 cm^3 K mol^{-1}) for **1**, 24.0 K (8.5 cm^3 K mol^{-1}) for **2**, 20.0 K (8.1 cm^3 K mol^{-1}) for **3**, and 18.5 K (5.9 cm^3 K mol^{-1}) for **4** followed by a sharp increase at lower temperatures with maxima between 6 and 9 K. The decrease of $\chi_m T$ with the temperature may be attributed to antiferromagnetic Mn−Cr interactions mediated through the X_2An^{2-} bridges, as observed in $[NBu_4]^+$ and $[(H_3O)(phz)_3]^+$ salts containing similar $[Mn^{II}Cr^{III}(X_2An)_3]^-$ layers (X = Cl, Br, I and H).[14a] Because the ground spin states of Cr^{III} and Mn^{II} are different (3/2 and 5/2, respectively), this interaction leads to an antiferromagnetic coupling that results in a $\chi_m T$ minimum, followed by an increase of $\chi_m T$ below ca. 18−22 K, and finally by a ferrimagnetic long-range ordering at low temperatures for the four compounds. Furthermore, structural data may help to understand the contribution of the spin crossover to the observed decrease of $\chi_m T$. Thus, as the Fe−N and Fe−O bond lenghts of **1**, **2**, and **3** at 120 K indicate that the Fe(III) ions are HS at this temperature, we conclude that only a small fraction of Fe(III) ions in **1**, **2**, and **3** undergo spin crossover from 300 to 120 K. An additional proof of the absence of a significant spin-crossover transition in these three compounds is the linear behavior of the χ_m^{-1} versus T curve in the 50−300 K temperature range. This plot can be fitted to a Curie−Weiss law ($\chi_m^{-1} = (T - \theta)/C$) leading to Weiss constants, $\theta = -20.0$ K for **1**, $\theta = -15.1$ K for **2**, and $\theta = -13.1$ K for **3**, which are close to those of other 2D $Mn^{II}Cr^{III}$ anilate-based networks.[14a] In the case of compound **4**, Fe−N and Fe−O bond lengths at 120 K indicate that the Fe(III) complex is predominantly LS at this temperature. Therefore, the $\chi_m T$ value of **4** at 300 K and the approximately constant difference of $\chi_m T$ of **1**, **2**, and **3** with respect to that of **4**, indicate that most of the Fe(III) ions of this compound are in the LS state from 300 to 120 K. An additional proof of the absence of a significant spin crossover in **4** is the linear behavior of the χ_m^{-1} versus T curve in the 50−300 K temperature range (θ value of −13.5 K). Mössbauer measurements are needed to confirm the LS/HS Fe(III) ratios of these compounds with the temperature, but they could not be performed due to the small amount of sample available.

The confirmation of the long-range order and a more accurate determination of the ordering temperatures can be obtained from the susceptibility measurements performed with an alternating magnetic field (AC susceptibility). These measurements show a frequency-independent peak in the in-phase molar susceptibility (χ_m') and out-of-phase molar susceptibility (χ_m'') of the four 2D compounds (Figure 8). In the case of **1**, the χ_m'' is very weak and only appears at the lowest frequencies (1 and 10 Hz). On the contrary, **2**, **3**, and **4** show clear frequency-independent peaks in χ_m' and χ_m'' (Figure 8). In some cases, secondary peaks appear at lower temperatures that could be explained by formation of magnetic domains and domain-wall movement, as in the oxalate-based networks.[12] The ordering temperature, T_c, determined as the temperature at which χ_m'' becomes nonzero is ca. 10 K for **1**, 10.4 K for **2**, 10.2 K for **3**, and 9.8 K for **4**. These T_c values are much higher than those found for the $[NBu_4]^+$ and $[(H_3O)(phz)_3]^+$ salts containing similar $[Mn^{II}Cr^{III}(Cl_2An)_3]^-$ or $[Mn^{II}Cr^{III}(Br_2An)_3]^-$ layers (5.5 and 6.3 K),[14a] in contrast to oxalate-based 2D compounds, where T_c remains constant for a given 2D $[M^{II}M^{III}(C_2O_4)_3]^-$ lattice, independently of the inserted cation. We can, therefore, conclude that the magnetic coupling and, accordingly, the ordering temperatures of these heterometallic 2D anilate-based networks are much more sensitive to the changes of the inserted cations than the corresponding oxalate ones. The possible reasons to explain this effect are the presence of intermolecular interactions between the anilate ligands and Fe(III) complexes ($\pi-\pi$

dx.doi.org/10.1021/ic5016803 | *Inorg. Chem.* 2014, 53, 12014−12026

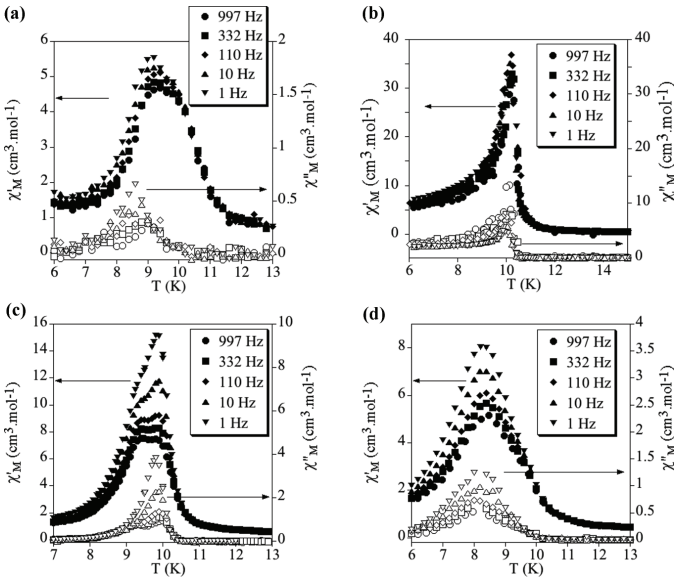

Figure 8. Temperature dependence of the in-phase AC susceptibility (χ') (filled symbols) and the out-of-phase AC susceptibility (χ'') of **1** (a), **2** (b), **3** (c), and **4** (c).

interactions and NH···O and NH···Cl/Br interactions mentioned above), which are not observed in $[NBu_4]^+$ and $[(H_3O)(phz)_3]^+$ salts containing similar $[Mn^{II}Cr^{III}(Cl_2An)_3]^-$ or $[Mn^{II}Cr^{III}(Br_2An)_3]^-$ layers. Some of these interactions could result in an increase of the Mn(II)−Cr(III) coupling constant through the anilate ligand and, accordingly, of T_c. In fact, these exchange interactions have shown to be very sensitive to small electronic changes introduced in the anilate bridge. Thus, in the series $(NBu_4)[Mn^{II}Cr^{III}(X_2An)_3]$, a change in the electron density in the anilate ring by changing X from Cl to H has resulted in an increase of T_c from 5.5 K up to 11.0 K.[14a] Interestingly, this modulation of T_c with the inserted cation (or even with solvent molecules), besides the already observed modulation with X,[14a] represents an additional advantage of the anilate-based networks compared with the oxalate ones.

The ferrimagnetic nature of the long-range ordering is confirmed by the isothermal magnetization measurements at 2 K that show a sharp increase of the magnetization at low fields that becomes more gradual at higher fields (Figure 9). At low fields (H < 0.2 T), the magnetizations of the four compounds increase with a high slope reaching values in the range 1.4−1.6 μ_B at H = 0.1 T (inset in Figure 9). At higher fields, the magnetization of the four compounds shows a gradual and nonlinear increase, which is higher in the case of **1**, **2**, and **3** (7.1 μ_B for **1**, 6.3 μ_B for **2**, and 7.2 μ_B for **3** at 5 T) than in **4** (4.0 μ_B at 5 T). These values are still far from saturation. The magnetization at lower fields is close to the expected value for a ferrimagnetic $Mn^{II}Cr^{III}$ network (M_s = 5 μ_B − 3 μ_B = 2 μ_B, possibly reduced by spin-canting effects in the anilate network). The gradual nonlinear increase observed at higher fields may be due to the contribution of the paramagnetic Fe(III) plus the result of the competition between the antiferromagnetic couplings and the Zeeman interaction with the external

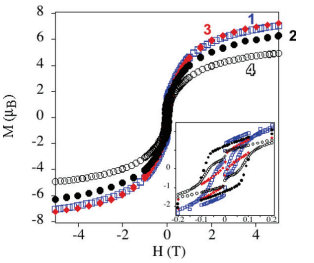

Figure 9. Isothermal magnetization at 2 K of **1** (empty blue squares), **2** (full circles), **3** (full red diamonds), and **4** (empty circles).

magnetic field. The higher increase in **1**, **2**, and **3** compared to that in **4** indicates that most of the Fe(III) of **1**, **2**, and **3** are in the HS state, whereas those of **4** are in the LS state at **2** K, in agreement with susceptibility measurements. These isothermal magnetization measurements also provide an additional proof of the magnetic ordering exhibited by these compounds because they present hysteresis below the ordering temperatures with coercive fields of ca. 35 mT for **1**, 87 mT for **2**, 10 mT for **3**, and 66 mT for **4** (Figure 9).

The χ_mT of **5** is shown in Figure 10. It presents at 300 K a value of 11.2 cm^3 K mol^{-1}. This value is close to the expected one for noninteracting Mn(II) and Cr(III) plus the contribution of two HS Fe(II) ion (12.25 cm^3 K mol^{-1} for g = 2) in agreement with crystal structure at 220 K, which suggests that most of the Fe(II) are in the HS. From 280 to 100 K, χ_mT shows a continuous decrease reaching a value of 8.4 cm^3 K mol^{-1} at 100 K. The decrease of χ_mT in this range of temperature (∼3 cm^3 K mol^{-1}) corresponds to the expected one for the spin crossover of half of the Fe(II). This is

dx.doi.org/10.1021/ic5016803 | Inorg. Chem. 2014, 53, 12014−12026

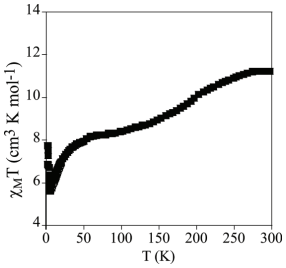

Figure 10. Temperature dependence of the product of the molar magnetic susceptibility times the temperature ($\chi_m T$) of **5** with an applied field of 0.1 mT.

supported by the structural data at 120 K, which indicate that 50% of Fe(II) are in the HS at this temperature (see above). At lower temperatures, $\chi_m T$ presents a gradual decrease that becomes very abrupt below 50 K to reach a minimum at 4.8 K followed by a sharp increase at lower temperatures. This behavior may be attributed to the antiferromagnetic Mn−Cr interactions mediated through the X_2An^{2-} bridges within the chains, as observed in the other compounds in this paper. This is supported by the magnetic data of other Mn^{II}−Cr^{III} chains of similar structure to that of **5** with diamagnetic counterions, obtained very recently by us, that show a very gradual decrease of $\chi_m T$ from 300 K (6.3 cm^3 K mol^{-1}) to 100 K (6.1 cm^3 K mol^{-1}) and an abrupt decrease below 50 K with a minimum at 6 K (2.5 cm^3 K mol^{-1}) followed by a sharp increase at lower temperatures.[25]

AC measurements show a frequency-independent peak in χ_m' and χ_m'' at temperatures below 2.6 K (Figure 11). This

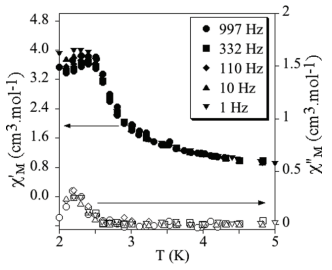

Figure 11. Temperature dependence of the in-phase AC susceptibility (χ') (filled symbols) and the out-of-phase AC susceptibility (χ'') of **5**.

indicates that the compound presents a magnetic long-range ordering below this temperature. The lack of frequency dependence of the AC peaks excludes a single- chain magnet (SCM) behavior.

The ferrimagnetic nature of the long-range ordering is confirmed by the isothermal magnetization measurements at 2 K that show a sharp increase of the magnetization at low fields (1.5 μ_B at H = 0.2 T) that becomes more gradual at higher fields (Figure S8 in the SI). As in the four previous compounds, the magnetization at lower fields is close to the expected value for a ferrimagnetic $Mn^{II}Cr^{III}$ network (M = 5 μ_B − 3 μ_B = 2 μ_B), while the gradual nonlinear increase observed at higher fields may be due to the contribution of the paramagnetic HS Fe(II). The hysteresis loop does not show a measurable coercive field. Therefore, this compound behaves as a soft magnet. The magnetic ordering must be the result of the ferromagnetic interchain interactions, induced by dipolar interactions and also by a possible superexchange pathway that can work through the halogen−halogen interchain interactions (see above). The synthesis of other compounds with a similar structure (replacement of $[Fe^{II}(tren(imid)_3)]^{2+}$ by diamagnetic complexes or of Cl_2An by Br_2An) is in progress in order to understand the role played by spin-crossover complexes and X_2An ligands in the interchain interactions.

CONCLUSION

Five novel compounds formed by $[Fe^{III}(sal_2\text{-trien})]^+$, $[Fe^{III}(5\text{-Cl-sal}_2\text{-trien})]^+$, $[Fe^{III}(sal_2\text{-epe})]^+$, $[Fe^{III}(4\text{-OH-sal}_2\text{-trien})]^+$, and $[Fe^{II}(tren(imid)_3)]^{2+}$ and anionic bimetallic coordination polymers based on the anilate ligand have been prepared and characterized. Two-dimensional anilate-based networks with a honeycomb structure have been obtained with the $[Fe^{III}(sal_2\text{-trien})]^+$ complex and derivatives (compounds **1**−**4**), whereas a one-dimensional (1D) anilate-based network has been obtained with $[Fe^{II}(tren(imid)_3)]^{2+}$ (compound **5**).

The first consequence of the replacement of oxalate by anilate ligands for $[Fe^{III}(sal_2\text{-trien})]^+$ and derivatives is that the formation of 2D compounds is favored when the larger anilate ligands are used. With oxalate ligands, one obtains either 2D or 3D networks, depending on the substituent of sal_2-trien. A second consequence is that, due to the larger size of anilate ligands, the distances between the Fe(III) complexes inserted between the anilate-layers are larger. This leads in some cases to the absence of intermolecular interactions between the spin-crossover complexes belonging to the same layer (**1** and **2**) or to the presence of isolated dimers of Fe(III) complexes (**3** and **4**). Furthermore, this results in the presence of large voids filled with disordered solvent molecules. Finally, a third consequence of the substitution of oxalate by anilate is the presence of π−π stacking interactions between the anilate ligands and the phenolate rings of the spin-crossover complexes, which is not observed in the oxalate-based compounds. These π−π interactions, more important in compounds **1** and **2**, lead to a larger trigonal distortion of the octahedral geometry of Fe(III) in these compounds. The rigidity imposed by π−π stacking with the anilate ligands and the lack of intermolecular interactions between the Fe(III) complexes may be at the origin of the absence of a significant spin crossover in the 2D compounds. Thus, the magnetic properties indicate that most of the inserted Fe(III) cations remain in their HS (**1**, **2**, and **3**) or LS state (**4**). At the same time the anilate network presents a ferrimagnetic ordering at ca. 10 K, which is significantly higher than the ordering temperatures obtained for oxalate networks with the same metal ions (ca. 5 K) or for 2D anilate networks with other templating cations (ca. 6 K for $[NBu_4]^+$ and $[(H_3O)(phz)_3]^+$ salts). Notice that the presence of pores in these structures and the chiral character of some of them could lead to new functionalities, in addition to the magnetic ordering such as solvent adsorption, proton conduction or chirality.

The preparation of anilate-based compounds combining spin crossover and magnetic ordering has been achieved with the use of $[Fe^{II}(tren(imid)_3)]^{2+}$ complex, which do not present spin crossover in bimetallic oxalate-based compounds.[12g] Compound **5** presents a 1D anionic anilate-based network surrounded by $[Fe^{II}(tren(imid)_3)]^{2+}$ complexes, Cl^- anions, and solvent molecules. The main difference with the previous

dx.doi.org/10.1021/ic5016803 | Inorg. Chem. 2014, 53, 12014−12026

series of 2D compounds is that the spin-crossover complexes do not show $\pi-\pi$ stacking interactions with the anilate ligands and present numerous intermolecular contacts among them. As a result of this, **5** shows coexistence of spin crossover of half of the Fe(II) complexes from 280 to 100 K and a ferrimagnetic coupling within the chains that gives rise to a magnetic ordering below 2.6 K. Photomagnetic measurements are in progress to study the possible effect of a photoinduced spin crossover in the magnetic properties of the anilate-based network in the search for a magnetic responsive material.

Finally, an additional advantage provided by this type of networks that remains to be explored is the functionalization of the anilate ligands with substituents leading to strong intermolecular interactions between the ferrimagnetic network and the spin-crossover complex or even covalent bonding between the two networks in order to enhance the interactions between them and to improve their responsive character.

■ ASSOCIATED CONTENT

Supporting Information

Structural views of **1**, **2**, **3**, **4**, and **5**. Changes of the unit cell parameters with the temperature and isothermal magnetization of **5** at 2 K. This material is available free of charge via the Internet at http://pubs.acs.org.

■ AUTHOR INFORMATION

Corresponding Authors

*E-mail: miguel.clemente@uv.es. Fax: (+34) 96 354 3273. Tel: (+34) 96 3544415.

*E-mail: eugenio.Coronado@uv.es.

Notes

The authors declare no competing financial interest.

■ ACKNOWLEDGMENTS

We thank the EU (SPINMOL ERC Adv. Grant), the Spanish MINECO (CTQ-2011-26507, and MAT2011-22785) and the Generalitat Valenciana (Prometeo and ISIC-Nano programs) for financial support. The authors also thank J. M. Martínez-Agudo and Dr. G. Agustí-López, University of Valencia, for magnetic characterization.

■ REFERENCES

(1) (a) Coronado, E.; Day, P. *Chem. Rev.* **2004**, *104*, 5419−5448. (b) Coronado, E.; Martí- Gastaldo, C.; Navarro-Moratalla, E.; Ribera, A.; Blundell, S. J.; Baker, P. J. *Nat. Chem.* **2010**, *2*, 1031−1036. (c) Coronado, E.; Martí-Gastaldo, C.; Navarro-Moratalla, E.; Burzuri, E.; Camon, E.; Luis, F. *Adv. Mater.* **2011**, *23*, 5021−5026. (d) Bourzami, R.; Eyele-Mezui, S.; Delahaye, E.; Drillon, M.; Rabu, P.; Parizel, N.; Choua, S.; Turek, P.; Rogez, G. *Inorg. Chem.* **2014**, *53*, 1184−1194.

(2) Coronado, E.; Mínguez Espallargas, G. *Chem. Soc. Rev.* **2013**, *42*, 1525−1539.

(3) See for general reviews: (a) Spin Crossover in Transition Metal Compounds. *Topics in Current Chemistry*; Gütlich, P., Goodwin, H. A., Eds.; Springer Verlag: Berlin-Heidelberg- New York, 2004; Vols. 233−235. (b) *Spin-Crossover Materials: Properties and Applications*; Halcrow, M. A., Ed.; Wiley: New York, 2013.

(4) Clemente-León, M.; Coronado, E.; Martí-Gastaldo, C.; Romero, F. M. *Chem. Soc. Rev.* **2011**, *40*, 473−497.

(5) (a) Clemente-León, M.; Galán-Mascarós, J. R.; Gómez-García, C. J. *Chem. Commun.* **1997**, 1727−1728. (b) Coronado, E.; Galán-Mascarós, J. R.; Gómez-García, C. J.; Martínez-Agudo, J. M. *Adv. Mater.* **1999**, *11*, 558−561. (c) Coronado, E.; Galán-Mascarós, J. R.; Gómez-García, C. J.; Ensling, J.; Gutlich. *Chem.—Eur. J.* **2000**, *6*, 552−563.

(6) (a) Bénard, S.; Yu, P.; Audière, J. P.; Rivière, E.; Clèment, R.; Ghilhem, J.; Tchertanov, L.; Nakatami, K. *J. Am. Chem. Soc.* **2000**, *122*, 9444−9454. (b) Aldoshin, S. M.; Sanina, N. A.; Minkin, V. I.; Voloshin, N. A.; Ikorskii, V. N.; Ovcharenko, V. I.; Smirnov, V. A.; Nagaeva, N. K. *J. Mol. Struct.* **2007**, *826*, 69−74.

(7) (a) Coronado, E.; Galán-Mascarós, J. R.; Gómez-García, C. J.; Laukhin, V. *Nature* **2000**, *408*, 447−449. (b) Alberola, A.; Coronado, E.; Galán-Mascarós, J. R.; Giménez-Saiz, C.; Gómez- García, C. J. *J. Am. Chem. Soc.* **2003**, *125*, 10774−10775. (c) Galán-Mascarós, J. R.; Coronado, E.; Goddard, P. A.; Singleton, J.; Coldea, A. I.; Wallis, J. D.; Coles, S. J.; Alberola, A. *J. Am. Chem. Soc.* **2010**, *132*, 9271−9273. (d) Coronado, E.; Galán-Mascarós, J. R.; Gómez-García, C. J.; Martínez-Ferrero, E.; Van Smaalen, S. *Inorg. Chem.* **2004**, *43*, 4808−4810. (e) Zhang, B.; Zhang, Y.; Zhu, D. *Chem. Commun.* **2012**, *48*, 197−199.

(8) (a) Okawa, H.; Shigematsu, A.; Sadakiyo, M.; Miyagawa, T.; Yoneda, K.; Ohba, M.; Kitagawa, H. *J. Am. Chem. Soc.* **2009**, *131*, 13516−13522. (b) Pardo, E.; Train, C.; Contard, G.; Boubekeur, K.; Fabelo, O.; Liu, H.; Dkhil, B.; Lloret, F.; Nakagawa, K.; Tokoro, H.; Ohkoshi, S.-I.; Verdaguer, M. *J. Am. Chem. Soc.* **2011**, *133*, 15328−15331. (c) Sadayiko, M.; Okawa, H.; Shigematsu, A.; Ohba, M.; Yamada, T.; Kitagawa, H. *J. Am. Chem. Soc.* **2012**, *134*, 5472−5475. (d) Okawa, H.; Sadakiyo, M.; Yamada, T.; Maesato, M.; Ohba, M.; Kitagawa, H. *J. Am. Chem. Soc.* **2013**, *135*, 2256−2262.

(9) (a) Endo, T.; Akutagawa, T.; Noro, S. I.; Nakamura, T. *Dalton Trans.* **2011**, *40*, 1491−1496. (b) Pardo, E.; Train, C.; Liu, H.; Chamoreau, L.-M.; Dkhil, B.; Boubekeur, K.; Lloret, F.; Nakatani, K.; Tokoro, H.; Ohkoshi, S.-i.; Verdaguer, M. *Angew. Chem., Int. Ed.* **2012**, *51*, 8356−8360.

(10) (a) Andrés, R.; Gruselle, M.; Malézieux, B.; Verdaguer, M.; Vaissermann, J. *Inorg. Chem.* **1999**, *38*, 4637−4646. (b) Andrés, R.; Brissard, M.; Gruselle, M.; Train, C.; Vaissermann, J.; Malézieux, B.; Jamet, J. P.; Verdaguer, M. *Inorg. Chem.* **2001**, *40*, 4633−4640. (c) Clemente- León, M.; Coronado, E.; Dias, J. C.; Soriano-Portillo, A.; Willett, R. D. *Inorg. Chem.* **2008**, *47*, 6458−6463. (d) Train, C.; Gheorghe, R.; Krstic, V.; Chamoreau, L. M.; Ovanesyan, N. S.; Rikken, G. L. J. A.; Gruselle, M.; Verdaguer, M. *Nat. Mater.* **2008**, *7*, 729−734. (e) Train, C.; Nuida, T.; Gheorghe, R.; Gruselle, M.; Ohkoshi, S. *J. Am. Chem. Soc.* **2009**, *131*, 16838−16843. (f) Gruselle, M.; Li, Y.; Ovanesyan, N.; Markhaev, V.; Shilov, G.; Mushenok, F.; Train, C.; Aldoshin, S. *Chirality* **2013**, *25*, 444−448.

(11) Clemente-León, M.; Coronado, E.; Gómez-García, C. J.; López-Jordà, M.; Camón, A.; Repollés, A.; Luis, F. *Chem.—Eur. J.* **2014**, *20*, 1669−1676.

(12) (a) Clemente-León, M.; Coronado, E.; Giménez-López, M. C.; Soriano-Portillo, A.; Waerenborgh, J. C.; Delgado, F. S.; Ruiz-Pérez, C. *Inorg. Chem.* **2008**, *47*, 9111−9120. (b) Clemente-León, M.; Coronado, E.; López-Jordà, M.; Mínguez Espallargas, G.; Soriano-Portillo, A.; Waerenborgh, J. C. *Chem.—Eur. J.* **2010**, *16*, 2207−2219. (c) Clemente-León, M.; Coronado, E.; López-Jordà, M. *Dalton Trans.* **2010**, *39*, 4903−4910. (d) Clemente-León, M.; Coronado, E.; López-Jordà, M.; Waerenborgh, J. C. *Inorg. Chem.* **2011**, *50*, 9122−9130. (e) Clemente-León, M.; Coronado, E.; López-Jordà, M.; Desplanches, C.; Asthana, S.; Wang, H.; Létard, J.-F. *Chem. Sci.* **2011**, *2*, 1121−1127. (f) Clemente-León, M.; Coronado, E.; López-Jordà, M. *Eur. J. Inorg. Chem.* **2013**, *2013*, 753−762. (g) Ben Djamâa, A.; Clemente-León, M.; Coronado, E.; López- Jordà, M. *Polyhedron* **2013**, *64*, 142−150. (h) Clemente-León, M.; Coronado, E.; López-Jordà, M.; Waerenborgh, J. C.; Desplanches, C.; Wang, H.; Létard, J.-F.; Hauser, A.; Tissot, A. *J. Am. Chem. Soc.* **2013**, *135*, 8655−8677.

(13) Coronado, E.; Galán-Mascarós, J. R.; Giménez-López, M. C.; Almeida, M.; Waerenborgh, J. C. *Polyhedron* **2007**, *26*, 1838−1844.

(14) (a) Atzori, M.; Benmansour, S.; Mínguez Espallargas, G.; Clemente-León, M.; Abhervé, A.; Gómez-Claramunt, P.; Coronado, E.; Artizzu, F.; Sessini, E.; Deplano, P.; Serpe, A.; Mercuri, M: L.; Gómez-García, C. J. *Inorg. Chem.* **2013**, *52*, 10031−10040. (b) Atzori, M.; Artizzu, F.; Sessini, E.; Marchiò, L.; Loche, D.; Serpe, A.; Deplano,

P.; Concas, G.; Pop, F.; Avarvari, N.; Mercuri, M: L. *Dalton Trans.* **2014**, *43*, 7006−7019.
(15) (a) Tweedle, M. F.; Wilson, L. J. *J. Am. Chem. Soc.* **1976**, *98*, 4824−4834. (b) Griffin, M.; Shakespeare, S.; Shepherd, H. J.; Harding, C. J.; Létard, J. F.; Desplanches, C.; Goeta, A. E.; Howard, J. A. K.; Powell, A. K.; Mereacre, V.; Garcia, Y.; Naik, A. D.; Müller-Bunz, H.; Morgan, G. G. *Angew. Chem., Int. Ed.* **2011**, *50*, 896−900.
(16) Nemec, I.; Herchel, R.; Salitros, I.; Trávnícek, Z.; Moncol, J.; Fuess, H.; Ruben, M.; Linert, W. *CrystEngComm* **2012**, *14*, 7015−7024.
(17) Sunatsuki, Y.; Ohta, H.; Kojima, M.; Ikuta, Y.; Goto, Y.; Matsumoto, N.; Iijima, S.; Akashi, H.; Kaizaki, S.; Dahan, F.; Tuchagues, J.-P. *Inorg. Chem.* **2004**, *43*, 4154−4171.
(18) Altomare, A.; Burla, M. C.; Camalli, M.; Cascarano, G. L.; Giacovazzo, C.; Guagliardi, A.; Moliterni, A. G. G.; Polidori, G.; Spagna, R. *J. Appl. Crystallogr.* **1999**, *32*, 115−119.
(19) Sheldrick, G. M. *Acta Crystallogr.* **2008**, *A64*, 112−122.
(20) Farrugia, L. J. *J. Appl. Crystallogr.* **2012**, *45*, 849−854.
(21) Spek, A. L. *J. Appl. Crystallogr.* **2003**, *36*, 7−13.
(22) (a) Kitagawa, S.; Kawata, S. *Coord. Chem. Rev.* **2002**, *224*, 11−34. (b) Michaelides, A.; Papadimitriou, C. D.; Plakatouras, J. C.; Skoulika, S.; Veltsistas, P. G. *Polyhedron* **2004**, *23*, 2587−2593. (c) Morikawa, S.; Yamada, T.; Kitagawa, H. *Chem. Lett.* **2009**, *38*, 654−655. (d) Yamada, T.; Morikawa, S.; Kitagawa, H. *Bull. Chem. Soc. Jpn.* **2010**, *83*, 42−48.
(23) Llunell, M.; Casanova, D.; Cirera, J.; Bofill, J. M.; Alemany, P.; Alvarez, S.; Pinski, M.; Avnir. D. *SHAPE*, version 2.0; University of Barcelona, 2010.
(24) Mínguez Espallargas, G.; Brammer, L.; Allan, D. R.; Pulha, C. R.; Robertson, N.; Warren, J. E. *J. Am. Chem. Soc.* **2008**, *130*, 9058−9071.
(25) Abhervé, A.; Clemente-León, M.; Coronado, E.; Gómez-García, C. J. Unpublished results.